Global Implications of Arctic Climate Processes and Feedbacks

Report of the Arctic Climate Workshop
Alfred Wegener Institute for Polar and Marine Research
Potsdam (Germany), 5 - 7 September 2005

Edited by Annette Rinke und Klaus Dethloff

Ber. Polarforsch. Meeresforsch. 520 (2006)
ISSN 1618 - 3193

Annette Rinke, Alfred Wegener Institute, Research Unit Potsdam, Telegrafenberg A43, 14473 Potsdam, Germany

Klaus Dethloff, Alfred Wegener Institute, Research Unit Potsdam, Telegrafenberg A43, 14473 Potsdam, Germany

Table of Contents

1 Introduction 1

2 Program of the Workshop 3

3 Extended Abstracts 7

A new sea ice albedo parameterization in ECHO-G and its global consequences
A. Benkel and M. Køltzow 9

The Arctic water cycle in ECHO-G scenarios
A. Benkel, B. Rockel, and F. Gonzalez-Rouco 13

Changes in synoptic weather patterns in the Arctic during the 21st century
J.J. Cassano, P. Uotila, and A.H. Lynch 17

ERA40 driven ORCM simulations of today's climate for the Arctic and Nordic regions
J. Debernard 21

Intercomparison of the GLIMPSE coupled RCMs
J. Debernard 26

Overview and main results of the EU project GLIMPSE "Global implications of Arctic climate processes and feedbacks"
K. Dethloff and GLIMPSE group 29

Sensitivities in the Rossby Centre Arctic models
R. Döscher, H.E.M. Meier, and K. Wyser 36

Sea ice simulations with the AWI's coupled regional atmosphere-ocean-ice model HIRHAM-NAOSIM
W. Dorn, K. Dethloff, A. Rinke, S. Frickenhaus, R. Gerdes, M. Karcher, and F. Kauker 41

Influence of horizontal resolution on Arctic Ocean model results
R. Gerdes and K. Fieg 45

On the impacts of extreme events on the coastal zone of a small Alaskan community: multi-scale modeling approaches
K. Görgen, A.H. Lynch, E.N. Cassano, L. Xie, L. Lestak, and R. Brunner 47

Winter climate regimes in forced atmosphere-ocean GCM simulations
D. Handorf, M. Sempf, K. Dethloff, C. Casty, E. Zorita, F. Gonzales-Rouco, M. Stendel, and J.H. Christensen 51

Reconstruction of past climate changes in the Arctic regions of Russia and Canda
S. Holzkämper and P. Kuhry 58

Frost flowers on sea ice: A multi-disciplinary research effort for the upcoming International Polar Year 2007/09
L. Kaleschke, A. Richter, J. Burrows, G. Heygster, J. Notholt, H.-W. Jacobi,, R. Weller, S. Kern, R. Sander, J. Hollwedel, and R. von Glasow 62

Arctic climate projections for the 21st century with the new generation of AOGCMs
V. Kattsov 66

Fresh water balance of the Arctic Ocean and adjacent seas: Results from NAOSIM-LRM hindcast experiments
C. Köberle and R. Gerdes 71

Atmospheric sensitivity to surface forcing in a regional climate model
M. Køltzow 73

Assessing Climate Change Impacts in the European North: The BALANCE project
M.A. Lange 77

A global adaptive barotropic model of the atmosphere
M. Läuter, D. Handorf, and K. Dethloff 82

How to deal with sea ice deformation in the Arctic: Four approaches in a continuum sea ice model
T. Martin 83

On recent changes in sea ice and ocean conditions and their potential feedback to Arctic climate
M. Maslowski 84

Retrieval of total water vapour over the Arctic from space-borne microwave radiometer data
C. Melsheimer and G. Heygster 85

Interactions between the surface, clouds, aerosols, and radiation in a meso-scale model of the Western Arctic
H. Morrison 89

Intercomparison of Arctic atmospheric RCMs: Spatiotemporal patterns of large-scale flow and temperature
A. Rinke, GLIMPSE and ARCMIP groups 90

Modeling of permafrost in a regional climate model and its influences on present and future Arctic climate
S. Saha, A. Rinke, K. Dethloff, and P. Kuhry 94

Multidecadal variability: What are the causes?
T. Schmith and M. Stendel 99

How does the ocean move beneath the sea ice? Problems and implications concerning model studies and observations
D. Schröder 100

Arctic Oscillation regime behaviour in an idealized atmospheric circulation model as a result of almost-intransitivity
M. Sempf, K. Dethloff, D. Handorf, and M.V. Kurgansky 103

Effects of climatic forcing on the marine ecosystem of the Barents and the Greenland Seas
D. Slagstad, I. Ellingsen, M. Reigstad, and P. Wassmann 104

Modeling the summer Arctic boundary layer
S. Söderberg, M. Tjernström, and M. Zagar 107

AOGCM sensitivity studies using Eliassen Palm fluxes as a diagnostic tool
E. Sokolova, K. Dethloff, A. Benkel, and A. Rinke 112

Sensitivity of the Arctic Oscillation to volcanic forcing in the IPCC AR4 climate models
G. Stenchikov 116

Simulation of climate evolution for the period 1500-2000 with all relevant natural and anthropogenic forcings
M. Stendel and J.H. Christensen 123

Modeling the Arctic boundary layer
M. Tjernström, S. Söderberg, and M. Zagar 128

Comparison of a regional landsat image based land cover classification to global data sets in Northeast European Russia
T. Virtanen and P. Kuhry 133

Comparison of modeled and observed clouds and radiation in the Arctic
K. Wyser, C. Jones, R. Döscher, and H.E.M. Meier 139

4 Appendix 145

Appendix 1: Work packages of the GLIMPSE project 147

Appendix 2: Participants of the workshop 148

Appendix 3: Author index 151

1 Introduction

The polar region is seeing major climate and environmental changes due to the effects of natural variability and global warming. Fifty-three experts from the United States, Canada, Europe and Russia gathered at the Alfred Wegener Institute for Polar and Marine Research in Potsdam from September 5-7, 2005 to address regional Arctic climate processes and their global feedbacks. The workshop was organized by Klaus Dethloff and Annette Rinke.

The workshop was organized as the final meeting of the European Union project "Global Implications of Arctic Climate Processes and Feedbacks" (GLIMPSE; http://www.awi-potsdam.de/www-pot/atmo/glimpse/). The main objectives of GLIMPSE (see Appendix 1 for the description of the six work packages) were the following:

- The project will address and reduce the deficiencies in our understanding of the Arctic by developing improved physical descriptions, understanding and parameterizations of regional Arctic climate feedbacks in atmospheric regional climate models and coupled atmosphere-ocean-sea-ice regional climate models with high horizontal and vertical resolution on the basis of data from the Surface Heat Budget of the Arctic Ocean project (SHEBA; Uttal et al., 2002) and of the network of meteorological stations over land. The involved Arctic regional models will be intercompared as part of the international Arctic Regional Climate Model Intercomparison Project (ARCMIP; http://curry.eas.gatech.edu/ARCMIP/ ; Curry and Lynch, 2002).
- The improved parameterizations from Arctic regional models will be implemented into state-of-the-art global coupled Atmosphere-Ocean General Circulation Models (AOGCMs), to determine and understand their global influences and consequences for Arctic climate feedbacks and decadal-scale climate variations. These results will be used to assess the probability of abrupt climate changes on decadal time scales in the past and in the future. The impact of Arctic climate changes on Northern ecosystems and communities will be investigated.

To arrive on more credible present-day Arctic simulations and estimates of possible Arctic climate changes, an improved understanding and modeling of the Arctic climate processes is necessary. One useful approach for this intention is the application of regional climate models (RCMs) on the Arctic region. The rationale for constructing a high-resolution RCM of the Arctic atmosphere is that the treatment of orography, land-sea mask and the physical processes are limited in GCMs by both vertical and horizontal model resolution. Use of RCMs with specified "perfect" lateral boundary conditions (from data analysis) eliminates problems originating from lower latitudes in contaminating the results in the Arctic. One of the results of GLIMPSE is the first detailed and coordinated evaluation of three ensembles of Arctic RCMs: 8 atmospheric RCMs have been compared for a 1-year-long (1997/98) simulation over the Western Arctic and 3 atmospheric RCMs have been compared for 10-year-long (1990-99) simulation over the pan-Arctic domain. 3 coupled atmosphere-ice-ocean RCMs have been developed for the pan-Arctic, and intercompared for the same 10-year-long simulation. The results of these evaluations and intercomparisons are described in the contributions of Debernard, Dethloff, Döscher, Dorn, Rinke, Tjernström, Wyser.

Further, deficiencies of GCMs in describing the Arctic climate are at least partly due to inadequate parameterizations of important Arctic physical processes. GLIMPSE investigations have indicated the importance of accurate representation of momentum, heat

and moisture exchange in the planetary boundary layer, surface albedo, and cloud-radiation interaction for Arctic simulations. The surface albedo has been recognized as one of the key parameterization in climate models and the ice-albedo feedback is the most important factor for the polar amplification of global warming, summarized by ACIA (2005). Within GLIMPSE it could be showed that a changed sea ice/snow albedo parameterization impacts the large-scale flow over high and middle latitudes (contributions of Benkel, Dethloff, Sokolova). They are connected with changes in the planetary wave fluxes (accompanied by changes in the storm track activity). This is one example of the direct feedback from Arctic changes on global climate processes (Dethloff et al., 2005a). To understand the global influences and consequences for Arctic climate processes and feedbacks, the understanding of decadal-scale climate variations comes into play. GLIMPSE investigations confirmed the capability of AOGCMs in reproducing regime-like behaviour and in simulating regional climate anomalies like the Late Maunder Minimum (contributions of Handorf, Stendel). Future climate changes projected by AOGCMs (and downscaled by RCMs) have a distinct uncertainty and impacts on the Arctic ecosystem (contributions of Kuhry, Saha, Slagstad).

The GLIMPSE final results (see for an overview the contribution of Dethloff) have been put during the workshop in context of the ongoing international Arctic research and related activities like the upcoming International Polar Year.

In addition to this workshop report, the main workshop results have been published in the weekly newspaper of the geophysical sciences EOS (Dethloff et al., 2005b). The online access is available at http://www.agu.org/pubs/eos.html.

References

ACIA (2005) Impacts of a warming Arctic: Arctic Climate Impact Assessment. Overview Report, Cambridge University Press, Cambridge, United Kingdom, 146 pp.

Curry JA, Lynch AH (2002) Comparing arctic regional climate models. EOS Trans Amer Geophys Union 83:87.

Dethloff K, coauthors (2005a) A dynamical link between the Arctic and the global climate system, GRL, submitted, Geophys. Res. Lett., submitted.

Dethloff K, coauthors (2005b) Global impacts of Arctic climate processes. EOS Trans Amer Geophys Union, accepted

Uttal T, coauthors (2002) Surface energy budget of the Arctic ocean. Bull Am Meteorol Soc 83:255-275.

2 Program of the Workshop

The Arctic climate workshop was held in Potsdam, Germany, on September 5-7, 2005. Participants[2] from Australia (1), Canada (2), Denmark (3), Germany (29), Norway (4), Russia (1), Sweden (6), and the United States (3) attended. The Alfred Wegener Institute, Research Unit Potsdam, Potsdam (Germany) organized the local logistics for the workshop.

During the first day of the workshop, the final GLIMPSE (http://www.awi-potsdam.de/www-pot/atmo/glimpse/) results were presented. Beside the overview of the main results given by the GLIMPSE coordinator K. Dethloff, reports of the six working packages[1] and individual participants were presented.

The second day of the workshop was dedicated to two topics: regional and global modeling with an Arctic emphasize. The morning session aimed on Arctic regional modeling studies which use atmosphere-alone and coupled ocean-sea ice regional models and are connected with the international projects ARCMIP (http://curry.eas.gatech.edu/ARCMIP/) and AOMIP (http://fish.cims.nyu.edu/project_aomip/overview.html). 11 scientific papers were presented. The afternoon session was focused on the global impacts of Arctic processes. 5 scientific contributions using AOGCMs were given. In the evening, 3 activities planned for the upcoming International Polar Year (IPY) were introduced and further steps of the regional climate model intercomparison have been discussed.

The third day of the workshop was used for the presentation of projections of future Arctic climate changes by the new generation global models (IPCC AR4 models; http://www-pcmdi.llnl.gov/ipcc/about_ipcc.php) and its impacts on the ecosystem and the communities. The impact was presented for the two regions of the European North (Nordic Seas and particularly the Barents Sea) and of Alaska. The workshop was closed with a discussion of the observed Arctic climate changes and of the uncertainties of the climate projections by the climate models.

Following the workshop, an excursion to Park Sanssouci and the New Palace in Potsdam (http://www.spsg.de/index.php?id=163) had been offered.

[1] The description of the work packages is given in Appendix 1.
[2] The list of participants is given in Appendix 2.

Monday, Sept. 5	**GLIMPSE Results: Session head: K. Dethloff**
08.00-09.00	Registration Building H on Telegrafenberg
09.00-09.15	**G. Amanatidis, EU, Opening**
09.15-09.45	K. Dethloff "Overview and main results of GLIMPSE"
09.45-10.00	A. Rinke "Intercomparison of Atmospheric RCMs"
10.00-10.15	S. Saha "Modelling of permafrost in a RCM"
10.15-10.30	K. Wyser "Validation of RCMs with respect to clouds"
10.30-11.00	**Coffee break**
11.00-11.15	M. Koltzow "Influence of surface forcing on the Arctic climate in a regional atmospheric model"
11.15-11.30	J. Debernard "ERA40 driven ORCM simulations of today's climate for the Arctic and Nordic regions"
11.30-11.45	J. Debernard "Intercomparison of coupled RCMs"
11.45-12.00	W. Dorn "Sea-ice anomaly simulations in HIRHAM-NAOSIM"
12.00-12.15	R. Döscher, K. Wyser, H. E. Meier, and S. Gollvick "Sensitivity studies with SMHIs coupled ocean-ice-atmosphere model for the Arctic (RCAO)"
12.15-12.30	A. Benkel "A new sea-ice albedo parameterisation in ECHO-G and its global consequences"
12.30-12.45	B. Rockel "The Arctic water cycle in ECHO-G scenarios"
12.45-14.00	**LUNCH**
14.00-14.15	E. Sokolova "AOGCM validation using Eliassen palm fluxes as a diagnostic tool"
14.15-14.30	M. Stendel "Simulation of climate evolution for the period 1500-2000 with all relevant natural and anthropogenic forcings"
14.30-14.45	T. Schmith and M. Stendel "Multidecadal variability: What are the causes?"
14.45-15.00	D. Handorf "Atmospheric Regime behaviour in AOGCMs"
15.00-15.30	**Coffee break**
15.30-15.45	J. H. Christensen " Generating long regional temperature series combining RCM and GCM information"
15.45-16.00	S. Holzkaemper and P. Kuhry "Paleoclimate proxy series from selected arctic regions".
16.00-16.15	S. Saha "Influence of permafrost on climate scenarios"
16.15-16.30	P. Kuhry "Terrestrial ecosystems"
16.30-16.45	D. Slagstad, P. Wassmann "Oceanic ecosystems"
16.45-17.30	General discussion
19.00-22.00	**Ice breaker party on Telegrafenberg**

Tuesday, Sept. 6	RCMs and AOGCMs
09.00-09.30	**ARCMIP & AOMIP Session head: A. Rinke** **H. Morrison ''Interactions between the surface, clouds, aerosols, and radiation in a meso-scale model of the western Arctic" Invited talk**
09.30-09.45	M. Tjernström & S. Söderberg "Modelling the Arctic boundary layer"
09.45-10.00	J. Cassano "Changes in synoptic weather patterns in the Arctic in the 20th and 21 st centuries"
10.00-10.15	S. Söderberg, M. Tjernström & M. Zagar "Modelling the summer Arctic boundary layer"
10.15-10.30	C. Melsheimer & G. Heygster "Retrieval of total water vapour over the Arctic from spacebourne micro-wave radiometer data"
10.30-11.00	**Coffee break**
11.00-11.15	D. Schröder "How does the ocean move beneath sea ice? Problems and implications concerning model studies and observations"
11.15-11.45	**R. Gerdes "Influence of horizontal resolution on Arctic Ocean Model results" Invited talk**
11.45-12.00	W. Maslowski "On recent changes in sea-ice and ocean conditions and their potential feedback to Arctic climate"
12.00-12.15	M. Karcher ""Atlantic Water in the Arctic Ocean: recent results of AOMIP simulations, implications for further studies and their relation to IPY"
12.15-12.30	T. Martin "How to deal with sea ice deformation in the Arctic: Four approaches in a continuum sea ice model"
12.30-12.45	C. Koeberle "Fresh water balance of the Arctic Ocean and adjacent seas "
12.45-13.30	**Lunch**
13.30-14.30	**Walk through the Telegrafenberg D. Fritsche**
14.30-15.00	**AGCM & AOGCM Session head: Jens Hesselbjerg Christensen** **L. Bengtsson "Natural variability of the global climate and Arctic response mechanisms" Invited talk**
15.00-15.30	**G. Stenchikov "Intercomparison of sensitivity of the Arctic Oscillation to volcanic forcing in the IPCC AR4 climate models" Invited talk**
15.30-16.00	**Coffee break**
16.00-16.15	E. Raschke "An assessment of two global radiation budget data sets"
16.15-16.30	M. Sempf "Nonlinear dynamics of atmospheric circulation regimes in an idealised atmospheric model"
16.30-16.45	S. Brand "A coupled climate model with a simplified stratospheric chemistry"

16.45-17.00	R. Treffeisen et al. "Arctic study of tropospheric aerosols, clouds and radiation (ASTAR 2004)"
17.00-17.30	**Coffee break**
17.30-17.45	**IPY 2007-2008** K. Dethloff "The German IPY and ARCMIP within the IPY THORPEX lead project"
17.45-18.00	L. Kaleschke "Frost flowers on sea ice - a multi-disciplinary research effort for the upcoming IPY"
18.00-18.15	C. Jones "Opportunities offered by new satellite missions for research into the Arctic water cycle: A Canadian IPY proposal"
18.30-19.00	**Next steps and connection to IPY** **ARCMIP (A. Rinke), AOMIP (R. Gerdes), CRCMs (W. Dorn), DAMOCLES (R. Döscher)**

Wednesday, Sept. 7	**Impact and endusers: Session head P. Kuhry**
09.00-09.30	**V. Kattsov "Arctic climate projections for the 21 st century with the new generation of AOGCMs" Invited talks**
09.30-10.00	**M. Lange ""Assessing climate change impacts in the European North: The BALANCE project"" Invited talk**
10.00-10.30	**Coffee break**
10.30-11.00	D. Slagstad, I. Ellingsen, M. Reigstad, & P. Wassmann,"Climatic impact on primary production in the Nordic Seas under extreme phases of the NAO" Invited talk
11.00-11.30	**K. Goergen "On the impacts of extreme events on the coastal zone of a small alaskan community: multi-scale modelling approaches" Invited talk**
11.30-12.00	**Discussion**
	"Current biases, uncertainties and future changes of Arctic climate" Session head: K. Dethloff
12.00-12.15	K. Dethloff et al. "Circulation patterns and storm tracks"
12.15-12.30	A. Rinke et al. "Regional Atmospheric changes"
12.30-12.45	P. Kuhry et al. "Permafrost changes"
12.45-13.00	R. Döscher et al. "Sea-ice changes"
13.00-14.00	**Lunch**
14.00-14.15	R. Gerdes et al. "Ocean changes"
14.15-14.30	D. Slagstad et al. "Ecosystem changes"
14.30-15.15	Discussion, Press release for EOS, Extended abstracts in Berichte zur Polarforschung Deadline 31. Oktober 2005
15.15-15.30	Final remarks, G. Amanatidis and K. Dethloff
16.20-18.20	**Visit to New palace and Park Sanssouci**

3. Extended Abstracts

(alphabetical by first author)

A new sea ice albedo parameterisation in ECHO-G and its global consequences

A. Benkel[1] and M. Køltzow[2]

[1] Institute for Coastal Research, GKSS Research Centre, Geesthacht, Germany
[2] Norwegian Meteorological Institute, Oslo

Introduction

Recent observations document a reduction in Arctic sea ice thickness [e.g. *Rothrock et al.,* 1999; *Wadhams and Davis,* 2000; *Perovich et al.,* 2003; *Yu et al.,* 2004] and a decrease in its extent during the last two decades, especially in summer [e.g. *Cavalieri et al.,* 2003; *Serreze et al.,* 2003]. Climate scenario simulations with coupled atmosphere ocean general circulation models (AOGCMs) indicate an even more pronounced reduction in summertime Arctic sea ice thickness during the 21st century [e.g. *Walsh and Timlin,* 2003; *ACIA,* 2004]. An appropriate description of sea ice thickness and coverage in AOGCMs plays a key role in modelling latent and sensible heat fluxes over the Arctic Ocean where a most accurately characterised sea ice albedo is essential for computing the absorbed solar radiation over the ice-covered ocean. Due to positive albedo feedback effects small changes in absorbed solar radiation can excite large changes in sea ice thickness and coverage on a local scale as well as on up to whole Arctic scales.

In this investigation studies with the state-of-the-art AOGCM ECHO-G [*Legutke and Voss,* 1999] are carried out to analyse the impact of improved schemes for cryospheric albedo on the Northern Hemispheric sea ice and also the atmospheric circulation pattern. ECHO-G proved its eligibility in simulating paleoclimate variability in different studies [e.g. *Zorita et al,* 2005; *von Storch et al.,* 2004].

Køltzow et al. [2003] validated existing sea ice albedo schemes currently used in climate models with albedo measurements at the SHEBA site (surface heat budget of the Arctic Ocean). They also suggest a new surface temperature dependent parameterisation that shows less deviation from SHEBA sea ice albedo measurements than several existing schemes, including the ECHAM4 scheme. Their suggested new sea ice albedo scheme is a combination of several albedo values assigned for melting/non-melting conditions for pure sea ice and snow covered sea ice. The albedo values were inferred by *Køltzow et al.* [2003] from literature. *Køltzow et al.* [2003] also included literature estimations for meltpond albedo and they additionally developed an estimation of a temperature depending meltpond fraction on sea ice. Compared to the observed sea ice albedo at the SHEBA location the ECHAM4 scheme absorbs too much solar radiation (3.8 Wm^{-2} too much in average for the period of measurements (March to August)), whereas the new scheme results in the same amount as the measured absorbed solar radiation, accompanied by fewer deviations from the observed values in each month than existing albedo schemes.

Model and set-up of the experiment

ECHO-G consists of the spectral atmospheric GCM ECHAM4 [*Roeckner et al.,* 1996] and the ocean model HOPE-G [*Wolff et al.,* 1997]. In this study ECHAM4 is run in T30 resolution and HOPE-G in T42 resolution. ECHO-G is flux-corrected with a flux adjustment constant in time that is adapted to present day climate conditions. The newly developed parameterisation schemes for sea ice and snow albedo [*Køltzow et al.,* 2003] were implemented into ECHO-G, but are applied to the Northern Hemisphere only. ECHO-G was run for two control simulations with fixed present day forcing conditions for greenhouse gas concentrations and the solar constant. One control integration was performed using the newly developed sea ice and snow albedo parameterisations, and the other control run was done with the original ECHAM4 parameterisations. Each run had been integrated for 510 years. To exclude spin-

down effects according to the implementation of the new scheme only the last 400 years of each run were analysed.

The new sea ice albedo parameterisation according to *Køltzow et al.* [2003] has in the case of bare sea ice conditions a much lower albedo than the original ECHAM4 scheme for all surface temperatures. Also in the case of snow over ice the new scheme generally gives a lower albedo, especially for temperatures above freezing point. Only within a surface temperature range between –9°C and –1°C the new scheme returns a higher albedo for snow over sea ice conditions. In the run with the new parameterisations the original ECHAM4 scheme for snow albedo over un-forested land areas was replaced by the *Roesch et al.* [2000] spectral approach that gives a higher albedo above –10°C and exactly the same albedo below –10°C. The new snow albedo scheme has therefore a higher albedo over at least partly forested areas above –10°C and in all other cases exactly the same albedo as the ECHAM4 scheme.

Results: Changes in snow cover, sea ice extent and thickness and circulation changes

Unless indicated otherwise all differences described within this section are differences of the new albedo run to the old albedo run.

As a direct result of the generally higher snow albedo the snow cover duration over Eurasia and North America is increased in every season with biggest differences in the spring season over the Ural region and in the summer season over northeast Siberia and north Alaska compared to the old albedo scheme run.

The sea ice thickness increased within the central Arctic domain up to 0.8 m in March and 1.8 m in September between Queen-Elizabeth-Islands and the North Pole. In each season in all Northern Hemispheric seas south of the Arctic Circle, in the Baffin Bay and southern Greenland Sea the sea ice thickness was reduced, which can also be detected for all seasons for the sea ice coverage with the exception of an increased sea ice coverage in the Sea of Okhotsk. Whereas in winter and spring a decrease of sea ice coverage in the Labrador Sea and the seas around south and middle Greenland is obvious, an increase in summer and autumn in the Arctic Ocean occurs. Both increase and decrease yield to a minimized annual cycle of Northern Hemispheric sea ice extent and area with lower maximum extent (area) and higher minimum extent (area) (Figure 1).

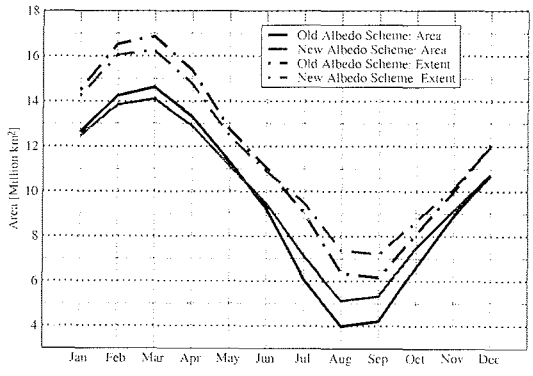

Figure 1: Annual cycle of Northern Hemispheric sea ice area (solid lines) and extent (dashed lines), averaged over 400 years. Grey lines indicate the annual cycle as a result of the new parameterisation.

Largest differences in near surface air temperature (T2m) occur around Greenland (warming, especially in winter and spring) and over the Kara, Laptev and East Siberian Sea in autumn (cooling). In general over all seasons a cooling occurs over the whole Northern Hemisphere with the exception of the Greenland area. The cooling increases from subtropical to polar latitudes (Figure 2). Statistically significant changes in T2m are nearly totally restricted to regions with changes in sea ice coverage or snow cover duration.

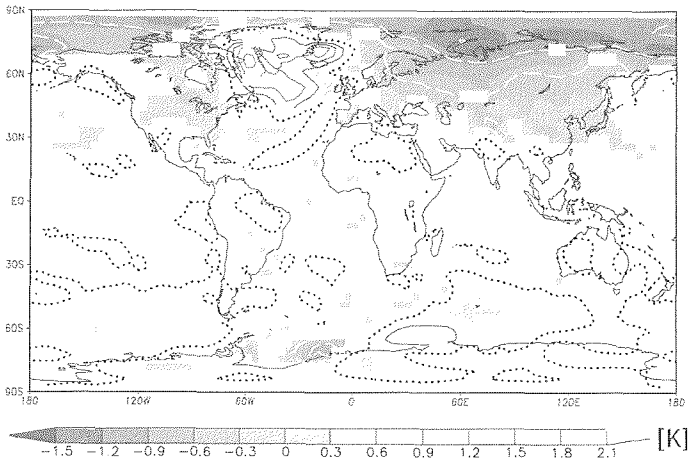

Figure 2: Difference in annual mean near surface temperature (T2m). New albedo parameterisation (snow and sea ice) run minus control run, averaged over 400 years. Shaded areas denote 95 % significance level. Contour lines are in 0.5 K intervals.

Sea level pressure (SLP) increases over snow-covered areas and in those sea ice covered regions with no decrease in sea ice coverage. All regions without cryosphere show a decrease in SLP. A similar pattern of regional changes occurs for the T2m. Statistically significant changes can also be identified in the winter seasonal mean geopotential height (Figure 3), which prove the exertion of circulation changes by surface radiation balances and – due to changes in the sea ice – by latent and sensible heat flux changes in the Arctic seas. The retreat of the Labrador Sea Ice goes along with thermally induced circulation changes: A lowered sea level pressure in the Labrador Sea and a rise of the 500 hPa geopotential height between Greenland and Iceland.

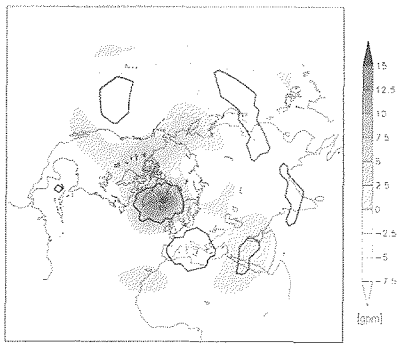

Figure 3: Winter (DJF) geopotential difference (gpm) at 500 hPa. New albedo parameterisation (snow and sea ice) run minus control run, averaged over 400 years. Thick black lines denote the 95 % significance level.

Discussion and Conclusion

Compared to observations of Arctic sea ice extents (*Parkinson and Cavalieri,* 2002) the run with the new albedo scheme shows improvements in simulating the annual cycle of Northern Hemispheric sea ice coverage, reducing the overestimation of the annual cycle from 2.3 x 10^6 km^2 to 0.7 x 10^6 km^2. The improved description of the annual cycle is a result of the much more realistic simulation of the sea ice extent in the sea around Greenland.

Slight changes in cryospheric albedo parameterisation lead to statistically significant near surface air temperatures and circulation changes.

References

ACIA, Impacts of a warming Arctic: Arctic Climate Assessment. Overview Report, *Cambridge University Press, Cambridge,* United Kingdom, 146 pp., 2004.

Cavalieri, D. J., C. L. Parkinson, and K. Y. Vinnikov, 30-Year satellite record reveals contrasting Arctic and Antarctic decadal sea ice variability, *Geophys. Res. Lett., 30(18),* 1970, doi:10.1029/2003GL01803, 2003.

Køltzow, M., S. Eastwood, and J. E. Haugen, Parameterization of snow and sea ice albedo in climate models, *Research Report no. 149, Norwegian Meteorological Institute,* 2003.

Legutke S. and R. Voss, The Hamburg atmosphere-ocean coupled model ECHO-G. *Technical Report No. 18, German Climate Computer Center (DKRZ), Hamburg, Germany,* 1999.

Parkinson C. L. and D. J. Cavalieri, A 21 year record of Arctic sea-ice extents and their regional, seasonal and monthly variability and trends, *Annals of Glaciol., 34, 441-446,* 2002.

Perovic, D. K., T. C. Grenfell, J. A. Richter-Menge, B. Light, W. B. Tucker III, and H. Eicken, Thin and thinner: Sea ice mass balance measurements during SHEBA, *J. Geophys. Res., 108(C3),* 8050, doi:10.1029/2001JC001079, 2003.

Roeckner, E., K. Arpe, L. Bengstson, M. Christoph, M. Claussen, L. Dümelil, M. Esch, M. Giorgetta, M. Schlese, and U. Schulzweida, The atmospheric general circulation model ECHAM4: model description and simulation of present-day climate, *Rep. 218, Max-Planck-Institut für Meteorologie, Bundesstr. 55, Hamburg, Germany,* 1996.

Roesch, C. A., Assessment of land surface schemes in climate models with focus on surface albedo and snow cover, *Zürcher Klimaschriften 78,* ETH Geographisches Institut, Zürich, 2000.

Rothrock, D. A., Y. Yu, and G. A. Maykut, Thinning of the Arctic Sea-Ice Cover, *Geophys. Res. Lett., 26(23),* 3469-3472, 1999.

Serreze, M. C., J. A. Maslanik, T. A. Scambos, F. Fetterer, J. Stroeve, K. Knowles, C. Fowler, S. Drobot, R. G. Barry, and T. M. Haran, A record minimum arctic sea ice extent and area in 2002, *Geophys. Res. Lett., 30(3),* 1110, doi:10.1029/2002/GL016406, 2003.

von Storch, H., E. Zorita, J. M. Jones, Y. Dimitriev, F. González-Rouco, and S. F. B. Tett, Reconstructing Past Climate from Noisy Data, *Science, 306, 679-682,* doi:10.1126/science.1096109, 2004.

Wadhams P. and N. R. Davis, Further evidence of ice thinning in the Arctic Ocean, *Geophys. Res. Lett., 27(24),* 3973-3975, 2000.

Walsh J. E. and M. S. Timlin, Northern Hemisphere sea ice simulations by global climate models, *Polar Research, 22(1),* 75-82, 2003.

Wolff J., E. Maier-Reimer, and S. Legutke, The Hamburg primitive equation model HOPE. *Technical report No. 13, German Climate Computer Center (DKRZ), Hamburg, Germany,* 1997.

Yu. Y., G. A. Maykut, and D. A. Rothrock, Changes in the thickness distribution of Arctic sea ice between 1958-1970 and 1993-1997, *J. Geophys. Res., 109,* C08004, doi:10.1029/2003JC001982, 2004.

Zorita E., J. F. González-Rouco, H. von Storch, J. P. Montávez, and F. Valero, Natural and anthropogenic modes of surface temperature variations in the last thousand years, *Geophys. Res. Lett., 32,* L08707, doi:10.1029/2004GL021563, 2005.

The Arctic Water Cycle in ECHO-G scenarios

A. Benkel, B. Rockel and González-Rouco

Institute for Coastal Research, GKSS Research Centre, Geesthacht, Germany

Introduction

Within a warming climate the hydrological cycle is expected to intensify yielding to more precipitation over the Arctic [*IPCC report* [*(Houghton et al.,* 2001]]. Changes in P-E (precipitation minus evaporation) over the Arctic and changes in river runoff discharge into the Arctic seas change the total freshwater flux into the Arctic Ocean and the northern North Atlantic and therefore affect the thermohaline circulation (THC). In most coupled climate model integrations the THC weakens as carbon dioxide increases [*IPCC report* [*Houghton et al.,* 2001]].

Although under global warming conditions the P-E budget over the Arctic (north of 65°N) increases on a higher rate than the Arctic river runoff, Arctic river runoff still contributes 70 to 80 % of the total freshwater flux (P-E and runoff) into the Arctic [*Wu et al.,* 2005]. Therefore the Arctic river runoff dominates the freshwater input into the polar oceans. Due to the large uncertainties in determining the P-E budget over the polar seas the Arctic river runoff may be a variable suitable for validating the freshwater input into the Arctic seas in model simulations.

Another important role of the Arctic water cycle is played by the cryosphere. Under climate change scenarios the positive feedback effects of snow cover - and even more important - sea ice cover changes are key processes for the polar amplification of a global warming.

Model and set-up of the experiment

ECHO-G [*Legutke and Voss,* 1999] is a coupled global atmosphere ocean general circulation model (AOGCM) and consists of the spectral atmospheric GCM ECHAM4 [*Roeckner et al.,* 1996] and the ocean model HOPE-G [*Wolff et al.,* 1997]. In this study ECHAM4 is run in T30 resolution and HOPE-G in T42 resolution. ECHO-G is flux-corrected with a flux adjustment constant in time that is adapted to present day climate conditions. ECHO-G is forced with many relevant natural and anthropogenic forcing such as variable greenhouse gas concentrations and a variable effective solar constant due to volcanic eruptions according to *Crowley* [2000]. A new albedo parameterisation for northern hemispheric snow and sea ice after *Køltzow et al.* [2003] was implemented into ECHO-G. Three forced integrations with ECHO-G using the new albedo scheme were performed and analysed: a paleoclimate run from 1450 to 1990 and two scenario simulations (IPCC SCRES A2 and B2, respectively). Additionally three forced runs with original ECHAM4 albedo parameterisation (a paleoclimate run (1000-1990), an A2 and a B2 scenario run) [*González-Rouco et al.,* 2003] were analysed.

Results

Although the new albedo parameterisation has an important influence on northern hemispheric sea ice coverage and thickness as well as on snow coverage (resulting in a better description of the annual cycle of sea ice coverage and in a northern hemispheric cooling that is even more pronounced within the Arctic [*Benkel and Køltzow*, 2005]) there is no obvious difference in multi-decadal time scales in the temporal evolution of the Pan-Arctic integrated annual mean P-E budget and of the Arctic long-term annual mean P-E amount itself (Figure 1). Therefore in the case of the P-E budget and derived variables such as runoff the two runs with different parameterisations may be used as members of an ensemble run. The freshwater input into the polar cap seas (sea areas north of 66°N) consists of the Arctic river runoff into the Arctic basin and of the divergence of the atmospheric water content that can be identified

as the P-E budget over the polar cap seas. The temporal evolution of the annual mean P-E budget integrated over the Arctic sea area and the temporal evolution of the annual mean runoff into the Arctic basin follow the temporal evolution of the global annual near surface air temperature (T2m) on multi-decadal to centennial time scales (Figure 1). As global annual T2m decreases from the Medieval Warm Period to the Little Ice Age, the freshwater input into the Arctic Ocean and northern North Atlantic decreases. With increasing carbon dioxide concentrations and global annual mean T2m since the beginning of the 20th century the freshwater input into the Arctic seas increases (Figure 1). The increase of freshwater input into the Arctic seas is even more pronounced under the warmer A2 high carbon dioxide emission scenario (not shown).

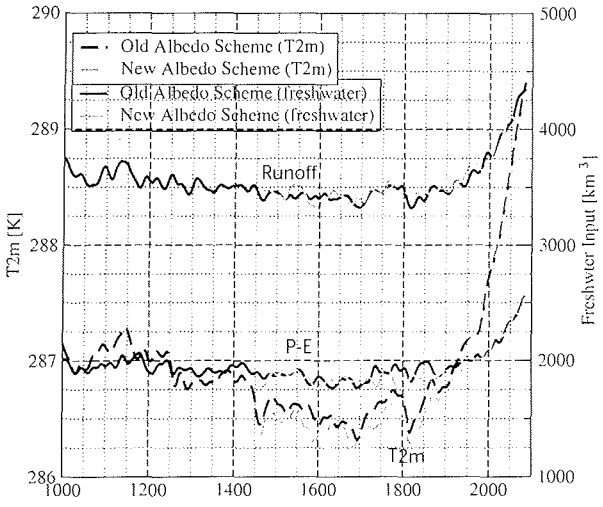

Figure 1: Freshwater input into polar cap oceans (sea areas north of the Arctic circle) and global annual mean T2m. Curves are smoothed with a 30-year low pass filter. Black lines indicate the old albedo scheme; grey lines indicate the new albedo scheme. Dashed lines indicate T2m whereas solid lines indicate the freshwater input (P-E over the polar cap oceans or the river runoff into the Arctic Ocean and the northern North-Atlantic, respectively). Forcing includes variable greenhouse gas concentrations, a variable solar and volcanic forcing (1000 – 1990). Forcing conditions from 1991 to 2100 according to IPCC SRES B2.

Under each global annual mean T2m within these simulations the Arctic River runoff is approximately twice the amount of the atmospheric part of the freshwater input into the Arctic seas. Nevertheless, the proportion of the atmospheric part to the total freshwater flux is slightly increasing as the global annual mean T2m increases (Figure 1). The centennial mean ratio of the P-E budget over the polar cap seas to the total freshwater input into those seas increased from 0.349 in the 17th century to 0.352 in the 20th and 0.363 in the 21st century (0.348 / 0.357 / 0.362 in the old albedo scheme run).

Atmospheric water vapour flux across 65°N (not shown) has no variations in location (longitudes of maximum net transport). It also has only very few changes in the amount on centennial time scales within the paleoclimate run although there are changes in the P-E budget within the Arctic domain and despite changes in global annual T2m. Regions with maximum net atmospheric water vapour flux into the Arctic are Greenland, the Norwegian Sea and Alaska.

Figure 2 shows the decrease of the northern hemispheric sea ice as well as the influence of the new albedo parameterisation on the simulated sea ice coverage. Under IPCC SRES B2 forcing conditions the simulated September northern hemispheric sea ice area will minimize to 2.8 x 10^6 km^2 (1.9 x 10^6 km^2 with the old scheme) until the end of the 21st century.

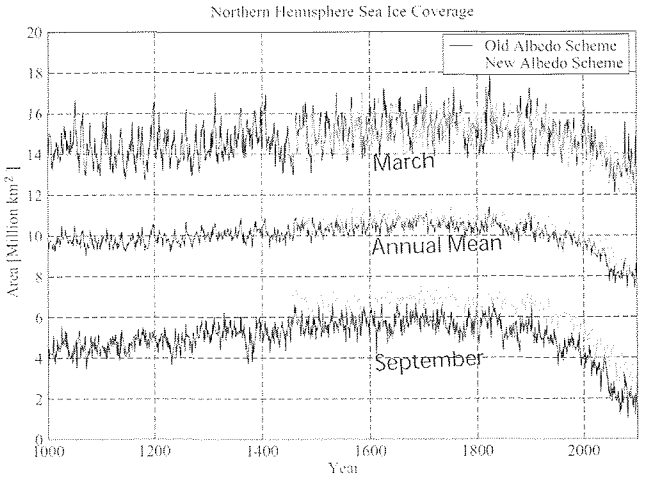

Figure 2: Northern Hemispheric sea ice area evolution for spring, fall and the annual mean. Forcing includes variable greenhouse gas concentrations, a variable solar and volcanic forcing (1000 – 1990). Forcing conditions from 1991 to 2100 according to IPCC SRES B2.

Figure 3 gives an impression of the even more pronounced reduction of the summertime Arctic sea ice area under the IPCC SRES A2 forcing conditions. ECHO-G using the new sea ice albedo scheme simulates only 1.2 x 10^6 km^2 of the northern hemisphere which will be covered with sea ice as a September mean for the last decade of the 21st century.

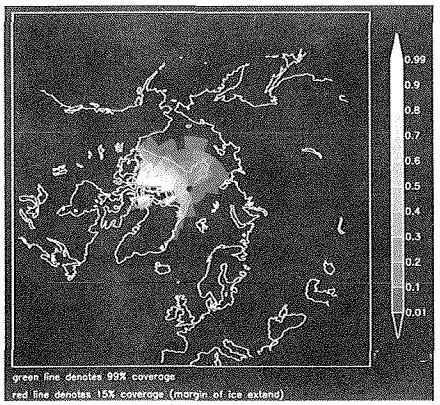

Figure 3: September mean sea ice coverage, averaged from 2091 to 2100, under IPCC SRES A2 forcing conditions.

Discussion and Conclusion

Compared to Global Discharge Data Centre (GRDC) estimated runoff volume into the polar cap seas for 65°N to 90°N (3346 km^3/a) [*Maurer,* 2004] the runoff in ECHO-G is overestimated by approx. 300 km^3/a. The observed increase of Russian river runoff into the Arctic Ocean from 1936 to 1999 (7%) [*Petersen et al.,* 2002] is reproduced well in ECHO-G. The mean of the two ECHO-G simulations (6%) agrees with the findings of *Wu et al.* [2005] who addressed the increase of Arctic river runoff they detected in the AOGCM HadCM3 to be anthropogenic and assumed that the observed increase [*Petersen et al.,* 2002] and the simulated increase are part of a long term increase in Arctic river discharge.

The paleoclimate and scenario runs with ECHO-G underline the assumption a warmer climate leads to a more pronounced freshening of the Arctic Ocean. ECHO-G also prognoses a nearby sea ice free Arctic in September at the end of the 21st century under IPCC SRES A2 conditions.

References

Benkel, A. and Køltzow, M., A new sea ice albedo parameterisation in ECHO-G and its global consequences, Berichte zur Polarforschung, Alfred-Wegener-Institut, Bremerhaven, submitted, 2006.

Crowley, T. J., Causes of climate change over the past 1000 years. Science, 289, 270-277, 2000.

IPCC, 2001: Climate Change 2001: The Scientific Basis. Contribution of Working Group I to the Third Assessment Report of the Intergovernmental Panel on Climate Change [Houghton, J. T., Y. Ding, D. J. Griggs, M. Noguer, P. J. van der Linden, X. Dai, K. Maskell, and C. A. Johnson (eds)]. Cambridge University Press, Cambridge, United Kingdom and New York, NY, USA, 881 pp.

González-Rouco F., H. von Storch, and E. Zorita, Deep soil temperature as proxy for surface air-temperature in a coupled model simulation of the last thousand years, Geophys. Res. Lett., 30, doi:10.1029/2003GL018264, 2003.

Køltzow, M., S. Eastwood, and J. E. Haugen, Parameterization of snow and sea ice albedo in climate models, Research Report no. 149, Norwegian Meteorological Institute, 2003.

Legutke S. and R. Voss, The Hamburg atmosphere-ocean coupled model ECHO-G. Technical Report No. 18, German Climate Computer Center (DKRZ), Hamburg, Germany, 1999.

Maurer, T., Discharge to the Arctic Ocean. GRDC contribution to: The Observed Arctic Hydrological Cycle, chapter edited by B. Rudolf, ACSYS Book (in prep.), 2004. http://grdc.bafg.de/

Peterson, B. J., R. M. Holmes, J. W. McClelland, C. J. Vörösmarty, R. B. Lammers, A. I. Shiklomanov, I. A. Shiklomanov, and S. Rahmstorf, Increasing River Discharge to the Arctic Ocean, Science, 298, 2133-2137, 2002.

Roeckner, E., K. Arpe, L. Bengstson, M. Christoph, M. Claussen, L. Dümelil, M. Esch, M. Giorgetta, M. Schlese, and U. Schulzweida, The atmospheric general circulation model ECHAM4: model description and simulation of present-day climate, Rep. 218, Max-Planck-Institut für Meteorologie, Bundesstr. 55, Hamburg, Germany, 1996.

Wu, P., R. Wood, and P. Stott, Human influence on increasing Arctic river discharges, Geophys. Res. Lett., 32, doi:10.1029/2004GL021570, 2005.

Wolff J., E. Maier-Reimer, and S. Legutke, The Hamburg primitive equation model HOPE. Technical report No. 13, German Climate Computer Center (DKRZ), Hamburg, Germany, 1997.

Changes in synoptic weather patterns in the Arctic during the 21st century

John J. Cassano[1], Petteri Uotila[2], and Amanda H. Lynch[2]

[1] Cooperative Institute for Research in Environmental Sciences and Program in Atmospheric and Oceanic Sciences, University of Colorado, USA

[2] School of Geography and Environmental Science, Monash University, Australia

1. Introduction

The field of synoptic climatology provides a powerful method to study the climate of a region by stratifying large volumes of data (daily or higher temporal resolution fields of the atmospheric state) into a small number of categories on a physically meaningful basis. An important step in this type of analysis is developing a robust classification scheme that can be applied to large volumes of data. For our analysis, we use the method of self-organizing maps (SOMs) (Kohonen, 2001) to derive a synoptic climatology for the Arctic from an ensemble of current and 21st century climate simulations conducted in support of the Intergovernmental Panel on Climate Change (IPCC) 4th Assessment Report (AR4). This synoptic climatology is then used as a framework to analyze trends in temperature over the same time periods.

2. Methods

2.1 Data

The synoptic climatology and analysis in this paper is based primarily on coupled atmosphere-ocean general circulation model forecasts. Daily fields of sea-level pressure (SLP) and surface temperature for the December-January-February (DJF) season for the time periods 1991-2000, 2046-2055, and 2091-2100 are interpolated to an EASE grid of 42x42 points, centered on the pole, with 200 km grid spacing. The model output for the 1991-2000 period are taken from climate of the 20th century model experiments (20C3M) while the 21st century data are taken from 720 ppm CO_2 stabilization experiments (SRES A1B). Global atmospheric reanalysis data from the European Centre for Medium-Range Weather Forecasts 40-year reanalysis (ERA-40) for the time period 1991-2000 are used to evaluate the ability of the GCMs to simulate the correct distribution of synoptic circulation patterns during the 20th century.

2.2 Description of the Self-organizing map algorithm

The Self-Organizing Map (SOM) algorithm is a neural network algorithm that uses an unsupervised learning process to find patterns in data. Formally, the SOM may be described as a non-linear mapping of high-dimensional input data onto the elements of a regular low dimensional array (Kohonen, 2001). The use of self organizing neural networks to analyze and organize atmospheric circulation data represents a new way to create synoptic climatologies (Hewitson and Crane, 2002).

Application of the SOM algorithm to a high-dimensional input data set results in the creation of a low-dimensional array, called a map. This map is a 2-dimensional array of reference vectors that are representative of the probability density function of the input data. For the analysis presented here the input data to the SOM algorithm is daily gridded SLP data from ten IPCC model simulations and the resulting reference vectors (also called nodes) depict the synoptic circulation patterns that span the input data space. The synoptic pattern classification derived from this data using the SOM algorithm is shown in Figure 1, and is referred to as the master SOM.

3. Results

3.1 20th Century Circulation: Models and Reanalysis

Once the master SOM has been defined, data from individual models, the entire ten model ensemble, atmospheric reanalyses, or for different time periods can be mapped to the SOM, allowing the residence frequency of each synoptic pattern, represented by the individual nodes in Figure 1, to be determined for a particular dataset.

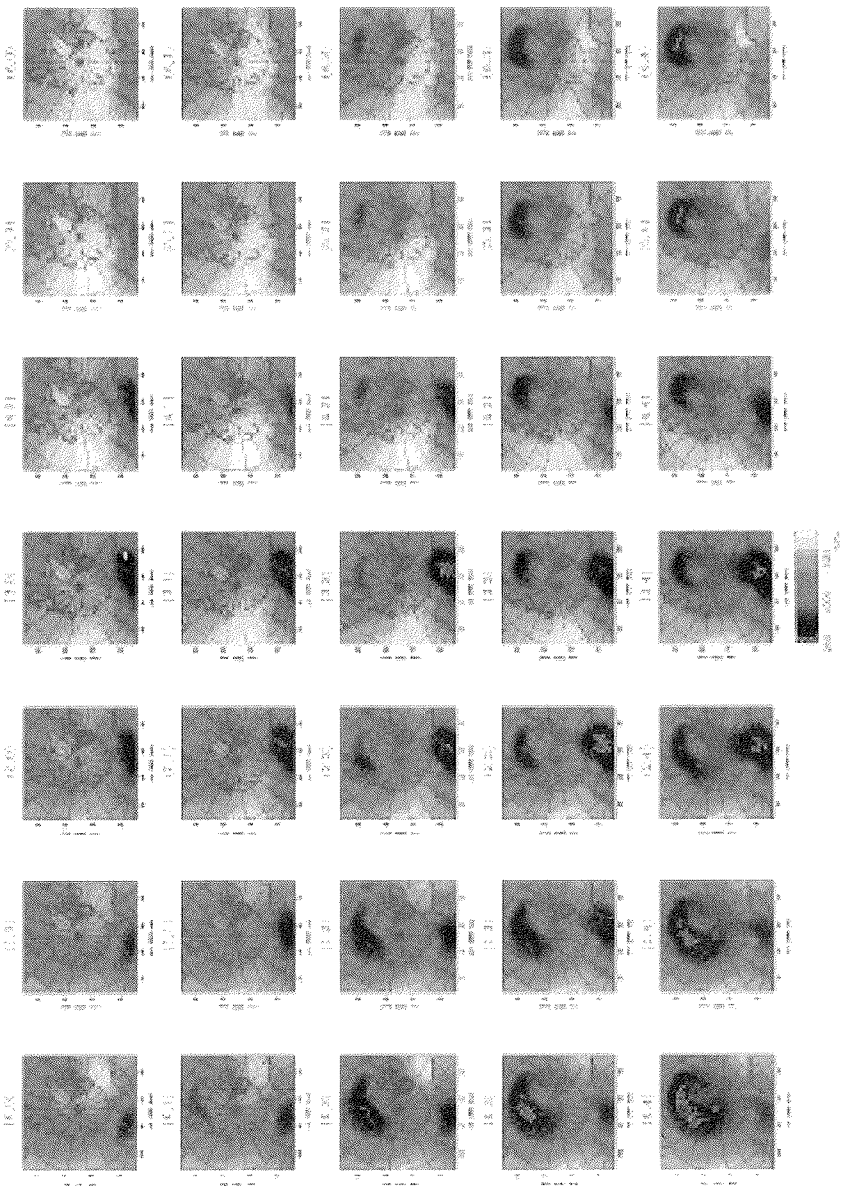

Figure 1. Master SOM for DJF, with sea-level pressure values shown by shading.

Figure 2a displays the residence frequency of each node for the ten model ensemble for the DJF 1991-2000 time period. This figure indicates that nodes near the top right corner of the map, associated with strong high pressure over Asia and/or the Arctic Ocean, and the top left corner of the map, associated with a moderate Aleutian Low and high pressure over western Canada and Alaska, occur most frequently.

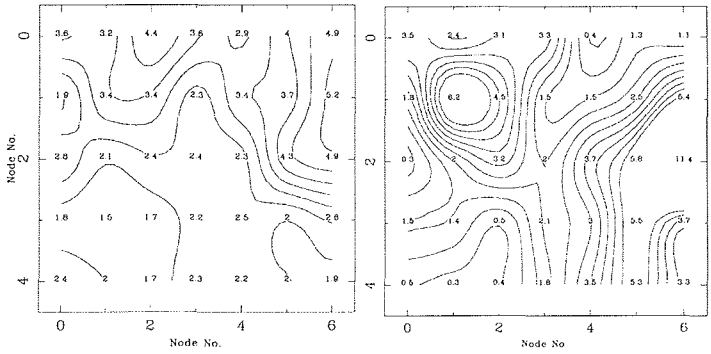

Figure 2. Node residence proportions for DJF during the period 1991-2000 for (a; left) the ten model ensemble and (b; right) the ERA40 reanalysis data.

These results can be compared to residence frequencies calculated with the ERA-40 reanalysis data for the same time period (Figure 2b). The reanalysis data have high residence frequencies (generally greater than 3%) for nodes on the right side of the map (somewhat weaker and spatially confined Icelandic low patterns) and upper left corner of the map (moderate to strong Aleutian low patterns with limited areas of high pressure over the Arctic land areas), and low residence frequencies for nodes with very strong high pressure dominating the Arctic (upper right corner) and nodes with an extended North Atlantic storm track and/or strong Aleutian low (lower right corner). The residence frequencies of the model ensemble differs from the ERA-40 data in the that the models predict a greater occurrence of strong, sometimes excessively strong, Arctic high pressure patterns (upper right) at the expense of Icelandic low patterns (middle right).

3.2 21st Century Trends

Figure 3 displays the relative change in node residence frequency between the 1991-2000 and 2046-2055 time periods. The relative change is calculated as the difference in the node residence frequency between the two time periods divided by the averaged node residence frequency for the two time periods. The largest increases, in excess of 30%, are found in the lower left portion of the map (extended North Atlantic storm track patterns) and the largest decreases, in excess of –30%, are found in the upper right corner of the map (strong Arctic high pressure patterns). During the second half of the 21st century (not shown) the trend of decreasing occurrence of strong Arctic high patterns continues, although with smaller magnitude. Moderate increases in the node residence frequency is found from the lower right to upper left corner of the map (Icelandic and Aleutian low patterns) with some decreases in the extended North Atlantic storm track pattern that increased in the first half of the century. Overall, during the 21st century the ensemble of simulations indicate a large relative decrease in the occurrence of strong Arctic high pressure patterns with large increases in strong Icelandic low patterns (both spatially confined and with an extended storm track into the eastern Arctic basin).

Temperature anomalies for each node are calculated as the node averaged temperature minus the whole dataset averaged temperature (not shown). The largest cold anomalies, in excess of -5 K, are found over Eurasia, the Arctic basin, and northwestern North America and are

associated with strong Arctic high pressure patterns. As seen in Figure 3 it is these patterns that are forecast to occur less frequently during the 21st century. The largest warm anomalies, in excess of 5 K, are most pronounced over Eurasia with some warming in northwestern North America as well, and are associated with nodes in the lower left corner of the map, that are predicted to occur more frequently during the 21st century. The warm patterns are driven by the extended North Atlantic storm track, which acts to transport warm air into Eurasia, and a strong Aleutian low which advects warm air into northwestern North America.

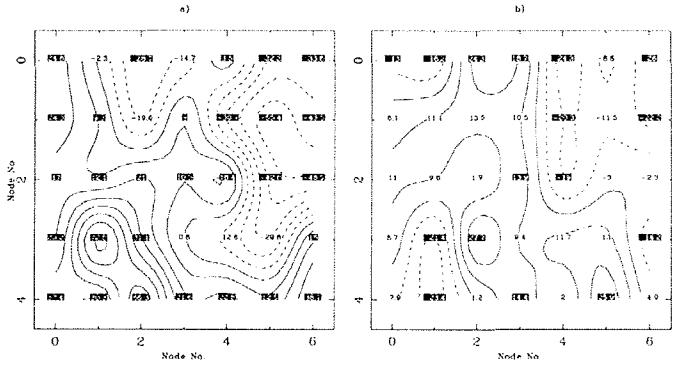

Figure 3. Percentage difference in node residence proportions for DJF for the time periods (a) 2046-2055 vs 1991-2000 and (b) 2091-2100 vs 2046-2055. Statistically significant trends at the 95% confidence level are highlighted in black.

4. Future Work

Cassano et al. [2005] present additional results from this analysis, while a similar analysis for the Antarctic can be found in Lynch et al. [2005]. Future work will expand upon this analysis, with an emphasis on the impacts of changing atmospheric circulation patterns on other components of the Arctic climate system. Two key areas of interest are changes in the freshwater cycle of the Arctic and changes in the atmospheric forcing of the Greenland ice sheet mass balance. Sea ice transport within and export from the Arctic basin is another area for future analysis.

References

Cassano, JC, Uotila, P, Lynch, A. 2005. Changes in synoptic weather patterns in the polar regions in the 20th and 21st centuries, Part 1: Arctic. *International Journal of Climatology*. Accepted pending revisions.

Hewitson BC, Crane RG. 2002. Self-organising maps: applications to synoptic climatology. *Climate Research* 22: 13-26.

Kohonen T. 2001. *Self-Organizing Maps,* Springer, 501pp.

Lynch, A, Uotila, P, Cassano, JC. 2005. Changes in synoptic weather patterns in the polar regions in the 20th and 21st centuries, Part 2: Antarctic. *International Journal of Climatology*. Accepted pending revisions.

Acknowledgements

We acknowledge the international modeling groups for providing their data for analysis, the Program for Climate Model Diagnosis and Intercomparison (PCMDI) for collecting and archiving the model data, the JSC/CLIVAR Working Group on Coupled Modeling (WGCM) and their Coupled Model Intercomparison Project (CMIP) and Climate Simulation Panel for organizing the model data analysis activity, and the IPCC WG1 TSU for technical support. The IPCC Data Archive at Lawrence Livermore National Laboratory is supported by the Office of Science, U.S. Department of Energy. This research uses data provided by the Community Climate System Model project (www.ccsm.ucar.edu), supported by the Directorate for Geosciences of the National Science Foundation and the Office of Biological and Environmental Research of the U.S. Department of Energy. This analysis was supported by research grants ARC FF0348550, NSF OPP-0100120 and NSF OPP-0229649.

ERA40 driven ORCM simulations of today's climate for the Arctic and Nordic regions

Jens Debernard

Norwegian Meteorological Institute, Oslo

Introduction

The Oslo Regional Climate Model (ORCM) is a fully coupled regional atmosphere – sea ice – ocean model developed at the Norwegian Meteorological Institute (met.no). It was developed for coupled dynamical downscale studies for the present and future climate, and has mainly been constructed with the Arctic Ocean, northern North Atlantic and Europe as target areas.

The motivation for building a coupled regional climate model is that global coupled models will for a long time have too coarse resolution to give an adequate description of a climate at regional scales. Also, global climate models have generally considerable difficulties in reproducing the observed Arctic climate [*Walsh et al.* 2002, *Covey et al.* 2003]. This might be both due to insufficient resolution, but also due to poor parameterization and representation of physical processes. Coupled regional climate models can generally afford to use higher resolution than global models and thereby improve the first of these points. Second, simulations with these models forced with reanalyzed data are generally more constrained, and thereby closer to the synoptic situation than global models, which make them easier to use in dedicated process studies. This last point is important because then it should be easier to test parameterizations in a well working fully coupled regional model, and compare with observations, than in a fully coupled global model. The fully coupled approach is important for many of the Arctic processes that involve strong feedback from the sea ice. This approach can improve and add value to the regional downscaling of global climate scenarios by reducing the uncertainties due to unrealistic lack of feedback processes in stand-alone atmospheric RCMs. Also, due to the rather poor sea ice and SST distributions in many global coupled models, a large regional coupled model domain can in some aspects change, and improve the Arctic circulation over that in the global model. This will improve the creditability of dynamical downscale experiments in areas near the Arctic by reducing the uncertainty due to unrealistic forcing fields.

Description of ORCM

ORCM version 1 [*Debernard and Køltzow*, 2005] consists of the atmosphere model HIRHAM, the sea ice model MI-IM and the ocean model MICOM, coupled interactively together. HIRHAM is described in *Christensen et al.* [1996]. The dynamics of the model is taken from the limited area weather forecast model HIRLAM (version 2), and the physical parameterization is from the ECHAM4 model with some minor changes. The model uses 19 vertical sigma-p layers in the vertical. These are terrain following near the surface and equals pressure-surfaces in the free atmosphere.

The ice model MI-IM is described in detail by *Røed and Debernard* [2004]. It has intermediate complexity thermodynamics with one ice layer that includes fully prognostic internal energy, ice concentration and ice mass, while the heat capacity of the snow layer is neglected. The snow is insulating, reflective and has a latent heat contribution to the total heat budget of the model. The momentum equations in MI-IM are discretized with the elastic viscous plastic rheology of *Hunke and Dukowicz* [1997].

The ocean component of ORCM is a local *met.no* version of MICOM (Miami Isopycnic Coordinate Ocean Model), which is a three-dimensional, barotropic-baroclinic, general ocean circulation model, utilizing potential density as its vertical coordinate [*Bleck et al.* 1992, see also references therein]. Thus the vertical coordinate is Lagrangian in this model. The particular version used here is based on an earlier version described in *Shi et al.* [2001], with the additions of added rivers [*Debernard and Røed,* 2002], and new nesting conditions at

open boundaries [*Røed and Debernard,* 2005]. The configuration of the 27 density layers is similar to that used by *Røed and Debernard* [2004] and *Debernard and Røed* [2005], and intents to span the range of water masses from the brackish Baltic to heavy bottom water.

HIRHAM uses a rotated spherical grid of 0.5x0.5 degree resolution covering the Arctic Ocean, most of Europe and the Atlantic Ocean north of approximately 55 degrees north (Figure 1.) MI-IM and MICOM uses a grid with the same orientation as the atmospheric grid, but with a resolution of 0.25x0.25 degree.

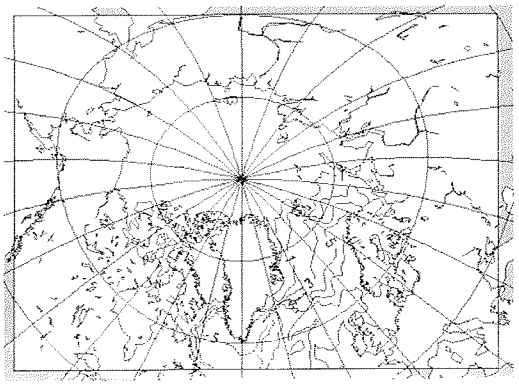

Figure 1. ORCM computational domain, with sea ice concentration from the ice model (light grey shading) and SST from the ocean model (black lines), the fields are average January conditions for the years 1995-1999 from EXP26. The darker shading over land denotes undefined points in the ice-ocean component, where the atmosphere models uses ERA40 data as the lower boundary condition.

Setup of ERA40 driven experiments

As an initial test of the capabilities of the coupled system several experiments with the ORCM has been run for the ten year period 1990-1999. Boundary data for the atmospheric model is taken from the ERA-40 reanalysis from the European Centre for Medium range Weather Forecasts (ECMWF). These data are applied directly at the open boundaries of HIRHAM (Figure 1), nested through a relaxation zone. As initial field, the ERA-40 analysis is used to give a cold start of the atmosphere model 1.1.1990. Thus there is no additional spin up of HIRHAM before the coupling to the ice and ocean models. Due to the lack of consistent, reanalysed ocean fields that are applicable as initial, as well as open boundary conditions for the ice-ocean component, a two-step approach is used to give MICOM-consistent boundary fields for ORCM.

First, the stand-alone ice-ocean component is run at an Atlantic domain, covering the Arctic Ocean and the Atlantic south to approximately 30 degrees S. Then, fields from this run are used at the open boundaries of the ORCM domain. In the inner domain, the ocean model uses a new FRS implementation tailored for MICOM [*Røed and Debernard*, 2005]. To give initial fields for the ORCM simulation at the inner domain (Figure 1), the stand-alone ice-ocean model is run at least one year before the fully coupled model is started in 1990, also utilizing boundary data from the Atlantic model. In all stand-alone ice-ocean simulations the atmospheric surface forcing is deduced from the ERA40 reanalysis. Initial hydrographic fields for the stand-alone simulations are taken from the Polar Science Center Hydrographic Climatology (PHC) [*Steel et al.* 2001], version 3.0. At the southern boundary of the Atlantic domain, MICOM used an buffer zone with relaxation of hydrography towards the climatology of from the World Ocean Atlas 2001 (WOA01) [*Stephens et al.,* 2002, *Boyer et al.,* 2002].

Discussion of preliminary results

Figure 2 shows ice area and ice volume, respectively. The solid and dashed lines represent results from two experiments that differ only in the initial condition used for the ice and ocean components. In the first experiment (EXP26, solid line), the system is started as described in the previous section, with one year spin-up of the ice and ocean components. The simulation is then run for 10 years. Restart files at the end of this first experiment are then taken as initial fields for the ocean and ice models in the second experiment (EXP27, dashed line), while the atmosphere model uses the same initial field as in the first experiment (ERA40 1.1.1990 analysis). In this way, we get two different realizations of the decade that only differ in the initial ice and ocean state. The open boundary forcing in the simulations are the same for all models.

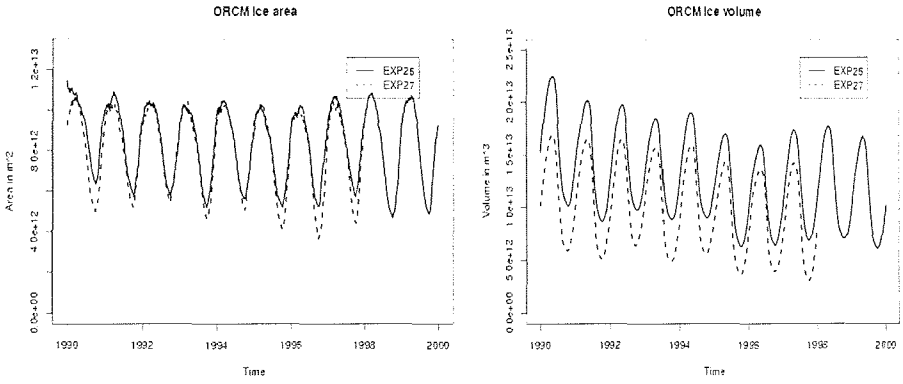

Figure 2. Time series of total ice area and of ice volume from two different simulations that only differ in the initial condition for the ice-ocean component of ORCM. The solid line is from the first experiment, and the dashed from the second.

In these preliminary experiments, it is evident that the ice volume and area in the Arctic Ocean is decreasing through the simulation, giving too little and too thin ice at the end of the last experiment. The reason for the small ice area is partly due to too little ice in the Labrador Sea due to a too strong sub-polar gyre in the ocean model, and partly due to too little ice in the Greenland Sea and Barents Sea (Figure 1). In the Greenland Sea, this may partly be an effect of a too strong recirculation of Atlantic water masses in the Fram Strait. Too little of this water continue into the Arctic Ocean as a subsurface current. In addition, there is a rather strong decrease in ice volume during the experiments, and the volume is decreasing faster than the area, which implies a reduction in the sea ice thickness. Although this is a situation that probably has occurred in the Arctic during the 1990's, the decrease seems to be overestimated in the present version of the model. One reason for this may be that the ice model is producing thin ice to fast. It is then closing the ice cover during winter, preventing new freezing of ice. In this way, the total ice volume is decreasing in the model. From the experiments, it seems to be more a problem of too small ice growth during winter, than to much ice melt during summer in these two experiments. At the end of the second experiment, the reduction in ice thickness is so large that it strongly influences the summer ice area. The mechanism involved is the strong positive ice albedo feedback in a coupled system. Too little ice gives too much absorption of solar heat in the ocean mixed layer, which then gives too strong ice melt. This situation clearly demonstrates the vulnerability of the summer sea ice to a warmer climate.

One interesting observation from Figure 2 is that the inter-annual variation in ice volume is quite similar in the two experiments. Clearly, the average drift is larger in the first experiment (solid line), but both realizations show a clear reduction in ice volume during 1995, with a small increase again in the later years of the decade. Because the ocean and ice state in these two experiments are rather different, this reduction must be caused by the coupled system response to the time varying open boundary conditions that are equal in both experiments. Although the atmosphere model uses the same initial condition in both experiments, but this has no influence on the situation after 5 years. It is not analysed if this sudden decrease in volume in the middle of the decade is due to pure atmospheric forcing, or if it is a remote effect of an atmospheric driven change in ocean conditions. If the latter is the case, this has to be a rather fast response in the system.

Concluding remarks

The ORCM has been successfully set up and preliminary test experiments for the 1990 decade show in general reasonable agreement with observations. However, there are some problems with the ocean circulation that needs to be considered. Also, the model shows a too strong reduction of the Arctic ice cover. This can partly be corrected with a more realistic increase in ice area when new and thin ice forms in the model. Although these first experiments are enlightening for the coupled system behaviour, it is found a little difficult to asses the results from the model during such a short period as 10-years, and especially during the 1990's, where there have been considerable changes in the Arctic climate. To meet these challenges, new and longer simulations are planned that cover more of the Arctic climate variability experienced during the last century.

Acknowledgement

Morten Ødegaard Køltzow, Lars Petter Røed and Jan Erik Haugen are all important members of the ORCM-group at met.no. The contributions from each of them are all instrumental for the development of the system. This work is supported by the Research Council of Norway under the project RegClim (grant no. 155976/720) and by the EU-project GLIMPSE (EVK2-2001-00337).

References

Bleck, R., C. Rooth, D. Hu, and L. T. Smith (1992) Salinity-driven thermohaline transients in a wind and thermohaline-forced isopycnic coordinate model of the North Atlantic, J. Phys. Oceanogr., 22, 1486–1515.

Boyer, T. P., Stephens, C., J. I. Antonov, M. E. Conkright, R. A. Locarnini, T. D. O'Brien, H. E. Garcia, 2002: *World Ocean Atlas 2001, Volume 2: Salinity*. S. Levitus, Ed., NOAA Atlas NESDIS 50, U.S. Government Printing Office, Wash., D.C., 165 pp., CD-ROMs.

Christensen, J. H., O. B. Christensen, P. Lopez, E. van Meijgaard and M. Botzet (1996): The HIRHAM4, Regional Atmospheric Climate Model, Danish Meteorological Institute – Scientific Report – Copenhagen.

Covey, C., K.M. Achuta Rao, U. Cubasch, P. Jones, S.J. Lambert, M.E. Mann, T.J. Phillips, and K.E. Taylor (2003): An overview of results from the Coupled Model Intercomparison Project, *Global and Planetary Change*, 37, 103-133.

Debernard, J., and M. Ø. Køltzow, 2005: Technical documentation of Oslo Regional Climate Model, Version 1.0, *In: RegClim Tech. Rep. No. 8*, Eds. T. Iversen and M. Lystad, 51-68. [Available from the Norwegian Meteorological Institute, P.O. Box 43 Blindern, 0313 Oslo, Norway]

Debernard, J., and L. P. Røed, 2002: Implementations of rivers in met.no's MICOM version. *In: RegClim Tech. Rep. No. 6*, Eds. T. Iversen and M. Lystad, 115-118. [Available from the Norwegian Meteorological Institute, P.O. Box 43 Blindern, 0313 Oslo, Norway]

Debernard J and L P Røed, 2005: Simulations with a North Atlantic coupled ice-ocean model. *In: RegClim Tech. Rep. No. 8*, Eds. T. Iversen and M. Lystad, 69-81. [Available from the Norwegian Meteorological Institute, P.O. Box 43 Blindern, 0313 Oslo, Norway]

Hunke, E., and J. Dukowicz, 1997: An elastic-viscous-plastic model for sea ice dynamics, J. Phys. Oceanogr., 27, 1849–1867.

Røed, L. P. and J. Debernard, 2004: Description of an integrated flux and sea-ice model suitable for coupling to an ocean and atmosphere model. *met.no Report No. 4*. ISSN 1503-8025.

Røed, L. P., and J. Debernard, 2005: Documentation of the method for nesting of MICOM variables into met.no's MICOM version (in preparation).

Shi, X.B, L.P. Røed, and B. Hackett, 2001: Variability of the Denmark Strait overflow: A numerical study, *J. Geophys. Res,* 106(C10), 22,277-22,294.

Steele, M., R. Morley, and W. Ermold, 2001: PHC: A Global Ocean Hydrography with a High-Quality Arctic Ocean, *J. Climate,* 14, 2079-2087.

Stephens, C., J. I. Antonov, T. P. Boyer, M. E. Conkright, R. A. Locarnini, T. D. O'Brien, and H. E.Garcia, 2002: *World Ocean Atlas 2001, Volume 1: Temperature.* S. Levitus, Ed., NOAA Atlas NESDIS 49, U.S. Government Printing Office, Wash., D.C., 167 pp., CD-ROMs.

Walsh, J.E., V.M. Kattsov, W.L., Chapman, V. Govokova, and T. Pavlova, 2002: Comparison of Arctic Climate Simulations by Uncoupled and Coupled Global Models, *J. Climate*, 15, 1429-1446.

Intercomparison of the GLIMPSE coupled RCMs

Jens Debernard

Norwegian Meteorological Institute, Oslo

Introduction

During the EU-project GLIMPSE, three different regional coupled climate models (coupled RCMs) have been developed and improved. The main motivation for introducing coupled RCMs is that global coupled models for a long time will have too coarse resolution to give an adequate description of a climate at regional scales. Also, global climate models have generally considerable difficulties in reproducing the observed Arctic climate [*Walsh et al.* 2002, *Covey et al.* 2003]. This might be both due to insufficient resolution, but also due to poor parameterization and representation of physical processes. Coupled regional climate models can generally afford to use higher resolution than global models and then improve the first of these points. Second, simulations with these models forced with reanalyzed data are generally more constrained, and thereby closer to the synoptic situation than global models, which make them easier to use in dedicated process studies. This last point might be important. It should be easier to test parameterizations in a well working fully coupled regional model, and compare with observations, than in a fully coupled global model.

Traditionally, dynamical downscale experiments have been done with stand-alone, regional atmosphere only models. However, due to the poor quality of the sea surface temperature and sea ice distribution in many global climate models that are used as boundary forcing for the coupled regional models, the uncertainty in the downscaled climate might be substantial. With better resolution, and in some senses better process-handling in coupled regional models, we might hope that we can improve some aspect of the local regional climate in a coupled regional model compared to stand-alone regional models and fully global coupled models. The fully coupled approach is especially important for many of the Arctic processes that involve strong feedback from the sea ice.

Model description

The three coupled regional models used in GLIMPSE are: HIRHAM-NAOSIM from Alfred Wegner Institute (AWI) [*Rinke et al.* 2003, *Dorn et al.* 2005], Rossby Centre Atmosphere Ocean model (RCAO) from the Rossby Centre [*Döscher et al.* 2002], and Oslo Regional Coupled Model (ORCM) from the Norwegian Meteorological Institute [*Debernard and Køltzow,* 2005].

All the coupled models use atmospheric components that are derived from the limited area weather forecast model HIRLAM [*Källén*, 1996]. HIRHAM-NAOSIM and ORCM use the model HIRHAM [*Christensen et al.* 1996] with dynamics from the HIRLAM model and physical parameterizations from the ECHAM4 model, while RCAO uses the Rossby Centre regional Atmospheric Model (RCA), which is another climate extension of the HIRLAM code [*Rummukainen et al*, 2001]. All models utilize rotated spherical grids with 0.5x0.5 degree resolution that cover the whole Arctic Ocean. However, there are individual differences of the size of the computational domains.

The model diversity is somewhat larger between the ice and ocean components of models. NAOSIM [*Karcher et al.*, 2003; *Kauker et al..*, 2003]) is a z-level ocean model based on MOM2 [*Pacanowski,* 1995], coupled to a dynamic-thermodynamic sea ice model [*Lemke et al.*, 1997]. RCAO uses the ocean model RCO [*Meier et al.* 2003], which is a z-level model based on the OCCAM model [*Webb et al.*, 1997; 1998], and ORCM uses an local version of the Miami Isopycnic Ocean Model (MICOM) [*Bleck et al.* 1992; *Debernard and Røed*, 2002; *Røed and Debernard*, 2005]. Thus, this latter model uses a Lagrangian vertical coordinate that makes it rather different from the other z-level models. The ice models are all quite similar,

but different. All models use the EVP rheology according to *Hunke and Dukowicz* [1997], and somewhat different versions of the 2-categorie (thick ice and thin ice / open water) thermodynamical formulation [*Lemke et al.* 1997; *Hibler* 1979; *Røed and Debernard* 2004]. All ice-ocean components covers the whole Arctic Ocean and the North Atlantic south to approximately 50 degrees north, utilizing 0.25x0.25 degrees (HIRHAM-NAOSIM and ORCM), or 0.5x0.5 degrees resolution in a rotated spherical grid.

Experiments and preliminary remarks

The GLIMPSE coupled RCMs have all simulated the whole or parts of the Arctic Climate during the 1990's with reanalysed ERA40 data as lateral boundary forcing in the atmospheric components. Some preliminary results from an intercomparison of these simulations show that all the models are working technically and that they give reasonable results. However, all systems have some deficiencies that should be improved in future versions. Of more general observations are:

All models show a warm winter-time bias in 2-meter temperature compared with ERA40. This might be due to too thin or too open Arctic ice during the winter.

The HIRHAM-NAOSIM system has a smaller atmospheric domain than RCAO and ORCM. This gives more external (ERA40) control of the circulation patterns and thereby a closer agreement with the ERA40 data in the interior of the Arctic. In some senses, local biases that are identified in this small domain are enhanced in the larger domains of the two other systems. This clearly demonstrates one choice that should be made in setting up the system. If the goal is to do a detailed downscaling of the global data (here ERA40), by adding value to the data by the coupled approach and by having better resolution, but still keep a large scale circulation that are as close as possible to the global data, then a small and constrained domain is feasible. However, if the goal is to correct parts of the large scale simulation due to deficiencies in the global models, the domain should be large enough so that the circulation within the regional model is allowed to deviate partly from the results from the global model.

A deeper and more detailed intercomparison and analysis of the equalities and differences between the simulations from the coupled RCMs are on the schedule for the near future.

Acknowledgement

The intercomparison of these models is dependent on people in the different model development groups, and could not be done without help from Wolfgang Dorn in the HIRHAM-NAOSIM-group, Ralf Döscher from the RCAO-group and Morten Ø. Køltzow from the ORCM-group. The intercomparison is supported by the EU-project GLIMPSE (EVK2-2001-00337).

References

Bleck, R., C. Rooth, D. Hu, and L. T. Smith (1992) Salinity-driven thermohaline transients in a wind and thermohaline-forced isopycnic coordinate model of the North Atlantic, J. Phys. Oceanogr., 22, 1486–1515.

Christensen, J. H., O. B. Christensen, P. Lopez, E. van Meijgaard and M. Botzet (1996): The HIRHAM4, Regional Atmospheric Climate Model, Danish Meteorological Institute – Scientific Report – Copenhagen.

Covey, C., K.M. Achuta Rao, U. Cubasch, P. Jones, S.J. Lambert, M.E. Mann, T.J. Phillips, and K.E. Taylor (2003): An overview of results from the Coupled Model Intercomparison Project, *Global and Planetary Change*, 37, 103-133.

Debernard, J., and M. Ø. Køltzow, 2005: Technical documentation of Oslo Regional Climate Model, Version 1.0, *In: RegClim Tech. Rep. No. 8*, Eds. T. Iversen and M. Lystad, 51-68. [Available from the Norwegian Meteorological Institute, P.O. Box 43 Blindern, 0313 Oslo, Norway]

Debernard, J., and L. P. Røed, 2002: Implementations of rivers in met.no's MICOM version. *In: RegClim Tech. Rep. No. 6*, Eds. T. Iversen and M. Lystad, 115-118. [Available from the Norwegian Meteorological Institute, P.O. Box 43 Blindern, 0313 Oslo, Norway]

Dorn, W., K. Dethloff, A. Rinke, S. Frickenhaus, R. Gerdes, M. Karcher, and F. Kauker, 2005: Simulations of the Arctic sea-ice anomaly during summer 1998 with a coupled regional atmosphere-ocean-ice model, *Submitted to Geophys. Res. Letters.*

Döscher, R., U. Willén, C. Jones, A. Rutgersson, H.E.M. Meier, U. Hansson, and L.P. Graham, 2002: The development of the coupled regional ocean-atmosphere model RCAO. *Boreal Env. Res.* 7, 183-192.

Hibler, W.D., III, 1979, A dynamic thermodynamic sea ice model, *J. Phys. Oceanogr.*, 9, 815-846.

Hunke, E., and J. Dukowicz, 1997: An elastic-viscous-plastic model for sea ice dynamics, J. Phys. Oceanogr., 27, 1849–1867.

Karcher, M.J., R. Gerdes, F. Kauker, and C. Köberle, 2003: Arctic warming: Evolution and spreading of the 1990s warm event in the Nordic seas and the Arctic Ocean, *J. Geophys. Res.*, 108, 3034, doi:10.1029/2001JC001265.

Kauker, F., R. Gerdes, M. Karcher, C. Köberle, and J.L. Lieser, 2003: Variability of Arctic and North Atlantic sea ice: A combined analysis of model results and observations from 1978 to 2001, *J. Geophys. Res.*, 108, 3182, doi:10.1029/2002JC001573.

Källén, E. (ed), 1996: HIRLAM documentation manual. System 2.5, pp 178 + pp 55 Apendix

Lemke, P. W. E. Hibler, G. Flato, M. Harder, and M. Kreyscher, 1997: On the improvement of sea ice models for climate simulations: The Sea Ice Model Intercomparison Project, Ann. Glaciol., 25, 183-187.

Meier, H. E. M., R. Döscher, and T. Faxén, 2003: A multiprocessor coupled ice-ocean model for the Baltic Sea: Application to salt inflow. *J. Geophys. Res.* 108:C8, 3273, doi:10.1029/2000JC000521.

Pacanowski, R.C, 1995: MOM 2 documentation: User's guide and reference manual, *GFDL Ocean Group Tech.* Rep. 3, 232 pp., Geophys. Fluid Dyn. Lab., Princeton Univ., Princeton, N. J.

Rinke, A, R. Gerdes, K. Dethloff, T. Kandlbinder, M. Karcher, F. Kauker, S. Frickenhaus, C. Köberle, and W. Hiller, 2003: A case study of the anomalous Arctic sea ice conditions during 1990: Insights from coupled and uncoupled regional climate model simulations. *J. Geophys. Res.*, 108(D9), 4275, doi:10.1029/2002JD003146.

Rummukainen, M., J. Räisänen, B. Bringfelt, A. Ullerstig, A. Omstedt, U. Willén, U. Hansson, and C. Jones, 2001: A regional climate model for northern Europe: model description and results from the downscaling of two GCM control simulations, *Clim. Dyn.*, 17, 339-359.

Røed, L. P. and J. Debernard, 2004: Description of an integrated flux and sea-ice model suitable for coupling to an ocean and atmosphere model. *met.no Report No. 4.* ISSN 1503-8025.

Røed, L. P., and J. Debernard, 2005: Documentation of the method for nesting of MICOM variables into met.no's MICOM version (in preparation).

Walsh, J.E., V.M. Kattsov, W.L., Chapman, V. Govokova, and T. Pavlova, 2002: Comparison of Arctic Climate Simulations by Uncoupled and Coupled Global Models, *J. Climate*, 15, 1429-1446.

Webb, D.J., B.A. de Cuevas, and A.C. Coward, 1998: The first main run of the OCCAM global ocean model, Internal report of James Rennell Div., *Southampton Oceanog. Cent.*, 50 pp., Southampton, England, U.K.

Webb, D.J., A.C. Coward, B.A. de Cuevas, and C.S. Gwillam, 1997: A multiprocessor ocean general circulation model using message passing, *J. Atmos. Oceanic Technol.*, 14(1), 175-183.

Overview and main results of the EU project GLIMPSE-Global Implications of Arctic climate processes and feedbacks

Klaus Dethloff for the GLIMPSE group

Alfred Wegener Institute for Polar- and Marine Research, Research Unit Potsdam

GLIMPSE group: K. Dethloff (1), A. Rinke (1), S. Saha (1), E. Sokolova (1), W. Dorn (1), D. Handorf (1), J. E. Haugen (2), M. Ø. Køltzow (2), J. Debernard (2), L. P. Roed (2), J. H. Christensen (3), M.Stendel (3), P. Kuhry (4), S. Holzkämper (4), P. Wassmann (5), M. Reigstad (5), B. Rockel (6), A. Benkel (6), R. Döscher (7), K. Wyser (7), M. Meier (7)

(1) Alfred Wegener Institute for Polar and Marine Research, Research Unit Potsdam, Germany, (2) Norwegian Meteorological Institute Oslo, Norway, (3) Danish Meteorological Institute Copenhagen, Denmark, (4) Stockholm University, Sweden, (5) University Tromsoe, Norway, (6) Institute of Coastal Research, GKSS, Germany, (7) Rossby Center, SMHI, Sweden.

Motivation

Polar regions are the heat sink of the planet and connected with the energy source in the tropics. This meridional energy gradient drives the planetary dynamical circulation in the atmosphere and the oceans. Polar ice cores make it possible to write the history of recent climate change and to validate the climate simulation models. Polar regions hold the key to our climate future and thus the future of humanity. The polar regions are seeing major changes due to the effects of natural variability and global warming. The Arctic is an important part of the European climate engine. Native communities in the Arctic with four million people are impacted by global climate changes concerning economic and food producing activities.

The main goal of the Glimpse project was to address the deficiencies in our understanding of the Arctic by :

- Developing in concert with the ARCMIP (Arctic Regional Climate Model Intercomparison Project), improved physical descriptions of Arctic climate feedbacks in atmospheric and coupled regional climate models.
- The improved parameterizations have been implemented into global climate system models to determine their global influencers and consequences for decadal-scale climate variations.
- These results have been used to assess the probability of abrupt climate changes on decadal time scales in the past and in the future.

Here we describe selected results of the GLIMPSE project concerning the

1. Evaluation of an ensemble of high resolution Arctic regional climate models and the climatic influence of aerosols.

2. Improved sea-ice and snow albedo parameterization and influence on atmospheric circulations.

3. Development and application of coupled regional AOI models to the Arctic.

4. Global impacts of Arctic feedbacks connected with teleconnection pattern.

5. Decadal-scale climate variations in paleo-climatic simulations and the structure of atmospheric circulation regimes.

6. Influence of improved permafrost description on future climate changes in the Arctic and impact on ecosystems.

1. Evaluation of an ensemble of high resolution Arctic regional climate models and the climatic influence of aerosols

The ARCMIP-Arctic Regional Climate Model Intercomparison Project for the small SHEBA domain and the big GLIMPSE domain was finished. Simulations for one year SHEBA period Sept 1997-Sept 1998 have been carried out with the participating model ARCSyM (USA), COAMPS (S, USA), HIRHAM (D, DK), CRCM (C), RCA (S), RegCM (N), REMO (D) and PolarMM5 (USA). For the pan-Arctic GLIMPSE domain simulations for a 10 year period January 1990 – December 2000 have been carried out with the models HIRHAM (D, DK), RCA (S), RegCM (N).

The simulations showed a remarkable scatter between the model temperature and humidity profiles due to different dynamics and parameterizations (radiation, clouds, PBL, soil schemes). The scatter between warmest and coldest model is in the order of 3°C. There is a need for improvements in the parameterizations of Arctic processes. The mentioned scatter is in the range of the model scatter of climate change scenarios. The stronger model deviations in winter are due to differences in the simulation of meso-scale cyclones, as discussed in Rinke et al. (2005). The direct climatic impact of Arctic Haze was investigated in Rinke at al. (2004) and shown that aerosols trigger changes in the development of cyclones over the Arctic Ocean and exert climate influence on global teleconnection pattern like the Barents Sea Oscillation.

2. Improved sea-ice and snow albedo parameterization and influence on atmospheric circulation

A new snow albedo scheme was developed with a surface temperature dependent scheme which is different for forested (linear dependency) and non-forested (polynomial approach) areas. A new sea ice albedo with_3 different surface types (snow covered ice, bare sea-ice, melt ponds and leads) and a surface temperature dependent scheme; linear dependency was developed by Køltzow et al. (2005).

By implementing this scheme into the HIRHAM model for the pan-Arctic GLIMPSE domain it was shown that the gross features of the annual surface albedo cycle are reproduced by such a surface temperature dependent scheme. A polynomial temperature dependency of snow albedo improves HIRHAM simulations in spring compared to the old linear temperature dependency and improves especially the surface air temperature in spring and autumn. This new scheme improves the mean sea level pressure in spring and autumn, but decrease MSLP skill in mid-summer compared to ERA40. HIRHAM is highly sensitive to the sea ice albedo for large Arctic area.

The new snow and sea-ice albedo scheme decreased the temperatures in the Arctic energy sink and the question appears which regional impacts in the coupled climate system and influence on sea-ice melt and freezing in the Arctic are connected with this feature? The decreased temperatures in the Arctic energy sink lead to an increased energy gradient between tropics and Arctic and could result in global implications?

3. Development and application of coupled regional climate models to the Arctic

Coupled regional climate models of the Arctic climate system has been developed based e. g. at AWI on the atmospheric model HIRHAM, parallelized version, 110×100 grid points, horizontal resolution 0.5° and 19 vertical levels and the ocean–ice model NAOSIM, which uses MOM-2 with elastic-viscous sea-ice rheology, 242×169 grid points, horizontal resolution 0.25°and 30 vertical levels. The boundary forcing is based on ERA-40 data. Figure 1 shows the total volume of Arctic sea-ice for a 11 year long simulation 1989-2000 starting from different initial sea-ice conditions. Blue solid and dashed lines show two experiments with HIRHAM-NAOSIM starting from different initial conditions. One other coupled model

experiment was carried with the Oslo RCM (ORCM). There is a spin up of about 6-10 years to reach realistic sea-ice volume. The year to year variations in ice volume for HIRHAM-NAOSIM and ORCM shows similar fluctuations and are probably connected with variability in the external atmospheric driving fields in the ERA-40 data.

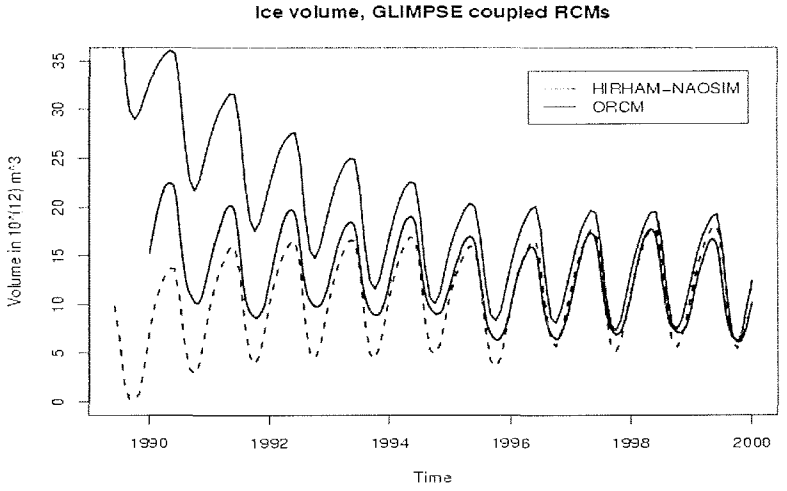

Figure 1. Total volume of Arctic sea-ice for a 11 year long simulation 1989-2000 starting from different initial sea-ice conditions with two coupled regional climate models.

Sea-ice concentration simulations with the AWI model by Dorn et al. (2005) were able to reproduce the big sea-ice anomaly of the Arctic Ocean of September 1998 with the new ice albedo scheme. The ice thickness simulation is affected by the parameterization of ice growth during winter and the relationship between lateral and basal sea-ice growth.The ice albedo parameterization is a crucial factor for ice melting during summer due to its impact on the energy fluxes via the ice–albedo feedback. The regional sea-ice distribution during summer is modified by the atmospheric circulation and vice versa.

The effect of ocean temperature and salinity initial conditions was investigated by Döscher et al. (2005). For the order of 10 year long runs, the ocean initialization is a dominating factor for the ice extent, effecting even the atmospheric circulation. Figure 2 shows the effect of ocean temperature and salinity initial conditions on the mean sea level pressure. Start from decadal length ocean-stand-alone spinup is decribed by the run"coup63" and start from the Polar Science Centre climatology (PHC) climatology is the run "coup65". Shown is only the active (modelled) ocean part, other values over water surfaces are from ERA data.

The choice of ocean initial conditions affects the atmospheric circulation via a different sea ice distribution. Different pressure patterns can be seen with largest effects during the summer months. A proper ocean spin-up is a necessary condition for a realistic coupled simulation.

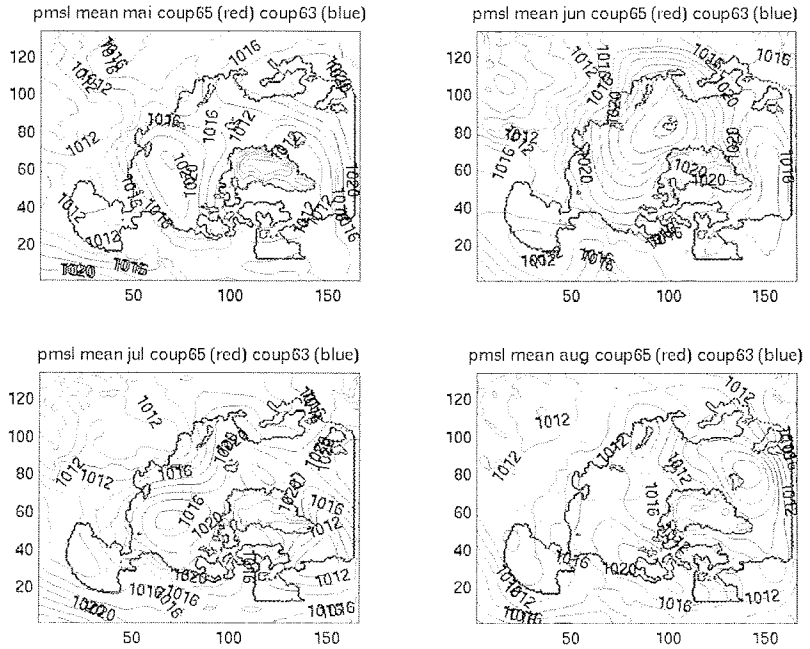

Figure 2. Effect of ocean temperature and salinity initial conditions on the mean sea level pressure (hPa) starting from an ocean-stand-alone spinup "coup63-red" and starting from the Polar Science Centre climatology (PHC) climatology "coup65-blue".

4. Global impacts of Arctic feedbacks connected with teleconnection pattern

Sensitivity run over 250 years with fixed solar constant (1365 W/m^2) and CO_2 (353 ppm) and a new ice- and snow albedo scheme for the Arctic has ben carried out by use of the state-of-the-art coupüled climate model ECHO-G. As shown by Benkel et al. (2005) the Arctic sea ice coverage within ECHO-G improved, especially the minimum extend and area in summer. There is an Arctic cooling in winter and summer owing to the improved albedo parameterisation similar to the results in the regional coupled climate models. Strongest global impacts occur during winter.

Diagnostic studies have been carried out by computing the localized Eliassen-Palm fluxes, which describes the interaction between the time mean state and the transient eddies. Figure 3 shows the localised Eliassen-Palm flux differences for the old and the new snow and sea-ice albedo scheme for ECHO-G "New albedo minus Control" for 8 years. Colours display the magnitude of the differences and the arrows describe the differences in the EP vector propagation. Changes in the planetary wave trains between tropics and Arctic over the Pacific and the Atlantic are visible and described in Sokolova et al. (2005). Changes occur also in the storm tracks over Northern America and Northern Europe owing to the improved Arctic albedo parameterisation.

The global impact of improved Arctic sea-ice and snow albedo leads to annular mode structures similar to the Arctic Oscillation. This implies an influence on the meridional coupling between the energy sources in the tropics and the energy sink in the Arctic and would have strong implications for CO_2 scenario runs as shown in Dethloff et al. (2005).

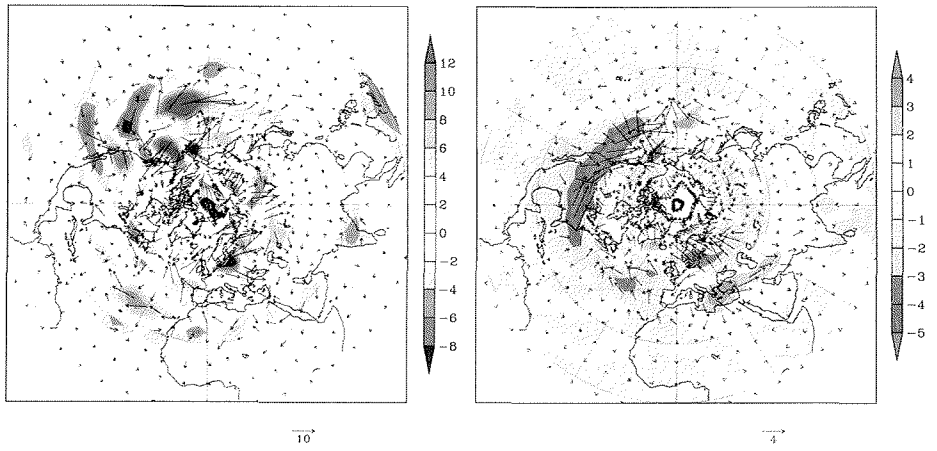

Figure 3. Eliassen-Palm flux differences (m^2s^{-2}) (left low-pass filtered, 10-90 days, right high-pass filtered, 2-6 days) for winter conditions for 8 years.

5. Decadal-scale climate variations in paleo-climatic simulations and the detection of atmospheric circulation regimes

1000 year long simulations the state-of-the-art AOGCMs ECHAM4/OPYC and the ECHO-G with the old and the new snow and sea-ice albedo scheme have been carried out and described by Benkel et al. (2005) and Stendel et al. (2005).

Multi-decadal circulation anomalies are seen, e. g. the Maunder Minimum and both models are able to simulate cold and warm 25 year long lasting anomalies as deviations from the 200 year mean 1500-1700. The models are driven with most relevant forcings, both natural (solar variability, volcanic aerosol) and anthropogenic (greenhouse gases, sulphate aerosol, land-use changes).

In contrast to previous GCM studies, Stendel et al. (2005) have taken into account the latitudinal dependence of volcanic aerosol and the changing land cover for a period covering several centuries. There is a clear signature of large volcanic eruptions in the simulated temperature record. Strong warming is simulated after 1850, in particular over land, going along with an increase of the positive North Atlantic Oscillation (NAO). The cooling events at the end of the 17 th century and early 18 th century are connected with a decrease in pressure difference between low and high latitudes and a decrease of the NAO. This favours positive ice anomalies east of Greenland and around Iceland, leading to widespread negative temperature anomalies over Europe. There develop also characteristic blocking patterns over Western Europe which contribute to the advection of cold air.

Figure 4 shows the temporal development of the first Principal Component of sea level pressure in the Atlantic-European sector and the associated empirical orthogonal function, which explains 37 % of the variance. A strong increase in the positive phase during the last decades of 20 the century is clearly visible.

These long-term simulations have been used by Handorf et al. (2005) to search for multiple atmospheric circulation regimes. Three multiple regimes have been detected with the Pacific North America pattern (PNA), the Cold Ocean Warm Land (COWL) and the Arctic Oscillation (AO).

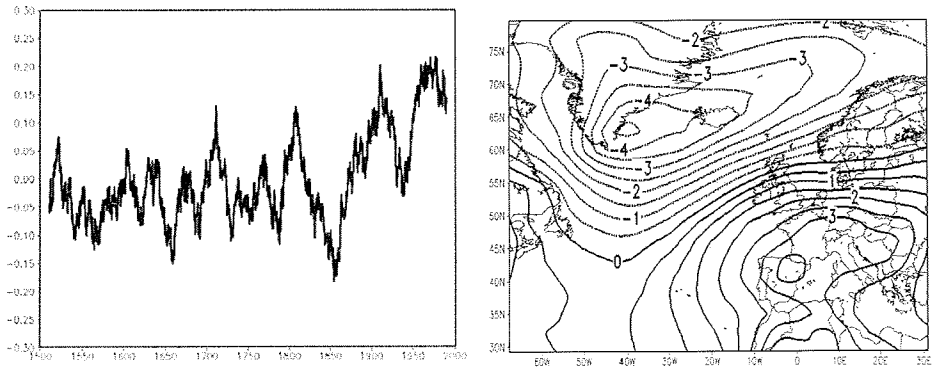

Figure 4. Temporal development of the 1st Principal Component (normalised) of sea level pressure in the Atlantic-European sector from 1500 until 200 and the associated empirical orthogonal function (hPa).

6. Influence of improved permafrost description on future climate changes and impact on ecosystems

A new land-surface model (LSM) from NCAR has been coupled with HIRHAM in the Arctic permafrost region taking into account six moisture layers in the soil as described by Saha (2005) and Saha et al. (2005). The new coupled atmosphere-soil model has reduced the cold winter bias in the soil and improved also the summer soil structure.

The new land surface scheme has a significant influence on the future projection of the Arctic temperature, precipitation and mean sea level pressure. Figure 5 shows the temperature differences between the HIRHAM4 coupled LSM and the old HIRHAM4 projections for the time period (2037-2042) minus (2024-2029) using the IPCC B2 scenario of ECHO-G. The uncertainty of Arctic climate scenarios due to an improved permafrost scheme is in the range of -2 and +2 °C.

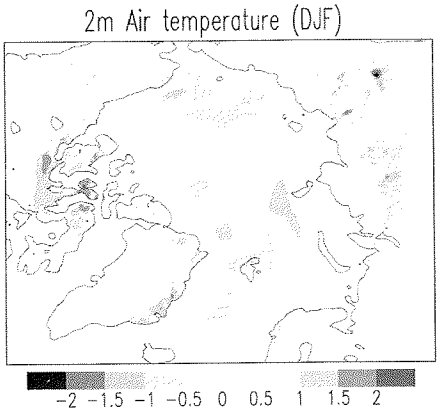

Figure 5. Temperature difference (°C) "HIRHAM4 coupled LSM minus HIRHAM4 projections" for the time period (2037-2042) minus (2024-2029).

7. Summary of selected GLIMPSE results

Arctic regional climate models (RCMs) have been validated in very close connection with process studies (SHEBA), ERA data and satellite data for a small and a pan-Arctic domain. Arctic specific parameterizations for surface ice– and snow albedo and aerosols have been improved and sensitivity studies with regional climate models have been carried out. Coupled system models for the simulation of Atmosphere-Ocean-Ice-Land-Snow-Soil feedbacks in the Arctic have been developed. The description of radiation, clouds, sea-ice albedo, permafrost processes, spin-up of ocean circulation and initial sea-ice cover in RCMs have been improved. A more realistic sea-ice and snow albedo treatment changes the ice-albedo feedback and the radiative fluxes in the A-O-I system. Many new ideas for improving AOGCMs has been developed. Global implications appear due to changes in the barotropic planetary wave trains. Arctic sea-ice and snow albedo treatment triggers the occurrence of the Arctic Oscillation. This has implications for future climate change scenarios. Decadal-scale climate variability in the past is connected with shifts between different atmospheric circulation regimes under the influence of external forcing factors.

References

Benkel et al., 2005, this issue.
Dethloff et al., 2005, A dynamical link between the Arctic and the global climate system, GRL, submitted.
Dorn et al., 2005, Simulation of the Arctic sea-ice anomaly with during summer 1998 with a regional coupled atmosphere-ocean-ice model, J. Geophys. Res., submitted.
Döscher et al., 2005, this issue.
Handorf et al., 2005, this issue.
KØltzow et al., 2005 this issue.
Rinke, et al., 2004, Regional climate effects of Arctic Haze, Geophys. Res. Lett, 31, L16202.
Stendel et al., 2005, Influence of various forcings on global climate in historical times using a coupled atmosphere-ocean general circulation model, Climate Dyn., in press.
Rinke et al., 2005, Evaluation of an ensemble of Arctic regional climate models: Spatiotemporal fields during the SHEBA year, Climate Dyn., submitted.
Saha, S., 2005, The influence of an improved soil scheme on the Arctic climate in a RCM, PhD thesis, University Potsdam, Institute of Physics, 115 pp.
Saha et al., 2005, this issue.
Sokolova et al., 2005, this issue.

Sensitivities in the Rossby Centre Arctic models

Ralf Döscher, H.E. Markus Meier and Klaus Wyser

SMHI/Rossby Centre, Norrköping, Sweden

Introduction and model set-up

The development of regional coupled climate models for the Arctic has been carried out within the GLIMPSE project to test parameterizations under conditions better controlled as possible in global models (GCMs). The Rossby Centre coupled model RCAO (Döscher et al. 2002) consists of the ocean component RCO and the atmosphere model RCA. The model domains (Fig.1) cover the complete Arctic Ocean, the Bering Sea and parts of the subpolar North Atlantic.

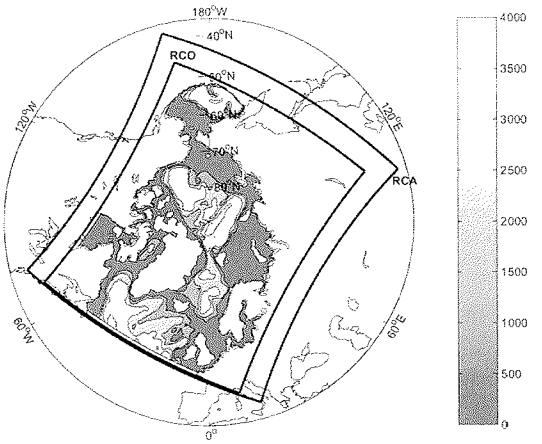

Figure 1. Model domains for RCAO. The inner/outer limits mark the RCO/RCA model boundaries, T-grid points are located on identical positions to facilitate flux coupling. Contour areas within the RCO domain represent ocean depth.

The atmosphere grid extension is somewhat larger than the ocean domain due to boundary nudging effects. The model grid points for temperature are located at identical positions. Inter-model communication is handled by the coupler OASIS (v2.4). RCO has initially been developed for the Baltic Sea (Meier et al, 2003) and has now been applied to the Arctic. A special feature is its low-diffusion advection (Webb et al. 1998) which enables simulations of centennial length with maintained halocline. This is an important precondition for a realistic representation of sea surface quantities in the Baltic Sea and the Arctic Ocean. RCA is based on the weather forecast model HIRLAM and the basic version of RCA is described by Jones et al. (2004). RCA has been applied to several regions. This has improved model evaluation possibilities by widening the range of conditions under which the model is tested, and facilitated benefiting from special observational data sets. A newly developed land surface scheme, an improved treatment of snow on sea-ice, shallow convection, a better turbulence scheme and radiation scheme have been introduced into RCA. The most noticeable improvement was the representation of snow cover on sea-ice, which shows a much more realistic seasonal cycle. The new scheme explicitly solves the energy balance for the snow-pack, which leads to a more realistic snow melt in spring and summer, much in agreement with observations from the SHEBA site.

In the coupled version RCAO, information is exchanged by generally having the ocean sending relevant fields of surface state variables and surface albedo to the atmosphere, which is responding with fluxes of heat and freshwater.

Spin-up

Sensitivity experiments with RCAO are carried of for a subset of the ERA40 period (1958-2002). Coupled integrations require initial fields for ocean and atmosphere. While snapshot fields for the atmosphere are available from ERA40, ocean start fields must be generated by ocean-standalone spin-up runs. At least the time scale of an advective ocean spin-up should be covered by a 30-year run.

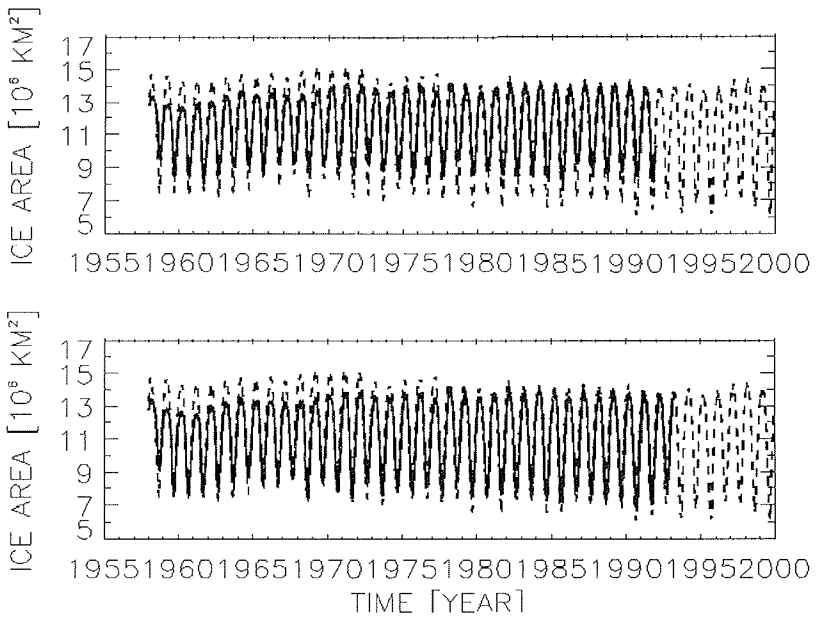

Figure 2. Sea ice extent in ocean standalone spinup-up runs (full lines) and ERA40 (dashed lines). The model run in the upper panel (a) is based on RCO standard formulations for ice albedo and radiative surface fluxes. The annual amplitude is generally underestimated. The run in the lower panel (b) shows distinct improvements due to modifications of ice albedo and radiative flux formulations as recommended by the AOMIP project.

As a first validation of the spin-up and later coupled runs, the Arctic sea ice extent is used here as a sensitive indicator for the quality of simulations. Fig. 2 shows the sea ice extent for two ocean spin-up runs in comparison to observation-derived values from the ERA40 data set (almost identical to the GSFC-nasateam time series starting 1978). The first run (Fig. 2a) shows a systematically underestimated ice extent amplitude. Parameterizations for ice albedo (constants for dry snow/wet snow/dry ice/wet ice = 0.87/0.77/0.7/0.3) and surface radiative fluxes are derived for Baltic Sea conditions based on observations in that area. The second run (Fig. 2b) features modifications of ice albedo (constants for dry snow/wet snow/dry ice/wet ice = 0.80/0.70/0.6/0.5) and surface radiative fluxes as recommended by the AOMIP project (http://fish.cims.nyu.edu/project_aomip/forcing_data/atmosphere/radiative_heat.html). As a result, the annual amplitude of ice extent is much improved after an adjustment period of about 15 years. These differences indicate the non-universal character of certain parameterizations, which work well in marginal seas such as the Baltic Sea but not that well

for extreme arctic conditions. This poses even a problem within our large Arctic domain which includes both central arctic as well as marginal ice areas. Similar needs to modification are found for other parameterizations as well (lateral melting and freezing). We conclude that the degree of universality of key parameterizations needs to be raised in order to gain robustness in different application domains. This appears especially necessary for global models.

Sensitivity of the ocean model to variations of the Atlantic lateral boundary condition

The influence of North Atlantic temperature and salinity conditions (T/S) on the Arctic sea ice extent are of special interest. As a sensitivity test, we replaced the seasonally varying monthly mean T/S profiles prescribed at the Atlantic open boundary of RCO by summer profiles. The effect on the arctic sea ice extent appears to be negligible on the 30-year timescale of the experiment. This implies that the subpolar and arctic heat exchange processes at the ocean/atmosphere interface are more important than the lateral inflow characteristic to shape the arctic ice extent. Stronger and more deep-reaching changes at the southern boundary must be expected to give stronger effects on arctic sea ice (see Kauker et al. 2005).

Sensitivities in the coupled model

When employing the coupled model, ocean/ice-atmosphere interaction comes into play, which adds positive (destabilizing) or negative (stabilizing) feedback mechanism at the interface. In addition, biases in exchange fluxes can lead to problems not seen in standalone runs.

A strong sensitivity with respect to ice albedo formulation is found in the coupled model. Replacing our standard scheme of constant albedo values (see above) with a pure temperature-dependent formulation, (Køltzow, 2003) results in a disappearance of perennial arctic sea ice within three years. This unrealistic behavior is triggered by an unrealistically strong ice-albedo feedback during the onset of the melting phase in spring. The surface temperature dependence has been derived from SHEBA observations. We argue that the formulation unrealistically increases our model's sensitivity because influences other than surface temperature, such as the snow age and the surface type are not taken into account. Similar to other parameterizations (see above) the surface temperature – albedo relation might be valid for SHEBA conditions in the central arctic, but not necessarily for the complete model domain including more marginal areas. On the other hand side, other GLIMPSE models (regional models of AWI, met.no and the global models ECHO-G and ECHAM4-OPYC3 of GKSS and DMI) do not show this strong sensitivity. Apparently, the models differ in their sea-ice related background sensitivity, i.e. the general sensitivity of the model with respect to ice forcing and ice parameter changes in its specific parameter space position. A more detailed comparison of GLIMPSE regional coupled models is conducted by Debernard et al. (2006) in this issue.

Methods to affect the background sensitivity are explored in further sensitivity experiments. Parameterizations of lateral melting and lateral freezing play an important role for the ice extent. The thickness parameter for lateral freezing controls the relation between newly frozen area (i.e. concentration) and thickness. For Baltic Sea applications (Meier et al. 2003) less than 10 cm are sufficient. In the Arctic, RCAO requires 50-150 cm to prevent a rapid drift towards too little ice extent. 50 cm has been recommended by Hibler (1979). The step from 50 cm to 150 cm leads to an increased ice thickness, which reduces the background sensitivity of RCAO.

Lateral melting is not necessary at all for our Baltic Sea applications, where the vertical thermodynamic processes work sufficient to simulate the annual cycle of relatively thin sea ice. In the Arctic, RCAO needs a certain amount of lateral melting to resemble the amplitude

of the annual cycle of sea ice extent. Sea ice models often overestimate lateral melting to compensate for their failure to resolve first year ice (Schmidt et al. 2004). In our case, a lateral melting proportional to the ice concentration is necessary.

In our integrations, sea ice thickness is the most important variable with respect to a conversion into a state of no perennial sea ice. Several sensitivity tests with respect to radiation-relevant cloud quantities indicate that summer ice disappears if the annual/spatial mean ice thickness falls below a value of 1 m. This occurs after O(10 years) long thickness decreases after starting from an average thickness of 2.3 m. When sea ice parameterizations or ocean initial conditions are chosen in a way to favor thicker ice, the coupled sensitivity ("background sensitivity") is reduced.

Mean Sea Level Pressure

Different sea ice conditions as given in several coupled sensitivity runs generally affect the atmospheric circulation. Variations of e.g. the reference thickness of lateral ice freezing or T/S initial conditions can lead to reversed wind directions over large basins of the Arctic Ocean. This sensitivity is in agreement with Rinke et al. (2003). On the other hand side, the atmospheric circulation feeds back on the ice distribution.

When validating the simulated large scale air circulation, represented by the mean sea level pressure (MSLP), we generally find a good agreement with ERA40 fields if the coupled model is used instead of the standalone atmosphere model. Monthly mean fields (and RMS differences between model fields and ERA40 data) for Aug to Nov 1990 are shown in Fig. 3 as an example.

Results are typical even for other versions of RCAO and RCA. In almost all cases, the RMS differences are distinctly smaller in the coupled cases. Possible explanations are seen in (a) the ocean/ice-atmosphere coupled processes as indicated above and in (b) the different representation of sea ice/snow surface temperature. RCAO is applying a thermodynamic ice model with two layers of ice and one layer of snow with variable thickness and bottom heat flux, while the RCA standalone component features a simpler representation with constant ice thickness and bottom flux. RCA is forced with ERA40 ice concentrations, which should be better than RCAO's. Thus, the difference in ice surface temperature appears to dominate the differences in MSLP.

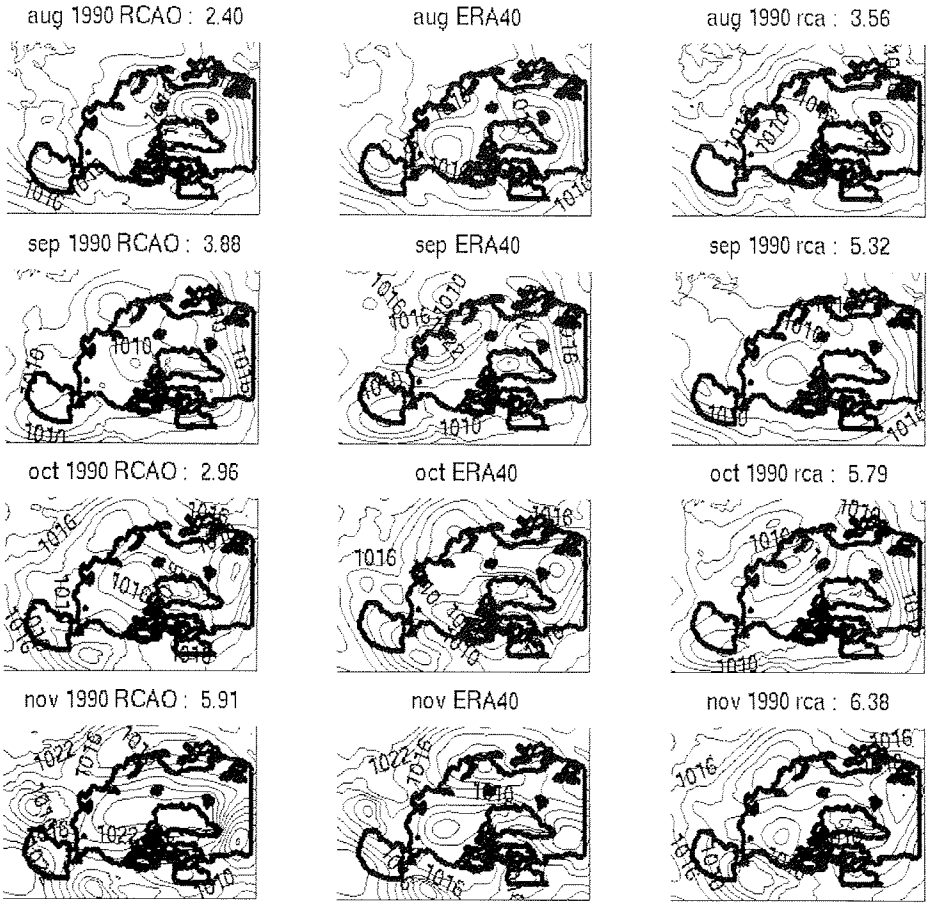

Figure 3. Monthly mean sea level pressure for the coupled model RCAO (left column), ERA40 (center column) and RCA standalone (right column), for months aug, sep, oct, nov. Contour interval: 3 hPa. The coupled model RCAO resembles ERA pressure fields more closely compared to the standalone RCA. The visual impression is supported by RMS differences (in hPa) as given on the right hand side in the titles of the individual figures.

References

Debernard, J., this issue

Döscher, et al, The development of the coupled ocean-atmosphere model RCAO. Boreal Env. Res. 7, 183-192, 2002.

Hibler III, W.D., A dynamic thermodynamic sea ice model. J. Phys. Ocean., vol .9, pp. 815-846, 1979

Jones, C. G., Wyser, K., Ullerstig, A. and Willén, U., The Rossby Centre Regional Atmospheric Climate model Part II: Application to the Arctic Climate. Ambio 33:4-5, 211-220, 2004.

Kauker, F., R. Gerdes, M. Karcher, and C. Koeberle, Impact of North Atlantic Current changes on the Nordic Seas and the Arctic Ocean. J. Geophys. Res., 2005. (accepted).

Køltzow, M, Eastwood, S. and Haugen, J. E, Parameterization of snow and sea ice albedo in climate models, Research Report no. 149, Norwegian Meteorological Institute, 2003

Meier, H. E. M., Döscher, R. and Faxen, T., A multiprocessor coupled ice-ocean model for the Baltic Sea: Application to salt inflow. J. Geophys. Res., 108(C8), 3273, doi:10.1029/2000JC000521, 2003.

Rinke, A., et al., A case study of the anomalous Arctic sea ice conditions during 1990: Insights from coupled and uncoupled regional climate model simulations, J. Geophys. Res., 108, 4275, 2003.

Schmidt, G.A., C.M. Bitz, U. Mikolajewicz, and L.-B. Tremblay,. Ice-ocean boundary conditions for coupled models. Ocean Modelling 7, 59-74, doi:10.1016/S1463-5003(03)00030-1, 2004.

Webb, D.J., de Cuevas, B.A. & C.S. Richmond, Improved advection schemes for ocean models. J. Atm. Oceanic Technology, 15, 1171-1187, 1998

Sea-ice simulations with AWI's coupled regional atmosphere–ocean–ice model HIRHAM–NAOSIM

W. Dorn, K. Dethloff, A. Rinke, S. Frickenhaus, R. Gerdes, M. Karcher, F. Kauker

Alfred Wegener Institute for Polar and Marine Research, Potsdam and Bremerhaven, Germany

Introduction

Recent coupled model intercomparison studies have shown that different atmosphere–ocean–ice models produce quite different sea-ice thickness and extent already in their present-day climate [see *Holland and Bitz*, 2003, their Figure 4]. Hence, it is not surprising that projections of the 21st century ice extent by these models differ considerably from each other and are strongly dependent on the models' simulations of present-day ice extent [*Walsh and Timlin*, 2003; *Holland and Bitz*, 2003; *Flato and Participating CMIP Modelling Groups*, 2004]. The outcome of this is a wide range in the projected polar amplification of climate change and thus in the magnitude and regional pattern of high-latitude warming and its potential consequences.

The uncertainty in modeling present-day Arctic sea-ice conditions and its implications for climate projections indicates the need for improved descriptions of physical processes involved in atmosphere–ice–ocean feedbacks. A realistic simulation of these feedbacks is one of the major challenges in Arctic climate modeling, hampered by the scarcity of available observational data from polar regions and the resulting fragmentary knowledge of the underlying mechanisms of feedbacks. In order to gain deeper insight into Arctic climate processes and feedback mechanisms acting at the interface between atmosphere, ocean, and sea-ice, a series of sensitivity experiments has been conducted with the pan-Arctic coupled regional atmosphere–ocean–sea-ice model HIRHAM–NAOSIM developed at the Alfred Wegener Institute (AWI).

Model Description

The coupled regional model is a composite of two stand-alone models of the Arctic: the regional atmospheric climate model HIRHAM [*Dethloff et al.*, 1996], which incorporates the physical parameterization package of the general circulation model ECHAM4 [*Roeckner et al.*, 1996], and AWI's high-resolution regional ocean–sea-ice model NAOSIM [*Karcher et al.*, 2003; *Kauker et al.*, 2003], which is based on the Modular Ocean Model MOM-2 [*Pacanowski*, 1995]. The NAOSIM version used for the coupled model incorporates a dynamic–thermodynamic sea-ice model with elastic-viscous-plastic (EVP) dynamics according to *Hunke and Dukowicz* [1997] and zero-layer thermodynamics based on the widely-used two-level sea-ice model by *Hibler* [1979] with two ice thickness categories (thick ice and thin ice/open water).

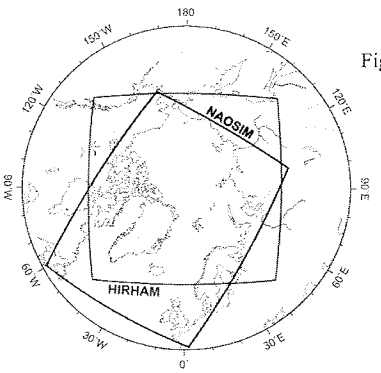

Figure 1: Geographical position of the model domains of the coupled model's atmosphere component HIRHAM and its ocean–ice component NAOSIM. Both model components use rotated latitude–longitude grids at a horizontal resolution of 0.5° (~50 km) for atmosphere and 0.25° (~25 km) for ocean–ice, respectively.

The model domains of the atmosphere and the ocean–ice component are shown in Figure 1. In the present model configuration, the atmosphere and ocean–ice computations are implemented on different grids with different resolutions and necessitate a complex coupling procedure for the exchange of variables between the grids. More information on the model configuration, including a detailed description of the coupling between HIRHAM and NAOSIM, is given by *Rinke et al.* [2003].

HIRHAM–NAOSIM simulations were carried out for the period from May 1989 to December 1999 as well as for some shorter periods. In each case, the model was driven by ECMWF (European Centre for Medium-Range Weather Forecasts) re-analyses (ERA-40) at HIRHAM's lateral boundaries and also at HIRHAM's lower and NAOSIM's upper boundary points that lie outside of the overlap area of the two model domains. The initial ocean and sea-ice fields were taken from a stand-alone run of NAOSIM described by *Karcher et al.* [2003], while the atmospheric fields were initialized with ERA-40 data.

Experiment	Description
h1.2-std	control run with h_0 = 1.2 m and standard ice initialization
h1.2-uni	as h1.2-std but with uniform initial ice thicknesses of 1 m
h0.5-std	as h1.2-std but with h_0 = 0.5 m
h1.2-alb	as h1.2-std but with new snow and ice albedo scheme
h2.0-alb	as h1.2-alb but with h_0 = 2.0 m

Table 1: HIRHAM–NAOSIM sensitivity experiments with respect to initial ice thickness, lead closing parameter (h_0), and ice albedo scheme. The lead closing parameter is a fixed reference thickness for lateral freezing of sea-ice and determines the relationship between basal and lateral sea-ice growth during the cold season. The new snow and ice albedo scheme is based on suggestion 2 of *Køltzow et al.* [2003] and tends to result in a stronger reduction of the ice albedo for melting conditions when snow has already disappeared.

Simulation Results

The top panel of Figure 2 shows the total sea-ice volume from three long-term simulations with different lead closing parameter or initial ice thickness as described in Table 1. All simulations are far from a steady-state at the beginning but arrive at a quasi-stationary cyclic state of equilibrium after about 8–10 years. This equilibrium is only little affected by the initial sea-ice state, even though the initial ice volume differs by a factor 4 (note that formation of thick ice takes a longer time than decay of too thick ice so that h1.2-uni comes close to h1.2-std only at the end of the simulation).

On the other hand, the coupled model's state of equilibrium depends significantly on the rate of increase in ice concentration given by h_0. The simulation with h_0 = 0.5 m results in a mean ice volume that is just about half as large as using h_0 = 1.2 m. This dependency on h_0 is in qualitative agreement with findings of *Holland et al.* [1993] who found an increase in mean ice thickness of about 1 m when decreasing the growth rate of ice concentration to 50% (equivalent to a doubling of h_0). A rough comparison with available ice thickness observations shows that the simulation with h_0 = 0.5 m clearly underestimates the ice volume, while the simulation with h_0 = 1.2 m is much closer to these observations, even though the modeled sea-ice is also thinner than observed.

The corresponding sea-ice extent of the h_0 experiments is shown in the bottom panel of Figure 2 in comparison with SSM/I satellite derived data using the NASA Team algorithm [*Cavalieri et al.*, 1990, updated 2004]. The model generally overestimates the sea-ice extent during winter, and none of the experiments has been able to reduce this shortcoming substantially. In contrast, both simulations also overestimate summer ice extent during the first years, but the simulation with h_0 = 1.2 m agrees quite well with the observations after some years, while the simulation with h_0 = 0.5 m now tends to underestimate the summer ice extent considerably.

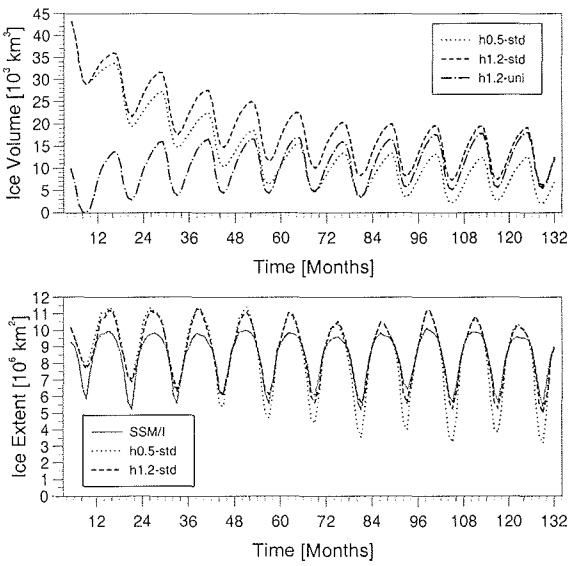

Figure 2: Simulated monthly means of sea-ice volume (top) and sea-ice extent (bottom) within the model domain from May 1989 (Month 5) to December 1999 (Month 132). The sea-ice extent is here defined as the area of all grid cells with at least 15% sea-ice concentration. For comparison, the SSM/I satellite derived sea-ice extent (solid line) was calculated for the same domain. The model simulations were carried out with h_0 = 0.5 m (h0.5-std, dotted lines), with h_0 = 1.2 m and standard ice initialization (h1.2-std, dashed lines), and with h_0 = 1.2 m and initialization with uniform 1 m ice thickness (h1.2-uni, dot and dash line).

A similar underestimation of ice volume and extent is also found in the experiment with the new snow and ice albedo scheme (h1.2-alb). As the new scheme decreases the ice albedo for melting conditions, the energy input into the ocean–ice system is increased, leading to quicker decay of sea-ice during summer and accordingly to reduced ice volume at the end of the summer. However, the impact on ice volume is not as strong as due to the change of h_0. On the other hand, there is not only an indirect influence on summer sea-ice by the changed ice volume but also a direct modification of atmospheric and sea-ice conditions by the changed albedo scheme [*Dorn et al.*, 2005]. Nevertheless, stronger decay of ice mass during summer (as due to a reduced ice albedo) can be compensated by stronger ice growth during winter by means of an increased lead closing parameter. Another experiment with the new snow and ice albedo scheme and h_0 = 2.0 m shows a quite similar seasonal cycle of ice extent as the control run (h1.2-std) and also similar atmospheric circulation patterns.

Sensitivity experiments have also been conducted with respect to the atmospheric heat exchange and drag coefficients, but the impact of these parameters on the ice volume is rather small. Nevertheless, they play an important role for the simulation of the atmospheric circulation, which in turn modifies the regional sea-ice distribution by their influence on energy transport and ice drift. In order to achieve a realistic regional distribution of sea-ice in late summer, it also requires that the coupled model reproduces the observed atmospheric circulation during the preceding summer months. But in contrast to the clear response of the sea-ice cover to the atmospheric circulation, the atmospheric response to incorrect sea-ice cover is not that definite. Unrealistic sea-ice cover, owing to incorrect thermodynamic ice loss, favors model deviations in atmospheric circulation, but these deviations can clearly differ in their strength, probably as a result of regional feedback processes.

Conclusions

A common result of all experiments is that summer ice extent is significantly correlated with the ice volume at the beginning of the melting period (ensemble correlation coefficient of 0.92 between ice volume in April and ice extent in September). The ice thickness simulation, in turn, is significantly affected by the lead closing parameter and the ice albedo parameterization and rather insignificantly by atmospheric drag and heat exchange coefficients and the initial ice thickness distribution after an adequate spin-up time of about 8–10 years. A comparison with observed sea-ice concentrations and thicknesses suggests that the simulated summer sea-ice extent is closer to reality when the simulated ice thickness distribution corresponds approximately with observed values. It has particularly become evident that the overall performance of the coupled models depends strongly on the models' ability to reproduce observed sea-ice conditions.

Furthermore, it has turned out that the widely-used, but rather intuitively reasoned parameterization of ice growth, which is especially reflected in an arbitrary parameter h_0, provides an opportunity to tune a coupled model without giving rise to direct physical inconsistencies. On the other hand, this physical uncertainty in ice growth can be a potential source of error in modeled Arctic sea-ice conditions. It is supposed that the underestimation of ice volume and the overestimation of winter ice extent originates not only from uncertainties in parameterizations of atmospheric fluxes, as related to albedo, clouds, or atmospheric boundary layer, but also from an oversimplified treatment of lateral freezing and melting of sea-ice. An improved thermodynamic ice scheme, which allows for a separate and more sophisticated treatment of the atmospheric surface fluxes over open water and sea-ice, is presently being developed and tested.

References

Cavalieri, D., P. Gloerson, and J. Zwally (1990, updated 2004), DMSP SSM/I monthly polar gridded sea ice concentrations, 1988 to 2003, edited by J. Maslanik and J. Stroeve, National Snow and Ice Data Center, Boulder, CO, digital media.

Dethloff, K., et al. (1996), Regional climate model of the Arctic atmosphere, *J. Geophys. Res.*, *101*, 23,401–23,422.

Dorn, W., et al. (2005), Simulation of the Arctic sea-ice anomaly during summer 1998 with a coupled atmosphere– ocean–ice model, *Geophys. Res. Lett.*, submitted.

Flato, G. M., and Participating CMIP Modelling Groups (2004), Sea-ice and its response to CO2 forcing as simulated by global climate models, *Clim. Dyn.*, *23*, 229–241, doi: 10.1007/s00382-004-0436-7.

Hibler, W. D., III (1979), A dynamic thermodynamic sea ice model, *J. Phys. Oceanogr.*, *9*, 815–846.

Holland, D.M., L.A. Mysak, D.K. Manak, and J.M. Oberhuber (1993), Sensitivity study of a dynamic thermodynamic sea ice model, *J. Geophys. Res.*, *98*, 2561–2586.

Holland, M.M., and C.M. Bitz (2003), Polar amplification of climate change in coupled models, *Clim. Dyn.*, *21*, 221–232, doi:10.1007/s00382-003-0332-6.

Hunke, E. C., and J. K. Dukowicz (1997), An elastic-viscous-plastic model for sea ice dynamics, *J. Phys. Oceanogr.*, *27*, 1849–1867.

Karcher, M. J., R. Gerdes, F. Kauker, and C. Köberle (2003), Arctic warming: Evolution and spreading of the 1990s warm event in the Nordic seas and the Arctic Ocean, *J. Geophys. Res.*, *108*, 3034

Kauker, F., R. Gerdes, M. Karcher, C. Köberle, and J. L. Lieser (2003), Variability of Arctic and North Atlantic sea ice: A combined analysis of model results and observations from 1978 to 2001, *J. Geophys. Res.*, *108*, 3182, doi:10.1029/2002JC001573.

Køltzow, M., S. Eastwood, and J. E. Haugen (2003), Parameterization of snow and sea ice albedo in climate models, *Research Report 149*, Norwegian Meteorol. Inst., Oslo, Norway, 37 pp.

Pacanowski, R. C. (1995), MOM 2 documentation: User's guide and reference manual, *GFDL Ocean Group Tech. Rep. 3*, Geophys. Fluid Dyn. Lab., Princeton Univ., Princeton, N.J., U.S.A., 232 pp.

Rinke, A., et al. (2003), A case study of the anomalous Arctic sea ice conditions during 1990: Insights from coupled and uncoupled regional climate model simulations, *J. Geophys. Res.*, *108*, 4275

Roeckner, E., et al. (1996), The atmospheric general circulation model ECHAM-4: Model description and simulation of present-day climate, *MPI Rep. 218*, Max Planck Inst., Hamburg, Germany, 90 pp.

Walsh, J. E., and M. S. Timlin (2003), Northern Hemisphere sea ice simulations by global climate models, *Polar Res.*, *22*, 75–82.

Influence of horizontal resolution on Arctic Ocean model results

Rüdiger Gerdes and Kerstin Fieg

Alfred Wegener Institute for Polar- and Marine Research, Bremerhaven, Germany

Processes on small scales have a significant impact on the large scale oceanic circulation. Examples are boundary currents that have typical width comparable to the local internal Rossby radius and flow of dense water through narrow channels like the Denmark Strait and the Faeroe Bank Channel. The internal oceanic scales are especially small, just a few kilometers, in certain regions of the Nordic Seas and in the Arctic Ocean. We thus expect that ocean model results for those regions are especially sensitive to changes in grid resolution. The NAOSIM (North Atlantic-Arctic Ocean-Sea Ice Model) hierarchy of the Alfred-Wegener-Institut offers the possibility of systematic experiments to explore the influence of grid resolution. Here, we compare selected results from three ocean-sea ice models with different horizontal and vertical resolution. A focus is on Fram Strait where long term measurements can be compared with model results.

The NAOSIM hierarchy consists of three basic ocean-sea ice models: LRM (low resolution model, 1° horizontal resolution, 19 levels, covering the whole Atlantic north of 20°S and the Arctic Ocean); HRM (high resolution model, 0.25°, 33 levels, northern North Atlantic north of approximately 50°N); FRM (fine resolution model, 0.08°, 50 levels, model domain identical to HRM). The HRM is part of the regional coupled climate model HIRHAM (Rinke et al., 2003). All models are based on the MOM2 code (Pacanowski 1995) of the Geophysical Fluid Dynamics Laboratory. To avoid the singularity of geographical spherical coordinates at the pole the model is formulated on a rotated spherical grid where the equator coincides with the geographical 30°W meridian (Köberle and Gerdes, 2003). The ocean model is coupled with a dynamic-thermodynamic sea ice model that has been developed by Harder (1996) from the original Hibler (1979) model. The models are coupled following the procedure devised by Hibler and Bryan (1987). The most important feature of their approach is that the stress acting on the uppermost level containing sea ice as well as liquid water consists of the sum of wind stress and internal ice stresses. This ensures that in an ice covered ocean the convergence of ice is considered in the Ekman convergence. The sea ice component calculates the surface heat fluxes from standard bulk formulae using prescribed atmospheric data and SST predicted by the ocean model. The forcing follows the AOMIP protocol (http://fish.cims.nyu.edu/project_aomip/overview.html) except that the first model level contains a restoring towards prescribed surface salinity in most experiments (in all experiments discussed here). The time constant for the restoring is 180 days.

Sea ice volume and Arctic Ocean liquid water content are similar in all model versions and their temporal behaviour does not indicate sensitivity to numerical resolution. Sea ice was initialised with very different values but converged in the LRM and HRM results after around ten years. The same is true for ice export through Fram Strait. On the further way to Denmark Strait, sea ice is exposed to warmer waters depending on the width of different components of the East Greenland Current. The width and intensity of the recirculating branch of Atlantic Water depends on resolution and with it the melting rate of sea ice drifting southward along the East Greenland Coast. Large differences between models exist in the transport through the Canadian Archipelago. The requirement of southward oceanic transport through the Archipelago necessitates an excessively broad opening in the LRM. A realistic piling up of sea ice in the narrow straits of the Archipelago is thus not possible, resulting in unrealistic large sea ice export in the LRM.

The oceanic circulation in Fram Strait is dominated by an intense recirculation that surpasses the net volume exchange between the Arctic Ocean and the Nordic Seas by a factor of three to five. The intensity of the recirculation in models depends very much on resolution. Only the highest resolution model (FRM) shows individual northward and southward volume transports that are comparable to the estimates based on observations. The other model version feature much smaller transport components. However, the net exchange is again very similar among the model versions.

Another phenomenon that depends on resolution is the sinking in the Greenland Sea. Apparently independent of convective activity, there is a general downward motion in the Greenland Sea as evidenced by the sinking of isothermals and the warming of the deep Greenland Sea over recent decades (Karstensen et al., 2005). Only the FRM reproduces this sinking which could be due to a better lateral exchange between the interior Greenland Sea and the currents surrounding it. Only FRM produces an intense eddy field in the Nordic Sea and it is conceivable that these eddies are instrumental in supplying Atlantic water to the upper water column in the Greenland Sea.

While the FRM shows many features that are more realistic than in the lower resolution versions of the model, it has some shortcomings that it shares with other high resolution models of the northern North Atlantic (Treguier et al., 2005). The model shows very intense barotropic currents following the topographic features in the subpolar gyre area, especially the Reykjanes Ridge. These currents bring warm and salty water into the Labrador Sea. The cooling there leaves very dense water behind. Convection intensity and depth becomes too large in the Labrador Sea. This might introduce a positive feedback that further enhances the subpolar gyre and the supply of warm and saline water to the Labrador Sea. The cause of this problem is not yet known but might be associated with insufficient supply of fresh water to the Labrador Sea, either through the East Greenland Current or the Canadian Archipelago.

References

Harder, M. (1996) Rauhigkeit und Alter des Meereises in der Arktis - Numerische Untersuchungen mit einem großskaligen Modell. *Berichte zur Polarforschung*, **203**, Alfred-Wegener-Institut. (Ph. D. thesis, in German with English summary.)

Hibler, W.D. (1979) A Dynamic Thermodynamic Sea Ice Model. *J. Phys. Oceanogr.*, **9**, 815-846.

Hibler, W. D. and K. Bryan (1987) A Diagnostic Ice-Ocean Model. *J. Phys. Oceanogr.*, **17**, 987-1015.

Karstensen, J., P. Schlosser, D. W. R. Wallace, J. L. Bullister, and J. Blindheim (2005), Water mass transformation in theGreenland Sea during the 1990s, J. Geophys. Res., 110, C07022, doi:10.1029/2004JC002510.

Köberle and Gerdes (2003) Mechanisms determining the variability of Arctic sea ice conditions and export, J.Climate, 16, 2843-2858.

Pacanowski, R.C. (1995) MOM 2 Documentation, user's guide and reference manual. *GFDL Ocean Group Technical Report*, **3**. Geophysical Fluid Dynamics Laboratory/Princeton University, Princeton, NJ, 232pp.

Rinke, A., Gerdes, R., Dethloff, K., Kandlbinder, T., Karcher, M., Kauker, F., Frickenhaus, S., Koeberle, C., Hiller, W.(2003). A case study of the anomalous Arctic sea ice conditions during 1990: Insights from coupled and uncoupled regional climate model simulations, Journal of geophysical research, Vol. 108, No. D9, 4275, DOI: 10.1029/2002JD003146

Treguier, A.M., S. Theetten, E. P. Chassignet, T. Penduff, R. Smith, L. Talley, J. O. Beismann and C. Böning. (2005) The North Atlantic Subpolar Gyre in Four High-Resolution Models. Journal of Physical Oceanography: Vol. 35, No. 5, pp. 757–774.

On the Impacts of extreme events on the coastal zone of a small Alaskan community: multi-scale modeling approaches

K. Görgen[1], A.H. Lynch[1], E.N. Cassano[2], L. Xie[3], L. Lestak[2], and R.D. Brunner[4]

[1]School of Geography and Environmental Science, Monash University, Melbourne, Australia
[2]CIRES, University of Colorado at Boulder, Boulder, Co, U.S.A.
[3]Coastal Fluid Dynamics Lab, North Carolina State University, Raleigh, NC, U.S.A.
[4]Political Science, University of Colorado at Boulder, Boulder, Co, U.S.A.

Introduction

The main impacts of intense storms during the ice-free season on the community of Barrow, Alaska, are flooding and coastal erosion. This vulnerability arises from Barrow's location on a low lying coastal plain at the northernmost point of the United States, facing the Chukchi Sea to the west. The community of around 5000 inhabitants is concerned about their ability to adapt to their perhaps increasing vulnerability in the future. Over the past six years, a joint project of Monash University (Australia), University of Colorado at Boulder (U.S.A.), the National Center for Atmospheric Research (U.S.A.) and the Barrow Arctic Science Consortium has worked to expand the range of informed options open to the community. This has been done through an integrated assessment of the impacts of climate variability and change on things of value to the community. The need for exceedingly specific and local information is in this context the driver for the research that we conduct. This bottom-up approach is highly policy relevant, requiring close collaboration with both policy scientists and community leaders. Multi-scale modeling approaches that also heavily incorporate observational data are used in support of these goals to study the storms and their impacts for the last 50 years [*Brunner et al.*, in press; *Lynch et al.*, 2004].

Threats to Barrow

The continuous community development and modernization since the 1950s mean that more lives, property, and other things of value are at risk. Aside from many buildings in close proximity to the shoreline, some things of special importance include the old Barrow Townsite, Ukpeagvik, with important archeological and ancestral remains at stake, the underground utilidor corridor that provides sewage and water, and the freshwater reservoir. Threats include the two sewage lagoons and the landfill, where toxic materials are buried. Human induced changes to the coastal environment include gravel mining of the beach and a beach nourishment program.

Major changes in the natural system especially contribute to an increased vulnerability. Rising temperatures result in permafrost thaw and therefore a weakening the unconsolidated bluffs. At the same time the length of the open-water season increases as sea-ice retreat has accelerated in the Beaufort and Chukchi Seas during the past two decades. Since ice can effectively protect the coast from wave action and storm surges this has a strong impact on vulnerability.

Atmospheric environment

Statistical models of Barrow wind speed data from the National Weather Service over the last 60 years do not show any significant linear trends of highest wind events during the ice-free season, but a very large and increasing variability is evident. This is coupled with a non-stationary relationship between strongest wind events and their return periods. This complexity inhibits the use of wind speed data alone for any prognostics.

A neural network analysis using self organizing maps based on NCEP/NCAR mean sea level pressure re-analysis data is used to characterize the synoptic conditions associated with high wind events at Barrow. Strong easterly winds are associated with a large Aleutian cyclone and/or a strong Beaufort-Chukchi high pressure ridge. These are by far the most frequent

causes of high winds at Barrow. Unfavorable impacts however are primarily linked to westerly winds which cause storm surges and damaging waves. These situations are associated with strong Beaufort-Chukchi cyclones, a weather pattern that has increased somewhat during the last 50 years. Important for the storm's destructiveness is its intensity, the proximity to the coast, fetch to the sea ice for waves to build up, and its life-span.

Polar MM5 experiments are performed for all storms of the past 50 years to better understand the atmospheric conditions and the development processes during the storms. In addition, these high-resolution realizations can be used as forcing datasets for other impact models. It is evident that only a detailed high resolution model simulation can capture all relevant small-scale features (e.g. polynyas and leads) for an adequate storm reproduction [*Lynch et al.*, 2003].

Flooding and Erosion

Short term impacts of individual storms are addressed using an impacts model due to the lack of a sea level gauge at Barrow. The inundation modeling is done by North Carolina State University's CAPES model [*Peng et al.*, 2004]. In one example, the comparison of the simulated composite flood extent with a flood debris line mapped after the record 1963 storm (Figure 1) shows a good overall agreement, with many detailed features being reproduced [*Hume and Schalk*, 1967]. This supported the use of this model to simulate other, less well documented, flood events. The inundation was derived using the Polar MM5 winds as the sole atmospheric forcing to CAPES. Uncertainties include the influence of wave height, and the fact that some topographic features have changed over the years. The use of the CAPES model coupled with the SWAN model to incorporate the wave setup, wave height and wave run-up is expected to further improve the results.

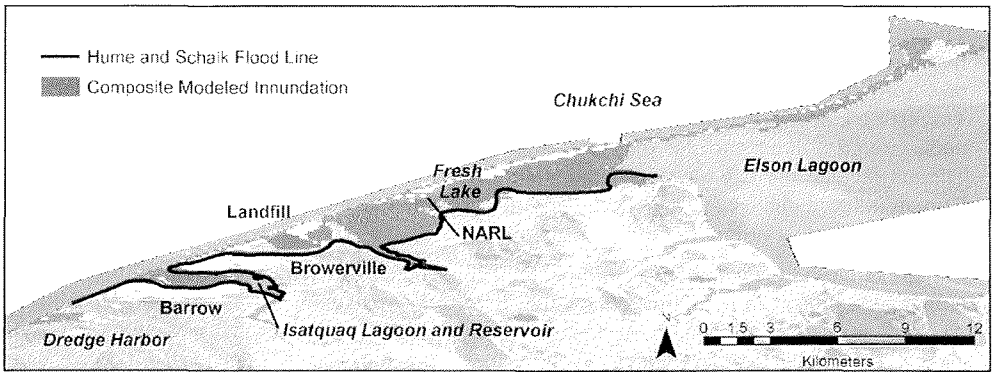

Figure 1. Inundation as simulated by the CAPES model for the October 1963 storm. All flood-water affected grid cells during the storm are combined into one composite layer. The *Hume and Schalk* [1967] mapped floodline is overlaid. Underlying is a Quickbird satellite image from 2002.

The high-resolution monitoring and mapping of coastline erosion by means of remote sensing, GPS field surveys and geographic information systems (GIS) is needed to complete our overall process knowledge. The overall rate of erosion in the town of Barrow is relatively small compared to the rest of the Barrow peninsula. In Figure 2 minimum erosion rates of about 0.2 m 50 yr^{-1} are found south of Barrow's gravel pit. Maximum erosion rates along the unconsolidated permafrost bluffs north of the gravel pit adjacent to the Barrow town site reach values of up to 34 m 50 yr^{-1}. Consistent with the episodic nature of erosion processes, it has been established that about 20% of the bluff erosion happened during the record storm of 1963.

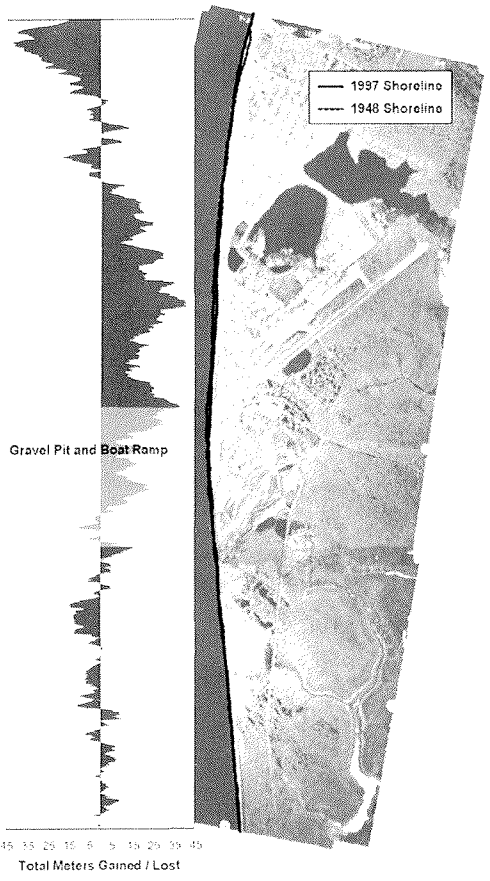

Figure 2. Coastal retreat (negative values) or aggregation (positive values) between 1948 and 1997 (left). Orthorectified aerial photography from 1997 of Barrow and Browerville, overlaid are shoreline positions in 1948 and 1997 (right).

Policy responses and mitigation strategies

Flooding is primarily a short-term emergency management problem while the erosion can be regarded mainly as a planning policy and engineering problem. With regard to the potential policy responses to these problems, a number of different "soft" and "hard" adaptation strategies compete with each other. For example, the beach nourishment program was intended to gain time for the re-location of very exposed parts of the town to slightly higher locations further inland, but while the hard option of nourishment was pursued, the soft counterpart of relocation was not. A feasibility study by the U.S. Army Corps of Engineers focuses on the increase of the elevation of the coastal road and thereby forming a sea wall. Other potential policy responses include the protection of the old landfill site, some re-locations of especially threatened buildings, and changes in planning and zoning regulations. In response to results similar to those presented here, the new hospital will be located outside the October 1963 floodline and the design and the location of the new Barrow Global Climate Change Research Facility is influenced by 1963 flood levels.

The community, being self-empowered, is responsible for making these decisions. This project seeks to inform those decisions, using the guiding principles of reserves, redundancy and resilience. So far, the physical science in this project, by the use of various model and observational methodologies, has provided an environmental context for local policy to build upon.

References

Brunner, R. D., A. H. Lynch, J. Pardikes, E. N. Cassano, L. Lestak, and J. Vogel, An Arctic disaster and its policy implications, *Arctic*, in press.

Hume, J. D., and M. Schalk, Shoreline Processes near Barrow, Alaska: A Comparison of the Normal and the Catastrophic, *Arctic*, *20*, 86-103, 1967.

Lynch A. H., Cassano E. N., Cassano J. J., and Lestak L. R., Case studies of high wind events in Barrow, Alaska: Climatological context and development processes. *Mon. Weather Rev.*, *131*, 719-732, 2003.

Lynch, A. H., J. A. Curry, R. D. Brunner, and J. A. Maslanik, Toward an integrated assessment of the impacts of extreme wind events on Barrow, Alaska, *Bull. Am. Meteorol. Soc.*, *85*, 209-221, 2004.

Peng, M. C., L. Xie, and L. J. Pietrafesa, A Numerical Study of Storm Surge and Inundation in the Croatan-Albemarle-Pamlico Estuary System, *Estuarine, Coastal and Shelf Science*, *59*, 121-137, 2004.

Winter climate regimes in forced Atmosphere-Ocean-GCM simulations

D. Handorf[1], M. Sempf[1], K. Dethloff[1], C. Casty[2], E. Zorita[3], F. Gonzales-Rouco[4], M. Stendel[5], J. Hesselberg-Christensen[5]

[1] Alfred Wegener Institute for Polar and Marine Research, Potsdam
[2] Climate and Environmental Physics, University of Bern
[3] Institute for Coastal Research, GKSS Research Centre, Geesthacht
[4] Department of Astrophysics and Atmospheric Sciences, University of Madrid
[5] Danish Climate Centre, Danish Meteorological Institute, Copenhagen

Introduction

It has long been recognized that the midlatitude planetary-scale flow is characterized by a few preferred circulation patterns (Rossby, 1939), which can be defined on a monthly time scale as climate regimes. The concept of climate regimes provides a framework for explaining, at least partly, low-frequency variability by transitions between distinct regimes (Palmer, 1999). The concept has been proven in studies with low-order nonlinear dynamical systems (e.g., Charney and DeVore, 1979) and in observational studies (Stephenson et al., 2004, and references therein). Here, we aim at investigating the capability of complex coupled atmosphere-ocean GCMs in representing recurrent climate regimes. Therefore, we compare the regime variability of several 500-year long, control and externally forced model simulations.

The quantitative method for the detection of climate regimes is based on the general property of recurrence. Thus, climate regimes are often identified by detecting local density maxima in the reduced state space of atmospheric data (e.g., Kimoto and Ghil, 1993; Hsu and Zwiers, 2001). In order to account for the nonlinear dynamics of regimes, a Nonlinear

Principal Component Analysis (NLPCA) (Monahan, 2000) is applied additionally. The detection of climate regimes is performed on monthly 500 hPa geopotential height data with focussing on winter (D, J, F) data for the Northern hemisphere (north of 20° N) as the main patterns of variability are more pronounced during that season.

Data Sets

The modelled data sets have been obtained from four 500-year long integrations of two different coupled atmosphere-ocean general circulation models, both belonging to the ECHAM family.

Three runs have been carried out with ECHO-G. This model consists of the atmospheric GCM ECHAM4 (Roeckner et al., 1996; 19 vertical layers up to 10hPa, horizontal resolution T30 corresponding to a grid of 3.75°x3.75°) and the global version of the Hamburg Ocean Primitive Equation GCM HOPE-G (Wolff et al., 1997; 20 vertical layers, horizontal resolution T42 (2.8°x2.8°), dynamic-thermodynamic sea-ice model with snow cover). For the long-term simulation an annual mean flux correction for heat and fresh water is applied to avoid an unrealistic climate drift of the coupled system. ECHO-G has been run in control mode, that is the forcing functions for the solar insolation, the aerosol loading and the greenhouse gases have been fixed to present day values. Additionally, two simulations with prescribed time-evolving external forcing functions for the solar insolation, the aerosol loading and the greenhouse gases concentration have been carried out for the period 1500 to 1990 (Zorita et al., 2003) and for the period 1000 to 1990. For the latter run, only the period from 1500 onwards has been analysed for this study.

The fourth analysed long-term simulation has been performed with ECHAM4/OPYC, that is the atmospheric model ECHAM4 in T42 resolution (corresponding grid 2.625°x2.625°) has been coupled to the global isopycnic ocean model OPYC in T42 resolution (Oberhuber,

1993). The external time-dependent forcings differs from those for the ECHO-G runs by applying latitudinal dependent volcanic aerosol forcing and by including land use changes (Stendel et al., 2005).

Methodology

It has been proven that climate regimes can be identified by studying the state space structure of atmospheric motions (e.g., Kimoto and Ghil, 1993; Hsu and Zwiers, 2001). Usually, the probability density function (PDF) of a low-dimensional (mostly 2-dimensional) reduced state space is analyzed regarding the frequency of occurrence of regimes. Recurrent climate regimes are defined as patterns which correspond to areas of the state space with an unexpected high recurrence probability.

As the two basis functions of the reduced state-space the first two EOFs (Empirical Orthogonal Function) have been choosen. The corresponding standardized time series (principal components; PCs) of the EOFs form the state variables of the reduced state space. For all model simulations the first two EOFs explain approximately 30% of the total 500hPa winter geopotential variance. The most dominant patterns are very similar among the model runs, revealing an annular structure similar to the Arctic Oscillation in EOF1. The main feature of EOF2 is the wave train of the Pacific-North America pattern.

The joint PDF of the state space is calculated with a Gaussian kernel estimator with conservative settings for all parameters to avoid spurious multimodality of the PDF (Silverman, 1986). State space areas with an unexpected high recurrence probability are estimated by means of adequate Monte Carlo simulations (MC, e.g., Kimoto and Ghil, 1993; Hsu and Zwiers, 2001, Casty et al., 2005a). Therefore 1000 pairs of random (PC1, PC2) time series are simulated with the same mean, variances, and one-lag autocorrelation coefficients as the original (PC1, PC2) time series. The areas with an unexpected high recurrence probability are defined by using the 95% confidence interval.

In order to account for the nonlinear dynamics of regimes, additionally the NonlinearPrincipal Component Analysis (NLPCA, Monahan, 2000) has been applied for regime detection. This method is applied in the space spanned by the first 10 leading linear PC modes accounting for about 80% of the total variance. The first NLPCA mode is characterised by a curve in this 10-dimensional space and corresponds to a sequence of spatial maps. The temporal evolution along the NLPCA1 curve can be characterized by a time series $\lambda(t)$, which measures the distance along the curve to one endpoint of the NLPCA1 curve. This time series is an analogue to the linear PC time series. Recurrent climate regimes are then defined as patterns in the state space, which correspond to maxima of the PDF of $\lambda(t)$. Again, the PDF has been calculated with a Gaussian kernel estimator.

Recurrent Climate Regimes

Fig. 1 shows the PDFs for the winter 500 hPa geopotential height fields for 1500-1990 for all model runs. Regions of unexpected recurrence probabilities estimated by the Monte Carlo approach are indicated by grey-shaded areas with thick contour lines. Furthermore, the u-shaped curves of the first NLPCA mode are overlaid. The PDFs of the corresponding NLPCA1-time series $\lambda(t)$ (not shown) reveal three maxima for each model run. In Fig. 1, their exact positions on the NLPCA1 curves are indicated by the symbols, whereas the starting and endpoints are marked by > and o, respectively. The u-shaped curves of the first NLPCA mode almost connect the significant areas determined by the Monte Carlo approach. Therefore, both methods detect similar climate regimes.

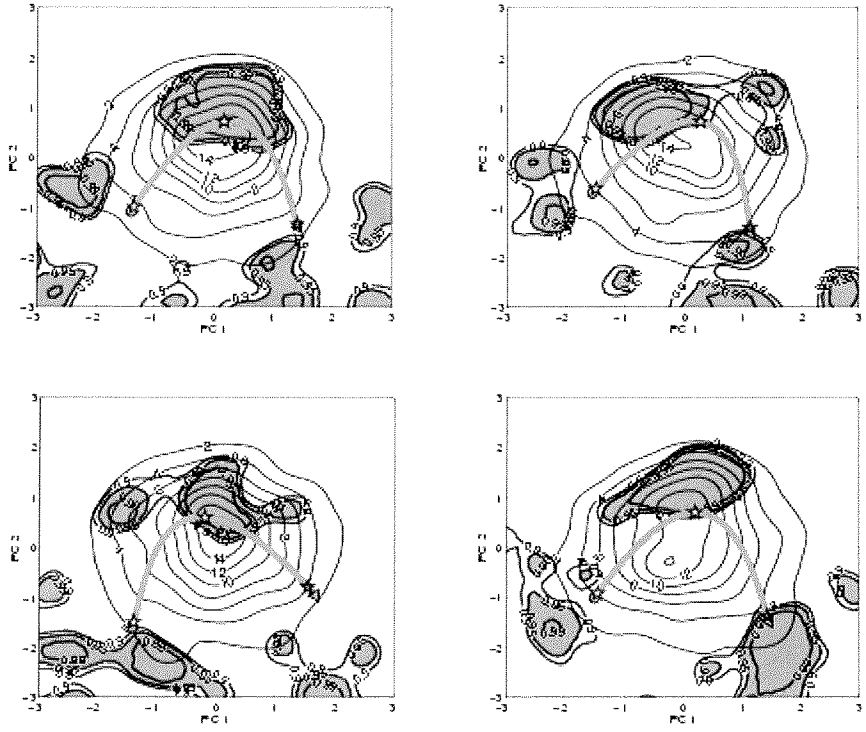

Fig.1: Probability density functions (PDF, contours in %) for monthly mean of winter (DJF) 500hPa geopotential data in the state space spanned by the first two EOFs for 4 model simulations. Grey shaded areas mark regions with an unexpected high recurrence probability on a confidence level of 95%, determined by means of a MC approach. Overlaid is the curve of the NLPCA1 mode. The symbols * indicate the positions of the climate regimes in the state space. The symbols > (o) indicate the starting (end) point of the NLPCA1 curve.Upper row from left to right: ECHO-G control run; ECHO-G forced run; started in 1500. Lower row from left to right: ECHO-G forced run, started in 1000 (data used since 1500); ECHAM4/OPYC forced run.

In the following, the spatial maps of these climate regimes, based on the results of the NLPCA, are discussed. Given the coordinates of the position of the climate regimes in the low-dimensional state space, the corresponding spatial 500hPa geopotential height anomaly patterns can be reconstructed. These patterns as well as their frequency of occurrence are very similar among the different model runs.

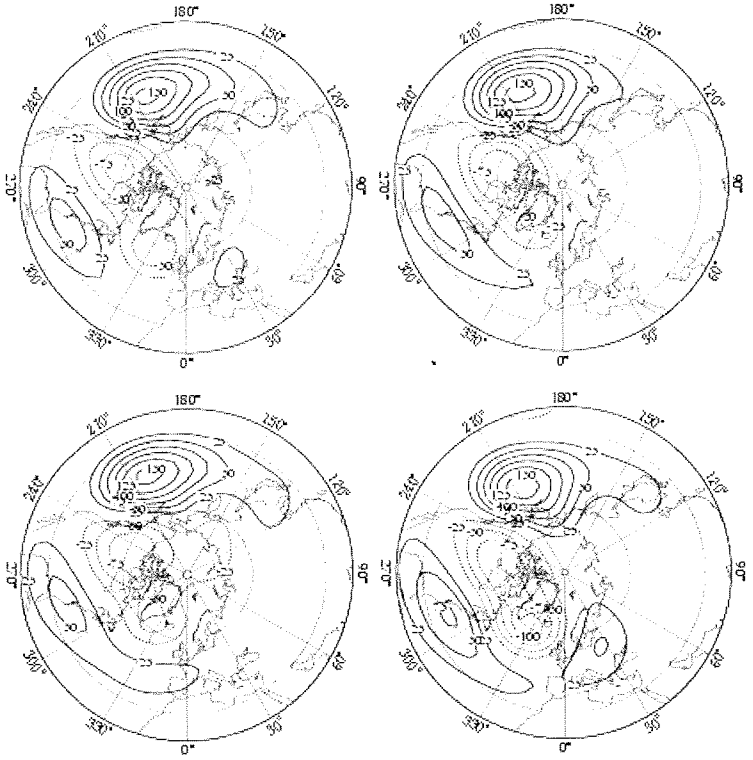

Fig.2: Anomaly patterns of the first winter climate regimes (PNA-) for the Northern Hemisphere (north of 20°N) for 4 model simulations. Upper row from left to right: ECHO-G control run; ECHO-G forced run; started in 1500. Lower row from left to right: ECHO-G forced run, started in 1000 (data used since 1500); ECHAM4/OPYC forced run.

Regime 1 (Fig. 2) resembles the Pacific-North America Pattern in its negative phase and has an occurrence of about 9%. This flow situation is connected with a westward retreat of the East Asian jet stream and enhanced blocking activity over the northern North pacific. The second regime (Fig. 3) reveals a weak Cold Ocean-Warm Land (COWL) pattern, which is connected with anomalously warm hemispheric mean temperature (Wallace et al., 1995). Over the Nort Atlantic, this pattern includes a weak positive dipole of the North Atlantic Oscillation (NAO). This pattern is the most frequent one with about 23%. Fig. 4 displays the last regime for each model run showing the Arctic Oscillation (AO) in its negative phase. Its frequency of occurrence varies between 7% and 11% and is slightly less frequent for the forced model simulations.

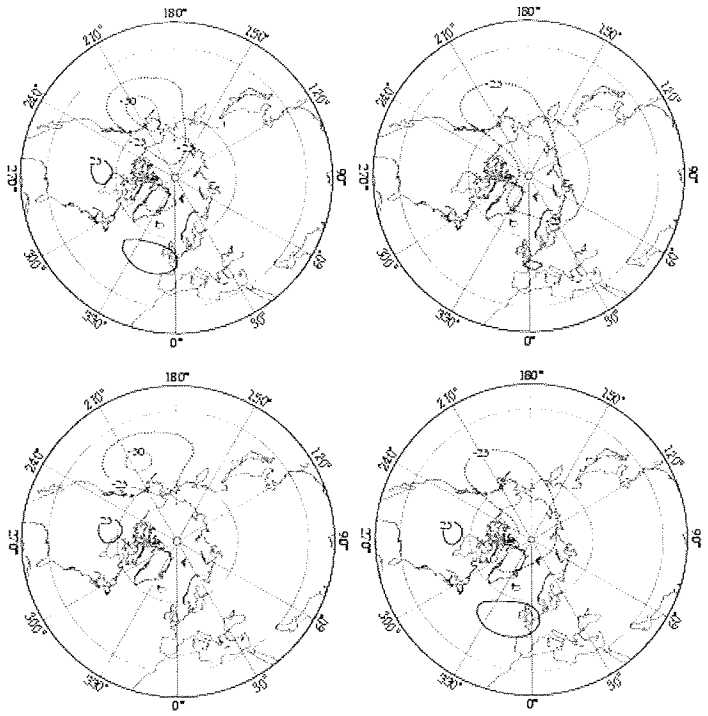

Fig.3: As in Fig. 2, but for the second winter climate regime (COWL).

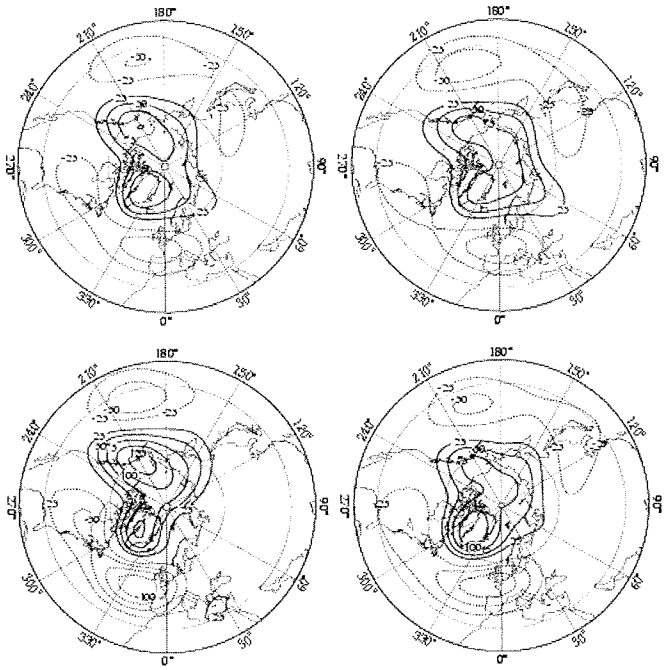

Fig.4: As in Fig. 2, but for the third winter climate regime (AO-).

By analysing the NLPCA1-time series λ(t), one get more insight into the temporal evolution of the regimes and their transitions. Thus, it is possible to attribute specific winter regime conditions to pronounced climate anomalies. For example, in the model simulation with ECHAM4/OPYC the onset period of the late Maunder Minimum (LMM, ~1675-1715) exhibits less occurrence of COWL and more frequent occurrence of the negative phase of AO then the end period of the LMM. Thus, this hemispheric analysis confirms the shift from NAO- to NAO+ estimated by Stendel et al. (2005) for the North Atlantic region. Another example is the second half of the last century. Since 1970, all three forced simulations show the tendency to more frequent COWL and less frequent AO- patterns in accordance with the observed circulation changes.

Conclusions and Outlook

Our study confirmed the capability of coupled atmosphere-ocean GCMs in reproducing regime-like behaviour. Furthermore, the climate regime analyses provides an sophisticated approach for the comparison of model simulations and also for model-data intercomparison (Casty et al., 2005a).

The comparison of the results for the regime analyses between the control and the forced runs has revealed that the external forcings does not change the spatial regime structure in accordance with the paradigma developed by Palmer (1999). For all model runs, unforced as well as forced, three regimes have been detected, connected with a PNA- flow situation, a COWL pattern and an AO- like pattern.Slight changes in the frequency of occurrence of regimes have been estimated for the AO- regime with less frequent occurrence for the forced model simulations.

The presented methods of regime detection allows not only the detection of the regime flow patterns but elucidates inherently their temporal structure regarding occurrence and regime transitions, as it has been exemplarily described for the LMM and the warming since 1970. Thus, further detailed studies on the attribution of specific winter regime conditions to pronounced climate anomalies known from proxy and observational data are possible.

For further research concerning the influence of external forcings versus internally generated climate variability there is the need of analysing ensembles of transient model runs together with different independent reconstruction approaches (Casty et al., 2005b) as a prerequisite for reliable assessments of future climate change.

Acknowledgments

The authors would like to thank the group ``Modelle und Daten" at the Max Planck Institute for Meteorology, Hamburg, for providing the data of the ECHO-G control simulation.

References

Casty, C., Handorf, D., Raible, C.C., Gonzalez-Rouco, F.J., Weisheimer, A., Xoplaki, E., Luterbacher, J., Dethloff, K., and H. Wanner (2005a), Recurrent climate winter regimes in reconstructed and modelled 500 hPa geopotential height fields over the North Atlantic/European sector 1659-1990, *Climate Dynamics, 24*, 809-822.

Casty, C., Handorf, D., and M. Sempf (2005b), Combined winter climate regimes over the North Atlantic/European sector 1766-2000, *Geophysical Research Letters, 32*, L13801, DOI: 10.1029/2005GL022431.

Charney, J. G., and J. G. DeVore (1979), Multiple flow equilibria in the atmosphere and blocking, *J. Atmos. Sci., 36*, 1205–1216.

Hsu, C. J., and F. Zwiers (2001), Climate change in recurrent regimes and modes of Northern Hemisphere atmospheric variability, *J. Geophys. Res., 106*, 20145-20159.

Kimoto, M., and M. Ghil (1993), Multiple flow regimes in the Northern Hemisphere winter, Part I: Methodology and Hemispheric regimes, *J. Atmos. Sci., 50*, 2625-2643.

Monahan, A. H. (2000), Nonlinear principal component analysis by neural networks: Theory and application to the Lorenz system, *J. Clim., 13*, 821– 835.

Oberhuber , J.M. (1993), The OPYC Ocean General Circulation Model, *DKRZ Tech. Rep. 7*, 148pp.,Hamburg.

Palmer, T. N. (1999), A nonlinear perspective on climate change, J. Clim., *12*, 575– 591.

Roeckner, E., K. Arpe, L. Bengtsson, M. Christoph, M. Claussen, L. Dümenil, M. Esch, M. Giorgetta, U. Schlese, and U. Schulzweida (1996), The atmospheric general circulation model ECHAM-4: Model description and simulation of present-day climate, *MPI Rep. 218*, 90pp., Hamburg.

Rossby, C. G. (1939), Relation between variations in the intensity of the zonal circulation of the atmosphere and the displacement of the semipermanent centers of action, *J. Mar. Res., 2*, 38– 55.

Silverman, B.W. (1996), *Density estimation for statistics and data analysis*, 175pp., Chapman & Hall, New York.

Stephenson, D. B., A. Hannachi, and A. O'Neill (2004), On the existence of multiple climate regimes, *Q. J. R. Meteorol. Soc., 130*, 583– 606.

Wallace, J. M., Y. Zhang, and J. A. Renwick (1995), Dynamic contribution to hemispheric mean temperature trends, *Science, 270*, 780-783.

Wolff, J.O., E. Maier-Reimer, and S. Legutke (1997), The Hamburg ocean primitive equation model, *DKRZ Tech. Rep.13*, 98pp., Hamburg.

Zorita, E., H. von Storch, J.F. Gonzales-Rouco, U. Cubasch, J. Luterbacher, I. Fischer-Bruns, S. Legutke, U. Schlese (2003), Simulation of the climate of the last five centuries, *GKSS Report 2003/12*, Geesthacht.

Reconstruction of past climate changes in the Arctic regions of Russia and Canada

Steffen Holzkämper and Peter Kuhry

Department of Physical Geography and Quaternary Geology, Stockholm University, Sweden

1 Climate reconstruction from proxy data

The reconstruction of past climate and environmental conditions can help to improve future climate model runs and to assess implications of the projected climate change for ecosystems. Direct calibration and validation of climate models with observed meteorological data is limited by the length of available time series and by the sometimes poor spatial data coverage at remote sites. Proxy data from e.g. ice cores, tree rings, lake sediments or peat deposits can provide valuable information to overcome this problem. The majority of former studies on past climate change has utilized single proxies only, e.g. tree ring widths or pollen sequences with their respective transfer functions. The significance of only a single climate proxy is, however, limited due to processes that are not directly related to climate, such as biological or local geographical factors (soil properties, hydrological conditions, wind exposure etc.). Therefore, the application of multi-proxy approaches is desirable, which takes several indicators of climate and environmental change into account, by that providing a more meaningful climate reconstruction. Another important issue is the chronological control of the studied records which puts the studied parameters into a solid time frame. Reservoir effects, dead carbon fractions of bulk sediments and missing rings in dendrochronology are critical questions which can be minimized by viewing a broader range of available proxies from one region, thus once more favouring the multi-proxy approach in comparison to single-proxy studies.

The overall aim of the EU-GLIMPSE project was to address and reduce the deficiencies in our understanding of the arctic climate and to improve the representation of arctic climate feedbacks in GCMs and RCMs. The contribution of Stockholm University included the development of a paleoclimatological database over the past ~1000 years for validation of climate model output, with an emphasis on the investigation of multi-centennial to multi-decadal variability in selected arctic regions. Our review of literature and new sampling and analysis focuses on two regions characterized by gradual lowland transitions in climate, vegetation and permafrost conditions, i.e. Northeast European Russia and the Central Canadian Arctic. As a first step, available meteorological data from various databases were collected for these two regions of special interest. The longest records from the north-western Russian weather stations go back to the late 19^{th} century and provide mean monthly air temperature, extreme minimum temperature, precipitation, and snow depth data. Many stations, however, have long gaps before 1950 and after 1990. The meteorological data are the basis for the calibration of the proxy data and indicate the degree of temporal and spatial variability. The next step was to find and evaluate other quantitative or semi-quantitative paleoclimatic or paleoenvironmental investigations which were carried out in the respective regions. Finally, the collection and analysis of new proxy data from the Russian and Canadian Arctic should improve the current status of data paucity and bring new insights in the climatic and environmental history of the selected Arctic regions over the past ~1000 years.

2 Observed meteorological data from the Arctic

Within the GLIMPSE project, the availability of observed meteorological data from the Russian and Canadian Arctic was checked and the data were collected and arranged in a single database. A selection of meteorological stations, measured parameters and length of available records is given in Figure 1.

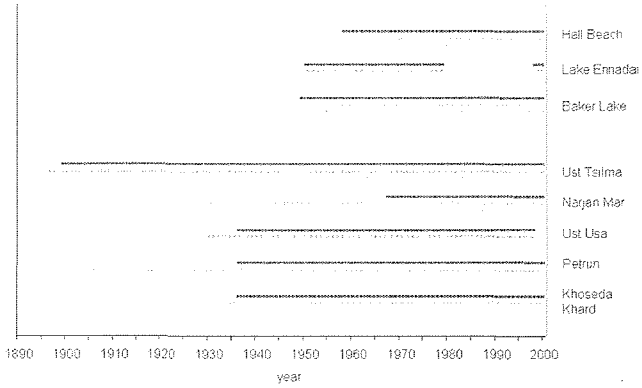

Figure 1: Selected weather stations with periods of observations of monthly mean air temperature (upper bars), precipitation (center bars), and snow depth (lower bars) for Central Canada and Northeast European Russia.

3 Published proxy data from Russian and Central Canadian arctic regions

The number of studies addressing the past one to two millennia in the Russian and Canadian Arctic is very small and most of them very limited in their significance when it comes to quantitative results. For Central Canada, a multi-proxy study was recently carried out in the boreal forest region near Lake Athabasca, and the semi-quantitative results suggest that the period between ~1700 and 1780 was relatively cold and dry, whereas the subsequent time interval until ~1940 was wet and warm. Since then, the climatic conditions are described as intermediate [*Wolfe et al.*, 2005]. Another study based on tree ring width comes to the conclusion that the climatic pattern over the past four centuries was significantly different in the region East of the Hudson Bay and West of the Hudson Bay [*Overpeck et al.*, 1997]. In comparison to the western side, the east was subject to larger fluctuations with a pronounced Little Ice Age and subsequent 20th century warming. In the western Russian Arctic, a quantitative climate reconstruction has been made for a site on Yamal Peninsula, which is based on ring width of trees. The reconstruction goes back until ~4000 years BP, and the data have been analyzed for statistical trends and variances [*Hantemirov and Shiyatov*, 2002]. A quantitative reconstruction of paleotemperatures covering the last hundreds of years was derived from diatom and chironomid transfer functions applied to lake sediment sequences in the Eastern European Tundra *(Solovieva et al.*, 2005). A large number of tree ring records was investigated over the whole Arctic region, but no regional climate reconstruction has yet been derived from this extensive data set [*Briffa*, 1995]. More studies exist which address the climate evolution of the entire Holocene, though with considerably lower temporal resolution [*Nichols*, 1967; *Solovieva et al.*, 2005; *Väliranta et al.*, 2003]. From the screening of available information on Arctic climate of the past 2000 years, the urge for additional data from these regions becomes clear.

New proxy data from Northeast European Russia and the Central Canadian Arctic

Over the last two years, we have collected and analyzed a large number of proxy samples and are currently working on the final analyses and interpretation of the data. We investigate climate proxies from two remote areas: the Moreju River catchment in the Northeast European Russian Arctic and the Kazan River catchment in the Central Canadian Arctic (Nunavut). The Moreju River, which we visited in summer 2004 (Figure 2), drains directly into the Barents Sea; the vegetation of the sampling area, which is located ~20 km south of the coast, is mainly shrub and lichen tundra, but favorable micrometeorological and

hydrological conditions along the river valley render the survival of small forest islands possible. The area has (dis)continuous permafrost. A frequent problem with field work in the Arctic is transportation. In order to cover a larger area for sampling, we used inflatable rubber boats which enabled us to float down the Moreju River with breakpoints at promising sites for sampling. However, the sampling strategy and equipment had to be adjusted to the limited load capacity. We were able to collect tree trunks, lake sediments and peat deposits for a detailed reconstruction of climate during the last 1000 years.

The Canadian study area was visited in summer 2005. Two sample sites near Lake Ennadai and Misaw Lake were chosen, where forest patches, small lakes and peatlands were abundant, thus enabling us to collect the same set of samples as during the Russian field trip. Again, the equipment had to be minimized, as both lakes are remote and accessible by float plane only. The applied methods to investigate the collected samples from Russia and Canada include tree ring analysis (ring width, wood density, $\delta^{13}C$ and $\delta^{18}O$ of the cellulose fraction), the study of lake sediments ($\delta^{18}O$ of aquatic cellulose, diatom-, chironomid-, and cladocera assemblages), and the analysis of peat deposits (macrofossil assemblage and $\delta^{18}O$ of the cellulose of *Sphagnum*). Dating of the samples is done by ^{14}C (lake sediments and peat), ^{210}Pb (lake sediments and peat), or dendrochronological software (trees). Here we present preliminary results for the Russian area.

Tree rings:

During the field trip in summer 2004, we have collected 5 disks of spruce which were growing close to the shore of the Moreju River. One of the trunks was partly buried by sand and lying on the river bench. The oldest tree sampled is 145 years old and started growing in ~1845 a.d. A 50 year old living tree was sampled to complete the time series to the present.

Lake sediments:

A small lake (~0.2 km^2) close to the Moreju River was chosen to core sediments. The sediment cores with a composite depth of 88 cm is currently being analyzed for diatom- and chironomid assemblages and oxygen isotope ratios and dated by the radiocarbon and ^{210}Pb methods. The first radiocarbon date indicates that the entire record sampled covers the period of the past ~2500 years. A specialty of the sediment is the presence of two peat layers which interrupt the clayish core at a depth of 64 and 72 cm. These may indicate periods when the lake has dried out and rendered the growth of mosses possible, probably due to phases of less precipitation and/or higher temperatures. Further radiocarbon dates will provide information on the precise timing and duration of these dry periods.

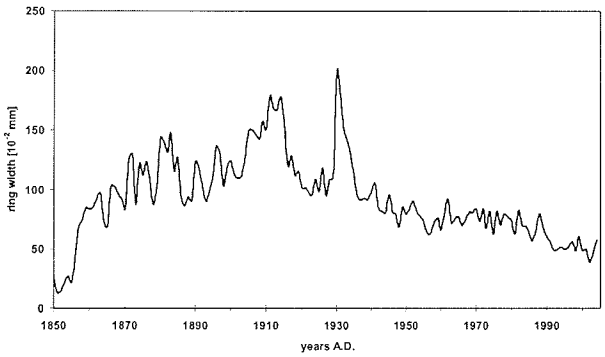

Figure 3: Preliminary results from ring width measurements of five spruce trees from the Moreju River catchment, northeastern European Russian Arctic. The curve is the undetrended mean value, uncorrected for possible missing rings

Peat profiles:

A 37 cm deep peat profile was sampled from a relatively wet area typical for the cracks in polygonal peat plateaus. Ongoing analyses include plant macrofossil and oxygen isotope analysis and radiocarbon dating. The first date at the bottom of the profile gave an age of 550 ^{14}C-years BP. The assemblage of the plant macrofossils is rather uniform throughout the profile. The main plant species identified is *Sphagnum lindbergii* which accounts for 75 to 85 % of the peat deposit. The remaining parts consist of varying percentages of *Dicranum*, *Drepanocladus* and *Polytrichum*. A preliminary conclusion that can be drawn from the ongoing analysis is a rather stable environment that did not force any major changes in plant assemblages in that area.

5 Conclusions and outlook

The general need for more well-dated climate archives from the Arctic region is obvious. With new proxy samples and analyses a step into that direction is taken. Our final results will provide important information about the climatic and environmental history of the Arctic and help to improve future climate model runs.

References

Briffa, K.R., Unusual twentieth-century summer warmth in a 1,000-year temperature record from Siberia, *Nature, 376*, 156-159, 1995.

Hantemirov, R.M., and S.G. Shiyatov, A continuous multimillennial ring-width chronology in Yamal, northwestern Siberia, *The Holocene, 12* (6), 717-726, 2002.

Nichols, H., The Post-glacial history of vegetation and climate at Ennadai Lake, Keewatin, and Lynn Lake, Manitoba (Canada), *Eiszeitalter und Gegenwart, 18*, 176-197, 1967.

Overpeck, J., K.A. Hughen, D. Hardy, R. Bradley, R. Case, M. Douglas, B. Finney, K. Gajewski, G. Jacoby, A. Jennings, S. Lamoureux, A. Lasca, G. MacDonald, J. Moore, M. Retelle, S. Smith, A. Wolfe, and G.A. Zielinski, Arctic environmental changes of the last four centuries, *Science, 278*, 1251-1256, 1997.

Solovieva, N., V.J. Jones, L. Nazarova, S.J. Brooks, H.J.B. Birks, J.-A. Grytnes, P.G. Appleby, T. Kauppila, B. Kondratenok, I. Renberg, and V. Ponomarev, Palaeolimnological evidence for recent climatic change in lakes from the northern Urals, arctic Russia, *Journal of Paleolimnology, 33*, 463-482, 2005.

Wolfe, B.B., T.L. Karst-Riddoch, S.R. Vardy, M.D. Falcone, R.I. Hall, and T.W.D. Edwards, Impacts of climate and river flooding on the hydro-ecology of a floodplain basin, Peace-Athabasca Delta, Canada since A.D. 1700, *Quaternary Research, 64* (2), 147-162, 2005.

Väliranta, M., A. Kaakinen, and P. Kuhry, Holocene climate and landscape evolution East of the Pechora Delta, East-European Russian Arctic, *Quaternary Research, 59*, 335-344, 2003.

Frost flowers on sea ice - a multi-disciplinary research effort for the upcoming International Polar Year 2007/09

L. Kaleschke[1], A. Richter[1], J. Burrows[1], G. Heygster[1], J. Notholt[1], H.-W. Jacobi[2], R. Weller[2], S. Kern[3], R. Sander[4], J. Hollwedel[5], R. von Glasow[5]

[1] Institute of Environmental Physics, University of Bremen
[2] Alfred Wegener Insitute for Polar and Marine Research, Bremerhaven
[3] Institute for Marine Research, University of Hamburg
[4] Max-Planck Institute for Chemistry, Mainz
[5] Institute of Environmental Physics, University of Heidelberg

Sea salt aerosol is a very important constituent of the polar troposphere. It plays a role in the phenomena of Arctic Haze and the so-called Bromine Explosion. Bromine radicals released from sea salt have a major influence on atmospheric chemistry, e.g. for ozone depletion and the biogeochemical mercury cycle. Sea salt ions captured in ice cores are of fundamental importance for the paleo-climatic interpretation of these. Recently it was hypothesized that salty frost flowers that grow on fresh sea ice are the major source of sea salt aerosol in the polar regions. This hypothesis has many implications in different fields of research. These sea ice related physico-chemical processes are key issues in the upcoming International Polar Year 2007/09. Here we provide a brief introduction.

It was already recognized by Fridtjof Nansen that the Arctic is not a pristine environment but is being influenced by air masses that are transported from midlatitudes. More recently it is apparent that the Arctic troposphere is a unique chemical reactor playing an important role for global change. The phenomenon of a dense Arctic Haze was frequently mentioned by U.S. pilots flying over the Arctic Ocean from the late 1940s to the early 1960s [Mitchell, 1957]. Since the 1970s the Arctic Haze phenomenon was investigated in numerous studies [e.g. Shaw, 1995; Barrie, 1986].

The first indication of photo-oxidant chemistry came from analysis of the atmospheric sulfur seasonal cycle by Barrie and Hoff [1984], who observed a significant decrease of the sulfur dioxide to sulphate ratio in spring. In 1988 Barrie et al. [1988] observed a drop of ozone at polar sunrise and a coincident increase in filterable bromine [Niki and Becker, 1993]. The bromine sources and involved chemical mechanisms were unknown at that time.

Fan and Jacob [1992] described a heterogeneous autocatalytic reaction that causes an exponential increase of gaseous bromine radicals. The primary bromine source was identified to be sea salt aerosol generated by breaking waves on the ocean surface. This reaction became known as the so-called bromine explosion [Wennberg, 1999]. The bromide activation is driven by ozone and hydroperoxyl on acidic aerosols in the presence of sunlight, and is catalyzed by hypobromous acid and chloride [Vogt et al., 1996]. The presence of reactive bromine has a strong impact on tropospheric chemistry and is therefore important for the air chemistry of polar regions as well as the global climate system [Gauchard et al. 2005; von Glasow et al., 2004].

The advent of the measurement of tropospheric trace gases from space by the Global Ozone Monitoring Experiment, GOME, led to the discovery of enhanced amounts of BrO close to regions of sea ice in the Northern and the Southern Hemisphere [Richter et al., 1998; Wagner and Platt, 1998].

From the analysis of Antarctic sea salt aerosol it was inferred that brine originating from the sea ice surface was the dominating sea salt source in winter [Wagenbach et al., 1998]. Ion analysis showed a strong, systematic depletion of sulfate with respect to bulk sea water which was explained by the crystallization and precipitation of mirabilite below -8 °C [Nelson and Thompson 1954].

Rankin et al. [2001] hypothesized that frost flowers could be the long sought salt source and showed strong implications for the interpretation of ice core records (Fig. 1). This changed the paradigm on the origin of the primary marine ions found in these climate archives [e.g. Legrand & Mayewski, 1997; Wolff et al. 2003].

Figure1: Frost flowers on sea ice. Photograph by Hans-Werner Jacobi

Frost flowers grow on thin young sea ice from the water vapor phase. These ice crystals grow on a liquid layer of concentrated brine. The liquid brine gets onto the crystals by capillary suction resulting in an ion concentration triple of that of sea water [Martin et al. 1995,1996; Perovich & Richter-Menge, 1994]. It is thought that the delicate crystals are easily blown away by the wind and thus can produce the salty aerosol [Hall and Wolff, 1998; Rankin et al., 2001; Wolff et al. 2003].

A model to estimate the potential frost flower (PFF) coverage was developed by Kaleschke et al. [2004]. The PFF-model is driven by the sea ice concentration derived from satellite measurements and the surface air temperature. Briefly, the model identifies the new ice regions with especially cold surface air temperatures. By using advanced algorithms for sea ice retrieval it is possible to identify the regions where the new sea ice production takes place [Kaleschke et al. 2001, 2004ab; Kern et al. 2003; Spreen et al. 2005]. The regions of high PFF values are frequently connected with regions of enhanced BrO concentrations through air trajectories on a timescale of up to about three days (Fig. 2).

The bromine explosion requires a slightly acidic environment [Fickert et al., 1999]. Today's surface ocean is saturated with respect to calcium carbonate and has a pH of about 8.2 [Orr et al., 2005]. The carbonate ions act as a buffer that stabilizes the pH. For this reason the bromine explosion has not been observed over the open ocean because the pH is above 7. This might be different on the sea ice surface or frost flower aerosol. $CaCO_3 \cdot 6H_2O$ is the first solid salt that appears when the sea water temperature drops below -2.2 C [Weeks and Ackley, 1986]. This probably removes the carbonate from the freezing brine. The remaining liquid will likely be much more sensitive to acidification and is therefore probably a strong potential source for the bromine activation. Very recent preliminary results of a sensitivity study using the atmospheric chemistry models MECCA and MISTRA demonstrated the dramatic influence of a carbonate removal.

The IGBP projects, IGAC and SOLAS, have jointly endorsed the task, Air-Ice Chemical Interactions (AICI), to determine the importance of some of the here mentioned processes, and assess how they would alter with a warming climate and shrinking sea ice cover. The Ocean-Atmosphere-Sea Ice-Snowpack Interactions Study (OASIS) will be the most important

IPY project for the Arctic. Updated information can be found on the OASIS project website at http://www.oasishome.net.

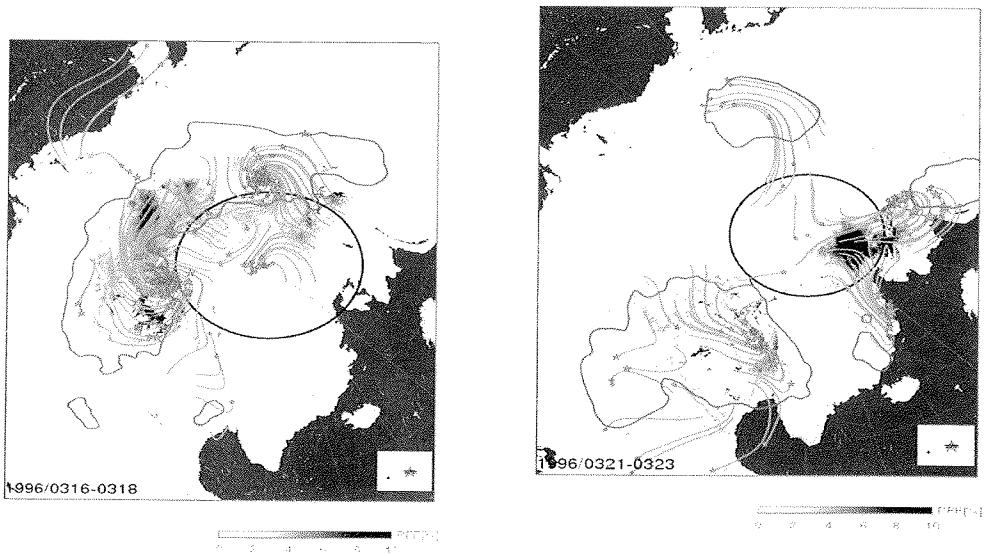

Figure 2: Example total PFF coverage (stars) and enhanced BrO amounts (isolines) over the Arctic. The maximum values of two consecutive days are shown: from 16 (21) to 17 (22) and 17 (22) to 18 (23) March 1996 for PFF and BrO, respectively. The stars mark the endpoints of 24h surface air trajectories starting at relatively large potential frost flower coverages, sampled every 187 km. The PFF field was smoothed to 300 km spatial resolution in order to approximately match the GOME resolution. The total PFF coverage is proportional to the size of the stars. Two stars of 1% and 10% area coverage are shown in the lower right corner for comparison. The isoline corresponds to enhanced BrO amounts of the mean plus one standard deviation. The black circle indicates the almost dark latitudes (solar zenith angle > 80°). Sea ice covered regions are presented in white and the open ocean is colored in black.

References

Barrie, L.A., R.M. Hoff, The oxidation rate and residence time of sulphur dioxide in the Arctic atmosphere, Atmos. Environ., 18, 2711-2722, 1984

Barrie, L.A., Arctic air pollution: an overview of current knowledge. Atmospheric Environment 20 (1986), pp. 643-663

Barrie, L. A., J. W. Bottenheim, R. C. Schnell, P. J. Crutzen, and R. A.Rasmussen, Ozone destruction and photochemical reactions at polar sunrise in the lower Arctic atmosphere, Nature, 334, 138-141, 1988.

Fan, S. M., and D. J. Jacob, Surface ozone depletion in Arctic spring sustained by bromine reactions on aerosols, Nature, 359, 524-552, 1992

Fickert, S., J. W. Adams, and J. N. Crowley, Activation of Br-2 and BrCl via uptake of HOBr onto aqueous salt solutions, J. Geophys. Res., 104(D19), 23,719-23,727, 1999.

Gauchard,P. et al. ; Study of the Origin of Atmospheric Mercury Depletion Events recorded in Ny-Alesund, Svalbard, spring 2003; Atmos. Env., in Press. 2005

Hall , J.S., and Wolff E.W., Causes of seasonal and daily variations in aerosol sea-salt concentrations at a coastal Antarctic station - the seasonal pattern of its chemical composition and radionuclide content, Atmos. Env., 32(21), 3669-3677, 1998

Kaleschke, L., Richter, A., Burrows, J., Afe, O., Heygster, G., Notholt, J., Rankin, A. M., Roscoe, H. K., Hollwedel, J., Wagner, T., Jacobi, H. W., Frost flowers on sea ice as a source of sea salt and their influence on tropospheric halogen chemistry, Geophysical research letters, 31, L16114. DOI: 10.1029/2004GL020655, 2004a.

Kaleschke, L. and G. Heygster, Towards multisensor microwave remote sensing of frost flowers on sea ice, Annals of Glaciology, 39, 219-222, 2004b.

Kaleschke, L., C. Lüpkes, T. Vihma, J. Haarpaintner, A. Bochert, J. Hartmann, G. Heygster: SSM/I Sea Ice Remote Sensing for Mesoscale Ocean-Atmosphere Interaction Analysis. Can. J. Remote Sensing 27,5, 526-537, 2001.

Kern, S. and L. Kaleschke and D. A. Clausi, A Comparison of two 85 GHz SSM/I Ice Concentration Algorithms with AVHRR and ERS-SAR, IEEE Trans. Geosci. and Remote Sensing, 41(10), 2294-2306, 2003.

Legrand, M., P. Mayewski, Glaciochemistry of polar ice cores: A review, Rev. Geophys., 35(3), 219-244, 10.1029/96RG03527, 1997.

Martin, S., R. Drucker, and M. Fort, A laboratory study of frost flower growth on the surface of young sea ice, J. Geophys. Res., 100(C4), 7027-7036, 1995.

Martin, S., Y. Yu, and R. Drucker, The temperature dependence of frost flower growth on laboratory sea ice and the effect of the flowers on infrared observations of the surface, J. Geophys. Res., 101(C5), 12,111-12,125, 1996.

Mitchell, J.M. Jr., Visual Range in the Polar Regions with Particular Reference to the Alaskan Arctic, Journal of Atmospheric and Terrestrial Physics, Special Supplement 1957):195-211

Nelson, K.H., and T.G. Thompson, Deposition of Salts from Sea Water by Frigid Concentration, Journal of Marine Research, 13(2), 166-182, 1954.

Niki, H., Becker K.H. (editors), The tropospheric chemistry of ozone in the polar regions, Proceedings of the NATO Advanced Research Workshop on the Tropospheric Chemistry of Ozone in the Polar Regions held at Wolfville, Nova Scotia, Canada, August 23 - 28, 1992, Springer, 1993

Orr, J.C. et al., Anthropogenic ocean acidification over the twenty-first century and its impact on calcifying organsims, Nature, 437, 681-686, 2005.

Perovich, D., and J. A. Richter-Menge, Surface characteristics of lead ice, J. Geophys. Res., 99(C8), 16,341-16,350, 1994.

Vogt, R., P. J. Crutzen, and R. Sander, A mechanism for halogen release from sea-salt aerosol in the remote marine boundary layer, Nature, 383, 327-330, 1996.

Rankin, A. M., E. W. Wolff, and S. Martin, Frost flowers: Implications for tropospheric chemistry and ice core interpretation, J. Geophys. Res., 107(D23), 4683, doi:10.1029/2002JD002492, 2002.

Richter, A., F. Wittrock, M. Eisinger, and J. P. Burrows, GOME observations of tropospheric BrO in Northern Hemispheric spring and summer 1997, Geophys. Res. Lett., 25(4), 2683-2686, 1998.

Shaw, G.E., The Arctic haze phenomenon, Bulletin of the American Meteorological Society, 76(12), 2403-2413, 1995.

Spreen, G., L. Kaleschke, G. Heygster, Sea Ice Remote Sensing Using AMSR-E 89 GHz Channels, J. Geophys. Res., subm. 2005.

von Glasow, R., R. Kuhlmann, M.G. Lawrence, U. Platt, P.J. and Crutzen, Impact of reactive bromine chemistry in the troposphere, Atmospheric Chemistry and Physics, Vol. 4, pp 2481-2497, 8-12-2004.

Wagenbach, D., F. Ducroz, R. Mulvaney, L. Keck, A. Minikin, M. Legrand, J. S. Hall, and E. W. Wolff, Sea-salt aerosol in coastal Antarctic regions, J. Geophys. Res., 103(D9), 10,961- 10,974, 1998.

Wagner, T., and U. Platt, Satellite mapping of enhanced BrO concentrations in the troposphere, Nature, 395, 486-490, 1998.

Weeks W.F. and S.F. Ackley (1986), The growth, structure, and properties of sea ice, in The Geophysics of Sea Ice, NATO ASI B146, edited by N. Untersteiner, pp. 9-164, Martinus Nijhoff, Zoetermeer, Netherlands, 1996.

Wennberg, P., Atmospheric chemistry: Bromine explosion, Nature 397, 299 - 301, 1999.

Wolff, E.W., Rankin, A.M., and Roethlisberger, R., An ice core indicator of Antarctic sea ice production? ,Geophysical Research Letters. Vol. 30, no. 22. Nov. 2003

Arctic climate projections for the 21st century with the new generation of AOGCMs

Vladimir Kattsov

Voeikov Main Geophysical Observatory, St.Petersburg, Russia

1. Introduction

The most current generation of AOGCM simulations has recently (late 2004 – early 2005) been completed for the Intergovernmental Panel on Climate Change (IPCC) in order to provide input to the IPCC's Fourth Assessment Report (AR4). The AR4 is scheduled for publication in 2007. The standard set of the AR4 simulations includes climate of the 20th century (20C3M), three SRES scenarios (A2, B1, and A1B) for the 21st century, and some others. Ensemble simulations with more than 20 models have become available for community-wide analysis (http://www-pcmdi.llnl.gov/ipcc/about_ipcc.php). A number of diagnostic subprojects within the IPCC modelling project (http://www-pcmdi.llnl.gov/ipcc/diagnostic_subprojects.php) address a range of aspects of arctic climate simulation, including reproducing current climate and its evolution through the 20th century, as well as projections of the future polar climate.

2. Developments since IPCC Third Assessment Report

Compared to the IPCC Third Assessment Report (TAR) (2001) generation of models also used in the recently published Arctic Climate Impact Assessment (ACIA) (Kattsov and Källén, 2005), advances have been demonstrated in developing coupled global AOGCMs. The advances include higher resolutions, improved numerical schemes and parameterizations (e.g. almost all AR4 models now have more or less comprehensive sea-ice dynamics components); decreased necessity in flux adjustments; and better simulations of some aspects of current climate and specific modes of variability. Improved computational strategies, e.g. larger ensembles of simulations, and multi-model ensembles have started to play an increasingly important role in understanding processes responsible for the range of model results.

3. Simulation of the current arctic climate

The ability of AOGCMs to reproduce current climate is among most important prerequisites for credible projections of future climate using these models. Compared to the TAR and ACIA, the AR4 multi-model ensemble has demonstrated some improvement is simulations of the basic surface climate variables (Chapman and Walsh, 2005; Kattsov et al., 2005). An example of such improvement is shown at Figure 1 comparing the model mean precipitation over the Arctic Ocean within 70°N latitude simulated by the AR4 models and their TAR versions against the updated observational regional arctic climatology of Bryazgin (1976) and the reanalysis data (ERA-40).

According to TAR, biases in simulations of the atmospheric and oceanic circulation in the high latitudes are among evident causes of biases in sea-ice simulations with individual models. E.g., the across-model variance of sea level pressure (SLP) is greater over the Arctic region than anywhere else in the Northern Hemisphere (NH). While generally decreased since TAR, at least in the northern polar region (Chapman and Walsh, 2005), SLP biases suggest that the wind fields driving the AOGCM sea-ice components, however advanced their dynamics are, are likely to be responsible for a significant part of the biases in simulated geographical distributions of sea-ice mass and velocities (Bitz et al., 2002; Walsh et al., 2002). So are surface heat fluxes, whose errors (Sorteberg et al., 2005) may result in particular from inadequate parameterizations of atmospheric boundary layer (under stable conditions such as over ice, in the night, and in the wintertime), high latitude cloudiness

demonstrating striking inter-model scatter in the current climate annual cycle (e.g. Kattsov and Källén, 2005), etc.

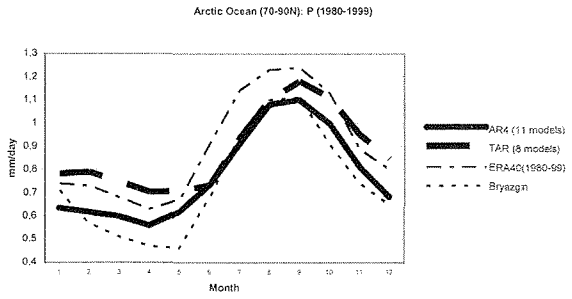

Figure 1. Precipitation seasonal cycle over the Arctic Ocean within 70°N latitude (1980-1999): model means for two subsets of models: 11 AR4 models whose earlier versions were available from TAR, and the corresponding 8 TAR versions.

4. Simulation of the arctic climate evolution through the 20th century

Arctic warming observed in mid-20th century has become one of burning issues in discussions of the attribution of the late 20th century warming. While there are a few mechanisms suggested to explain the mid-20th century arctic warming, there is a broad consensus that it was a manifestation of the natural variability inherent to the climate system. Some scientists believe that the late 20th century warming was of the same nature, however others find it very unlikely that it can be explained by the natural variability alone. It is also unlikely that further analysis of the available scarce data of historical instrumental observations in the Arctic will add a lot in the future to the current understanding of the phenomenon. On the other hand, AOGCM multi-member and multi-model ensemble simulations show considerable promise in this respect.

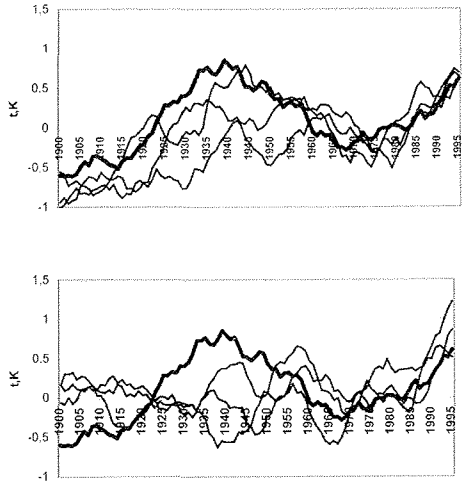

Figure 2. Surface air temperature (over the Arctic Ocean within 70°N latitude) anomalies in the 20th century (relative to 1961-1990) simulated by a subset of AR4 models (thin lines) as compared against the observational data (thick lines, Polyakov et al., 2003): ECHO-G (left) and ECHAM5/MPI-OM (right). 11-year smoothing is applied both to the simulation and observational data.

Most of the AR4 model ensembles show an encouraging ability to reproduce the warming trend in the Arctic for the late 20th century that is not seen in the control runs with the same models. Many, but not all, of the models are also able to capture the other major feature of the 20th century arctic climate (Figure 2, see also Wang et al., 2005). From the view point of AOGCM evaluation and credibility of projections of the future climate, it seems sufficient that the models are able to reproduce the amplitude and frequency, but not the phase (precise timing of the maxima and minima) of the long-term natural variability in the Arctic.

5. Projections of arctic climate change in the 21st century

A robust feature of climate models since early simulations of the climate system response to increases in atmospheric concentrations of greenhouse gases has been a poleward retreat of snow and ice and the 'polar amplification' of increase of air temperature in the lower troposphere, which is particularly strong in the Arctic. The polar amplification is usually attributed to positive feedbacks in the climate system, the cryosphere being of prime importance. While evaluating cryospheric feedbacks in recent years has been marked by a certain progress, substantial uncertainty remains as to their magnitudes, and their representation in AOGCMs (see e.g. NRC, 2003). This is one factor contributing to a spread of modelled climate responses in high latitudes. On the global scale the surface albedo feedback is positive in all the models, with a spread among the models much smaller than that of cloud feedbacks. Understanding and evaluating sea-ice feedbacks is complicated by their strong coupling to processes in the high-latitude atmosphere and ocean, particularly to polar cloud processes and ocean heat and freshwater transport. Scarcity of observations in polar regions (e.g. of sea ice thickness) also hampers evaluation. However, new techniques allowing for estimating the sea-ice and land-snow albedo feedbacks have been developed and applied to climate models (e.g. Winton, 2005).

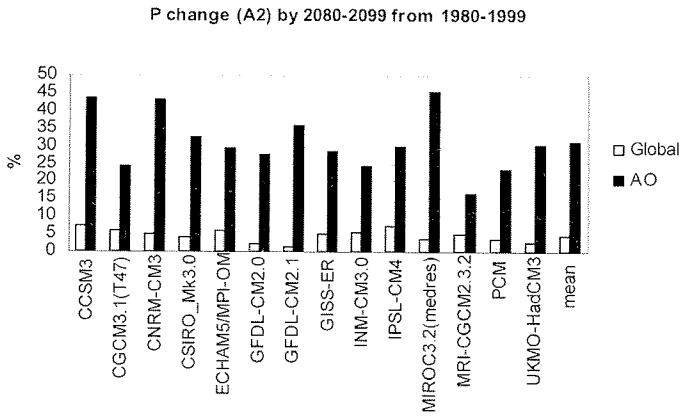

Figure 3. Annual mean precipitation changes (%) from 1980-99 by 2080-99 in A2 scenario: global and over the Arctic Ocean (70-90°N).

Along with the amplified warming, projected arctic climate changes include decrease of cold air outbreaks and frost days (Vavrus et al., 2005); sea level pressure decrease over the high latitudes (Chapman and Walsh, 2005); increased precipitation mean (Figure 3) and intensity and associated risk of flooding, as well as increased river discharge into the Arctic Ocean (Figure 4) (Kattsov et al., 2005; Meehl et al., 2005); and shrinkage of marine and terrestrial

cryosphere (Arzel et al., 2005; Zhang and Walsh, 2005). In a few projections, perennial arctic sea ice disappears by the end of the 21st century. While the above projected changes are relatively large in the Arctic, so are the interannual variabilities, which (together with the above mentioned inter-model scatters) prevent the projected changes in the arctic surface climate from becoming significant within next few decades (Chapman and Walsh, 2005; Kattsov et al., 2005). On the other hand, for the next several decades, models do not show dramatic differences in projections of the basic surface climate variables due to differences in the emission scenarios.

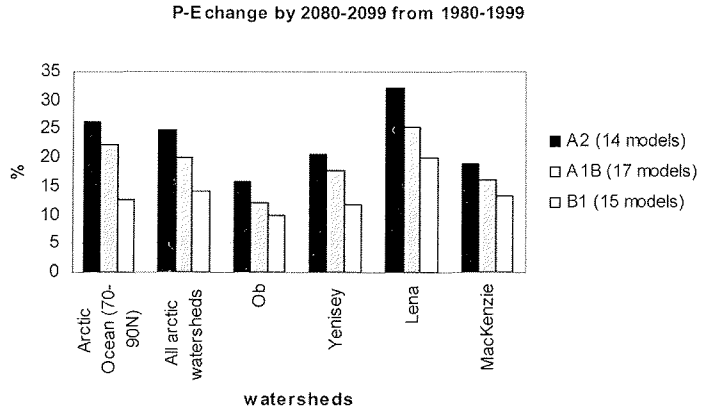

Figure 4. Annual mean P-E (discharge) change in A2, A1B, and B1 scenarios by the 2080-99 over different regions: the Arctic Ocean (70-90°N); All Arctic Ocean terrestrial watersheds; the Ob; the Yenisey; the Lena; and the Mackenzie watersheds.

6. Conclusions

New computational strategies and methods of model evaluation are developing, however defining a robust 'model metric' remains a challenge facing the climate modelling community. Having the large inter-model differences in sensitivity to external forcing, a quantitative likelihood weighting of different models in multi-model ensembles should improve credibility of the climate projections. Further progress in developing observational tests aimed at constraining climate sensitivity is hampered by the scarcity of observational data in the polar regions, sea ice thickness being a particular problem. Detailed satellite and in situ datasets should help to improve parameterizations of polar processes and their interaction and to develop appropriate metrics allowing to test against observations the AOGCM parameterizations and their effect on climate sensitivity. The observational and modelling activity expected during the International Polar Year 2007-2008 has a particular potential importance in this context.

Acknowledgements

We acknowledge the international modeling groups for providing their data for analysis, the Program for Climate Model Diagnosis and Intercomparison (PCMDI) for collecting and archiving the model data, the JSC/CLIVAR Working Group on Coupled Modelling (WGCM) and their Coupled Model Intercomparison Project (CMIP) and Climate Simulation Panel for organizing the model data analysis activity, and the IPCC WG1 TSU for technical support. The IPCC Data Archive at Lawrence Livermore National Laboratory is supported by the Office of Science, U.S. Department of Energy. This study was supported by the US National Science Foundation via the International Arctic Research Center of the University of Alaska Fairbanks

(subaward UAF05-0074 of OPP-0327664); by the Russian Foundation for Basic Research (Grants 05-05-65093 and 05-05-08064ofi_a) and INATS (Grant 03-51-4620). Thanks to Tatyana Pavlova, Bill Chapman and Veronika Govorkova for postprocessing AR4 model outputs and their analysis used in this study.

References

Arzel, O., T. Fichefet, and H. Goosse, 2005: Sea ice evolution over the 20th and 21st centuries as simulated by the current AOGCMs. *Ocean Modelling* (in press).

Bitz, C., G. Flato, and J. Fyfe, 2002: Sea ice response to wind forcing from AMIP models. *J. Climate*, 15, 523-535.

Bryazgin, N. N., 1976: Yearly mean precipitation in the Arctic region accounting for measurement errors. (In Russian) *Proc. Arctic Ant. Res. Inst.*, **323**, 40-74.

Chapman, W.L., and J.E. Walsh, 2005: Simulations of arctic temperature and pressure by global coupled models. *J. Climate* (in press).

Kattsov, V., and E. Källén, 2005: Future Changes of Climate: Modelling and Scenarios for the Arctic Region, in *Arctic Climate Impact Assessment (ACIA)*. Cambridge University Press, Cambridge, United Kingdom and New York, NY, USA. (in press) (also available from http://www.acia.uaf.edu/)

Kattsov, V., J.E. Walsh, W. Chapman, V. Govorkova, T. Pavlova, and X. Zhang, 2005: Simulation and Projection of Arctic Freshwater Budget Components by the IPCC AR4 Global Climate Models. *J. Hydrometeorology* (under revision).

Meehl, G.A., J.M. Arblaster, and C. Tebaldi, 2005: Understanding future patterns of precipitation extremes in climate model simulations. *Geophys.Res. Lett.* (in press).

NRC, 2003: National Research Council of the National Academies, 2003: Understanding climate change feedbacks. Washington D.C.: National Academies Press. 152 pp.

Polyakov, I., R. Bekryaev, G.Alekseev, U. Bhatt, R. Colony, M. Johnson, A. Makshtas, D. Walsh, 2003: Variability and trends of air temperature and pressure in the maritime Arctic, 1875-2000. *Journal of Climate*, 16, 2067-2077.

Sorteberg, A., V. Kattsov. J. Walsh, T. Pavlova, 2005: The Arctic Surface Energy Budget as Simulated with the IPCC AR4 AOGCMs. *Climate Dynamics* (under revision).

Vavrus, S.J., J.E. Walsh, W.L. Chapman, and D. Portis, 2005: The behavior of extreme cold air outbreaks under greenhouse warming. *Int. J. Climate* (under revision).

Walsh, J. E., V. Kattsov, W. Chapman, V. Govorkova, and T. Pavlova, 2002: Comparison of Arctic climate simulations by uncoupled and coupled global models. *J. Climate*, **15**, 1429-1446.

Wang, M., J.E. Overland, V. Kattsov, J.E. Walsh, X. Zhang, and T. Pavlova, 2005: Intrinsic Versus Forced Variation in Coupled Climate Model Simulations over the Arctic during the 20th Century, *J. Climate* (under revision).

Winton, M., 2005: Surface Albedo Feedback Estimates for the AR4 Climate Models. *J. Climate* (in press).

Zhang, X., and J.E. Walsh, 2005: Toward a seasonally ice-covered Arctic Ocean: scenarios from the IPCC AR4 model simulations. *J. Climate* (in press).

Fresh water balance of the Arctic Ocean and adjacent seas: Results from NAOSIM-LRM hindcast experiments

C. Köberle and R.Gerdes

Alfred Wegener Institute of Polar- und Marine Research, Bremerhaven

Available observations indicate large variability of components of the Arctic fresh water balance, namely the halocline and sea ice reservoirs and the export rates of sea ice and liquid fresh water through Fram Strait. The Arctic Ocean is a large fresh water source for the Atlantic and thus changes in its export rate to lower latitudes have the potential to affect the large scale Atlantic circulation.

We present results from a 54-year hindcast experiment with the low (1degree) resolution version of the coupled ocean-sea ice model NAOSIM. Forcing follows the AOMIP (Arctic Ocean Model Intercomparison Project) specifications. Experiments are designed to avoid excessive damping of anomalies that usually occurs with restoring of surface salinity to climatological values. We discuss the budgets of the Arctic Ocean fresh water components sea ice and liquid fresh water separately.

The volume of Arctic sea ice at a given moment is the result of net ice production- freezing minus melting- and ice exports through Fram Strait, Barents Sea Opening and the Canadian Archipelago. The export through Fram Strait is by far the largest component. As shown in Köberle and Gerdes 2003, ice production variability is more determined by the 2m air temperature, while the export at different times is either determined by the position of the local pressure field or by the thickness of the ice passing through Fram Strait. The latter is the result of this ice production's location and history.

The Arctic fresh water content at a given moment is the result of fresh water input through precipitation minus evaporation, net ice production, river runoff and a time constant correction flux and the export through the above mentioned straits. Large changes- even trends- are visible in fresh water content, but not in any of the components. From that we conclude that existing changes over longer times are the result of small but persistent imbalances between input and export. The input variability has a much shorter time scale and is mostly due to the variability of the net ice production. The export variability is dominated by Fram Strait export and exhibits a decadal timescale. Fram Strait export shows one extreme export event that develops from the end 50s to a peak in the early 60s and than returns to its former level until the beginning of the 70s. This event is most prominently visible in the East Greenland current and to a smaller degree in increased southward Barents Sea liquid fresh water transport. A decomposition of Fram Strait southward fresh water transport reveals the volume transport as the largest contribution. The vertically integrated stream function indicates a large difference also in the Barents Sea area. Barents Sea fresh water and sea ice export are increased. The salinity gradient on a section across Fram Strait is much smaller than before and after the transport event. From all this evidence we conclude, that an extreme amount of ice from the Barents Sea melts on its way with the northward recirculating Spits Bergen current. The resulting fresh water input decreases the density gradient across Fram Strait and thus leads to a reduced meridional velocity. The Fram Strait fresh water export during the whole 50 years of the integration is actually dominated by this one freak event, before and after the variability is comparably small.

Balances have also been calculated for the Greenland Sea the Canadian Archipelago and Baffin Bay. From that we calculate the amount of the liquid fresh water arriving at the Labrador Sea on the one hand via Fram and Denmark Strait and on the other hand via the Canadian Archipelago and Davis Strait. The total amounts arriving on either pathway are of similar magnitude. The transport convergence in the Labrador Sea is 2700 km^3 per year.

References

Köberle, C.; Gerdes, R. (2003): Mechanisms determining the variability of Arctic sea ice conditions and export, Journal of Climate, 16, 2843-2858

Köberle, C.; Gerdes, R. (2005): Simulated variability of te Arctic Ocean fresh water balance 1948-2003, in preparation.

Atmospheric sensitivity to surface forcing in a regional climate model

Morten Køltzow

Norwegian Meteorological Institute, Oslo

Introduction

The technical basis for future climate projection scenarios is the use of atmosphere-ocean general circulation models (AOGCMs). Due to limited computer resources, transient AOGCM simulations are made with a rather coarse resolution. Typical horizontal resolution is above 300km in the atmosphere and 150km in the oceans (Lambert and Boer, 2001). This resolution is insufficient for most impact studies of climate change, and may also constitute an important source of errors in climate simulations related to regional-scale patterns. Climate models have in general considerable difficulties in reproducing the observed Arctic climate (Walsh et al., 2002, Covey et al., 2003). This may be partly due to coarse resolution, inadequate model description of in situ physical processes, and from model imperfections causing errors at lower latitudes. If resolution is a dominating source of error, one way to improve Arctic and sub-Arctic climate simulations is to run a regional climate model (RCM). Given that the spread amongst AOGCM results at high latitudes probably also is connected with in situ physical processes involved in feedback chains for which sea-ice is a key factor (Curry et al., 1996), pure atmospheric downscaling is believed insufficient, and a coupled regional climate model is needed. The added value of a coupled RCM for the Arctic depends on (1) the quality of the coupled RCM itself, and (2) the relative importance of lateral atmospheric boundary conditions and the in situ surface forcing associated with the sea surface and sea ice surface. In the present study we want to study the relative importance of the surface forcing. This is carried out by doing sensitivity experiments with the regional atmospheric model HIRHAM. The atmospheric sensitivity to sea surface temperature, sea ice albedo, sea ice fraction and sea ice thickness is examined. One key factor for the relative importance of surface forcing is the size of the integration domain, but as will be shown, also in small domains the mentioned surface forcing may have a large impact.

HIRHAM is constructed with dynamics from the HIRLAM system and with physics from the ECHAM4 climate model at Max Planck Institute in Hamburg. The model is described in detail by Christensen et al. (1996). Different versions of the model have earlier been used for downscaling studies at several institutes (e.g. met.no, DMI and AWI). In the model, sea surface temperature and sea ice fraction and sea ice thickness are prescribed while sea ice surface temperature is calculated based on energy fluxes between the atmosphere and the surface, and the heat transport from the ocean and through the sea ice to the sea ice surface. For all experiments the horizontal resolution is 0.5°, with 19 vertical levels. The integration domain differs between the different experiments described.

Snow and sea ice albedo

Surface albedo is a key climate parameter deciding the amount of absorbed solar radiation at the surface. The parameterization of snow and sea ice albedo is especially important since a pronounced annual cycle is found due to changes in snow and sea ice features during the year (Winther et al., 2002, Perovich et al., 2002). The original albedo scheme in HIRHAM has been validated against observed albedo from the SHEBA experiment, and several deficiencies were found. In late winter and early spring when snow cover is present at the sea ice, too low sea ice albedo was calculated. And, in summer a too high surface albedo was used, due to neglecting the effect of melt ponds on the sea ice. A new scheme was then developed based on SHEBA data and literature studies (Køltzow, 2003). Presented here are results from the last 8 year of 9 year long simulations with the original and the new sea ice albedo scheme. The integration domain is shown in Figure 1. The new albedo scheme give higher sea ice albedo in winter and spring and lower sea ice albedo in summer (June and July) due to the

effect of snow cover and formation of melt ponds, respectively. Change in albedo also change absorbed solar radiation at the sea ice surface. In April and May, 4W/m2 less solar radiation is absorbed with the new scheme averaged for the integration domain. Furthermore, 2W/m2 more solar radiation is absorbed in the summer. For pure sea ice covered areas these changes are as high as up to 15W/m2 in monthly means. Clear impacts are seen in both 2m air temperature and mean sea level pressure.

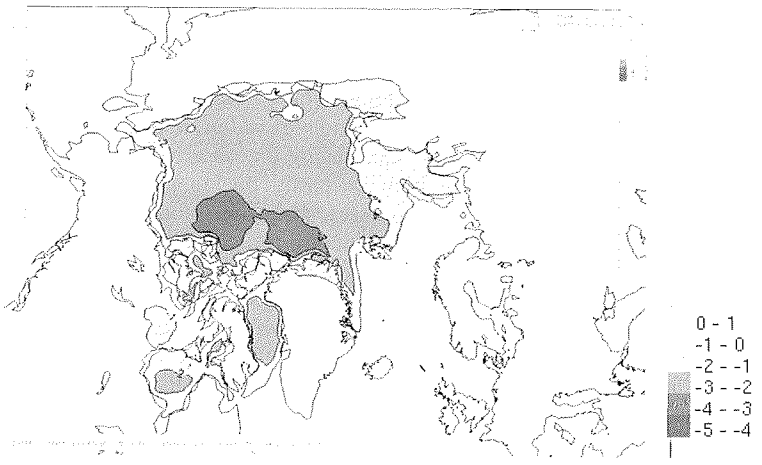

Figure 1. Differences between 2m air temperature average over March, April and May for 8 years from new and old sea ice albedo.

Figure 1 show difference in the 2m air temperature average over March, April and May with the new and old sea ice albedo scheme. For large parts of the Arctic the new scheme is 2-3 °C colder than the old. The new scheme is also in better agreement with ERA40 temperature, but still, HIRHAM has a warm bias in Arctic (not shown). A similar, but smaller response is evident in autumn during refreezing of the sea ice. In the summer season (June, July and August) and winter season (December, January, February) the difference in air temperature is small because the sea ice surface temperature is close to melting point, and the lack of solar radiation, respectively. An impact is also seen in mean sea level pressure. Differences of 3-4 hPa are observed. Compared to ERA40 a clear positive impact is seen in spring and autumn. However, during summer a too strong high centred above the North Pole (not shown) is found with the new scheme.

Sea ice thickness

High uncertainty is associated with sea ice thickness in the Arctic climate, from both an observational and climate modelling aspect. However, sea ice plays an important role in the Arctic (winter) climate as the sea ice acts like an insulator, so that the cold atmosphere don't feel the relative warm ocean beneath. The insulator effect is further highly dependent on sea ice thickness. A common approach when running an atmospheric model for sea ice covered areas is to prescribe constant sea ice thickness. To investigate the importance of this choice, we made three simulations for a small integration domain covering the Beaufort Sea, with prescribed sea ice thickness of 1m, 2m and 4m. Area average of minimum 2m air temperature in winter for all sea ice covered areas differed by 10°C in monthly mean between the thinnest and thickest sea ice, while the simulation with 2m sea ice were approximately 5°C colder than the simulation with 1m sea ice. This underlines the large uncertainty and the need for more accurate knowledge of sea ice thickness in order to achieve skilful modelling of the Arctic climate.

Sea surface temperature and sea ice concentration

To investigate the effect of sea surface temperature and sea ice concentration on the atmosphere two experiments with HIRHAM were performed. The first experiment is a downscaling of 15years of "today's" climate from the Max Planck Institute (MPI) Global Climate Model (ECHAM5/OPYC3). Downscaling domain is shown in Figure 2, and HIRHAM is forced with wind, temperature, pressure and humidity at the lateral boundary and with sea surface temperature and sea ice concentration at the surface boundary. All these variables are from the ECHAM5/OPYC3 model. In the second experiment, the surface forcing in the Atlantic and European part of Arctic are replaced with similar data from the Hadley centre Global Climate Model (HadAM3H).

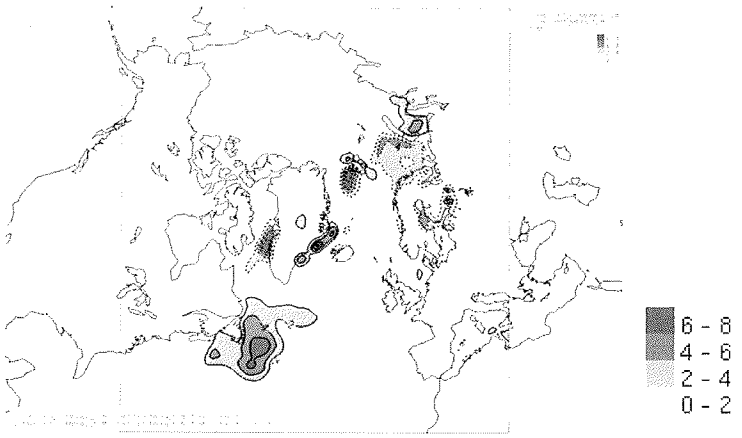

Figure 2. Differences between surface temperature from downscaling with Hadley centre data and MPI data in December (monthly mean over 15year). Solid lines indicate that Hadley Centre data is colder, and dashed lines implies MPI is colder.

Figure 2 show the difference in surface temperature between the experiments as a mean over 15 December months. The sea surface from the HADLEY model is colder than the MPI model east of New Foundland, while the opposite is true in the Barents Sea. Differences are also found associated with the sea ice boarder west and east of Greenland. The different surface forcing found in December is typical for all winter months, while the differences in summer months are smaller and more arbitrary. Looking at response in mean sea level pressure pattern, the highest signal is found in periods with highest surface forcing. In Figure 3, the difference between the mean sea level pressure for December in the two experiments is shown. The colder sea surface east of New Foundland is connected with a decrease in the strength of the Icelandic low, while a higher surface temperature in the Barents Sea decreases the surface pressure in the area. The resulting response seems reasonable with decreased storm-track activity associated with colder sea surface. However, even though the difference in surface forcing is very similar through the winter, the response in surface pressure differs from month to month (not shown). The response is more complex and not as easy to explain later in the winter. It seems reasonable to conclude that not only the location and strength of the surface forcing is important for the response, but also the flow pattern itself.

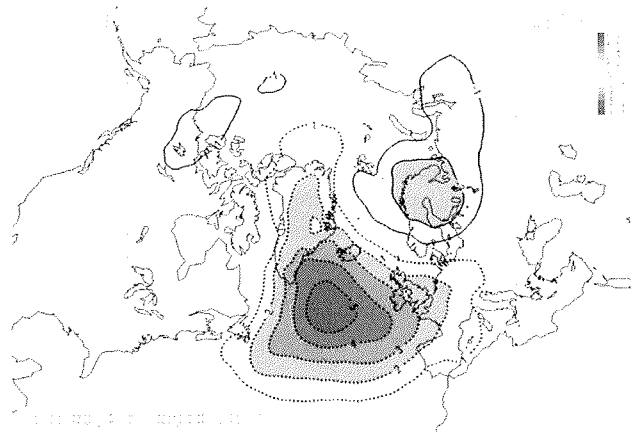

Figure 3. Differences between mean sea level pressure from downscaling with Hadley centre data and MPI data in December (monthly mean over 15year). Dashed lines indicate higher surface pressure with Hadley Centre forcing, and solid lines indicate lower surface pressure.

Summary

Through several different experiments it is shown that the atmosphere at high latitudes is sensitive to surface forcing in regional climate models. This implies that dynamical downscaling (better resolution) and better description of the surface forcing (e.g. a regional coupled model), can improve the simulated Arctic climate from global climate models. An example with change of the parameterization of sea ice albedo also showed that in some seasons the model climate may be improved compared to the ERA40 re-analyses with a more realistic description of physical processes.

Acknowledgement

Many thanks to Jan Erik Haugen, Jens Debernard and Lars Petter Røed for stimulating discussions and help during this work. This work is supported by the EU project GLIMPSE (EVK2-2001-00337) and by the Research Council of Norway under the national project RegClim (grant no. 155976/720).

References

Christensen, J. H., O. B. Christensen, P. Lopez, E. van Meijgaard and M. Botzet (1996), The HIRHAM4, Regional Atmospheric Climate Model, Danish Meteorological Institute – Scientific Report – Copenhagen.

Covey, C., K. M. AchutaRao, U. Cubasch, P. Jones, S. J. Lambert, M. E. Mann, T. J. Phillips, K. E. Taylor (2003), An overview of results from the Coupled Model Intercomparison Project, Global and Planetary Change 37, 103-133.

Curry, J. A., W. B. Rossow, D. Randall & J. L. Schramm (1996), Overview of Arctic Cloud and Radiation Characteristics, Journal of Climate, vol 9, 1731-1764.

Køltzow, M., S. Eastwood and J. E. Haugen (2003), Parameterization of snow and sea ice albedo in climate models, Research report no. 149, met.no.

Lambert, S. J. and G. J. Boer (2001), CMIP1 evaluation and intercomparison of coupled climate models, Climate Dynamics 17, 83-106.

Perovich , D. K., T. C. Grenfell, B. Light and P. V. Hobbs (2002), Seasonal evolution of the arctic sea ice albedo, Journal of Geophysical Research,vol 107, C10, SHE 20, 1-13.

Walsh, J. E., V. M. Kattsov, W. L. Chapman, V. Govokova and T. Pavlova (2002), Comparison of Arctic Climate Simulations by Uncoupled and Coupled Global Models, Journal of Climate, Volume 15, 1429-1446.

Winther, J-G, F. Godtliebsen, S. Gerland and P. E. Isachsen (2002), Surface albedo in Ny-Ålesund , Svalbard: variability and trends during 1981-1997, Global and Planetary Change 32, 127-139.

Assessing Climate Change Impacts in the European North: The BALANCE project

Manfred A. Lange
Institute for Geophysics, Westfälische Wilhelms-Universität Münster, Germany

Introduction/Background

Present predictions of global climate change models (GCMs) indicate an enhanced warming for most of the circumpolar North as compared to the rest of the globe. This is mostly due to a umber of important feedback mechanisms between atmospheric and cryospheric processes such as the ice-albedo feedback. However, global warming also implies that the impacts or consequences of such changes may be equally enhanced compared to other regions. This apprehension is exacerbated by the fact that environmental and human systems in the Arctic are particularly sensitive to changes in physical conditions. The response to climate change impacts in the Arctic, a highly complex but poorly understood system may lead to positive or negative feedback, thus at least potentially implying an enhanced vulnerability (*vulnerability*: the extent to which climate change may damage or harm a system; it is a function of both sensitivity to climate and the ability to adapt to new conditions). There is an urgent need to better understand these processes, which not only involve environmental but also societal processes and components. *Integrated Regional Impact Studies* (IRISs) provide a tool to tackle this problem and to determine the overall vulnerability of the European North to climate change [*Lange and BASIS consortium*, 2003].

This issue lies at the heart of the BALANCE project (*Global Change Vulnerabilities in the Barents Region: Linking Arctic Natural Resources, Climate Change and Economies*), whose major goal lies in *assessing the vulnerabilities of the Barents Sea system to climate change based on a common modelling framework for major environmental and societal components and on the quantification of linkages between these components through an integrated assessment model.*

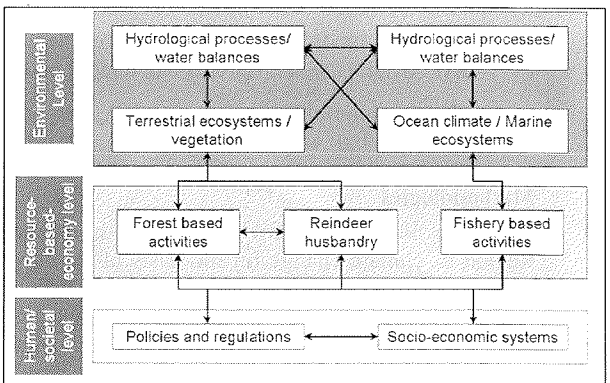

Figure 1: *The overall study framework of BALANCE, its main subject areas and their linkages*

Integrated assessments, when taken seriously, are a difficult and ambitious undertaking. They not only involve co-operation between different natural science disciplines but also between the natural and the human sciences. This notwithstanding, we are convinced that only an interdisciplinary/holistic approach will lead to results that will provide answers to the issue of climate change and its impacts in the Arctic. Splitting up this problem into a number of 'sub-units', e.g., one addressed by the physical sciences, the other by the biological and a third by the social or human sciences will not 'do the job'. In addition, whatever the results of an IRIS, its usefulness and ultimate validity will be measured not by scientists alone but primarily by the people in the region that is being studied. It is therefore mandatory in an IRIS to involve stakeholders in all phases of the project as early as possible. These requirements have been considered in the project design such that the key characteristics of BALANCE may be summarized by the following characteristics: *interdisciplinarity, stakeholder involvement, synthesis and integration of existing results.*

BALANCE is a continuation of an earlier EU-project, BASIS [Barents Sea Impact Study; see *Lange and BASIS consortium*, 2003], is funded by the *European Commission* (EVK2-CT2002-00169) and is being carried out by a consortium of 15 partners from six countries.

The study region and the scope of BALANCE

BALANCE focuses on the Barents Sea region of the European North, a region that truly deserves to be considered for an IRIS for a number of reasons.

- The unique environmental conditions both with regard to the terrestrial ecosystems as well as to the biophysical conditions in the Barents Sea;
- the rich occurrence of and the dependence of the regional economy on natural resources, particularly timber, fish, reindeer and hydrocarbons;
- the relatively high population density (particularly in the Russian part of the Barents Region) compared to other regions in the circumpolar North;
- and being the northernmost part of the *European Union*

are only a few of these reasons, which distinguish the BALANCE study region from other parts of the Arctic.

The overall scope and study framework is based on three distinct categories/levels: the environmental-, the resource-based-economy- and the human/societal level (Figure 1). Within each of these levels, subjects as shown in the figure are being addressed in BALANCE. A distinct characteristic of these subject areas are their mutual relationships with-, their linkages among- and their dependencies from each other. This characteristic is one of the major motivations for carrying out BALANCE holistically as an IRIS.

The spatial and temporal scope of our study comprises

- a common modelling scale of no larger than 20x20 km squares within the study area of BALANCE (i.e., the Barents Sea region) and
- seasonal (monthly) temporal resolution around two time slices at 2020 and 2050 (and possibly 2080) with integration over ± 10 years around this time.

Methodologies

The main objective of BALANCE lies in determining the vulnerabilities of the Barents Region to climate change on the basis of an integrated climate change impact assessment. This determines the major methodologies, which are described in more detail in Lange [2004]. Carrying out a climate change impact study requires the provision of baseline scenarios (*baseline scenarios* ignore climate change and consider only changes that are due to existing or projected changes in economic activities, societal characteristics, policies and regulations) and climate change scenarios (*climate change scenarios* account for greenhouse-gas-driven climate change) of the environmental and economic components given in Figure 1 and their comparison through an integrated assessment model (IAM). The construction of an IAM comprises a major task within BALANCE. This is being pursued through a two-pronged approach: by constructing an *IAM of intermediate complexity* (i.e., an IAM that does not comprise all of the components of the studied system and utilizes parameterized and/or somewhat simplified representations of cause-effect relationships with regard to the reaction of individual components of the system to climate change) on the one hand and a number of individual impact models for the considered components of the Barents Sea system. The latter approach builds on a sequential execution of models describing the response to climate change of individual components on the environmental-, resource-based-economy- and the human/societal level along so-called *impact chains* in the terrestrial, marine and freshwater

realm of the of the Barents Sea system (Figure 2). The impact models utilized in BALANCE include:

- a 3D-ocean model including the physical, chemical and biological components of the Barents Sea [see, e.g., *Slagstad, et al.*, 1999; *Slagstad and Støle-Hansen*, 1991],
- a fishery population model [see, e.g., *Gjøsæter, et al.*, 2002],
- a regional hydrological/surface snow model package [*Dankers*, 2002],
- a detailed surface flux model for local-scale hydrological investigations [*Harding and Lloyd*, 1998],
- a vegetation model (based on the *Lund-Potsdam-Jena vegetation model*) that allows estimates of ecotone shifts in response to climate change [*Wolf and Callaghan*, in prep.],
- a forest growth model that also takes into account forest pest outbreaks as a result of climate change [*Kozlov*, 1997],
- fishery economy models [*Eide and Flaaten*, 1998] and
- a forestry economy model [*Layton and Pashkevitch*, 1999].

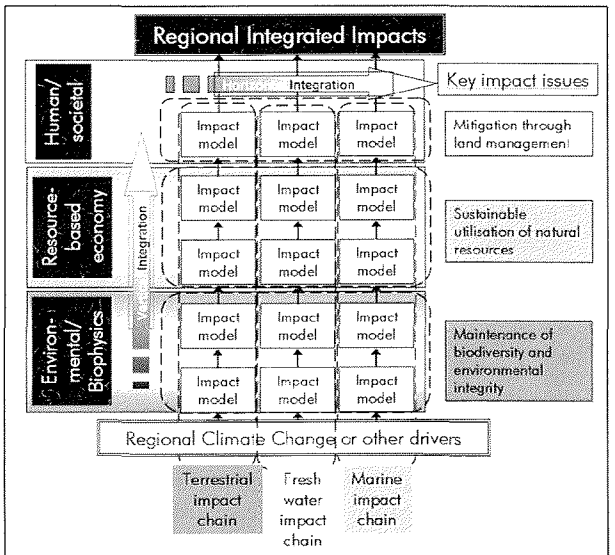

Figure 2: *Schematic depiction of major modelling strategy in BALANCE utilizing integration along vertical impact chains and horizontal key impact issues*

The environmental-level models are driven by climate scenarios as obtained from a dedicated regional climate model (REMO), which is in turn driven by a global circulation model (ECHAM4/OPYC3) which utilizes the B2 SRES emission scenario [*Nakicenovic, et al.*, 2000] as major driver.

Details of the *IAM of intermediate complexity* can be found elsewhere [*Grewe*, 2005] and will not be described here for lack of space.

Results and Discussion

Instead of attempting to give a more or less complete picture, I will try illustrate the suite of results by two examples which may provide insight into the kind of insight that may be generated by an IRIS.

Ocean climate and fishery

The conditions in the Barents Sea are mainly controlled by the general oceanographic conditions, which comprise the inflow of (relatively) warm Atlantic waters along the Norwegian coast in the south-west on the one hand and the advance of Arctic waters from the north-east [*Loeng*, 1991]. However, there is a strong link between the atmospheric conditions and ocean surface- as well as sea ice processes [see, e.g., *Sakshaug and Slagstad*, 1992]. Thus, the magnitude of Atlantic-water inflow influences the position of the sea ice edge in the northern Barents Sea: During 'warm years' (i.e., years with strong Atlantic-water influence)

the sea ice edge is found further to the north compared to 'cold years' (i.e., years with moderate to minor Atlantic-water influence).

The presence of a sea ice cover inhibits mixing of the ocean surface layer by surface winds thus preventing mixed-layer deepening and the upwelling of deeper and oxygen- as well as nutrient-rich waters. This in turn reduces significantly the magnitude of primary production in the surface layers and subsequently decreases productivity of higher trophic levels [*Sakshaug and Slagstad*, 1992]. Conversely, a decrease in sea ice cover will result in enhanced mixing and thus in the overall increase in oceanic productivity, given a continuous supply of nutrients from intermediate waters.

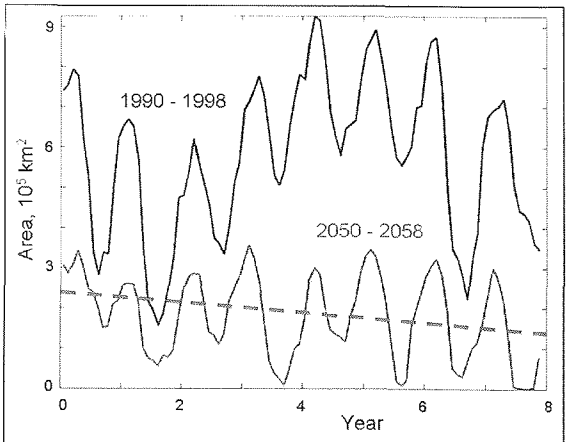

Figure 3: Variation of sea ice area in the Barents Sea as simulated by the a 3D-ocean model for 1990-98 (upper curve) and 2050-58 (lower curve) driven by the results of the REMO regional climate model; the dashed line gives an approximate trend in mean sea ice cover for the period 2050-58 [modified from Slagstad. pers. comm..]

It is expected that future climate change will result in an overall decrease in sea ice cover of the Arctic Ocean, particularly in the summer months [*ACIA*, 2004]. Our model studies demonstrate that this also applies specifically to the Barents Sea (Figure 3). As can be seen, not only is the magnitude of sea ice cover in 2050-58 approximately halved compared to the 1990-98 period, the decrease in sea ice area appears to be continuing over the 2050-58 period. Thus, it is expected that the reduction of sea ice will have significant impacts on the productivity of the Barents Sea as outlined above and may lead to enhanced fish stock sizes. This would ultimately provide increasing potential for the fishery industry in the Barents Sea region.

Length of snow cover season, ecotones shifts and reindeer herding

Somewhat similar to the above described sea ice changes, a warming trend is also expected to lead to a reduced length of the snow cover season in the Barents Sea region. As shown by Dankers [2002] for the Tana Basin of northern Finland, the equally expected increase in precipitation will only partly reduce this effect. As also demonstrated in the same study, the snow-free season is extended in a climate change scenario run [based on the B2 SRES scenario; *Nakicenovic, et al.*, 2000] compared to the control run representing present conditions. In combination with enhanced temperatures, this results in an extended growing season. Moreover, it is expected that the change in climatic conditions will result in significant shifts in vegetation zones, principally shifting the taiga-tundra ecotones (i.e., the mean boundary between the boreal forest and tundra vegetation) northwards as he warming trend is manifested [Wolf, pers. comm.].

The impact of these developments on reindeer herding activities are more complex than immediately obvious. While the shortening of the snow cover season and the increase in the length of the growing season can be considered favourable, the warming trend may also increase the number of refreezing events. Refreezing events comprise the temporal melting of snow surface layers followed by refreezing of the melt water and formation of an ice layer at the top of the snow cover. This reduces the ability of the reindeer to penetrate the snow layer in order to reach their forage. The result is a reduction of food supply for the reindeer with adverse effects for their overall conditions and their reproduction success. The shift in the

tundra-taiga ecotone also implies reduced food supply for reindeer as less area will be available for them for grazing. In addition, they will face enhanced pressure from forest owners who consider reindeer as disturbance to tree growth and forest development and who may not wish to see reindeer intruding on their welcome enhancement of timber production.

Acknowledgement

I would like to thank the *European Commission* for providing the funds to carry out BALANCE. I am grateful for the fruitful cooperation of my project partners and for providing me with unpublished data and results of their investigations. Finally, I would like to thank Prof. Klaus Dethloff (AWI Potsdam) for inviting me to present my paper at the *Arctic Climate Workshop*.

References

ACIA (2004), *Impacts of a Warming Arctic: Arctic Climate Impact Assessment*, 140 pp., Cambridge University Press, Cambridge, U. K.

Dankers, R. (2002), *Sub-arctic hydrology and climate change: a case study of the Tana River Basin in Northern Fennoscandia*, 240 pp., Faculteit Ruimtelijke Wetenschappen Universiteit Utrecht, Utrecht, The Netherlands.

Eide, A., and O. Flaaten (1998), Bioeconomic Multispecies Models of the Barents Sea Fisheries, in *Models for Multispecies Management*, edited by T. Rødseth, pp. 141-172, Physica-Verlag, Heidelberg, New York.

Gjøsæter, H., et al. (2002), Growth of Barents Sea capelin (*Mallotus villosus* Müller) in relation to zooplankton abundance, *ICES Journal of Marine Science, 59*, 959-967.

Grewe, C. (2005), Integrated assessment model for the Barents Sea region, BALANCE Project Deliverabel 4.3, 9 pp, Institute for Geophyiscs, University of Münster, Münster, Germany.

Harding, R. J., and C. R. Lloyd (1998), Fluxes of water and energy at three high latitude tundra sites in Svalbard, *Nordic Hydrology, 29*, 267-284.

Kozlov, M. V. (1997), Pollution impact on insect biodiversity in boreal forests: evaluation of effects and perspectives of recovery, in *Disturbance and Recovery in Arctic Lands: An Ecological Perspective. Proceedings of the NATO Advanced Research Workshop on Disturbance and Recovery of Arctic Terrestrial Ecosystems, Rovaniemi, Finland, 24-30 September 1995*, edited by R. M. M. Crawford, pp. 213-250, Kluwer Academic Publishers, Dordrecht, The Netherlands.

Lange, M. A. (2004), Global Changes and their impacts in the circumpolar North: Basic concepts and methods, in *IRISEN-II. Integrated Regional Impact Studies in the European North: Basic Issues, Methodologies and Regional Climate Models - II. Proceedings of an Advanced Study Course at Abisko Research Station, Sweden, from July 20 to August 3, 2002*, edited by M. A. Lange and D. Poszig, pp. 45-82, Centre for Environmental Research (CER), Münster, Germany.

Lange, M. A., and BASIS consortium (2003), The Barents Sea Impact Study (BASIS): methodology and first results, *Continental Shelf Research, 23*, 1673-1694.

Layton, I. G., and A. Pashkevitch (1999), Forestry and Forest Industries in the Arkhangelsk Oblast – their development and vulnerability to global change, GERUM Working Report, 1999-09-17, 90 pp, Umeå, Sweden.

Loeng, H. (1991), Features of the oceanographic conditions of the Barents Sea, *Polar Res., 10*, 5-18.

Nakicenovic, N., et al. (2000), *IPCC Special Report on Emission Scenarios*, 599 pp., Cambridge University Press, Cambridge, U.K. and New York, USA.

Sakshaug, E., and D. Slagstad (1992), Sea ice and wind: Effects on primary productivity in the Barents Sea, *Atmosphere-Ocean, 30*, 579-591.

Slagstad, D., et al. (1999), Modelling the carbon export and air-sea flux of CO_2 in the Greenland Sea, *Deep-Sea Research II, 46*, 1511-1530.

Slagstad, D., and K. Støle-Hansen (1991), Dynamics of plankton growth in the Barents Sea. Model studies, *Polar Res., 10*, 173-186.

Wolf, A., and T. V. Callaghan (in prep.), Modelling the vegetation change in the Barents Region.

A global adaptive barotropic model of the atmosphere

Matthias Läuter, Dörthe Handorf, Klaus Dethloff

Alfred Wegener Institute for Polar and Marine Research, Potsdam

Atmospheric multi-scale interactions generating planetary waves play an important role for atmospheric climate variability on timescales from seasons to decades. As well external forcings, e.g. by mountains, as internal forcings, e.g. by synoptic flow patterns, on spatial scales of about 1000 km generate planetary waves. Conversely, the planetary wave structure effects synoptic flow patterns by large-scale momentum and energy fluxes.

To simulate these atmospheric multi-scale interactions we present an adaptive barotropic model based on the spherical shallow water equations. We use an adaptive Lagrange-Galerkin method consisting of the finite element method and the semi-Lagrange method for the spatial and temporal discretization. Thereby the triangular unstructured grid is temporally variable und spatially adaptive.

Experiments with the model PLASMA show the applicability of the adaptive method to atmospheric processes for idealized atmospheric flows. Beside the successful reproduction of analytical solutions the modeling of the orographic forcing of planetary waves is shown. In sensitivity experiments the influence of different zonal wind velocities and different mountain heights on the plantary wave structure is analyzed.

How to deal with sea ice deformation in the Arctic: Four approaches in a continuum sea ice model

T. Martin

Alfred Wegener Institute for Polar and Marine Research, Bremerhaven

In the Arctic sea ice grows thermodynamically until an equilibrium thickness of 2-3m is reached. This formation of level ice is disturbed by deformation processes, which evolve under convergent and shear conditions of sea ice motion, rafting and ridging of the ice cover. This builds thicker ice, accounting for about two-thirds of the Arctic sea ice volume. It is important to describe these dynamical deformation processes in numerical models which are used to investigate climate change in Arctic and Subarctic regions.Efforts have been made during the last thirty years to implement these deformation processes to numerical models based on very different theories. In this study four different approaches to model a deformed sea ice cover are compared. The four different approaches include (1) an additional prognostic equation for ice roughness from which ridge parameters are diagnostically derived, applicable to single ice class models, (2) a redistribution model with two ice categories, level and ridged ice, including a statistical derivation of ridge parameters, (3) a set of prognostic equations for ridge parameters, i.e. ridge density and sail height, from which a ridged ice class is finally derived, and (4) a multi-category model, where sea ice is redistributed between several ice classes by deformation. Basically all four models were able to reproduce the governing spatial distribution of Arctic sea ice thickness. However, there are differences in structure and absolute values. The algorithm listed first tends to give a less discrete distribution of deformed ice while the third shows very distinct areas of heavy ridging. Approaches two and four are very similar in theory though the multi-category model lacks exact ridge information. Differences will be discussed and results compared to data from a control run of the model without ridging and measurement data.

On recent changes in sea ice and ocean conditions and their potential feedback to Arctic climate

W. Maslowski

Department of Oceanography, Naval Postgraduate School, Monterey, California, USA

One of the outstanding goals in climate modeling is proper representation of feedback processes between the atmosphere and ocean / sea ice. This is of particular importance in the polar regions where sea ice thickness distribution, ice edge position, winter leads and polynyas, and mesoscale patterns of sea surface temperature (SST) distribution have significant effect on the atmosphere via different than climatology heat fluxes. We use a coupled ice-ocean model of the Pan-Arctic region to study effects of variable atmospheric forcing on sea ice and ocean conditions at scales ranging from seasonal to decadal. In particular, we have completed an ensemble of four runs forced with realistic daily 1979-2003 ECMWF data and with variable restoring to surface temperature and salinity, to investigate Arctic climate change through a one-way coupling of the atmosphere to the sea

ice and ocean. The overall sea ice conditions are quite robust among the four cases and show dramatic melting of multi-year sea ice in the late 1990s and 2000s. In addition, our analyses indicate that increased oceanic advection of heat into the central Arctic might be in part responsible for the recent reduction in the sea ice extent and volume. We argue that such changes in sea ice conditions and the temperature distribution in the upper ocean must affect the surface atmospheric conditions and possibly vertical atmospheric structure over the Arctic Ocean. We conclude that a proper representation of air/sea ice/ocean interactions and feedbacks is needed and can be accomplished in a high-resolution regional climate model of the Arctic Ocean. This approach should advance our understanding of causes and effects of climate change in the Arctic, which is going to be one of the most important questions to address by field and modeling activities within the upcoming IPY in 2007-2008.

Retrieval of total water vapour over the Arctic from space-bourne microwave radiometer data

Christian Melsheimer and Georg Heygster

Institute of Environmental Physics, University of Bremen, Bremen, Germany

1. Introduction

The polar regions belong to the regions of which the least information is available about the current and predicted states of surface and atmosphere. We present advances in a method to determine the total (column) water vapour (TWV) of the polar atmosphere over open water, sea ice and land ice from space-bourne microwave radiometer data, in particular data from the sensor AMSU-B (Advanced Microwave Sounding Unit B) on the new generation polar orbiting satellites of NOAA (National Oceanic and Atmospheric Administration), NOAA-15, NOAA-16, and NOAA-17(AMSU-B reference); likewise, data from the sensor SSM/T2 (Special Sensor Microwave) on the DMSP (Defense Meteorological Satellite Program) satellites can be used. The frequencies and numbering of the AMSU-B channels are shown in the following table.

AMSU-B Channel:	16	17	18	19	20
Frequency [GHz]:	89	150	183.3±1	183.3±3	183.3±7

Table: AMSU-B channels and frequencies

The first two channels, 16 (89 GHz) and 17 (150 GHz), are window channels, while the remaining three are centred around the strong water vapour absorption/emission line at 183.3 GHz. The width of the imaged strip (swath) is about 2000 km, the resolution on the ground is between about 15 and 50 km, increasing from the centre to the edge of the swath. Since there are about 14 satellite passes a day, the whole globe is covered once daily, with a lot of overlap in the polar regions. The sensor SSM/T2 is very similar to AMSU-B, except for a lower resolution of 50 to 100 km.

2. Water vapour retrieval algorithm

While AMSU-B is designed and operationally used for humidity sounding, this fails over polar regions since there, (1) the total water vapour content of the atmosphere is so low that the contribution caused by surface emission is substantial and (2) the surface emission is poorly known and highly variable because of variable ice cover of the seas.

Our method which retrieves total water vapour is complementary in that it works exactly where the atmosphere is dry enough for the ground to be "seen" by the sensor, and it is mostly independent of the surface emissivity. The basic idea [*Miao et al.*, 2001] is to use three channels where the surface emissivity is similar but the water vapour absorption is different, such as the three AMSU-B channels centred around the 183.3 GHz water vapour line.

Starting from the radiative transfer equation for a not too opaque atmosphere in the approximation of *Guissard and Sobieski,* [1994], the following equation for the total water vapour W can be derived [*Miao et al.*, 2001]:

(Eq. 1) $$W\sec\theta = C_0+C_1\log[(T_i-T_j,-F_y)/(T_j-T_k-F_x)]$$

where θ is the viewing angle, T_i.is the brightness temperature measured by AMSU-B at channel no. i, while the three channels i, j,and k are sorted in such a way that for the corresponding water vapour absorption coefficients, κ_i, κ_j, κ_k, we have $\kappa_i < \kappa_j < \kappa_k$. The four parameters C_0, C_1, F_x, F_y, which we shall call "calibration parameters", have to be determined empirically. To do this, radiosonde data (Arctic, 1997 till 2001, about 27000 profiles), were taken as input for simulating AMSU-B brightness temperatures with the radiative transfer model ARTS (The Atmospheric Radiative Transfer Simulator, *Buehler et. al*, 2005), using a

range of different surface emissivities between 0.6 and 0.96. In addition, from the humidity data of each radiosonde profile, the total water vapour was calculated directly. Several linear regressions then yield the four calibration parameters C_0, C_1, F_x, F_y [details: *Miao*, 1998]

Using the three channels near the water vapour line (AMSU-B channels 20, 19, and 18, i.e., $(i,j,k)=(20,19,18)$), the method works up to total water vapour contents of about 1.5 kg/m^2. If we replace the most water-vapour sensitive channel 18 by the window channel 17 at 150 GHz, i.e., $(i,j,k)=(17,20,19)$, the method works up to total water vapour contents of about 6 kg/m^2. Such water vapour values are typical for the Arctic ocean, Siberia and Northern Canada in winter, and for Greenland almost year-round. So, if we have determined those four calibration parameters, the TWV can be calculated from AMSU-B brightness temperatures without any further input.

In order to extend the retrieved water vapour range to higher values, the channel 19 is replaced by the window channel 16 at 89 GHz, i.e., $(i,j,k)=(16,17,20)$. Since the emissivity of sea ice and ocean at 89 GHz is significantly different from the emissivity at 150 and 183 GHz, the emissivity does not cancel out any more, and instead of Eq. (1), we get the "extended algorithm"

(Eq. 2) $$W\sec\theta = C_0+C_1\log\{[(r_2/r_1)(T_i-T_j,-F_y)/(T_j-T_k-F_x)+C]-C\}$$

Here, $r_1 = 1-\varepsilon_{89}$ and $r_2 = 1-\varepsilon_{150}$ are the surface reflectivities, C depends on the water vapour absorption coefficients but can safely be approximated by 1 for TWV above 6 kg/m^2, and the other variables have the same meaning as in Eq. (1) above. This means that now, some information about the emissivity of sea ice at 89 and 150 GHz is needed. We have extracted this information from emissivity measurements over sea ice and open water during the SEPOR/POLEX (Surface Emissivities in Polar Regions-Polar Experiment; *Selbach*, 2003) campaign: Analysis of these data shows a moderately high correlation of the emissivities ε_{89} and ε_{150} of sea ice at 89 and 150 GHz, respectively. A linear regression yields

(Eq. 3) $$\varepsilon_{89} = 0.1809 + 0.8192\ \varepsilon_{150}$$

where we have imposed the additional constraint that $\varepsilon_{89}(\varepsilon_{150}=1) = 1$. Based on these data, the reflectivity ratio r_2/r_1 over sea ice can be approximated by a constant value of 1.22.

This means that for the extended algorithm, we need, in addition to the four calibration constants, information on the sea ice cover. The algorithm is then applied over sea ice. Since the emissivity of open water is rather well known [*Deblonde and English*, 2000], it is in principle possible to adapt the extended algorithm to the use over open water. However, we have not done this here since there are other remote sensing methods to retrieve TWV over open water, e.g., from other passive microwave sensors like SSM/I. Using this extended algorithm, the upper limit of the TWV that can be retrieved is about 12 kg/m^2. Thus, combining all three "sub-algorithms" mentioned so far (using channel triples 20,19,18; 17,20,19; 16,17,20), TWV values from 0 to about 12 kg/m^2 can be retrieved from AMSU-B data, using three sets of the four calibration parameters. Each sub-algorithm is used as long as both the numerator and the denominator in Eq. (1) are negative.

3. Validation

In order to validate the algorithm, we have collocated TWV data derived from AMSU-B data with TWV data from ECMWF reanalysis data (ERA 40). For the winter months, the correlation is 0.91, and the mean deviation of AMSU-B TWV from ECMWF TWV is 0.28 kg/m^2. Since the TWV values at that time of the year are below 6 kg/m^2 over most of the Arctic, the extended algorithm is not used, and the TWV retrieval is independent of the surface emissivity.

For late summer, when the ice extent is smallest and the TWV values are highest, the TWV retrieval relies mostly on the extended algorithm that uses the above-mentioned approximation of the reflectivity ratio. Consequently, the correlation is considerably lower, 0.61, but still meaningful. Likewise, the mean deviation of AMSU-B TWV from ECMWF TWV is higher, 2.8 kg/m^2. However, since there is currently no other way for remotely sensing total water vapour over sea ice, this is nevertheless valuable information.

4. Results

We have calculated TWV from all AMSU-B data north of 50°N for the years 1999 to 2003. Fig. 1 shows a map of a one-day average of TWV for X March, 2002 from NCEP (National Centers for Environmental Prediction) reanalysis data (left), and derived from AMSU-B data using our algorithm (right). Fig. 1 shows daily averages of TWV from AMSU-B data for 4 subsequent days in March 2002, The propagation of a humid air intrusion through the Bering Strait into the inner Arctic is clearly visible from March 18 to 20, and on the following day the humid air has started dispersing.

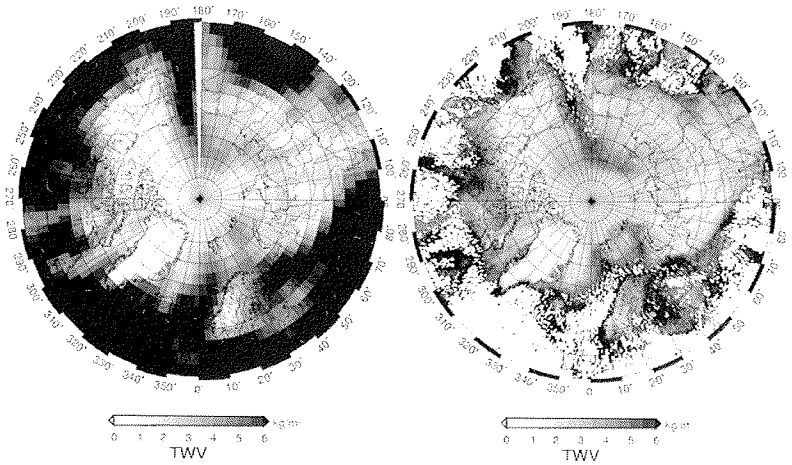

Fig 1: Left: TWV from NCEP reanalysis data; right: TWV derived from AMSU-B data. 19 March, 2001. White areas are areas where TWV is too high for the retrieval algorithm.

5. Summary and Outlook

With the method presented here, it is possible to retrieve total water vapour (TWV) up to about 6 kg/m^2 from AMSU-B data, independent of the potentially unknown surface emissivity. With the additional input of a rough estimate of sea ice emissivities, TWV over sea ice can be determined up to about 12 kg/m^2. Maps of the polar total water vapour derived by our method show details that are missed by, e.g., model or reanalysis data because of the sparsity of observations.

The possibility to assimilate total water vapour derived in such a way into numerical weather prediction models has been explored the EU project IOMASA (Integrated Observing and Modelling of the Arctic Sea Ice and Atmosphere). The total water vapour data might also be used together with regional models for water cycle investigations.

Since the emissivity of sea ice between 50 and 200 GHz has not been investigated thoroughly, data that complement the SEPOR/POLEX data on emissivity could help to refine the extended algorithm.

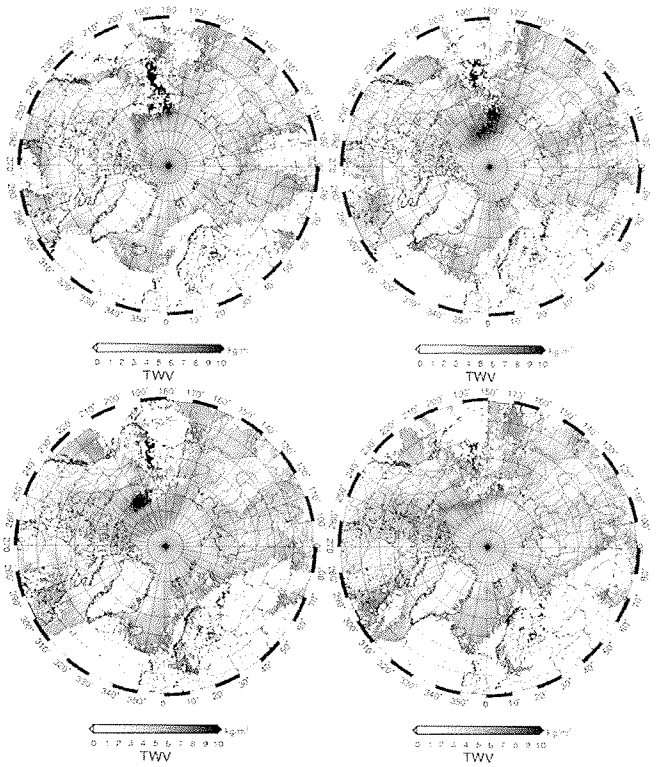

Fig 2: TWV derived from AMSU-B data for, left to right, top to bottom, 18, 19, 20, and 21 March, 2002

Acknowledgements

This study was supported by research grants EVK-CT-2002-00067 (EU) and HE-1746/9-1,2 (DFG).

References:

Buehler, S.A., P. Eriksson, T. Kuhn, A. von Engeln, and C. Verdes, ARTS, the Atmospheric Radiative Transfer Simulator, *J. Quant. Spectroscopy and Radiative Transfer 91*, 65-93, doi:10.1016/j.jqsrt.2004.05.051, 2005.

Deblonde, G., and S.J. English, Evaluation of the FASTEM-2 microwave oceanic surface emissivity model, *Proc. Int. TOVS Study Conf.*, Budapest, Hungary,ITWG/IAMAS, 67-68, 2000.

Guissard, A., P. Sobieski, A simplified radiative transfer equation for application in ocean microwave remote sensing, *Radio Science 29*(4), 881-894, Jul-Aug 1994.

Miao, J., K. Kunzi, G Heygster, T.A. Lachlan-Cope, and J. Turner, Atmospheric water vapor over Antarctica derived from Special Sensor Microwave/Temperature 2 data, *J. Geophys. Res. 106*(D10): 10187-10203, 2001.

Miao, J., *Retrieval of Atmospheric Water Vapor Content in Polar Regions Using Spaceborne Microwave Radiometry*, PhD Thesis, Department of Physics and Electrical Engineering, University of Bremen, and: Reports on Polar Research 289/1998, Alfred Wegener Institute for Polar and Marine Research, Bremerhaven, Germany, 109 pp., 1998.

Selbach, N, *Determination of total water vapor and surface emissivity of sea ice at 89 GHz, 157 GHz, 183 GHz in the Arctic winter*, PhD Thesis, Department of Physics and Electrical Engineering, University of Bremen, and Berichte aus dem Institut für Umweltphysik 21, Logos Verlag Berlin, 189 pp,2003.

Interactions between the surface, clouds, aerosols, and radiation in a meso-scale model of the western Arctic

H. Morrison

University of Colorado, Boulder, USA

Recent field experiments (SHEBA, MPACE, FIRE-ACE) have highlighted the common occurrence and importance of mixed-phase clouds in the Arctic. Interactions and feedbacks between the surface, clouds, aerosols, radiation, and synoptic-scale dynamics are described in the context of weakly-forced mixed-phase clouds occurring over the Arctic Ocean sea ice. These feedbacks are investigated on a regional scale using the polar version of the NCAR/PSU mesoscale model MM5. To improve the representation of clouds in MM5, a new two-moment microphysics scheme has been implemented that includes a detailed treatment of droplet and ice nucleation processes. The characteristics of the simulated mixed-phase cloud layer, and hence its impact on the surface, radiative transfer, and dynamics, are highly sensitive to the ice microphysics. In particular, the stability of the cloud layer is highly dependent upon the ice nucleation processes and the ice particle number concentration. In turn, the cloud properties are influenced by the surface, radiative transfer, and dynamics, representing several potential feedback pathways.

Intercomparison of Arctic atmospheric RCMs: Spatio-temporal patterns of large-scale flow and temperature

Annette Rinke, GLIMPSE and ARCMIP groups

Alfred Wegener Institute for Polar and Marine Research, Potsdam, Germany

GLIMPSE group: A. Benkel, J.H. Christensen, J. Debernard, K. Dethloff, R. Döscher, W. Dorn, D. Handorf, J. E. Haugen, S. Holzkämper, M. Køltzow, P. Kuhry , M. Meier, M. Reigstad, A. Rinke, B. Rockel, L.P. Roed, S. Saha, E. Sokolova, M.Stendel, P. Wassmann, K. Wyser

ARCMIP group: J.J. Cassano, J.H. Christensen, J.A. Curry, K. Dethloff, P. Du, E. Girard, J.E. Haugen, D. Jacob, C.G. Jones, M. Koltzow, R. Laprise, A.H. Lynch, S. Pfeife, A. Rinke, M.C. Serreze, M.J. Shaw, M. Tjernström, K. Wyser, M. Zagar

1. Introduction

To evaluate RCM simulations in the Arctic, the international project ARCMIP- Arctic Regional Climate Model Intercomparison Project (ARCMIP; Curry and Lynch 2002; http://curry.eas.gatech.edu/ARCMIP/ index.html) has been organized. The primary ARCMIP activities focus on coordinated simulations by different Arctic RCMs to determine the level of uncertainty in current Arctic RCM simulations. The simulation experiments are carefully designed so that each of the models is operating under approximately the same external constraints (same boundary conditions, horizontal resolution, and domain size). The first ARCMIP experiment has been conducted for the 1997/1998 period of the Surface Heat Budget of the Arctic Ocean (SHEBA; Uttal et al. 2002) project, which included extensive field observations and accompanying satellite analyses. For the single SHEBA station point, the different SHEBA-, satellite observations and analysis products have been compared to each other (Liu et al. 2004) and have been used to evaluate RCM simulations (Tjernström et al. 2005). Coordinated simulations over the 1 year September 1997 to October 1998 have been conducted by 8 RCMs over the SHEBA domain which covers the Beaufort and Chukchi Seas.

Within GLIMPSE, coordinated simulations over 10 years 1990-99 have been conducted by 3 RCMs over the pan-Arctic domain covering the polar cap north of ~65N.

The purpose of this paper is to evaluate and intercompare the spatiotemporal distributions of simulated Arctic temperature and large-scale flow fields produced by the different RCMs. The differences between the models will be assessed with the aim to quantify the scatter among them and therefore the magnitude of disagreement and unreliability of current Arctic RCM simulations. Such an estimate is important in the light of future Arctic climate change simulations.

2. Intercomparison of 8 RCMs over the SHEBA domain

The experimental design of the coordinated simulations was as follows: Simulations over 1 year, October 1997-September 1998 using the same SHEBA domain with 50 km horizontal resolution. All models used a common forcing for the lateral atmospheric boundary (6 hourly ECMWF operational analyses) and for the lower ocean/sea ice boundary (6 hourly SSM/I sea ice fraction, AVHRR ocean surface temperature). Dynamics and physics are different among the models. A detailed description of the experimental set-up and the participating models is given by Tjernström et al. (2005) and Rinke et al. (2005).

The 8-model ensemble average (or model ensemble mean) of the 850 hPa and 500 hPa geopotenial heights has been evaluated against the driving ECMWF analysis data. As the models are tightly constrained to follow the lateral forcing in such a small domain, small large-scale flow biases are expected. For the geopotential heights, the model ensemble performance bias is between -25 m and +5 m for winter and summer. As the uncertainty in the "observed"

geopotential heights as determined by the difference between the NCEP and ECMWF analyses is of about the same magnitude, one can say that the seasonal large-scale flow patterns are reproduced remarkably well by the model ensemble. An interesting feature is that the geopotential bias has the same pattern over the Beaufort/Chukchi Seas in all models, namely an underestimation of the height by the models compared to the ECMWF analysis. This bias feature is of barotropic nature, characterizing the entire column, and is seen for all seasons. Factors that may contribute to the bias are likely related to parameterized processes and different surface forcing used by this ARCMIP experiment and the operational ECMWF analysis. Examination of the bias in the 2 m air temperature shows that the model ensemble has a bias between -5 K and +5 K with the largest biases occurring along the coasts and over land with orographic structure. Factors responsible for the bias are the different orography/land-sea masks and horizontal resolutions in the RCMs relative to ECMWF. Differences in the downwelling surface radiation are associated with different 2 m air temperature over land. Additionally, different land surface schemes, soil moisture- and soil temperature initialization are used in the different models and ECMWF and contribute therefore to the differences. To unravel the different contributions is very difficult. Generally, the individual model performances are quite different. For the 2 m air temperature, the ensemble mean compares with the ECMWF analyses better than the individual models.

To characterize the across-model spread and the consistency among models, the intermodel standard deviation (sigma) has been calculated. A small sigma value, along with a small bias, indicates agreement among the models and shows that they capture the processes that govern the variable. A large sigma value indicates disagreement and unreliability in the simulations.

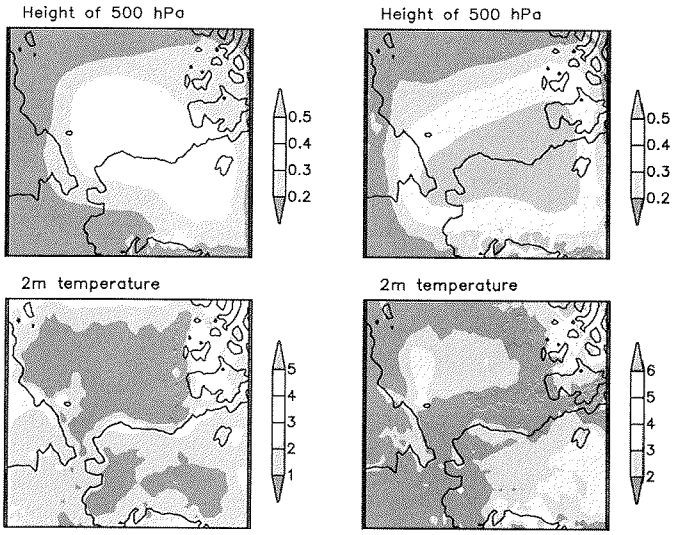

Fig. 1: Ratio of intermodel standard deviation to observed interannual variability for 500 hPa geopotential height and 2 m air temperature for winter (left) and summer (right).

The absolute magnitudes of the across-model scatter have been put into the context of the internal variability (observed interannual standard deviation from ERA40 data, period 1979-2001). A small ratio (less than one) indicates that the RCMs' agreement with each other is relatively high, compared with natural variability, i.e. the model spread is insignificant. A ratio much larger than one indicates that the model spread is significant. Figure 1 shows the ratio of the intermodel standard deviation to the observed interannual standard deviation, for

winter and summer temperature and geopotential, respectively. The across-model scatter in the geopotential heights is between 5 m and 20 m. However, compared with the interannual variability which is 2-5 times larger, the scatter is insignificant. The across-model scatter in the 2 m air temperature shows that the scatter is large over land areas and of the order of 1 K to 5 K. Compared to the ocean, this scatter arises because the land surface temperatures were not specified but were allowed to develop freely within each model. The different land-surface schemes as well as the differences in the radiation budget are responsible for the large intermodel land temperature scatter. The use of different orographic data sets contributes also to the relatively large across-model scatter in the 2 m temperature over islands and near the coasts. The across-model scatter over land is significant, and mostly ~2 times larger than interannual variability. In general, the across-model scatter is twice as large as the ensemble mean bias. The exceptions are both the 2 m temperature over ocean/sea ice and the geopotential over selected parts of the region (which depends on the season).

A detailed model evaluation against ECMWF data and model intercomparison of the large-scale flow, temperature, clouds and surface radiation is presented in Rinke et al. (2005).

3. Intercomparison of 3 RCMs over the pan-Arctic domain

Within GLIMPSE, the 3 models HIRHAM, HIRHAM.no, and RCA participated in this intercomparison. The experimental design of the coordinated simulations was as follows: Simulations over 10 years, 1990-1999 using a pan-Arctic domain with 50 km horizontal resolution. The domain sizes differ between the 3 models. All models used a common forcing for the lateral and lower boundary (ERA40 analyses). Dynamics and physics are different among the models.

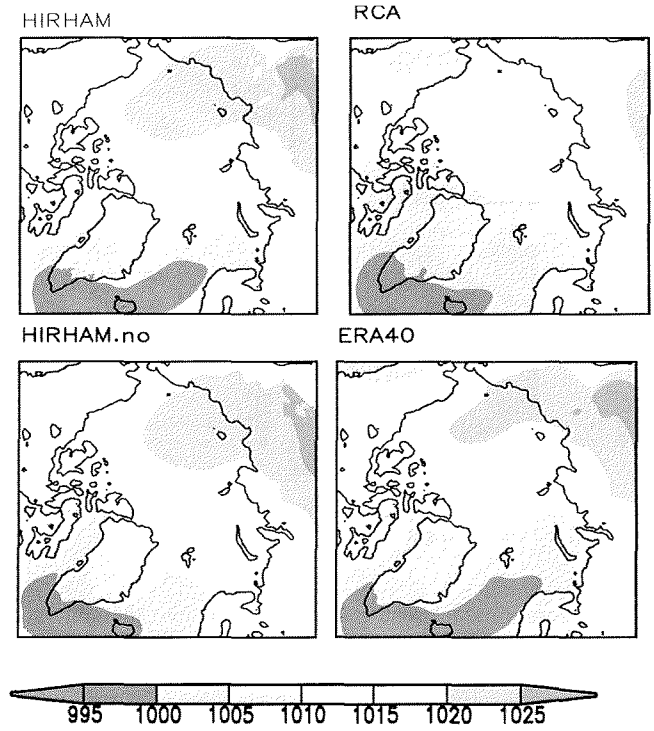

Fig. 2: Mean sea level pressure [hPa], winter, 1990-99, simulated by the 3 RCMs and from ERA40 analysis.

Figure 2 shows the comparison of the simulated mean sea level pressure (SLP) patterns with the ERA40 data. The winter pattern is characterized by the North Atlantic storm track extending east through Barents Sea into Kara Sea and south of Baffin Island and by an anticyclone over Siberia with an high pressure belt extending to the western Arctic. The models with a very large domain (RCA and HIRHAM.no) show a negative bias over the North Atlantic region associated with a truncation of North Atlantic strom tracks. Such a winter bias is known from the global models (Chapman and Walsh, 2005) and is consistent with the inability of North Atlantic storm track to penetrate Eurasian part. The observed summer SLP (not shown here) pattern is characterized by much weaker spatial gradients, especially over Eurasia. There is a local cyclone frequency maxima. A distinct summer cyclone maximum is also over the Arctic Ocean which is confirmed as a region of cyclolysis, associated with the decay of systems migrating from the Eurasian coast as well as along the weaker North Atlantic track (Serreze et al., 2001). The models show more agreement among each other in summer than in winter. And they have a common bias: The simulated SLP over the ice-covered Arctic Ocean is higher than the observed. In HIRHAM, the seasonal area-averaged root-mean-square error is 1-2 hPa. There are large differences in the individual model performances. All model tend to have the largest root-mean- square error in the cold season as also seen over the SHEBA domain results. However, even if some individual root-mean-square error was larger, the spatial correlation of patterns is always high. The simulated temperatures vary considerably across the models in winter, while they are more consistent in summer. Compared with ERA40, all models tend to be colder over ocean and warmer over land (with a whole area averaged root-mean square error of ~2 K) during summer.

4. Summary

With this work, we quantified the scatter among the models and therefore the magnitude of disagreement and unreliability of current Arctic RCM simulations. Even with a relatively constrained experimental design we notice a considerable scatter among the different RCMs. For the ARCMIP1 experiment, we found a large and significant across-model scatter in the 2 m temperature over land, in the surface radiation fluxes, and in the cloud cover which implies a reduced confidence level for these variables. In general, for the 2 m temperature, the ensemble means outperform the individual models. The simulated large-scale flow patterns reproduce observations and are in high agreement among the individual models. The first intercomparison for the pan-Arctic domain emphasize the larger influence of the domain size, forcings and internal variability on the simulations results. The results have to be discussed in relation to Arctic downscaled projections for future climate changes for which a similar across-model scatter can be expected and emphasizes the need for a multi-model ensemble approach for more reliable estimates.

References

Chapman, W.L., and J.E. Walsh, 2005: Simulations of arctic temperature and pressure by global coupled models. J. Clim., in press.

Curry, J.A. and A.H. Lynch, 2002: Comparing arctic regional climate models. EOS Trans Amer Geophys Union 83: 87

Liu J., Curry, J.A., Rossow, W.B., Key, J.R., Wang, X., 2004: Comparison of surface radiative flux data sets over the Arctic Ocean. J Geophys Res, submitted

Rinke and coauthors, 2005: Evaluation of an Ensemble of Arctic Regional Climate Models: Spatiotemporal fields during the SHEBA year, Clim. Dyn., submitted

Serreze, M.C., A.H. Lynch, and M.P. Clark, 2001: The summer Arctic frontal zone as seen in the NCEP/NCAR reanalysis, J. Clim. 14, 1550-1567.

Tjernström and coauthors, 2005: Modeling the Arctic boundary layer: An evaluation of six ARCMIP regional-scale models with data from the SHEBA project, Boundary-Layer Meteorol, in press

Uttal and coauthors, 2002: Surface energy budget of the Arctic ocean. Bull Am Meteorol Soc 83:255-275

Modeling of Permafrost in a regional climate model and it's influences on present and future Arctic Climate

S. Saha[1], A. Rinke[1], K. Dethloff[1], P. Kuhry[2], S. Holzkämper[2]

[1] Alfred Wegener Institute for Polar and Marine Research, Potsdam, Germany
[2] Department of Physical Geography and Quaternary Geology, Stockholm University, Sweden

The Regional Climate Model (RCM) HIRHAM4 [Christensen et al., 1992; Christensen et al., 1996; Dethloff et al., 1996] has been applied to investigate the soil processes in the Arctic. The strength and weakness of the RCM simulated soil and surface variables have been investigated using available observed and reanalysis data. The physical processes of the permafrost and active layer are very complex in nature. Therefore a complex Land Surface Model (LSM) [Bonan et al., 1996a] with advanced soil and vegetation scheme has been used in the current HIRHAM4 domain. Later, this LSM is coupled with the RCM HIRHAM4. The LSM coupled with HIRHAM4 (HIR-LSM) shows its strength and weakness in simulating soil temperature in the permafrost region. Using both of the model (HIRHAM4 and HIR-LSM), the IPCC B2 emission scenario climate has been simulated for three time slices (1990-1995, 2024-2029 and 2037-2042). The time slices 1990-1995 and 2024-2029 are associated with the negative North Atlantic Oscillation (NAO) index and the time slice 2037-2042 is associated with the positive NAO index. The NAO indices are calculated by using ECHO-G IPCC B2 scenario simulations. The influences of new soil, vegetation schemes and the coupling of HIRHAM4 with LSM on the future projection of permafrost have been investigated. Model lateral and lower boundary forcing data were from ERA-15 reanalysis and ECHO-G B2 scenario simulation.

1. The RCM HIRHAM4 and its soil processes in the Arctic

The HIRHAM4 is a high resolution model with a horizontal grid resolution of 0.5 degree in rotated latitude, longitude and 19 or 25 vertical levels in hybrid sigma coordinate. The model governing equations are based on the hydrostatic assumption. The model soil depth is about 10m and divided into 5 layers. For the soil moisture description, the model uses the bucket model and soil moisture, evaporation, drainage, surface runoff are parameterized. In the presence of snow, the heat flux through snow is calculated using prescribed snow thermal properties and snow density. Snow is treated as a single layer over the ground.

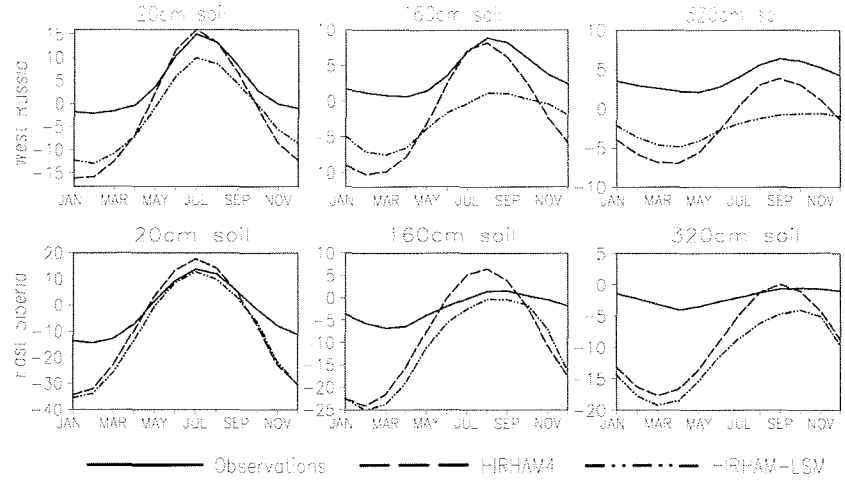

Figure 1: Monthly climatology mean soil temperature at 3 different depths. Average over all stations in West Russia and East Siberia are shown here.

Figure 1 shows the monthly climatology mean soil temperature, averaged over stations in West Russia and East Siberia. During summer, the model soil temperatures are better simulated compared to the observations. The biases in the model simulated summer soil are about ±5°C. During winter, the model soil temperature is too cold. The largest winter cold bias occurred in Eastern Siberia with a maximum of about 20°C. The magnitude of the winter air temperature signal has not been damped sufficiently when it has penetrated into the soil. This damping phenomenon is largely influenced by the freezing and thawing action of the soil moisture and the amount of snow on the ground surface. Since during winter, HIRHAM4 does not take into account soil moisture freezing, the model soil temperature rapidly goes down below 0°C. The winter precipitation is largely underestimated by the model. Also the model comparisons with the station measurements and satellite observations have shown a large deficiency in model snow water equivalent (SWE). A large part of the ground heat flux is used in the active layer for the phase transition of soil moisture. Also snow over the ground surface during winter prevents excessive cooling of soil to the colder air and during spring, a delay in snow melt cools down the summer soil temperature. Therefore, due to the absence of soil moisture freezing/thawing scheme and less ground insulation by the snow, the model soil has been cooled down during winter.

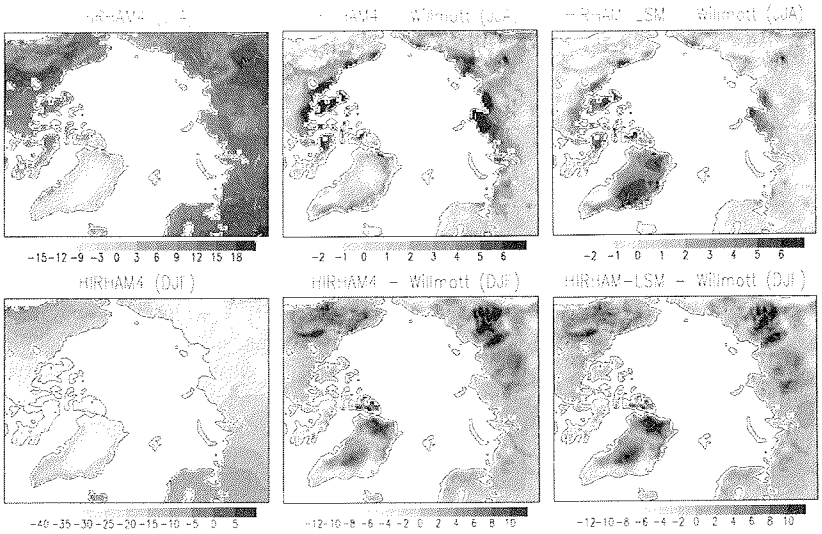

Figure 2: Summer (JJA) and winter (DJF) averages of HIRHAM4 monthly climatology mean (1979-1993) 2m air temperature, HIRHAM4 minus Willmott-Rawlins climatology and HIRHAM-LSM minus Willmott-Rawlins climatology 2m air temperature °C.

The model shows a very good agreement in monthly climatology mean 2m air temperature with all station measurements. Also, the large scale spatial patterns in Willmott and Rawlins [1999] climatology are captured well by the model (Figure 2). However during summer, the model has shown a warming of maximum 8°C at the Northern coastal part of Canada, Siberia and Alaska. During winter, the model 2m air is warmer than Willmott and Rawlins [1999] climatology in mountain regions of Eastern Siberia and Alaska.

2. Sensitivity studies with the HIRHAM4

Sensitivity studies have been performed with the HIRHAM4 to understand the cold winter biases in the soil temperature. Four sensitivity studies have been carried out by changing soil thermal conductivity, snow density and using revised stability functions under stable

condition and a new snow albedo scheme for snow over bare ground. In all sensitivity studies, the magnitude of the soil temperature change was within ±6°C. So, the change in one model parameter was not able to improve the winter soil temperature and to reduce the cold winter bias.

The revised stability function [Louis et al., 1982] under stable conditions increased the downward sensible heat flux. Therefore a warming in the winter soil was detected. The domain averaged warming in the winter soil was by a maximum of 0.5°C. An increase in sensible heat flux at the surface increased the surface temperature and hence the surface long wave radiation. The sum of these above changed fluxes was not positive everywhere, i.e. in some places it showed cooling and in some places it showed warming compared to the control HIRHAM4 simulation.

A decrease in soil thermal conductivity (1/3 of original value) was able to decrease the ground heat loss to the atmosphere during winter by a maximum of 6 Wm^{-2}. During summer the ground heat gain was decreased by a maximum of 6 Wm^{-2}. Warming and cooling signals due to the gain and loss of ground heat fluxes during winter and summer respectively were found in the deeper layers. At about *3m* depth, the soil was colder during summer by a maximum of 6°C and warmer during winter by a maximum of 3°C. The upper soil layer's thermal inertia seems to be small and therefore, it was able to reach very quickly close to the near surface air temperature.

During the snow density (100 kg/m^3 instead of original value 300 kg/m^3) sensitivity experiment, the soil temperature behaved in a same way like during the conductivity sensitivity experiment. A reduction in snow density i.e. an increase in snow depth during winter increased the winter soil temperature at the deeper layer by a maximum of 1°C (domain area average basis), whereas during summer a decrease of maximum 6°C in soil temperature was found at the same depth.

The new snow albedo scheme [Køltzow et al., 2003] was able to increase the surface albedo during the months April, May and June by a maximum of 0.12, which was underestimated by the model by a maximum of 0.5. Though the increase in surface albedo due to the new snow albedo scheme was small compared to the model bias, it was able to decrease the summer model bias in 2m air temperature by a maximum of 1.5°C in some places. The effects on the soil temperature due to the new snow albedo scheme were not so large but the improvement in surface albedo and summer 2m air temperature was in the right direction.

During all sensitivity experiments, the monthly climatology mean sea level pressure was changed compared to the control simulation by a maximum of ±6 hPa. The change of large-scale pressure patterns has an implication for global circulation.

3. The HIRHAM-LSM simulations

In the HIRHAM-LSM model, the LSM was driven by the atmospheric output from the HIRHAM4 and the four LSM variables (soil moisture, skin moisture, snow water equivalent, surface temperature) were given back to the HIRHAM4 at each time step. The idea behind this coupling was to maintain the present HIRHAM4 parameterizations of surface moisture and heat fluxes and to realize the effects of the updated surface variables from the LSM and the effects of coupling between the two models (HIRHAM4, LSM) in soil temperature.

A significant change in the surface energy budget of the HIR-LSM model was found during the summer season compared to the HIRHAM4. During winter however, the HIRHAM-LSM model was not much different from the control HIRHAM4. The spatial distributions of the soil moisture content in LSM and HIRHAM4 were not similar. Therefore in some places, the HIRHAM-LSM's surface heat fluxes differed from the HIRHAM4 during summer. During winter, the HIRHAM-LSM's soil temperatures have been improved at West Russian stations

compared to the HIRHAM4's soil temperature at all depths (Figure 1). The station averaged winter soil at Western Russia is now warmer than the HIRHAM4 simulation by about 3-5°C. There are still winter biases in the HIRHAM-LSM soil temperature compared to the station measurement at West Russian stations by about 7-10°C. At the East Siberian stations, the HIRHAM-LSM model does not show any improvement in winter soil temperature biases, but it has improved during summer. During summer the HIRHAM-LSM 's soil temperature has been cooled down everywhere in the land part. However the summer cooling has brought the coupled model soil temperature at East Siberian stations very close to the observations. At 10cm depth, the horizontal patterns of HIRHAM-LSM simulated soil temperature are warmer in Western Russia, Alaska and Scandinavia by a maximum of 6°C. Now the summer 2m air temperature bias in the coastal region has been reduced (Figure 2).

There are difficulties in comparing station data with the model simulation of 50×50 km horizontal resolution. Within the 50×50 km model grid area, large variations in soil temperature can not be ruled out. For example, 2 stations in West Russia; Petrun (60.49E, 66.26N) and Khoseda (59.23E, 67.05N) are very close to each other, but the monthly mean soil temperature at 20 cm depth differs by a maximum of 12°C during winter. During summer, the differences are relatively small (maximum of about 6°C).

4. IPCC B2 scenario simulations by HIRHAM4 and HIRHAM-LSM

The main objective of these simulations was to find out the influences of different soil and vegetation schemes on future Arctic climate projection, particularly on the future soil temperature projection. Both of the models have shown a large winter warming/cooling in 2m air temperature during the positive NAO (2037-2042) phase compared to the negative NAO (1990-1995) phase. The winter 2m air temperature over Eurasia and Western Europe has warmed up by a maximum of 10°C and cooled down over Alaska and East Siberia by a maximum of 6°C. Similar warming and cooling spatial patterns are seen also in the ECHO-G B2 scenario 2m air temperature (the ECHO-G IPCC B2 scenario simulation was used for lateral, lower forcing and initial condition of HIRHAM4 and HIRHAM-LSM simulations).

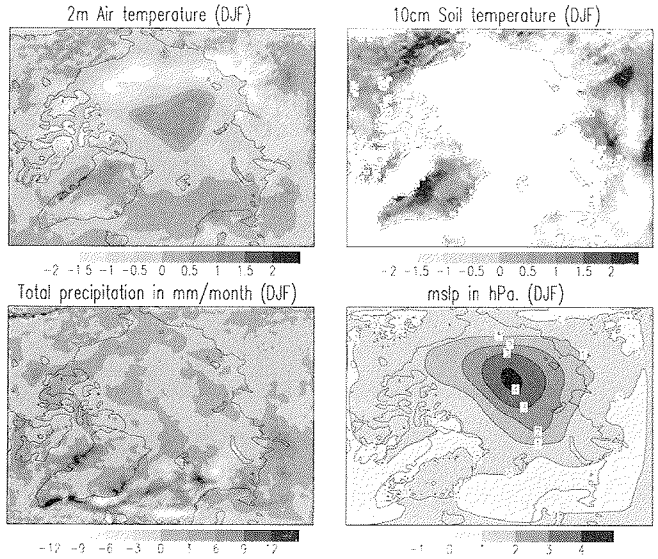

Figure 3: HIHAM-LSM projected change (2037-42 minus 1990-1995) minus HIRHAM4 projected change in 2m air and 10cm soil temperature (in °C), precipitation (in mm month^{-1}) and mean sea level pressure (in hPa).

The new land surface scheme and its coupling with the model HIRHAM4 have shown an influence on the winter soil temperature. The differences between the HIRHAM-LSM and HIRHAM4 simulated 2m air and soil temperatures are of the order of ±2°C (Figure 3). Therefore the future projection of Arctic air and soil temperature are uncertain by at least ±2°C due to only the land-surface scheme and it's interactions with the atmosphere. Also there are changes in summer precipitation by 12 mm month^{-1} in the HIRHAM-LSM model compared to the HIRHAM4 and their spatial distributions are very patchy. The mean sea level pressure was also changed in the HIRHAM-LSM model by a maximum of 4 hPa.

References

Bonan, G. B., A land surface model (LSM version 1.0) for ecological, hydrological and atmospheric studies: Technical description and user's guide, Tech. rep. NCAR/TN-417_STR, National Center for Atmospheric Research, NCAR, P.O. Box 3000, Boulder, Co 80307, 1996a

Christensen, J. H., E. van Meijgaard, On the construction of a regional climate model, DMI Tech. Rep. 92-14, Dan. Meteorol. Inst., Copenhagen, Denmark, 1992.

Christensen, J. H., O. B. Christensen, P. Lopez, E. van Meijgaard and M. Botzet, The HIRHAM4 regional atmospheric climate model, DMI Sci. Rep. 96-4, Dan. Meteorol. Inst., Copenhagen, Denmark, 1996.

Dethloff, K. A., A. Rinke, R. Lehman, J. H. Christensen, M. Botzet, B Machenhauer, Regional climate model of the Arctic atmosphere, J. Geophys. Res., 101, 23401-23422, 1996.

Køltzow, M., S. Eastwood, Comparison between temperature dependent parameterization schemes for snow albedo and estimated snow albedo from AVHRR, Research Note 98, Norwegian Meteorological Institute, 2003.

Louis, J. F., M. Tiedtke, J. F. Geleyn, 'A short history of the operational PBL-parameterization at ECMWF', in Proceeding of the ECMWF workshop on boundary layer parameterization, ECMEF, Reading, U.K., 1982.

Willmott, C. J., M. A. Rawlins, Arctic land-surface air temperature: Gridded monthly and annual climatologies (version 1.0), Center for Climate Research, Department of Geography, University of Delaware, Newark, DE 19716, 1999.

Multidecadal variability: What are the causes?

Torben Schmith and Martin Stendel

Danish Meteorological Institute, Copenhagen, Denmark

As a part of the GLIMPSE project we present some results from investigations on the nature of multidecadal variability in the ECHAM4/OPYC3 coupled model. More specifically, we analyse two runs of 500 year length each - one forced with reconstructed natural and antropogenic forcing and one unforced {{8216}}control{{8217}} run. We investigate the hypotheses, that the multidecadal variability seen in these runs (and in experiments with other models) is either generated by internal dynamics or externally forced. Also a third hypothesis: the combination, internally generated but phase-locked to the external forcing, e.g. in the form of the Gleisberg cycle in the solar irradiance, will be considered. We will mainly investigate oceanic quantities, such as sea surface temperatures and sea ice using spectral analysis tools, such as singular spectrum analysis supplemented by other statistical methods.

How does the ocean move beneath sea ice? Problems and Implications concerning model studies and observations

David Schröder

Meteorological Institute, University of Hamburg, Hamburg, Germany

Introduction

Near-surface ocean current is generally dominated by wind driving. According to Ekman theory net frictional stress balances Coriolis force with surface current perpendicular to both and about 45° to the right of wind. Inside the Ekman layer ocean velocity decreases and rotates clockwise with increase in depth (e.g., Pond and Pickard, 1979). If sea ice is present the Ekman layer is shallow and the rotation can occur within a layer of less than 30 m depth. This is approved my measurements from the 1972 AIDJEX Pilot Study (Mc Phee and Smith, 1976).

This study is based on simulations with a numerical dynamic-thermodynamic sea ice model for the Fram Strait region (2000 km x 1600 km area with a horizontal resolution of 9 km). The simulations are forced with 6-hourly atmospheric ECMWF analyses (European Centre for Medium-Range Weather Forecasts) and 6-hourly oceanic data of a MPI-OM-simulation (Max-Planck-Institute Ocean Model). The MPI-OM-simulation was forced with NCEP analyses and provided by Sein (MPI Hamburg). Sensitivity studies are carried out to analyze the impact of ocean current on sea ice. A detailed description of the sea ice model and the performed simulations is given by Schröder (2005). The applied ocean current of the MPI-OM-simulation is compared with DCM-measurements (Doppler Current Meter) provided by Hansen (Norwegian Polar Institute, Tromsø). The simulated sea ice drift and concentration of the sensitivity experiments are investigated and compared with drift measurements of 26 ice buoys - deployed during the two field experiments FRAMZY 1999 (Brümmer, 2000) and FRAMZY 2002 (Framstraßenzyklonen - Fram Strait Cyclones) (Brümmer et al., 2005) - during April 1999 and March 2002 and SSM/I data (ASI algorithm, horizontal resolution of 12.5 km, provided by Kaleschke, Uni Bremen).

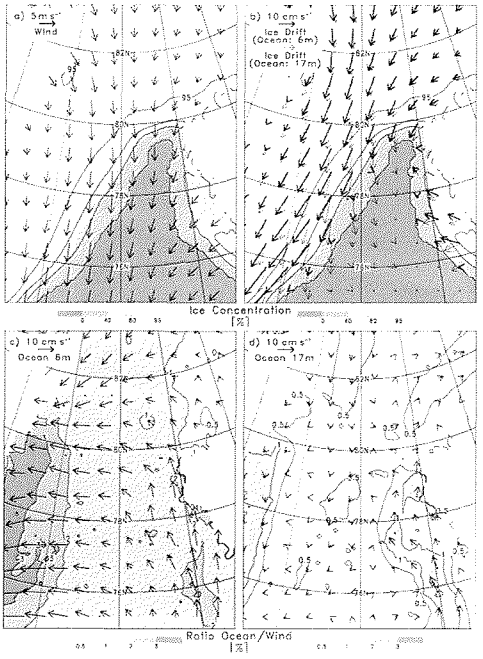

Figure 1: Mean 10m-wind field (ECMWF) (a), ice drift for the simulations forced with the ocean current at 6 m (thick arrows) and at 17 m (thin arrows) (b), ice concentration (shaded, a and b), ocean current (MPI-OM) at 6 m (c) and 17 m (d), and the ratio between ocean current and wind speed (shaded, c and d).

Results

March 2002 mean values of wind vector (ECMWF, height of 10 m), ocean current (MPI-OM, depths of 6 m and 17 m), and simulated ice drift are presented in Fig. 1 for the Fram Strait region (located between Greenland and Spitsbergen). In general, the ocean at the uppermost level (6 m, Fig. 1c) moves about 90° right of the wind (Fig. 1a) with 1 to 2 % of wind speed. The relative direction is in agreement with Ekman theory. The speed ratio is higher close to the coast of Greenland due to the East Greenland Current and the relative angle is larger in the southwest of Spitsbergen due to the West Spitsbergen Current. Outside these two currents the ocean current at 17 m representing the geostrophic current (Fig. 1d) is one order of magnitude smaller than at 6 m. The impact on the ice drift is shown on Figure 1b for both simulations: forced by uppermost ocean current (thick line) and forced by geostrophic current (thin line). The remarkable differences concerning ice drift speed and direction document impact and problem of the ocean current. It matters whether the geostrophic current (generally applied at uncoupled sea ice models (e.g., Dierer and Schlünzen (2005) and Zhang et al. (1999)) or the uppermost ocean current (generally applied at coupled sea ice models (e.g., Maslowski and

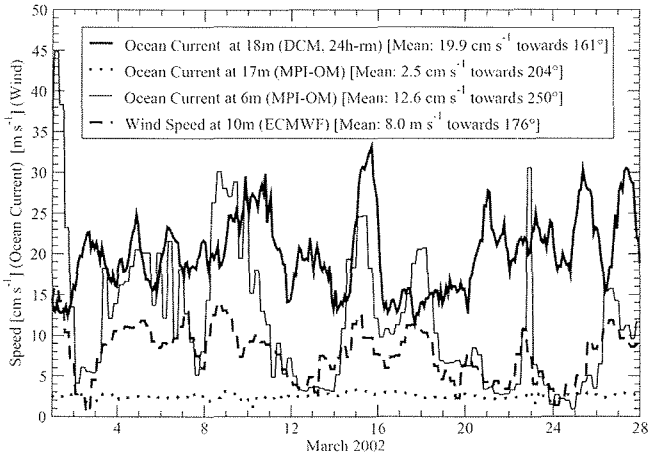

Figure 2: Time series of ocean current (measurements from a Doppler Current Meter and simulations of MPI-OM) and wind speed (ECMWF) at the location 79° N and 4° W for March 2002.

The ocean current measured by a Doppler Current Meter (18 m beneath sea ice at 79° N and 4° W) shows a high degree of variability at a time scale of days (thick line in Fig. 2). There are no similarities with the ocean current of MPI-OM (dotted line) at a comparable depth (17 m) which is one order of magnitude smaller and has a mean direction shifted by more than 40°. This statement is not only valid for one gridpoint but for the whole region. Studying the current at the uppermost level (thin line) the speed is similar to the observed speed, but the difference between the mean directions amounts to 90°. The comparison reveals that the simulation of the near-surface ocean current beneath sea ice in Fram Strait is a challenge not properly solved by the applied MPI-OM simulation in March 2002. Comparing the measured ocean current to the wind speed of ECMWF it is striking that the mean current is 15° left of the wind. It has to be mentioned that the quality of the current measurements is not known at short time scales (days to weeks).

Conclusions

The problems regarding the near-surface ocean current show that improved high frequency measurements are necessary at different depths to verify the current beneath sea ice in ocean models. Due to the impact on the divergence of sea ice (Schröder, 2005), it is important to measure horizontal distributions, e.g., by arranging DCMs in arrays. Beside complex coupled ocean-ice-atmosphere models simple uncoupled model studies are necessary to understand and verify sub-processes, separately.

Acknowledgement

I thank Burghard Brümmer, Amélie Kirchgäßner, and Gerd Müller for their support, Dimitry Sein for the MPI-OM simulations, Edmond Hansen for the DCM data, and Lars Kaleschke for the SSM/I data. The work was funded by the German Science Foundation under grant SFB 512/TP C2.

References

Brümmer, B. (Ed.), 2000: Field Experiment FRAMZY 1999 -- Cyclones over the Fram Strait and their impact on sea ice, Field report with examples of measurements. Ber. Zentrum für Meeres- und Klimaforschung, Univ. Hamburg, Met. Institut, Reihe A, 33, 178 pp.

Brümmer, B., J. Launiainen, G. Müller, and D. Schröder, 2005: Field Experiment FRAMZY 2002: Second experiment on cyclones over the Fram Strait and their impact on sea ice, Field report with examples of measurements. Ber. Zentrum für Meeres- und Klimaforschung, Univ. Hamburg, Met. Institut, Reihe A, 37, 134 pp.

Dierer, S. and K.H. Schlünzen, 2005: Influence parameters for a Polar mesocyclone development. Meteorologische Zeitschrift, submitted.

Maslowski, W. and W.H. Lipscomb, 2003: High resolution simulations of Arctic sea ice, 1979 – 1993. Polar Research 22 (1), 67-74.

McPhee, M.G. and J.D. Smith, 1976: Measurements of the turbulent boundary layer under pack ice. J. Phys. Oceanogr., 6, 696-711.

Pond, S. and G.L. Pickard, 1979: Introductory dynamic oceanography. Pergamon Press Ltd., Oxford, U.K., 241 pp.

Schröder, D., 2005: Wirkung von Zyklonen auf das Meereis in der Framstraße: Modellrechnungen und Beobachtungen. Ph.D. thesis, Fachbereich Geowissenschaften, Univ. Hamburg, 149 pp., http://www.sub.uni-hamburg.de/opus/volltexte/2005/2446.

Timmermann, R., A. Beckmann und H.H. Hellmer, 2002: Simulations of ice-ocean dynamics in the Weddel Sea -- 1. Model configuration and validation. J. Geophys. Res., 107 (C3), doi:10.1029/2000JC000741

Zhang, Y., W. Maslowski und A.J. Semtner, 1999: Impact of mesoscale ocean currents on sea ice in high-resolution Arctic ice and ocean simulations. J. Geophys. Res., 104 (C8), 18409-18429.

Arctic Oscillation regime behaviour in an idealized atmospheric circulation model as a result of almost-intransitivity

Mario Sempf[1], Klaus Dethloff[1], Dörthe Handorf[1], Michael V. Kurgansky[2]

[1] Alfred Wegener Institute for Polar and Marine Research, Potsdam, Germany
[2] Department of Geophysics, Faculty of Physics and Mathematics, University of Concepcion , Chile, On leave from A. M. Obukhov Institute of Atmospheric Physics, Moscow, Russia

A quasi-geostrophic, hemispheric three-level atmospheric model with horizontal T21 resolution is driven by Northern Hemisphere's T21 topography, whereas its thermal and surface forcing are determined by an automated, iterative tuning procedure. The zonal parts of the forcings are tuned to produce a realistic zonal wind profile for northern winter, while non-zonal thermal forcings are adjusted to obtain time-averaged non-zonal diabatic heating fields equal to wintertime observations. The perpetual winter model simulation reproduces observed wintertime climatology and patterns of low-frequency variability with accuracy. The model exhibits two significant circulation regimes which correspond to the positive and negative phase of the Arctic Oscillation (AO), respectively.

Steady solutions of the model equations have been determined, but they do not coincide with the regime centroids. They are even far outside of the system's attractor and therefore do not directly influence the model's dynamics. But an explanation of the dynamical structures underlying the model's regime behaviour is suggested by the results of a series of model experiments, in which the tuning procedure is repeated using lower values of surface friction. The weaker the surface friction is, the more distant and pronounced the two AO regimes become, indicated by increasing geopotential standard deviation at polar latitudes and also by the AO index distribution, the bimodality of which is becoming more and more extreme. The regime persistence, but also the model's sensitivity with respect to forcing changes dramatically increases. Due to this sensitivity, the tuning procedure fails to reproduce the observed zonal climate if the strength of the surface friction is below some critical value. Rather, the model's climate flips between the two extreme AO phases from one tuning iteration to another, but still allows for rare jumps to the other regime, respectively.

Based on these results, the two regimes observed in the control simulation are interpreted as a feature of the attractor's large-scale geometry in phase space, not necessarily requiring the existence of steady states embedded in the attractor. In the case of very low surface friction, the attractor evidently consists of two lobes connected by a thin channel, a structure qualitatively similar to Lorenz' attractor. The almost-intransitivity of the system generates the persistence of the regimes, the irregularity of the transitions and ultra-low frequency variability. Increase of the surface friction makes the two lobes approach each other and strengthens the connection between them, thus shortening the lifetime of regimes and increasing the frequency of transitions.

Effects of climatic forcing on the marine ecosystem of the Barents and the Greenland Seas

D. Slagstad[1], I. Ellingsen[1], M. Reigstad[2], and P. Wassmann[2]

[1] SINTEF Fisheries and Aquaculture, Trondheim, Norway
[2] University of Tromsø,, Norway

The seasonal ice zone (SIZ) is an area where annual and interannual variations in the physical conditions are large. In some years the SIZ may reach far into the Arctic Ocean, whereas in others there is much ice in the Northern Barents and the Greenland Seas even in late summer. The ecosystem in this zone must be able to tolerate and adapt to this large variability in ice cover. The SIZ is also an area where animals and algae of both Atlantic and Arctic origin coexist. Permanent change in the SIZ is expected to affect the biological productivity as well as the ecosystem structure.

In order to study the effect of climatic variability and climatic change on the ecosystem in the SIZ, we used an established ecological model (Wassmann et al., 2005) coupled to a hydrodynamic-ice model of the Arctic Ocean and the Nordic Seas (Slagstad and McClimans, 2005). The atmospheric inputs used are the NCEP/NCAR Reanalysis data (http:cdc.noaa.gov) for the period 1990 to 2004 and a GCM (ECHO-G) for two time slices choosing negative and positive phases of the NAO-index.

Model set-up and boundary conditions

The model domain encompassing the Nordic Seas and the Arctic Sea uses a horizontal grid point distance of 20 km. The model has 25 vertical levels. The levels which were modelled are the upper 10 m just below the sea surface, 10-15, 15-20, 20-25, 25-30, 30-35, 35-40, 40-50 m, then 50-75, 75-100, 100-150, 150-200, 200-250, 250-300, 300-400, 400-500, 500-700, 700-1000, 1000-1500, 1500-2000, 2000-2500, 2500-3000, 3000-3500, 3500-4000 and 4000-4500. The ice model is based on the EVP rheology described by Hunke and Dukowics (1997) and Hibler (1979).

On the open boundaries in the North Atlantic and the Arctic Ocean, the current velocities are specified (Slagstad and Wassmann, 1997). The inflow through the Bering Strait is assumed to be 1 Sv.

Four tidal components (M_2, S_2, K_1 and N_2) were imposed by specifying the various components at the open boundaries of the large-scale model. Data were taken from Schwiderski (1980).

The heat flux is calculated from air temperature, humidity, cloud cover. Initial values of temperature and salinity are taken from NODC World Ocean Atlas 1998 data (known also as the Levitus data base) provided by the NOAA-CIRES Climate Diagnostics Center, Boulder, Colorado, USA, from their Web site at http://www.cdc.noaa.gov/.

The ecological model (Wassmann et al., 2005) contains state variables for nitrate, ammonium, silicate, diatoms, flagellates, microzooplankton, DOC, heterotrophic flagellates, bacteria and two groups of mesozooplankton representing the Arctic and Atlantic species. The vertical export of carbon is represented with two state variables, fast and slow sinking detritus. This model is run online with the hydrodynamic model with a time step of 1800 s.

Results

The control run from 1990 to 2004 using NCEP as input data shows an annual mean primary production in the Greenland Sea of 86 g C m^{-2} (Fig. 1) and an interannual variability in the range of -22 to +35 %. The variability observed is mainly due to variations in the ice cover

during summer. Ice has a profound effect on primary production also after the ice melt. At high ice concentrations very little light is able to penetrate into the water, making phytoplankton growth light limited. As the ice melts during the summer more light can penetrate into the water column allowing the phytoplankton to grow. However, the ice melt stratifies the water. The nutrients are used quite rapidly in the euphotic zone, and the supply of nutrients from deeper water is inhibited by the stratification.

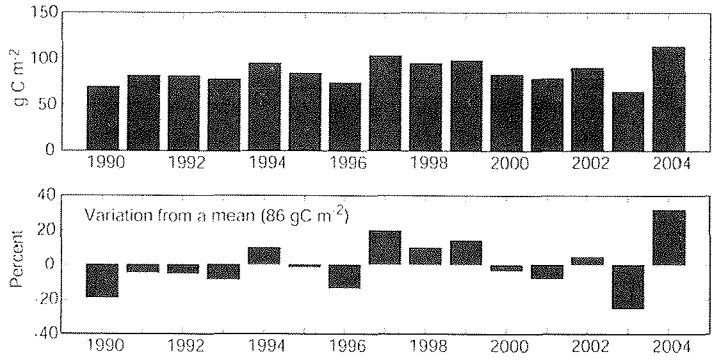

Figure 1. Simulated annual primary production (upper panel) and relative variability from the mean (lower panel) in the Greenland Sea using NCEP/NCAR atmospheric data as input.

In the Barents Sea, the average primary production (103 g C m^{-2}) is higher than in the Greenland Sea due to strong influence of Atlantic water (Fig. 2). The annual variability in the Atlantic water is low compared with the Arctic water. In the Northern Barents Sea, the annual production ranges from 20 to 80 g C m^{-2}, depending on ice cover and stratification.

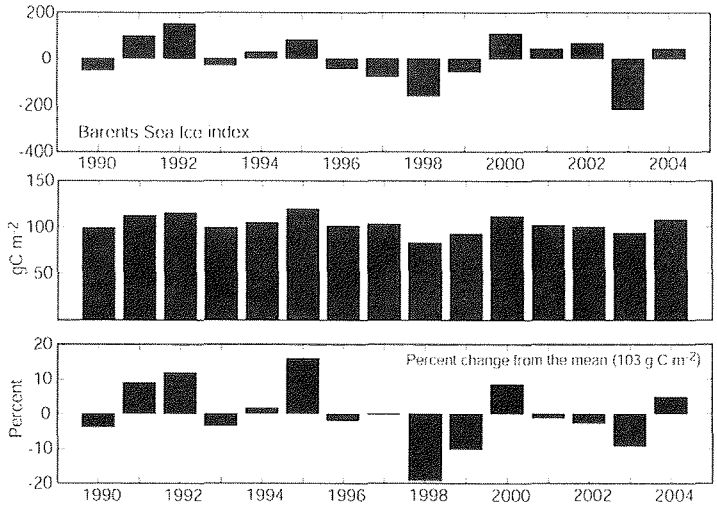

Figure 2. Upper panel: Barents Sea Ice index. Negative values indicate more ice and positive values less ice. Mid panel: Average annual production for the Barents Sea (g C m^{-2}). Lower panel: Variability in primary production from the mean (1990-2004).

Using ECHO-G as input

The Global Climate Model, ECHO-G (IPCC B2 scenario) was used as input to the coupled hydrodynamic and ecological models. Two time slices were selected based on the phase of the NAO, a negative phase (NAO^-) from 2024 to 2029 and a positive phase (NAO+) from 2037 to 2042. The initial conditions (ice, hydrography and biology) were taken from the NCEP simulations in December 2004. The annual mean primary production for both positive and negative NAO is 95 g C m^{-2}. This is 16% less than the annual average for this area using NCEP reanalysis data as model input. The interannual variability also appears to be less than for the NCEP simulations. Lower production is especially pronounced in the Atlantic water masses. The reason for this is that ECHO-G produce less vertical mixing in the upper water column that results in less supply of nutrients from the deep water. We speculate that this can be caused by underestimation of wind stress and low pressure passages through the Barents Sea in the GCM.

The model failed to find any difference in primary production in the Nordic Seas as consequences of different phases of NAO. This suggests that the winter (DJFM) NAO index has no significant effect on the primary production in the Nordic Seas. Wind and heat flux during the productive season (April –September) is much more important for primary production bringing up nutrients into the euphotic zone.

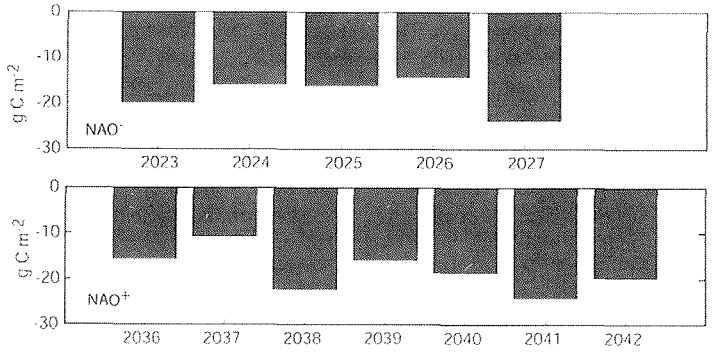

Figure 3. Deviation in primary production from the mean NCEP 1990-2000 simulation (113 g C m^{-2}) for the Nordic Seas. Upper panel: Negative phase of NAO. Lower panel: positive phase of NAO.

References

Hibler III, W.D., 1979. A dynamic thermodynamic sea ice model. J. Phys. Oceanogr., 9: 815-846.

Hunke, E.C. and Dukowicz, J.K., 1997. An elastic-viscous-plastic model for sea ice dynamics. J. Phys. Oceanogr., 27(9): 1849-1867.

Slagstad, D. and McClimans, T., 2005. Modelling the ecosystem dynamics of the Barents Sea including the marginal ice zone: I. Physical and chemical oceanography. J. Mar. Syst.

Slagstad, D. and Wassmann, P., 1997. Climatic change and carbon flux in the Barents Sea: 3-D simulations of ice-distribution, primary production and vertical export of particulate organic carbon. Mem. Natl Inst. Polar Res., 51(Special Issue): 119-141.

Wassmann, P., Slagstad, D., Riser, C.W. and Reigstad, M., 2005. Modelling the ecosystem dynamics of the Barents Sea including the marginal ice zone: II. Carbon flux and climate variability. J. Mar. Syst.

Modeling the summer Arctic boundary layer

Stefan Söderberg, Michael Tjernström and Mark Žagar

Stockholm University, Department of Meteorology, Stockholm, Sweden

1. Introduction

Recent years have seen an increased interest in the Arctic climate, partly because of its large sensitivity to anthropogenic climate change and partly due to the potentially large impacts to Arctic society and ecosystems of the projected climate changes for the next century [e.g. ACIA, 2004]. At the same time, the climate models used for climate projections perform worse in the Arctic than elsewhere and the inter-model scatter in future climate projections is also larger than for any other region on Earth [Walsh et al., 2005]. The Arctic Regional Climate Model Intercomparison project [ARCMIP, Curry and Lynch, 2002] aims at identifying model deficiencies and improving the description of Arctic climate processes in numerical models. This is achieved by controlled regional-modeling experiments. In the first ARCMIP experiment, several models were run for the SHEBA [Surface Heat Budget of the Arctic Ocean, Uttal et al., 2002] year, and results were intercompared and compared with SHEBA observations [Tjernström et al. 2005, Rinke et al. 2005].

This paper describes a similar experiment. The COAMPS^{TM} model [Hodur 1997] is used to simulate the Arctic Ocean Experiment 2001 [AOE-2001, Leck et al. 2004]. The AOE-2001 was an icebreaker-based experiment launched during July and August 2001. One specific component was a three-week ice drift, when the icebreaker *Oden* was moored to an ice floe around 89 °N and drifted in a generally southerly direction with the ice; both the icebreaker and the ice floe was utilized as measurements platforms. The experiment and some results are described in detail in Tjernström et al. [2004a, 2004b] and Tjernström [2005].

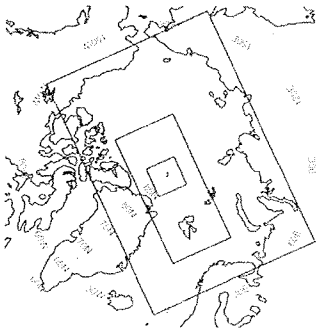

Figure 1. Model domains used for the AOE-2001 simulation. The three boxes show the three nested domains with the AOE-2001 ice-drift track shown inside the innermost domain. See the text for a discussion of the simulation set-up.

The model domains used for this experiment is shown in Figure 1. It consisted of an almost pan-Arctic outer domain, with a 54-km resolution, and two smaller nests, at 18 and 6 km resolution, respectively. The total simulation length was two months, from 1 July to 31 August 2001; the innermost nest was only used for the three-week ice drift, from 2 through 22 August. Similar to ARCMIP experiment 1, lateral boundary forcing was provided at six-hour intervals at the outer domain, using ECMWF (European Centre for Medium Range Weather Forecasts) analyses; COAMPS^{TM} then employs a system with instantaneous nesting for

subsequent nests with a factor-of-three resolution increase. Sea surface temperature (SST) and ice fraction were prescribed from AVHRR (Advanced Very High Resolution Radiometer) and SSMI (Special Sensor Microwave Imager) satellite observations, respectively, although SST in partially ice-covered areas was set to -1.8 °C. In contrast to the previous ARCMIP experiment, however, this simulation was performed using a thermodynamic ice model, allowing the surface temperature to respond to changes in surface radiation. The ice models carries separate energy balance relations for snow and bare ice, and also for the amount of snow on the ice. When the snow melts, a fraction of the melt water it is retained in the snow and is available for re-freezing if the temperature drops again.

2. Model results

2.1 Vertical structure

The vertical temperature structure of the lowest 4 km of the atmosphere is illustrated in Figure 2a and b, showing the observed temperatures from radiosoundings and from the model, respectively.

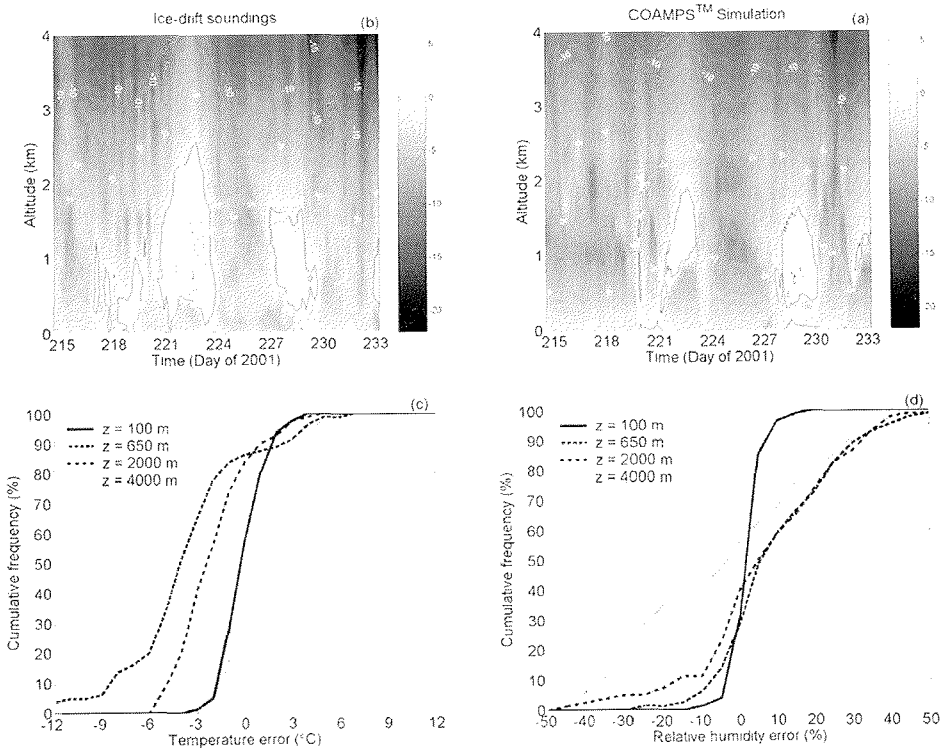

Figure 2. Time-height cross-sections of temperature from (a) the AOE-2001 soundings and (b) from the model simulation, and the cumulative frequency of the (c) temperature and (d) relative humidity errors, at a few selected heights (see the legend).

It appears that the model captures most of the variability in time, but creates a too deep cool layer at the surface. Two major warming events occurred during the ice drift, the first on JD 221 – 223 and the second on JD 227 – 229. The first of these has the warmest temperatures recorded during the ice drift, ~ 8 °C around ~ 600 m; the second event also has a significant warming above the boundary layer, but not as intense as the first. The model simulates both

events roughly correctly in time, but has a larger warming during the second than during the first event. The reason for the less warm air on top of the boundary layer seems to be a very rapid deepening in the modeled boundary-layer depth, indicating that cloud top entrainment on this day is too strong in the model, or possibly that the synoptic scale subsidence is too weak. To some degree the model also fails to simulate the very variable conditions during the first few days of the ice drift; this is even clearer in the simulated wind speeds aloft (not shown), Differences of this kind is likely at least partly a consequence of the large outer domain, allowing the model more freedom to develop its own internal dynamics that may deviate from that present in the ECMWF results that were imposed at lateral boundaries relatively far away from the area of interest.

Figure 2c and d compares the modeled temperature and relative humidity to that observed in the soundings at four heights: 100, 650, 2000 and 4000 m. The lowest should be within, while the second lowest should almost always be on top of, the boundary layer. The 4-km level should be representative of the free troposphere, while the 2-km level is in between and should be affected by local processes such as cloud formation. For the temperature, the lowest (boundary layer) and highest (free troposphere) layers have errors on average close to zero with an RMS error around ~1 °C. The boundary-layer level is strongly controlled by the melting and freezing processes at the surface, as in reality, while the upper presumably contains a strong signal from the analyzed boundaries. The two intermediate levels are significantly colder in the model than in reality, by 3 – 4 °C, although the RMS error is about the same. The 650-m level, with the largest mean error, is likely almost always in the cloud layer so a possible reason is a problem with the modeled clouds, although the 2-km level is more seldom inside clouds. Another potential cause of this error is the effects of shallow but intense synoptic systems evolving differently in the model than in reality; such shallow systems were encountered frequently [Tjernström et al. 2004a]. In the observations, these systems were often visible in the lowest few kilometers, except at the surface where the surface control dominated the conditions. The relative humidity error in the boundary layer is also close to zero with a reasonable scatter. At all the higher levels the results are more scattered and skewed towards more cases when the model is too moist except at the highest level, where the errors are about zero on average with a large scatter.

2.2 Clouds and boundary-layer conditions

The relative probability of the lowest cloud base and cloud top in the model and from the observations are shown in Figure 3a. In the observations, there are practically always low clouds present, with most common lowest cloud base around 100 m and the lowest cloud top mostly around 500 – 800 m [Tjernström 2005]. While the lowest cloud tops in the model correspond well with the observations, the modeled clouds are much to thin and the lowest clouds bases are therefore underrepresented; in fact it seems that the model tends to have its clouds distributed over one or only a few grid points in the vertical instead of the deeper more solid cloud layers that were observed by the cloud radar. The relative probability of boundary-layer depth, based on the same Richardson-number criteria in the model as in the observations, is shown In Figure 3b; the modeled results compare very favorable with the observations.

The near-surface conditions for temperature and relative humidity are illustrated in Figure 3c and d, respectively. Most commonly the near-surface temperature lies in the –2 to 0 °C range. This temperature interval is easily understood, observing that while fresh water melts at 0 °C, salty ocean water freezes at ~ -1.8 °C. Thus the temperature is restricted on the high side as long as ice persists in the water, while there is a latent heat of freezing is released at the lower temperature as long as there is open water present. The model seems to prefer to be on the cool side, closer to the lower value, while the upper value was more common observed. The model also almost entirely misses a cold event lasting a few days with temperatures down to ~

-6 °C. A closer inspection of the model results, however, reveals that the model actually simulates this event but slightly misplaces it in space. This illustrates both the problem of comparing model results with single-point observations and that of having a large outer domain. The model significantly underestimates the near-surface relative humidity (Figure 3d).

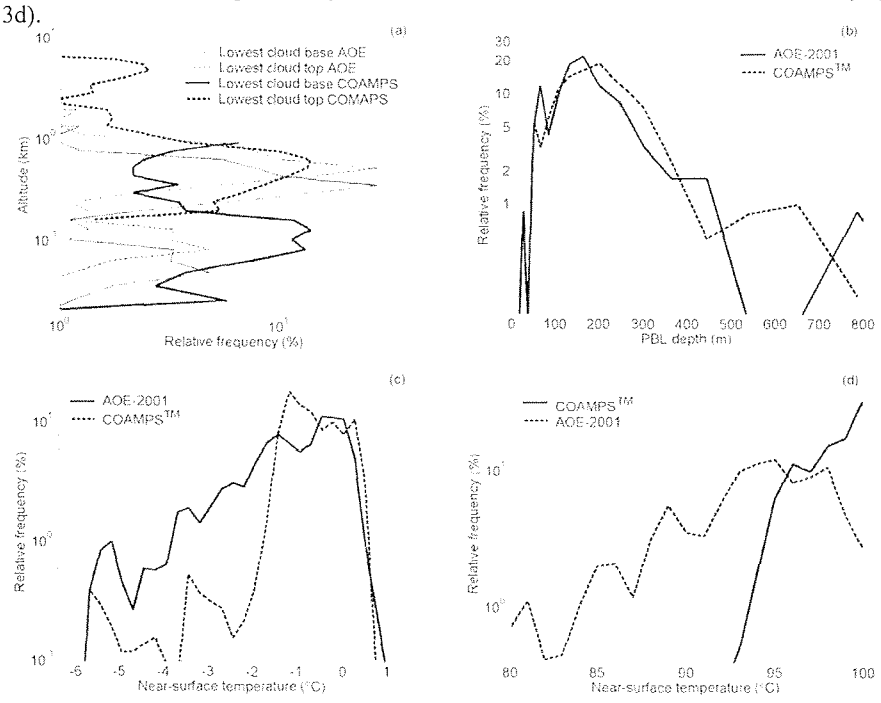

Figure 3. Probability density functions from the model and observations for (a) lowest cloud base and cloud top (km), (b) boundary layer depth (m), near-surface (c) temperature and (d) relative humidity

3. Summary

A two-month simulation for the Arctic Ocean Experiment 2001 (AOE-2001) is presented. In this paper the emphasis is on a model evaluation for the three week ice drift, from early August 2001, for which extensive observation data is available. The COAMPS™ model was applied to this experiment, using nested domains with a relatively large outer domain that was forced 6-hourly with analyzed fields from ECMWF. Ice concentrations and open-water SST was also prescribed from satellite data, while ice-surface temperature was calculated with a thermodynamic ice model. The forcing data as well as data for model evaluations for this experiment is available from the authors should any other modeling group want to repeat this experiment.

The comparison of the modeled results with the observations show that the model captures the main observed events, but that some synoptic scale events are missing in the model at the grid point closest to the experimental location. This is most likely a result of using a large outer domain, allowing the model large freedom to develop its own internal dynamics that, due to the chaotic nature of atmospheric flows, may become slightly different from what was prescribed at the lateral boundaries, without having to be incorrect from a physical point of view.

The largest difference between the model and the observations is found in temperature and humidity at moderate altitude, 0.5 – 2 km, and in the representations of the clouds, which at least to some degree occur in the same height interval. The modeled temperatures are too low and consequently the relative humidity is often too high. The clouds are much to thin in the model. While the cloud tops seem to be roughly correct, the lowest cloud bases are therefore much too high. Near-surface temperatures are reasonably well captured, but low-level relative humidity is too low, which may partly explain the relative lack of very low clouds.

References

ACIA, *Impacts of a warming Arctic, Arctic Climate Impacts Assessment*, Cambridge University Press, 2004.

Curry J.A. and A.H. Lynch, Comparing Arctic Regional Climate Models, *EOS Trans.*, 83, 87, 2002.

Hodur, R. M., The Naval Research Laboratory's coupled ocean/atmosphere mesoscale prediction system (COAMPS). *Mon. Wea. Rev.*, 125, 1414 — 1430. 1997.

Leck, C., M. Tjernström, P. Matrai and E. Swietlicki, Microbes, clouds and climate: Can marine microorganisms influence the melting of the Arctic pack ice? *EOS Transactions*, 85, 25 – 36, 2004

Rinke, A, K. Dethloff, J.J. Cassano, J.H. Christensen, J.A. Curry, P. Du, E. Girard, J.-E. Haugen, D. Jacob, C.G. Jones, M. Køltzow, R. Laprise, A.H. Lynch, S. Pfeifer, M.C. Serreze, M.J. Shaw, M. Tjernström, K. Wyser, M. Zagar, Evaluation of an Ensemble of Arctic Regional Climate Models: Spatiotemporal fields during the SHEBA year, Revised for *Clim. Dyn.*, 2005.

Tjernström, M., The summer Arctic boundary layer during the Arctic Ocean Experiment 2001 (AOE-2001). *Boundary-Layer Meteorology*, In press, 2005..

Tjernström, M., M. Žagar, G Svensson, J Cassano, S. Pfeifer, A. Rinke, K. Wyser, K. Dethloff, C. Jones and T. Semmler, Modeling the Arctic Boundary Layer: An evaluation of six ARCMIP regional-scale models with data from the SHEBA project, *Bound.-Layer Meteorol.*, In press, 2005

Tjernström, M., C. Leck, P. O. G. Persson, M. L. Jensen, S. P. Oncley and A. Targino, The summertime Arctic atmosphere: Meteorological measurements during the Arctic Ocean Experiment (AOE-2001), *Bull. Amer. Meteorol. Soc.*, 85, 1305 – 1321, 2004a.

Tjernström, M., C. Leck, P. O. G. Persson, M. L. Jensen, S. P. Oncley and A. Targino, Experimental equipment: A supplement to The summertime Arctic atmosphere: Meteorological measurements during the Arctic Ocean Experiment (AOE-2001). *Bulletin of the American Meteorological Society*, 85, 1322 – 1322, 2004b

Uttal, T., J. A. Curry, M. G. Mcphee, D. K. Perovich, R. E. Moritz, J. A. Maslanik, P. S. Guest, H. L. Stern, J. A. Moore, R. Turenne, A. Heiberg, M. C. Serreze, D. P. Wylie, P. O. G. Persson, C. A. Paulson, C. Halle, J. H. Morison, P. A. Wheeler, A. Makshtas, H. Welch, M. D. Shupe, J, M. Intrieri, K. Stamnes, R. W. Lindsey, R. Pinkel, W. S. Pegau, T. P. Stanton, T. C. Grenfeld, Thomas C, Surface Heat Budget of the Arctic Ocean, *Bull. Amer. Meteorol. Soc.*, 83, 255-276, 2002.

Walsh, J.E., S.J.Vavrus and W.L. Chapman, Workshop on modeling of the Arctic atmosphere, *Bull. Amer. Meteorol. Soc.*, 86, 845-852, 2005.

AOGCM sensitivity studies using Eliassen Palm fluxes as a diagnostic tool

E. Sokolova[1], K. Dethloff[1], A. Benkel[2], A. Rinke[1]

[1]Alfred Wegener Institute, Potsdam
[2]GKSS, Geesthacht

In order to investigate the feedbacks between regional Arctic climate processes and the global climate system, the atmosphere-ocean general circulation model ECHO-G has been applied with improved scheme, representing the sea-ice- and snow albedo interactions. The improved calculation of the snow albedo is based on new surface temperature dependent scheme; different for forested (linear dependency) and non-forested (polynomial approach) areas (Roesch, 2000). The sea ice albedo is calculated for 3 different surface types (snow covered ice, bare sea-ice, melt ponds and leads). In this case the scheme is linearly dependent on the surface temperature (Køltzow et al., 2003). These new parameterizations lead to a better agreement of the simulated model albedo and the Advanced Very High Resolution Radiometer (AVHRR) polar pathfinder (Xiong et al., 2002) as well as with the Surface Heat Budget of the Arctic Ocean (SHEBA) data (Uttal et al., 2002). In particular, the new scheme gives a higher and more realistic albedo in winter and early spring, improving the Arctic surface air temperatures representation (Saha, 2005) compared to climatological data set (Willmott, et al., 1999).

The ECHO-G atmospheric part is the ECHAM4 model with a horizontal resolution T30 (~ 3.75°x 3.75°) and 19 vertical levels. The used ocean model is HOPE-G, resolving the model area with T42 /L20 (~ 2.8°x2.8°) and 20 vertical levels (Zorita et al., 2004). The new albedo scheme is applied for the Northern hemisphere explicitly. The model was integrated for a 510 year period and forced with present day (1990) forcing conditions. A control run, with the same initial conditions but with the old sea ice and snow albedo parameterization is used for comparison in order to understand better the changes in the polar energy sink region.

Two 7 years periods are chosen for analysis, based on the area, covered by sea ice. First reference period is with significantly larger covered areas than the average values (high phase of sea ice), the second period is representative for smaller areas covered with sea ice than the average (low phase of ice snow) respectively.

The averaged annual surface air temperature difference between the new sea-ice and snow albedo run and the control run for this time slice is characterised by a cooling of the Arctic regions as a result of the increased albedo and a warming in a zonal belt covering the mid-latitudes. The annual cycle of Arctic sea-ice extent is found to be more realistic. The reason for the colder temperatures in the western Arctic is, that the polar vortex tends to be situated downstream of the northern Rocky Mountains. This preferred location is related to orographic forcing of planetary waves. The monthly and interannual variability of global temperature patterns is driven primarily by the interaction of the Arctic and mid latitude circulations through the strength and position of the polar vortex during winter (Dorn et al., 2000)

Fig. 1 shows the winter (DJF) averaged values for the temperature at 2m for the two periods - the one with high phase of ice cover (Fig. 1a) and with low phase of snow cover (Fig. 1b). For better comparison of the processes we show also the difference between these two periods in Fig. 1b and the sea ice cover (Fig. 1d). Lower temperatures at low phase of ice cover are observed over the Pacific area and the Davis Strait which corresponds directly to the higher values of sea ice cover. There is an increase in the temperatures over the Barents Sea, which is again a direct response of the smaller amount of sea ice cover. The relation between the higher temperatures over the North America and the ice cover is not that clear.

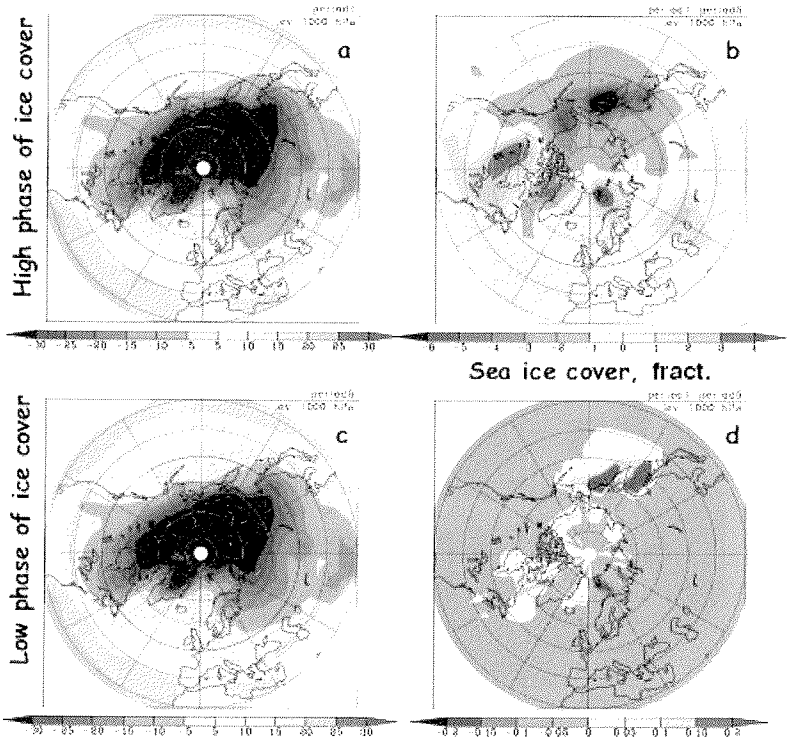

Fig. 1: Temperature at 2 m [deg.C] for the Northern Hemisphere, winter season (DJF) fort he periods of high phase of ice cover (a) and low phase of ice cover (c). (b) shows the difference between the periods (high-low). For comparison on (d) is shown the sea ice cover [frac.]

Figures 2a and 2c display the heat flux $(\overline{v'T'})$ on time scales of 2-6 days for winter for the two periods and the changes of it, compared to the control run, respectively (Fig. 2b and 2d). The heat flux on synoptical time scale corresponds clearly to the storm track activity in the Northern hemisphere. There is a small shift to the west of the centres of the storm tracks in the period with the low phase of snow cover (compare Fig.2a and 2c). Strongest changes occur over the North-American continent with a decrease of storm track activity due to a cooling of the Arctic related to the improved sea-ice and snow albedo simulations (Fig. 2b and 2d). Increased storm track activity occurs over the southern part of Greenland and the Fram Strait. The decreased storm track activity over the North Atlantic splits into two parts. One enters Northern Europe and decreases over Scandinavia, the other propagates to North Africa. A pronounced storm track increase appears over the Mediterranean Sea and Middle Asia. The storm track changes presented in Figure 3 are accompanied by changes in the zonal wind components over the northern hemisphere and a pronounced reduction in the North-American jet stream over the Pacific Ocean. It is not yet clear, whether the storm track changes are caused by or result from the large-scale circulation changes.

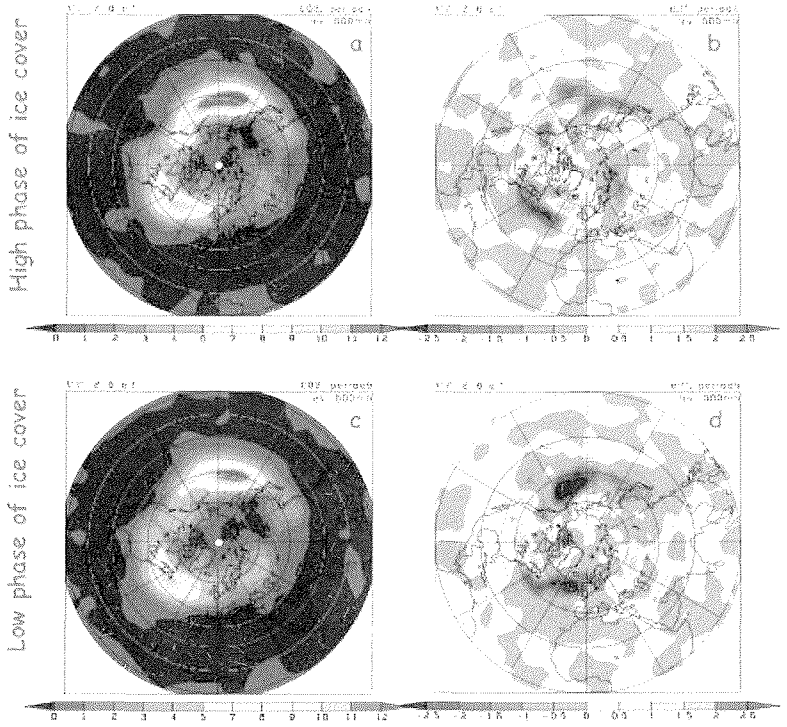

Fig. 2: Transient heat fluxes [Km/s] at 500 hPa, 2-6 days filter, for high phase of ice cover (a), low phase of ice cover (b) and differerences (new albedo–control run) for the high phase (c) and (new albedo-control run) for the low phase (d).

The atmosphere dynamics processes are analyzed also by using the localized Eliassen Palm (EP) fluxes. The applied method (Trenberth, 1986) is diagnostics of the impact of transient eddies on the time mean flow. There are number of advantages considering the EP flux. For quasi-geostrophic flow its divergence is proportional to the northward eddy flux of quasi-geostrophic potential vorticity. It provides a measure of the effects of wave transience and non-conservative effects.
According to Trenberth the localized EP flux for a quasi-geostrophic case is:

$$\vec{E}_u = \left[\frac{1}{2}\left(\overline{v'^2} - \overline{u'^2}\right), -\overline{u'v'}, f\frac{\overline{v'\phi_z'}}{S} \right] \qquad (1)$$

, where u and v are the velocity components, overbars represent a time average, f is the Coriolis parameter, S is the static stability, Φ is the geopotential height.

The first two components of (1) describe the barotropic feedback between the mean state and the transient waves due to momentum fluxes. The winter averaged barotropic part at 500 hPa of the EP fluxes is shown in Fig. 3. In Fig. 3a the EP flux is shown for the high phase ice cover period, and on Fig. 3b – the EP for the low phase of ice cover correspondingly. In both figures the zones of strongest flux correspond to the storm-track activities. The difference between the two periods (Fig. 3c) reveals that the feedback of the sea-ice and snow cover upon the atmospheric circulation is stronger in the Atlantic sector than in the Pacific. There is an indication for a wave train over the Pacific Ocean, connecting the tropics with the Arctic.

Changes in the Arctic sea-ice and snow cover introduced this change in the barotropic wave train at 500 hPa between the tropics and the Arctic over the Pacific.

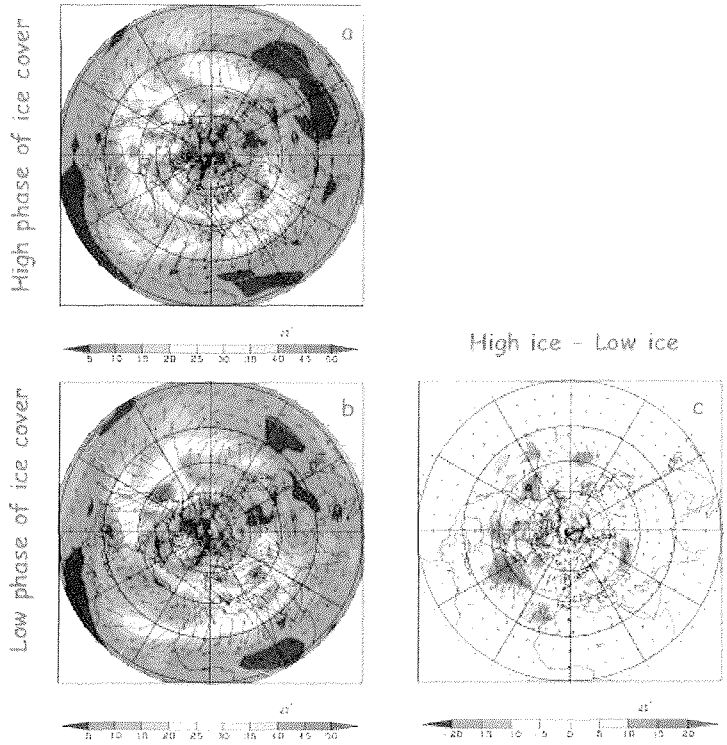

Fig. 3: Eliasses Palm (EP) flux [m^2/s^2] at 500 hPa, winter, barotropic part, for high phase of ice cover (a), low phase of ice cover (b) and difference high phase-low phase (c). Shades display the magnitude of the EP flux, the arrows describe the EP vector propagation.

Our results provide a physical mechanism to explain how regional sea-ice anomalies in the Arctic can exert a strong influence on the large-scale dynamical patterns of the atmospheric circulation patterns at seasonal and inter-annual time scales.

References

Dorn W., et al., Distinct circulation states of the Arctic atmosphere induced by natural climate variability, *J. Geophys. Res.* 105, 29.659-29.668 (2000).

Køltzow, M.Ø.,et al. Parameterization of snow and sea-ice albedo in climate models, *Res. Rep.* 149, Norwegian Meteorological Institute, Oslo, Norway (2003).

Roesch, C. A., Assessment of land surface scheme in climate models with focus on surface albedo and snow cover, *Zuercher Klimaschriften 78, ETH Geografisches Institut Zuerich* (2000).

Saha, S., The influence of an improved soil scheme on the Arctic climate in a RCM, PhD Thesis, University Potsdam, 115 pp (2005).

Trenberth, K. E., An assessment of the impact of transient eddies on the zonal flow during a blocking episode using localized Eliassen-Palm flux diagnostics, *J. Atmos. Sci.* 43, 2070-2087 (1986).

Uttal, T., et al., Surface heat budget of the Arctic Ocean, *Bull. Amer. Met. Soc.* 83, 255- 275 (2002).

Willmott, C. J.& M. A. Rawlins, Arctic Land-Surface Air temperature: Gridded monthly and annual climatologies (Version 1.01), Center for Climatic Research, University of Delware, Newark, 1999.

Xiong, X., K. Stammes & D. Lubin, Surface albedo over the Arctic Ocean derived form AVHRR and its validation with SHEBA data, *J. Appl. Met.* 41, 413-425 (2002).

Zorita, E., et al., Climate evolution in the last five centuries simulated by an atmosphere- ocean model: global temperatures, the North Atlantic Oscillation and the Late Maunder Minimum, *Meteorol. Z.* 13, 271 (2004).

Sensitivity of the Arctic Oscillation to Volcanic Forcing in the IPCC AR4 Climate Models

G. Stenchikov

Department of Environmental Sciences, Rutgers University, New Brunswick, NJ, USA

1. Introduction

The radiative perturbation caused by stratospheric aerosols produced by a major volcano provides a natural test of the ability of general circulation models (GCMs) to respond realistically to global-scale radiative forcing [*Stenchikov et al.*, 2002]. There are two main foci of such study, analysis of the simulation of global-mean surface temperature response and simulation of the response of the extratropical circulation in the NH winter season. With regard to the NH winter circulation, it is noteworthy that the observed long-term trends in the last few decades include a component that is consistent with a significant increase in the index of the AO [*Hurrell*, 1995; *Thompson and Wallace*, 1998]. This observed trend in the AO circulation is generally not well reproduced by current GCMs when forced with the historical trends of greenhouse gas and aerosol concentration [*Osborn*, 2004; *Knutson et al.*, 2005]. The models tend to underestimate AO variability and associated warming over land in high latitudes of the Northern Hemisphere (NH). These cause major deficiencies in the future NH polar climate projections. Low-latitude volcanic eruptions force a positive phase of the AO because of aerosol radiative heating in the equatorial lower stratosphere that strengthens the equator-to-pole temperature gradient in the lower stratosphere accelerating the polar vortex [*Kodera*, 1994; *Perlwitz and Graf*, 1995; *Ohhashi and Yamazaki*, 1999; *Shindell et al.*, 2001; *Black*, 2002]. This mechanism is based on a strong positive feedback between the polar NH winter vortex and vertical propagation of planetary waves. Here we test model AO sensitivity to volcanic forcing against available observation to better understand how well the up-to-date coupled climate models can reproduce AO variability.

2. Models and Experiments

As part of the IPCC intercomparison for the AR4, model groups performed historical "20th century" integrations. These generally started from the late 19th century and proceeded through 1999 or 2000. In these integrations, a detailed time series of atmospheric composition (long-lived greenhouse gases and atmospheric aerosols) was specified based on available observations. For the present study we examined the data from the "20th century" integrations from the 7 models accounted for the effects of volcanic aerosols (Table 1). Each model group adopted their own (but similar) specification of the volcanic aerosols based on [*Sato et al.*, 1993; *Hansen et al.*, 2002; *Stenchikov et al.*, 1998; *Ammann et al.*, 2003]. For comparisons with observed surface air temperature, we use the HadCRUT2v dataset (http://www.cru.uea.ac.uk/cru/data/temperature). This data set combines the land surface air temperature of *Jones and Mobley* [2003] with the HadSST1 SST data of *Parker et al.* [1995] and *Rayner et al.* [2003]. Variance adjustments have been applied to both land and ocean data. The HadSLP1 sea-level pressure data set for the period from 1871 to 1998 was obtained from http://hadobs.metoffice.com/gmslp/data/hadSLP1_1871-1998.asc.gz. It is an update of GMSLP2 using an improved land station data base, new interpolation scheme and the incorporation of local detail [*Basnett and Parker*, 1997].

To provide concise measures of the volcanic effects that can be compared among several models, composites of the anomalies in the periods following the 9 largest low-latitude (40°S-40°N) eruptions since 1860 were made for each field of interest for each model. The locations and dates of the nine eruptions considered are given in Table 2. We have defined

the anomalies in each post-volcano period relative to a reference period which is different for each eruption. The reference periods employed are given in Table 2.

3. Results

The strongest direct radiative effects of volcanic aerosols are expected in the stratosphere, and it is likely that much of the tropospheric circulation response is caused by the dynamical stratospheric influence on the troposphere. The model composites all show warming in the equatorial region at 50 hPa. In almost all cases there is net anomalous cooling over a region near the North Pole associated with strengthening of the polar vortex and negative anomalies of the 50 hPa geopotential height. The cooling observed near the pole is likely a dynamical consequence of the aerosol radiative perturbations, involving the effects of the mean conditions on the propagation of quasi-stationary planetary waves. The model composites for the 50 hPa geopotential anomaly display a rather wide range of behavior, although in each case there is at least a hint of the deepening of the polar low and consequent strengthening of the westerly vortex during the post-volcano winters.

3.1. Regional surface temperature response

Figure 1 depicts surface air temperature anomaly composites for each of the models along with the comparable observed pattern. The observed pattern of temperature anomaly is consistent with the expectation that the AO is in an anomalously positive phase in the post-eruption periods. Much of the observed warming reaches 90% confidence level in Northern Europe, Siberia, and eastern Asia.

In all the composites from the model simulations (Figs. 2a-2g), the Southern Oscillation cycle is reasonably well averaged out. Both GFDL (Figs. 2a-2b) and GISS (Figs. 2c-2d) models produce spatial patterns of winter warming over Eurasia that are in reasonable agreement with observations. The magnitude of the anomalies in the GISS model appears to be unrealistically small, however. The GFDL CM2.1 correctly produces maximum warming in Europe and eastern Asia but underestimates the amplitude of warming in eastern Asia. The composite anomaly maps for both NCAR models display maximum warming very far to the north. The MIROC-medres model shows warming mostly over Europe. All models produce cooling in the Middle East, but the observed cooling over Greenland is captured only by the GFDL models. The GFDL and NCAR models do not show significant warming over North America. Both GISS models tend to produce positive anomalies on the east coast of North America..

3.2 Sea level pressure response

The winter high-latitude warming seen in the observed post-volcano climate is consistent with anomalous circulation patterns featuring a strengthening of the tropospheric zonal wind and a poleward shift of storm tracks [*Hurrell*, 1995]. A composite of the observed sea level pressure (SLP) anomalies for the post-volcanic periods is shown in Fig. 2h along with the results from each of the models in Figs. 2a-g. The observed composite shows a strong low pressure anomaly centered near the North Pole. The high-latitude negative SLP anomaly is surrounded by a ring of positive SLP anomaly, but this is most pronounced over the Atlantic sector and the Mediterranean region. The SLP anomaly over the Azores in the observed composite is +2.5 hPa. The strong meridional SLP gradient in the Atlantic sector drives westerly surface wind anomalies that help account for the corresponding warm surface anomalies in Northern Europe and Asia.

In most of the model SLP composites there is a similar basic pattern of low pressure over the pole surrounded by a ring of anomalously high pressure. However, beyond that basic feature the models differ vary considerably in their SLP anomaly patterns. The GFDL and GISS model ensemble average results display the Atlantic dipole pattern of the observed sign, but

weaker than in the observed composite. The Azores maxima in all the GFDL and GISS models are about 0.5 hPa (Figs. 2a-2d). The two NCAR models and the MIROC model have less clearly developed Atlantic sector dipole responses, and generally a noisier SLP anomaly composite. The NCAR PCM composite SLP anomaly does not show the polar minimum that is seen in observations and the other model results.

4. Summary

In this study, the ensemble average response from the models for two NH winters (nine volcanoes and at least three different realizations) is compared to the single natural realization for the same nine volcanoes and two NH winters. In the two years following major eruptions, the NH winter tropospheric circulation has been observed typically to display features characteristic of an anomalously positive AO index situation. The models considered here display only limited success in reproducing these observed tropospheric post-volcano circulation and thermal anomalies. In both models and observations, sampling is an important issue. Due to the imperfect sampling of these noisy fields, one should not expect perfect agreement between the models and observations. Furthermore the increased averaging of the model response as compared with the observations, should produce a more statistically significant signal but with lower variability. But because the strongest simulated responses are 3-10 times weaker than observed (compare for example Fig. 2b and 2h for sea level pressure anomaly) we conclude that the model AO sensitivity is not as strong as in observations.

Determining why the model AO response is too weak would require additional analysis. However, one possibility is that the models may simply not have sufficiently fine resolution and sufficiently deep model domains to adequately treat stratospheric dynamics and the stratosphere-troposphere dynamical interactions. The GISS models do have the model top at 0.1 hPa, but these models have the coarsest vertical and horizontal resolution of those considered here (and coarse relative to most of the models in the IPCC intercomparison). .

One consequence of the inadequate treatment of stratospheric dynamics in the models may be a mean climate characterized by an unrealistically intense polar vortex. If the winter vortex is too strong it may be unrealistically resistant to penetration by planetary waves, and thus much too stable. This problem could be expected to weaken any wave feedback in the models, and possibly prevent the propagation of stratospheric signals into the troposphere. The NCAR CCM3, for example, has the strongest climatological zonal wind at 50 hPa.

It will also be interesting to compare the responses of the models to volcanic aerosol loading documented here with other aspects of the model behavior being analyzed in the IPCC AR4 projects. As noted above, most earlier hindcasts of 20th century climate do not reproduce the observed trends over recent decades in the AO component of the circulation, and thus do not capture the intensification of warming trends that has been observed over Northern Europe and Asia. There are various possible explanations for this discrepancy, but it is interesting to speculate that it could indicate that the models employed may have a basic inadequacy that does not allow a sufficiently strong AO response to large-scale forcing, and that this inadequacy could also be reflected in the simulated response to volcanic aerosol loading.

Acknowledgments.

We thank the international modeling groups for providing their data for analysis, the Program for Climate Model Diagnosis and Intercomparison for collecting and archiving the model data, the JSC/CLIVAR Working Group on Coupled Modelling and their Coupled Model Intercomparison Project and Climate Simulation Panel for organizing the model data analysis activity, and the IPCC WG1 TSU for technical support. The IPCC Data Archive at Lawrence Livermore National Laboratory is supported by the Office of Science, U.S. Department of Energy. GS supported by NSF grants ATM-0313592 and ATM-0351280 and NASA grant NNG05GB06G.

Table 1. IPCC models and their treatment of volcanic aerosols. The models are as follows: GFDL CM2.0 and CM2.1 – two versions of the GFDL coupled model with different atmospheric dynamical core; GISS EH and ER – two versions of the GISS coupled model with different ocean modules [http://www.giss.nasa.gov/tools/modelE]; NCAR CCM3 - Community Climate System Model, version 3.0 [http://www.ccsm.ucar.edu]; NCAR PCM1 – Parallel Climate Model; MIROC medres and hires – developed jointly at the Center for Climate System Research, University of Tokyo, National Institute for Environmental Studies, Frontier Research Center for Global Change, and Japan Agency for Marine-Earth Science and Technology [http://www.ccsr.u-tokyo.ac.jp/kyosei/hasumi/MIROC/tech-repo.pdf]; Meteorological Research Institute (MRI), Japan.

Mark	Model name	Spatial resolution	Model top (hPa)	Volcanic aerosols	Beginning of run	Ensemble members
a	GFDL CM 2.0	2°x2.5° L24	3.0	*Sato et al.* [1993], *Stenchikov et al.* [1998]	1861	3
b	GFDL CM2.1	2°x2.5° L24	3.0	*Sato et al.* [1993], *Stenchikov et al.* [1998]	1861	5
c	GISS-EH	4°x5° L20	0.1	*Sato et al.* [1993]	1880	5
d	GISS-ER	4°x5° L20	0.1	*Sato et al.* [1993]	1880	9
e	NCAR CCM3	T85 L26	2.2	*Amman et al.* [2004]	1870	6
f	NCAR PCM1	T42 L18	2.9	*Amman et al.* [2004]	1890	4
g	MIROC-medres	T42 L20	10.0	*Sato et al.* [1993]	1850	3

Table 2. Low-latitude volcanic eruptions chosen for compositing. "VEI" is the volcanic explosivity index. Averaged over an equatorial belt "Optical depth" is calculated using the volcanic aerosol data set of *Sato et al.* [1993].

Volcano name	Eruption date	Latitude	Winters analyzed	Reference period	VEI	Optical depth (λ = 0.55 μm) 30°S-30°N
Krakatau	August 27, 1883	6.10°S	1883-1884 1884-1885	1890-1901	6	0.20
Tarawera	June 10, 1886	38.23°S	1886-1887 1887-1888	1890-1901	5	0.07
Bandai	July 15, 1888	37.60°N	1888-1889 1889-1890	1890-1901	4	0.05
Santa María	October 24, 1902	14.76°N	1903-1904 1904-1905	1890-1901	6	0.10
Quizapu	April 10, 1932	35.65°S	1932-1933 1933-1934	1915-1931	5	0.02
Agung	March 17, 1963	8.34°S	1963-1964 1964-1965	1934-1955	4	0.11
Fuego	October 10, 1974	14.47°N	1975-1976 1976-1977	1965-1973	4	0.04
El Chichón	April 4, 1982	17.36°N	1982-1983 1983-1984	1976-1981	5	0.12
Pinatubo	June 15, 1991	15.13°N	1991-1992 1992-1993	1985-1990	6	0.18

References

Ammann, C., G. Meehl, W. Washington, and C. Zender (2003), A monthly and latitudinally varying forcing dataset in simulations of 20th century climate, *Geophys. Res. Lett.*, *30*, 1657, doi:10.1029/2003GL016875.

Basnett, T. and D. Parker, Development of the Global Mean Sea Level Pressure Data Set GMSLP2 (1997), *Climate Research Technical Note, 79*, Hadley Centre, Met Office, FitzRoy Rd, Exeter, Devon, EX1 3PB, UK

Hansen, J. E., et al. (2002), Climate forcing in Goddard Institute for Space Studies SI2000 simulations, *J. Geophys. Res.*, *107* (D18), doi:10.1029/2001JD001143.

Hurrell, J. W. (1995), Decadal trends in the North Atlantic Oscillation: Regional temperatures and precipitation, *Science*, *269*, 676-679.

Jones, P. D., and A. Mobley (2003), Hemispheric and large-scale surface air temperature variations: an extensive revision and an update to 2001. *J. Climate, 16*, 206-223.

Knutson, T. R., T. L. Delworth, K. W. Dixon, I. M. Held, J. Lu, D. V. Ramaswamy, D. Schwarzkopf, G. Stenchikov, and R. J. Stouffer (2005), Assessment of Twentieth-Century Regional Surface Temperature Trends Using the GFDL CM2 Coupled Models, J. Climate, in press.

Kodera, K., Influence of volcanic eruptions on the troposphere through stratospheric dynamical processes in the Northern Hemisphere winter (1994), *J. Geophys. Res.*, *99*, 1273-1282.

Ohhashi, Y., and K. Yamazaki, Variability of the Eurasian pattern and its interpretation by wave activity flux (1999), *J. Meteorol. Soc. Japan*, *77*, 495-511.

Osborn, T. J. (2004), Simulating the winter North Atlantic Oscillation: The roles of internal variability and greenhouse gas forcing, *Climate Dyn.*, *22*, doi: 10.1007/s00382-004-0405-1, 605-623.

Parker, D. E., C. K. Folland, and M. Jackson (1995), Marine surface temperature: Observed variations and data requirements, *Clim. Change, 31*, 559-600.

Perlwitz, J., and H.-F. Graf, The statistical connection between tropospheric and stratospheric circulation of the Northern Hemisphere in winter (1995), *J. Climate*, *8*, 2281-2295.

Rayner, N. A., D. E. Parker, E. B. Horton, C. K. Folland, L. V. Alexander, D. P. Rowell, E. C. Kent, and A. Kaplan (2003), Global analyses of sea surface temperature, sea ice, and night marine air temperature since the late nineteenth century, *J. Geophys. Res., 108* (D14), 4407, doi:10.1029/2002JD002670.

Sato, M., J. Hansen, M. P. McCormick, and J. Pollack (1993), Stratospheric aerosol optical depth, 1850-1990, *J. Geophys. Res.*, *98*, 22,987-22,994.

Shindell, D. T., G. A. Schmidt, R. L. Miller, and D. Rind (2001), Northern Hemisphere winter climate response to greenhouse gas, ozone, solar, and volcanic forcing, *J. Geophys. Res.*, *106*, 7193-7210.

Shindell, D. T., G. A. Schmidt, M. Mann, and G. Faluvegi (2004), Dynamic winter climate response to large tropical volcanic eruptions since 1600, *J. Geophys. Res.*, *109*, D05104, doi: 10.1029/2003JD004151.

Stenchikov, G. L., I. Kirchner, A. Robock, H.-F. Graf, J. C. Antuña, R. G. Grainger, A. Lambert, and L. Thomason (1998): Radiative forcing from the 1991 Mount Pinatubo volcanic eruption, *J. Geophys. Res.*, *103*, 13,837-13,857.

Stenchikov, G., A. Robock, V. Ramaswamy, M. D. Schwarzkopf, K. Hamilton, and S. Ramachandran (2002), Arctic Oscillation response to the 1991 Mount Pinatubo eruption: Effects of volcanic aerosols and ozone depletion. *J. Geophys. Res.*, *107* (D24), 4803, doi: 10.1029/2002JD002090.

Thompson, D. W. J., and J. M. Wallace (1998), The Arctic Oscillation signature in the wintertime geopotential height and temperature fields, *Geophys. Res. Lett.*, *25*, 1297-1300.

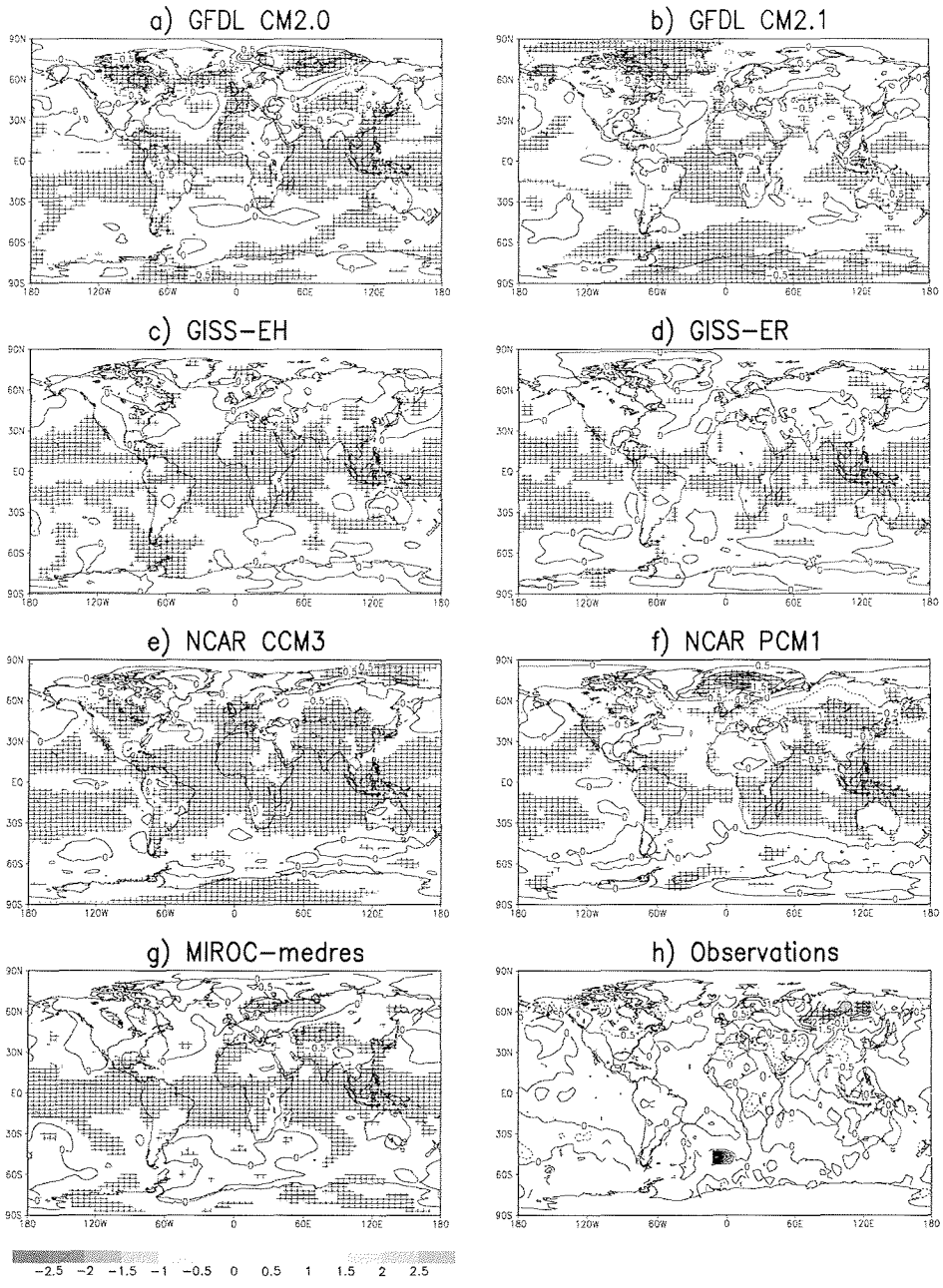

Figure 1. Surface winter (DJF) air temperature anomalies (K) composited for nine volcanic eruptions (see Table 2) and averaged for two seasons and all available ensemble members: a-g) IPCC model simulations marked as in Table 1; h) observations from HadCRUT2v dataset. Hatching shows 90% confidence level calculated using a two-tailed local t-test.

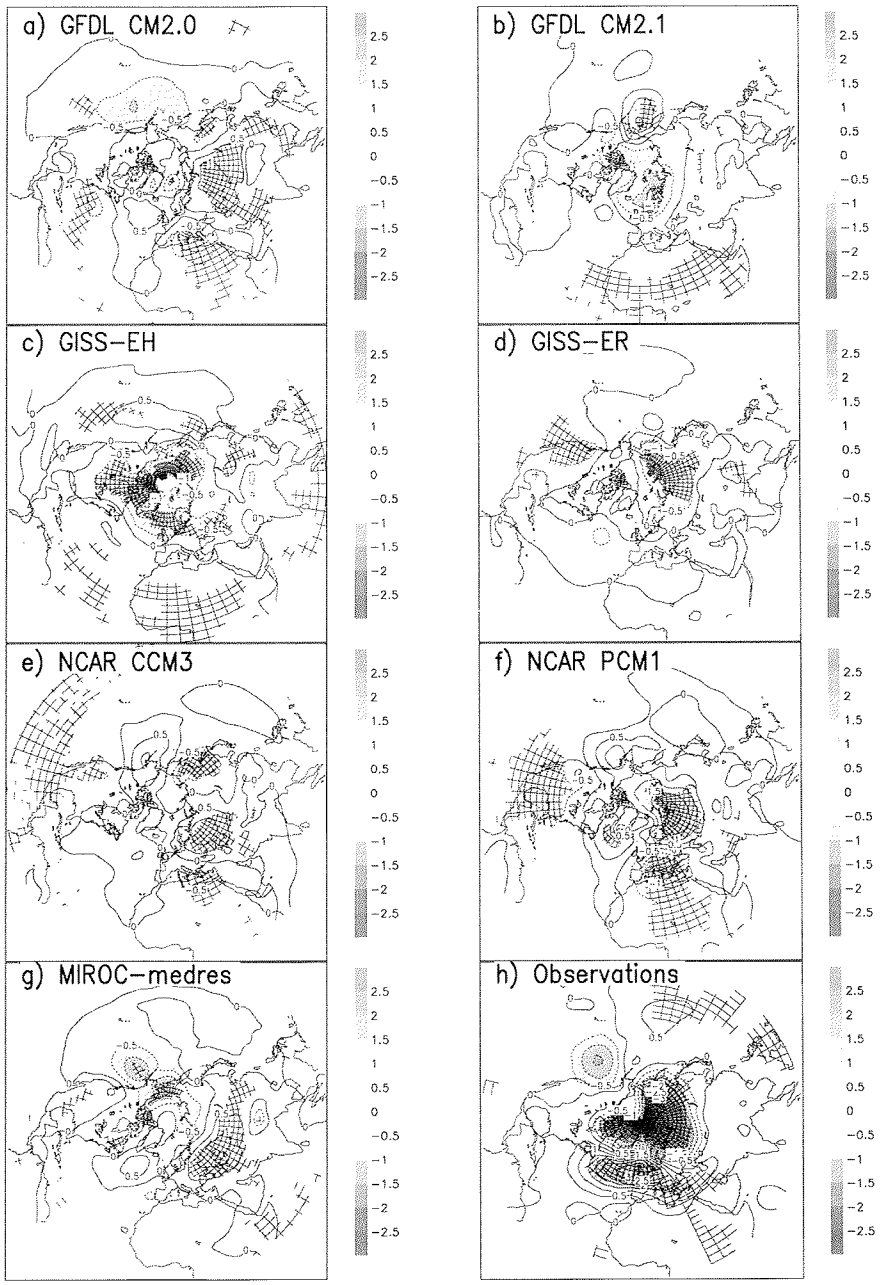

Figure 2. Sea level pressure anomalies (hPa) averaged for winter season (DJF) and composited for nine volcanic eruptions (see Table 2) and averaged for two seasons and all available ensemble members: a-g) IPCC model simulations marked as in Table 1; h) observations from HadSLP1 dataset. Hatching shows 90% confidence level calculated using two-tailed local t-test.

Simulation of climate evolution for the period 1500-2000 with all relevant natural and anthropogenic forcings

Martin Stendel and Jens Hesselbjerg Christensen

Danish Meteorological Institute, Copenhagen, Denmark

Introduction

Considerable attention has recently been paid to the evolution of climate and in particular temperature over the last couple of centuries. Since we do not have a sufficient amount of direct measurements prior to about 1850, proxy data (tree rings, ice cores, corals and historical documents) must be used to assess the climate of earlier times. In order to put the temperature evolution of the 20th century into a longer-term context, estimates of natural variability (internal variations of the climate system in absence of external forcings) as well as forced variability (both natural and anthropogenic) are required. Climate reconstructions based on proxies have inherent uncertainties. Multi-century transient climate simulations can help us to gain understanding of the temperature variations of past centuries and of the underlying physical processes when conducted with state-of-the-art coupled general circulation models. In order to conduct such a simulation, it is essential to be able to quantify all the various natural and anthropogenic forcings that are at play as realistic as possible. Our work differs from previous publications by two aspects: we have included a latitude dependence of volcanic aerosol and a description of land use changes in the forcing.

Model and experiment setup

We use the coupled ocean-atmosphere model ECHAM4-OPYC3. Its atmospheric part, ECHAM4, is described in Roeckner et al. (1999). The ocean model is an extended version of the OPYC model (Oberhuber, 1993), which consists of sub-models for the interior ocean, the surface mixed layer and sea-ice. Ocean and atmosphere are quasi-synchronously coupled, exchanging information once per day. An annual flux correction for freshwater and momentum is applied, based on present-day climate conditions. Further details are given, e.g., in Stendel et al. (2000), and references therein. The model was spun down from present-day to AD1500 conditions by applying the pre-industrial values of all the forcings described above. After a period of 500 years, the model variables had asymptotically approached nearly constant values. From this starting point, an unforced control simulation and a forced experiment including all forcings have been run for 500 years each.

Forcings

Natural forcings include solar irradiation variability and volcanic emissions, and anthropogenic forcings include time-dependent concentrations of greenhouse gases and chlorofluorocarbons (CFCs), land use changes and a simplified tropospheric sulphur cycle. Orbital variations can be neglected due to the comparatively short period that is investigated here. For solar irradiation, we used the annual data set of Lean et al. (1995, updated). Volcanic forcing is taken from the Robertson et al. (2001) annually and latitude-resolving volcanic optical depth dataset for the period 1500 to 1889. This index is obtained from the observation of sulfate aerosol in ice cores. From these, one can calculate the perturbation in optical depth, which can be expressed as anomalous radiative forcings at the tropopause for the solar and long wave part. From 1890 on, monthly-resolved model-based data of Ammann et al. (2003) were used. The annual concentrations of greenhouse gases (CO_2, CH_4 and N_2O) are also taken from Robertson et al. (2001). Halocarbon concentrations have been taken from observations described by Nakicenovic et al., 2000. In contrast to previous studies, we also take into account the effects of anthropogenic vegetation changes. So-called HYDE "A" data (Klein Goldewijk, 2001) is assigned to the ECHAM vegetation classes and interpolated to the model grid. Sulfur emissions are as in Roeckner et al. (1999).

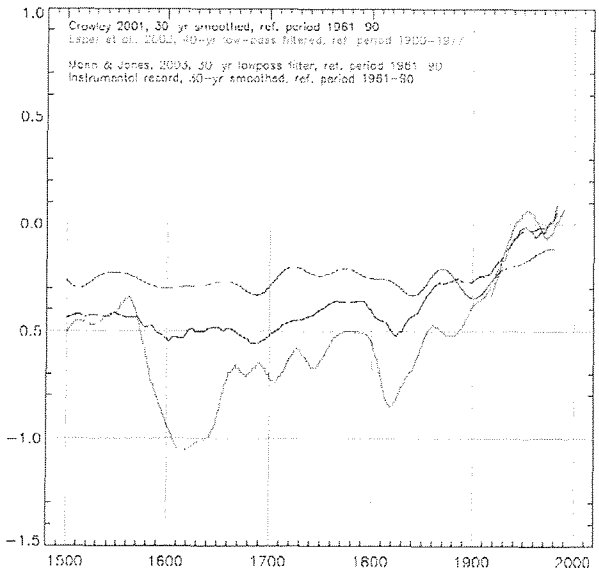

Fig. 1: Near surface temperature anomalies 1500-2000 for the instrumental record, the reconstructions of Huang et al. (2000), Esper et al. (2002) and Mann and Jones (2003), the model simulations of Crowley (2001) and Zorita et al. (2004) and for this study.

Evolution of surface temperature and comparison to proxy data

Fig. 1 shows the evolution of global near-surface temperature from instrumental observations and reconstructions by an energy balance model, dendrochronologies, borehole data, a multi-proxy approach and a model simulation using the same atmospheric model in coarser resolution. Temperatures in our study generally follow the proxy data, with negative anomalies during the Late Maunder Minimum (late 17th and early 18th century) and around 1830, as well as a strong temperature increase since the mid-19th century.

To assess the regional distribution of anomalies during the Late Maunder Minimum (LMM), we compare simulated and reconstructed seasonal temperature anomalies over Europe (Fig. 2). According to the reconstruction, the LMM was characterised by colder than average winter conditions over most of the continent and positive anomalies over most of Scandinavia. The model is able to depict this general pattern and thus seems to have skill to simulate large scale regional climate changes. Simulated cold anomalies in summer, however, extend too far south (not shown).

Multidecadal circulation anomalies

During cold periods in winter (DJF), we find positive sea ice anomalies in the Greenland / Iceland region, large cold anomalies over Northeast Europe due to anomalous snow cover and a general weakening of the zonal circulation by either anomalous high pressure in the polar region or anomalous low pressure over most of Eurasia. Both types of circulation anomalies favour positive sea ice anomalies near Iceland and along the east coast of Greenland. In summer (JJA), cold periods are also characterised by a weakening of the zonal circulation, caused by either anomalous high pressure over Greenland or anomalous low pressure over most of Europe/Asia. Both circulation patterns go along with a southwest displacement (and probably weakening) of the Azores high and generally tend to transport cool Atlantic air masses into most of Europe. The most striking circulation anomalies occur in autumn (SON, see Fig. 3) where, even in a 25 year average, 500 hPa anomalies of more than 20 gpm are simulated over Western Europe. Details are discussed in Stendel et al. (2005).

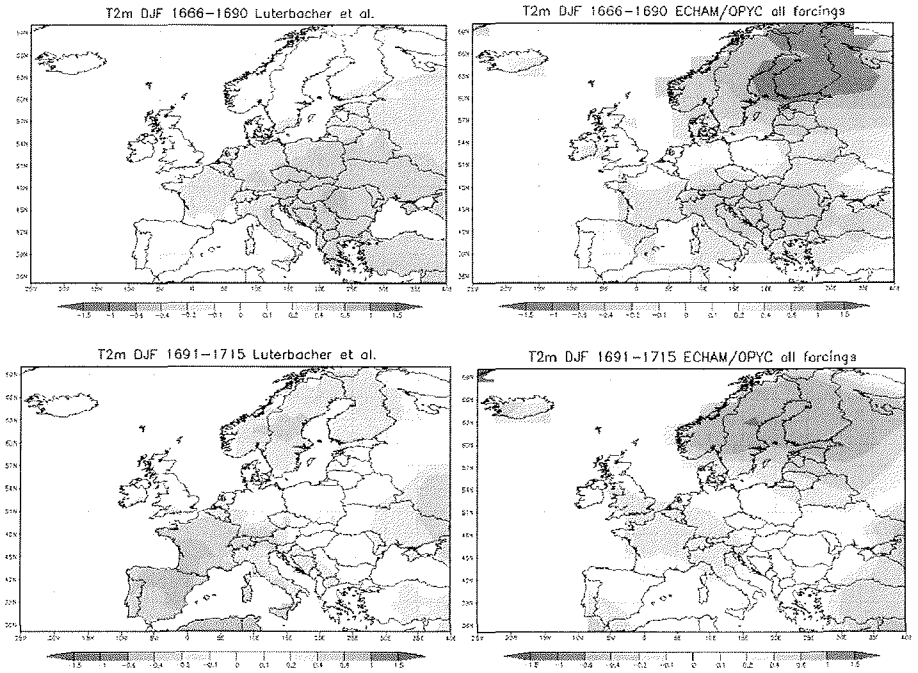

Fig. 2: Late Maunder Minimum winter (DJF) temperature anomalies [K] from the average 1500-1700 for 1666-1690 (upper panel) and 1691-1715 (lower panel). Left column: empirical reconstructions (Luterbacher et al., 2003), right column: this study.

There is evidence from reconstructions for a strong increase in zonality since the mid-19th century. Such an increase for the last 150 years - with the notable exception of the 1940s that were characterised by low NAO indices in the European-Atlantic region – is also visible in the first EOF (explaining 37% of the variance) of our simulation. A circulation pattern with high pressure over the British Isles is given by the second EOF, which explains almost a fifth of the variance. The corresponding PC has a large loading during most of the LMM, thus corroborating our findings about the increase of blocking patterns discussed above.

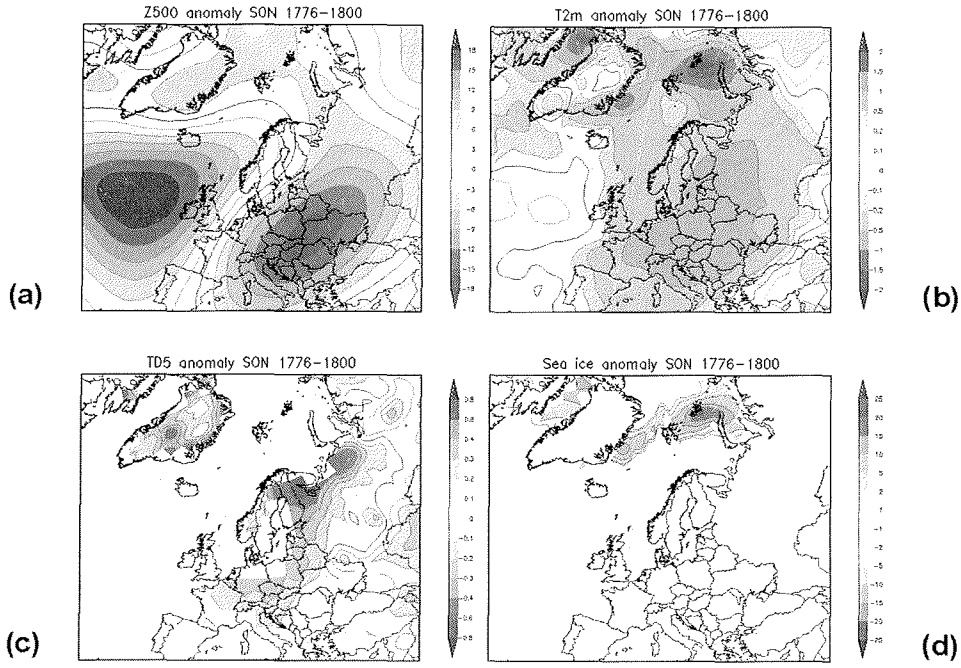

Fig. 3: 25 year (1776-1800) autumn (SON) anomalies from the mean 1500-1700 for (a) 500 hPa geopotential [gpm], (b) 2m temperature [K], (c) deep soil temperature [K] and (d) sea ice cover [%].

Discussion

Near-surface temperatures as well as deep soil temperatures well below the long-term average are simulated for extended periods, including the LMM. A decrease in radiative forcing, caused by less solar irradiation and/or volcanic aerosol, leads to a decrease in the upper tropospheric temperature gradient between tropics and high latitudes, a decreased northward momentum transport and therefore to a weakening of the NAO. This is the case in ECHAM despite the rather simplified representation of the stratosphere. Such quasipersistent circulation anomalies could lead to positive sea ice anomalies east of Greenland and around Iceland, regions that are particularly sensitive to circulation changes in ECHAM (Stendel et al., 2000), but probably also in reality.

In contrast to the mechanisms discussed above, the weakening of the ocean gyre circulation, as described in Zorita et al. (2004) does not seem to play a prominent role for the present model, as the local freshening in the northern oceans is compensated by the transport of anomalously saline waters (caused by anomalous evaporation) from the tropical Atlantic. This remote effect is able to compensate for the local effects in the North Atlantic which tend to decrease the density of surface water through warming and increase in freshwater flux (Latif et al., 2000).

In comparison to high resolution empirical climate reconstructions, the model is able to some extent to simulate regional climate anomalies, mainly in winter (DJF), suggesting that there is a memory effect for soil moisture that is not adequately covered in ECHAM's rather simple soil scheme. However, as can be seen in the years following large volcanic eruptions, it mainly reacts to the reduced insolation, but fails to reproduce the dynamical effects following such forcing anomalies.

Acknowledgments
This study has been conducted within the GLIMPSE project (Global implications of Arctic climate processes and feedbacks) which was supported by the European Commission under the 5th Framework Programme under contract EVK2-CT-2002-00164.

References

Ammann, C.M., G.A. Meehl, W.M. Washington and C.S. Zender, 2003: A monthly and latitudinally varying volcanic forcing dataset in simulations of 20th century climate. Geophys. Res. Lett. 30, 10.1029/2003GL016875.

Briffa, K.R., T.J. Osborn, F.H. Schweingruber, I.C. Harris, P.D. Jones, S.G. Shiyatov and E.A. Va-ganov, 2001: Low-frequency temperature variations from a northern tree ring density network. J. Geophys. Res. 106, 2929-2942.

Crowley, T.J., 2000: Causes of climate change over the last 2000 years. Science 289, 270-277.

Esper, J., E.R. Cook and F.H. Schweingruber, 2002: Low-frequency signals in long tree-ring chronologies fore reconstructing past temperature variability. Science 295, 2250-2253.

Huang, S.H., N.H. Pollack and P.Y. Shen, 2000: Temperature trends over the past five centuries reconstructed from borehole temperatures. Nature 403, 756-758.

Klein Goldewijk, K., 2001: Estimating global land use change over the past 300 years: the HYDE database. Glob. Biogeochem. Cycl. 15, 415-433.

Latif, M., E. Roeckner, U. Mikolajewicz and R. Voss, 2000: Tropical stabilization of the thermohaline circulation in a greenhouse warming simulation. J. Climate 13, 1809-1813.

Lean, J., J. Beer and R. Bradley, 1995: Reconstruction of solar irradiance since 1610: implications for climate change. Geophys. Res. Lett. 22, 3195-3198.

Mann, M.E. and P.D. Jones, 2003: Global surface temperatures over the past two millennia. Geophys. Res. Lett. 30, 10.1029/2003GL017814.

Nakicenovic, N. and 27 coauthors, 2000: IPCC special report on emissions scenarios. Cambridge University Press, Cambridge, UK and New York, NY, USA, 599 pp.

Oberhuber, J.M., 1993: Simulation of the Atlantic circulation with a coupled sea ice-mixed layer-isopycnal general circulation model. Part I: Model description. J. Phys. Oceanogr. 22, 808-829.

Robertson, A., J. Overpeck, D. Rind, E. Mosley-Thompson, G. Zielinski, J. lean, D. Koch, J. Penner, I. Tegen and R. Healy, 2001: Hypothesized climate forcing time series for the last 500 years. J. Geophys. Res. 106, 14783-14803.

Roeckner E., L. Bengtsson, J. Feichter, J. Lelieveld and H. Rodhe, 1999: Transient climate change simulations with a coupled atmosphere-ocean GCM including the tropospheric sulfur cycle. J. Climate 12, 3004-3032.

Stendel, M., T. Schmith, E. Roeckner and U. Cubasch, 2000: The climate of the 21st century: Transient simulations with a coupled atmosphere-ocean general circulation model. Danish Meteorological Institute Report 02-1, 51 pp.

Stendel, M., I.A. Mogensen and J.H. Christensen, 2005: Influence of various forcings on global climate in historical times using a coupled AOGCM. Clim. Dyn., in press.

Zorita, E. H. v. Storch, F.J. Gonzalez-Rouco, U. Cubasch, J. Luterbacher, S. Legutke, I. Fischer-Bruns and U. Schlese, 2004: Simulation of the climate of the last five centuries. Met. Z. 13, 271-289.

Modeling the Arctic boundary layer

Michael Tjernström, Stefan Söderberg and Mark Žagar

Stockholm University, Department of Meteorology, Stockholm, Sweden

1. Introduction

Recent years have seen an increased interest in the Arctic climate, partly because of its large sensitivity to anthropogenic climate change and partly due to the potentially large impacts to Arctic society and ecosystems of projected climate changes for the next century [e.g. ACIA, 2004]. At the same time, the climate models used for climate projections perform worse in the Arctic than elsewhere and the inter-model scatter in future climate projections is also larger than for any other region on Earth [Walsh et al., 2005].

The Arctic Regional Climate Model Intercomparison project [ARCMIP, Curry and Lynch, 2002] aims at identifying model deficiencies and improving the description of Arctic climate processes in numerical models. This is achieved by controlled regional-modeling experiments. In ARCMIP Experiment 1, several models were run for the SHEBA [Surface Heat Budget of the Arctic Ocean, Uttal et al., 2002] year; results are intercompared and compared with SHEBA observations. All models were run the same way, with a common model domain, covering ~ 3500 x 2750 km^2 of the western Arctic as determined by the SHEBA ice-drift track. To the south, it covers most of Alaska, the Bering Strait and northeastern Siberia and to the north it reaches into the pack ice, to about 85 °N. The target resolution of ~50 km is the same in all models, although details differ. Lateral boundary forcing was provided at six-hour intervals using ECMWF (European Centre for Medium Range Weather Forecasts) analyses, the same for all models. Sea surface temperature (SST) and ice fraction were also prescribed the same for all models from AVHRR (Advanced Very High Resolution Radiometer) and SSMI (Special Sensor Microwave Imager) satellite observations, respectively. Ice-surface temperatures were also prescribed from AVHRR data at a six-hourly resolution, although one model in this paper (COAMPS^{TM}) was re-run with thermodynamic ice model. The simulations were 13-month long, from September 1997 through September 1998. In summary, the models perform reasonably well for the resolved scale variables although deviations occur, differently in different models, but also display serious discrepancies for many parameterized processes. Detailed descriptions of the experiment and its results can be found in Tjernström et al. [2005] and Rinke et al. [2005].

2. Boundary layer turbulence

The fluxes of momentum and heat across the ice/atmosphere interface are important both for the atmosphere and for the ocean. An incorrect surface momentum flux affects the ice drift in a coupled model, and the life cycle of atmospheric synoptic scale systems. Incorrect turbulent heat fluxes affect the freezing and melting of sea ice. Tjernström et al. [2005] concluded that friction velocity in the ARCMIP simulations is reasonably accurate, although with a tendency to higher values than observed. The modeled turbulent heat fluxes, on the other hand, showed very little correlations to the observations. The functional relationships between the fluxes and the resolved-scale variables are, however, reasonable both for the momentum flux and for the heat flux.

Rather than examining the temporal agreement, Figure 1 compares the relative probability from the models with that of the observations. The systematic overestimation of the friction velocity, in particular in winter, is clear, while there is a systematic lack of occasions with low stress during both seasons, more in winter. The probability functions, for sensible and latent heat (Figure 1b and c; upward flux is defined positive), are centered near zero in both observations and models. In general, the modeled heat-flux probability distributions are much too wide, by at least a factor of two in both directions; there is an equal overestimation of both

up- and downward fluxes, slightly different for different models. The situation is somewhat better in summer than during winter. A somewhat surprising result is that the probability functions for both modeled and observed fluxes are similar between summer and winter, especially for sensible heat flux. For the latent heat flux, there are somewhat larger differences between the seasons. Quite a few of the models have a significant (unrealistic) downward water-vapor flux for an appreciable part of the year. It is often postulated that unrealistically modeled heat fluxes in the Arctic are due to the models being unable to resolve strong static-stability conditions, frequent in the Arctic winter. This is likely an over-simplification of the problem, as revealed by the results for the bulk Richardson number (Ri_b). The long tail in the probability function for the very stable conditions is quite well captured by the models. The main discrepancy is instead on the unstable side (negative Ri_b) where the models seem to overestimate the Ri_b magnitude.

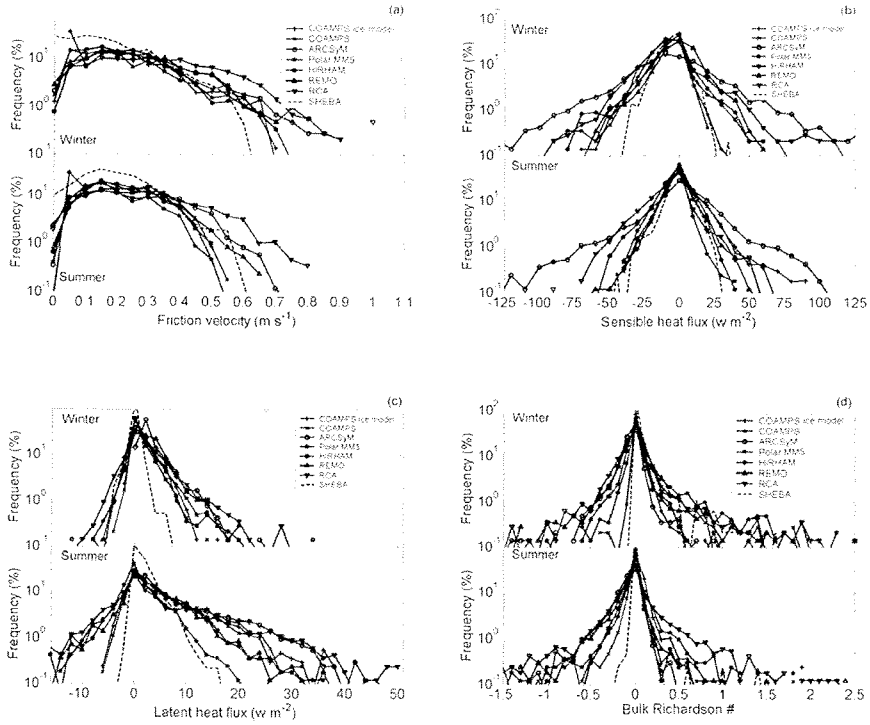

Figure 1. Relative probability density functions for (a) friction velocity (ms-1), (b) sensible and (d) latent heat flux (Wm-2), and (d) bulk Richardson number for seven model runs and from observations, for the SHEBA year. The results are separated into the "winter" (Oct-Mar) and "summer" (Apr-Sept) time periods.

3. Clouds and surface radiation

The over-all most important component for the energy balance at the surface is likely the radiation heat fluxes. The surface radiation is to large degree determined by the clouds, which in the Arctic are predominantly low-level stratus clouds [Intrieri, 2002; Tjernström et al., 2004]. One unexpected result from SHEBA was the presence of appreciable fractions of liquid water present in Arctic clouds even during winter at low temperatures [Intrieri, et al 2002]; this has potentially large consequences for the long-wave radiation at the surface.

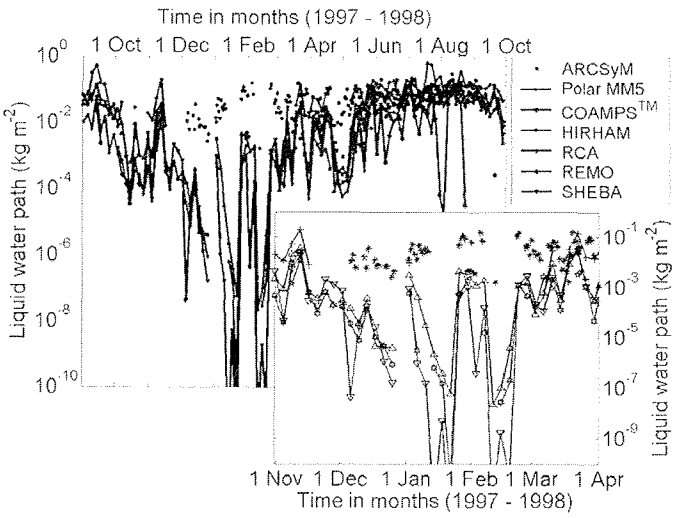

Figure 2. Time series of liquid water path from the models and from SHEBA; upper bigger panel shows weekly averages for the whole year, while the lower smaller panel shows daily averages for the winter season only.

While most models simulate a summer LWP of roughly the correct magnitude, they all severely underestimate winter LWP (Figure 2). Only three of the six models have any liquid water at all. These are models carrying only one prognostic cloud-water variable and distinguish phase based on temperature. The other models, carrying more complex formulations separating solid and liquid, cloud water and precipitation fails in winter. Figure 3a and b illustrate the effect of clouds on downward long-wave radiation. This must be done carefully, as an error in surface radiation may have many different reasons; a failure to simulate clouds when there should be, or vice versa, being the most likely. This is avoided by identifying periods when the models agree with observations on the presence of clouds. This is achieved by simultaneously demanding that the observed net long-wave radiation is small and the modeled cloud-water path is large; this isolates cloudy cases, and vice versa for clear cases. The probability functions of the error in down-welling long-wave radiation were then calculated for cloudy and clear conditions for winter and summer separately.

While the errors for clear conditions in winter are scattered rather narrowly around zero, the situation is different for cloudy conditions (Figure 3a). With significant clouds, the error probability function is wide, ranging from -75 – 25 Wm^{-2} with a model-ensemble median error around -25 Wm^{-2}. This is likely an effect of the fact that there is virtually no liquid water in the modeled clouds; liquid and ice clouds have very different properties for long-wave radiation. In summer the situation is somewhat reversed. For cloudy conditions, all models agree well with each other with a rather narrow probability function, while the clear case errors are more scattered; the dominant error indicates ~ 10-20 Wm^{-2} to little incoming long-wave radiation. An error of ~ -10 Wm^{-2} is consistent with a low-level temperature error of about -2 °C assuming a high emissivity. That is the error that many of these models show during summer (see Tjernström et al. 2005). As the median error seems independent of the presence clouds, this is a likely explanation.

The error in surface solar net radiation starts out positive, almost at 50% of the observed flux, changes sign in May and becomes negative but remains quite large through the summer. A large fraction of this error is related to the surface albedo (Tjernström et al. 2005). Most of the models have assumptions on the effects of snow age, reducing the albedo with time after

freshly fallen snow or as a function of temperature, but take too little account of melt-ponds. These start forming in spring and have a significant effect on the albedo in late summer. For a realistic annual albedo, the models often have too low winter and too high summer albedo. Examining the incoming part of the solar short-wave radiation, the error is close to zero until early May, then to early August, there is a negative error in many models, ranging from zero to ~ -100 Wm^{-2}. There is a correlation (as expected) between errors in incoming short-wave radiation and errors in LWP. On average, however, the error in summer LWP is around zero (not shown), thus it is unlikely that systematically too high LWP produces this error. Another potential reason might lie in the parameterizations of cloud albedo in the models. The summer Arctic is characterized by low concentrations of cloud condensation nuclei (e.g. Tjernström et al. 2004), which means that Arctic summer clouds are likely biased towards low droplet number concentrations. This should bias the actual cloud albedo to low values; this could explain the too low incoming solar radiation in the models as they systematically have a too high cloud albedo.

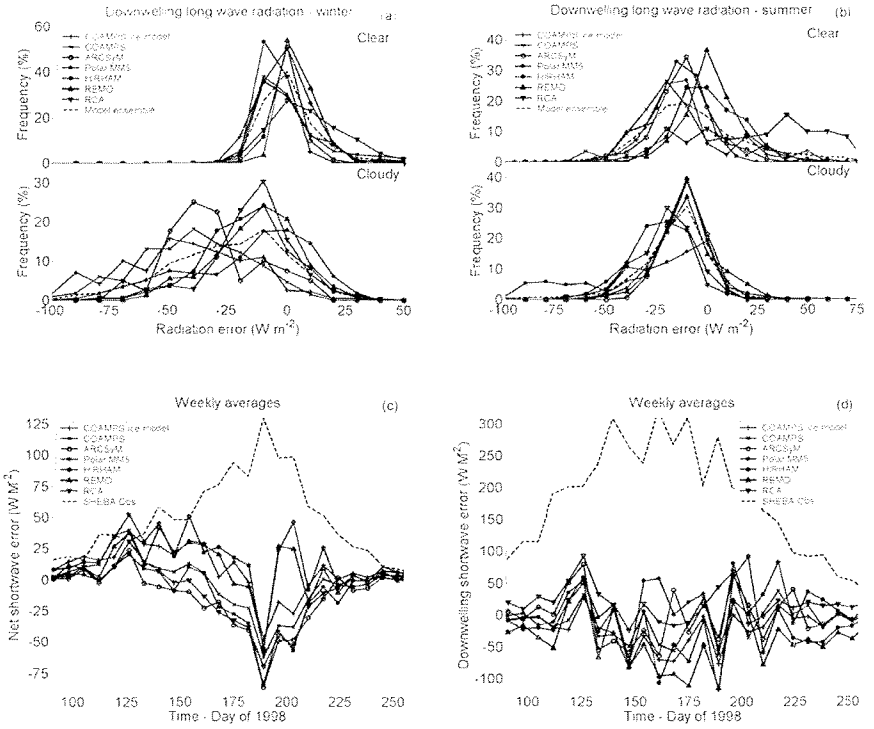

Figure 3. Plots of surface radiation errors. Top panels show the relative probability density functions for modeled and observed down-welling long-wave radiation (Wm-2), for (a) winter and (b) summer, for clear and cloudy situations separately. The two lower panels show time series the error in short-wave radiation, in (a) for the net and in (b) for the down-welling radiation. Included is also the observed time series for reference.

4. Summary

In ARCMIP Experiment 1, six models were run for a full year over a limited domain covering the SHEBA ice-drift track, facilitating comparisons between models and observations. The resolved-scale variables compare well with the SHEBA observations, but with different biases in different models; all the six models have their own set of problems and it is not possible to single out any model as being best. Examining sub-grid scale processes in the models, a somewhat different picture emerges. The surface momentum flux is reasonable, but the models in general overestimate the friction velocity, especially in high-wind winter conditions and miss many of the observed low-stress events. The probability functions of the turbulent surface heat fluxes are much too wide, indicating a preference in the models to overestimate the fluxes, regardless of sign. Errors in surface radiation fluxes are dominated by problems in modeling clouds and surface albedo. In winter there is a significant negative bias in incoming long-wave radiation for cloudy cases, likely due to a lack of water phase in the models; all models lack liquid water at low cloud temperatures whereas observations have significant liquid water all through the year. In summer there is a slight underestimation of incoming long-wave radiation. The error in the net short-wave radiation in summer is partly due to incorrect surface albedo in the models. Also the incoming short-wave radiation shows a negative error during much of summer, likely due to incorrect cloud albedo parameterizations in the models radiation codes.

References

ACIA, *Impacts of a warming Arctic, Arctic Climate Impacts Assessment*, Cambridge University Press, 2004.

Curry J.A. and A.H. Lynch, Comparing Arctic Regional Climate Models, *EOS Trans.*, **83**, 87, 2002.

Intrieri, J. M., M. D. Shupe, T. Uttal, and B. J. McCarty, An annual cycle of Arctic clouds characteristics observed by radar and lidar at SHEBA, *J. Geophys. Res,* 107, NO. C10, 10.1029/2000JC000423, 2002.

Rinke, A, K. Dethloff, J.J. Cassano, J.H. Christensen, J.A. Curry, P. Du, E. Girard, J.-E. Haugen, D. Jacob, C.G. Jones, M. Køltzow, R. Laprise, A.H. Lynch, S. Pfeifer, M.C. Serreze, M.J. Shaw, M. Tjernström, K. Wyser, M. Zagar, Evaluation of an Ensemble of Arctic Regional Climate Models: Spatiotemporal fields during the SHEBA year, Revised for *Clim. Dyn.*, 2005.

Tjernström, M., M. Žagar, G Svensson, J Cassano, S. Pfeifer, A. Rinke, K. Wyser, K. Dethloff, C. Jones and T. Semmler, Modeling the Arctic Boundary Layer: An evaluation of six ARCMIP regional-scale models with data from the SHEBA project, *Bound.-Layer Meteorol.*, In press, 2005

Tjernström, M., C. Leck, P. O. G. Persson, M. L. Jensen, S. P. Oncley and A. Targino, The summertime Arctic atmosphere: Meteorological measurements during the Arctic Ocean Experiment (AOE-2001), *Bull. Amer. Meteorol. Soc.*, **85**, 1305 – 1321, 2004.

Uttal, T., J. A. Curry, M. G. Mcphee, D. K. Perovich, R. E. Moritz, J. A. Maslanik, P. S. Guest, H. L. Stern, J. A. Moore, R. Turenne, A. Heiberg, M. C. Serreze, D. P. Wylie, P. O. G. Persson, C. A. Paulson, C. Halle, J. H. Morison, P. A. Wheeler, A. Makshtas, H. Welch, M. D. Shupe, J, M. Intrieri, K. Stamnes, R. W. Lindsey, R. Pinkel, W. S. Pegau, T. P. Stanton, T. C. Grenfeld, Thomas C, Surface Heat Budget of the Arctic Ocean, *Bull. Amer. Meteorol. Soc.*, **83**, 255-276, 2002.

Walsh, J.E., S.J.Vavrus and W.L. Chapman, Workshop on modeling of the Arctic atmosphere, *Bull. Amer. Meteorol. Soc.*, 86, 845-852, 2005.

Comparison of a regional Landsat image based land cover classification to global data sets in Northeast European Russia

Tarmo Virtanen[1] and Peter Kuhry[2]

[1] Department of Biological and Environmental Sciences, University of Helsinki, Finland
[2] Department of Physical Geography and Quaternary Geology, Stockholm University, Sweden

Introduction

The aim of this study is to assess deficiencies in the global land cover data sets used in climate modeling. Within the GLIMPSE project we are carrying out comparisons for four selected (sub)arctic regions between detailed regional land cover classifications based on Landsat images with extensive groundtruthing and four global data sets of increasing sophistication. These regions are the Usa Basin in Northeast European Russia, the Teno Basin in Northern Fennoscandia, the Kazan Basin in Central Canada, and the Khatanga area in Northern Siberia. In this paper we report on our findings for the first region.

The Usa Basin in Northeast European Russia covers an area of approximately 93 500 km^2. About 85% of this area corresponds to lowlands at elevations below 200 m. Forest in the southwestern and central lowlands occupies 25% of the total basin area. Tundra vegetation towards the North accounts for another 25%. Extensive peatlands can be found in both the taiga and tundra regions and cover 30% of the territory. The remaining area is occupied by meadows (2%), willow (7%), alpine areas (8%) and lakes (2%). Areas directly affected by human activities represent less than 1% (Figure 1).

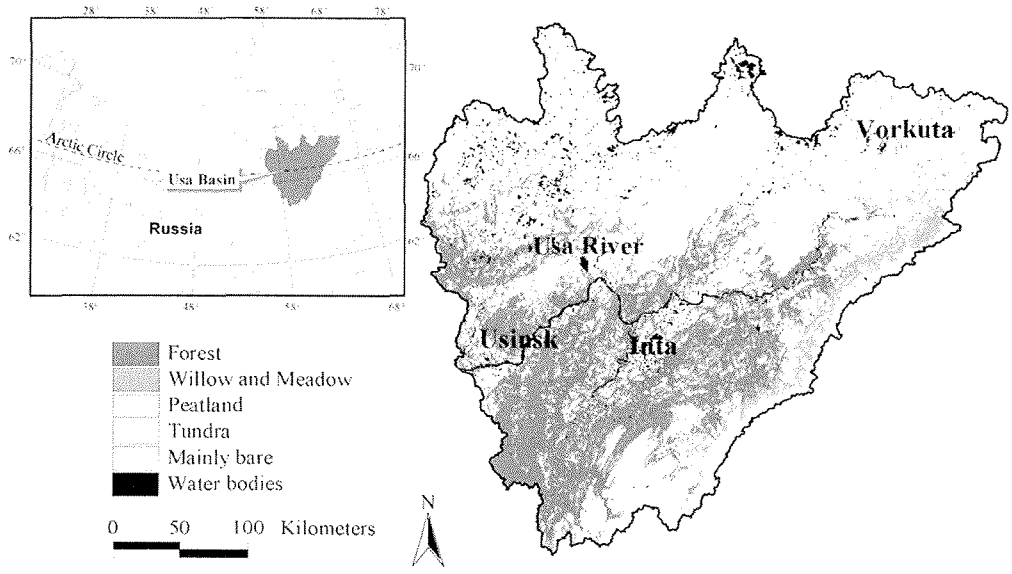

Figure 1. Location and major vegetation units of the Usa Basin.

The Usa Basin includes the important arctic treeline transition and is characterized by extensive peatland areas. Our comparisons will focus particularly on forest area and distribution, which affects such important parameters as surface albedo and roughness, and the areal extent of wetlands, which is important for such aspects as the hydrological cycle. Our analysis points to significant deficiencies in the global products, particularly in the less sophisticated data sets.

The regional and global data sets

The Usa Basin data set

The Usa Basin regional land cover classification was performed using a mosaic of spectrally adjusted Landsat TM5 images from five different dates, with ground reference data collected during the summers of 1998, 1999 and 2000 (Virtanen et al., 2004). The original classification has 21 land cover classes. The major vegetation units used for this study (forests, willow dominated stands and meadows, peatlands, tundra heaths, mainly unvegetated areas, and water bodies) were distinguished with relatively high accuracy: 84 % of the test points were classified correctly.

For the comparisons, we resample the 30m grid data from the regional classification to the 1 km cell size used in global data sets. The major class value found within each 1 km grid cell was assigned to each cell. We grouped our classes into the larger vegetation units mentioned above. In addition, water bodies were treated as their own class.

We cross-tabulate the areas of the major vegetation units between the regional classification and the global data sets for the exact same region. Limitations exist due to differences and ambiguities in the regional and global land cover classes, but by focussing only on major vegetation units these are largely avoided.

The global datasets

In the following we describe the four global data sets used in the comparisons.

The first two data sets have been created by the U.S. Geological Survey (USGS), the University of Nebraska-Lincoln (UNL) and the European Commission's Joint Research Centre (JRC). These are the Global Ecosystem (96 classes globally) and International Geosphere Biosphere Programme (17 classes globally) data sets (versions 1.2 and 2.0), and are freely available from [http://edcdaac.usgs.gov/glcc/glcc.html]. They were produced by the method described as "a multi-temporal unsupervised classification of NDVI (Normalized Difference Vegetation Index) data with post-classification refinement using multi-source earth science data" (Loveland et al., 2000). The base data were monthly AVHRR NDVI maximum value composites from April 1992 to March 1993. First, the seasonal greenness classes were defined using unsupervised classification. The seasonal greenness classes were further translated into land cover regions in the post-classification refinement using digital elevation, ecoregion data, and a collection of other land cover/vegetation reference data. To make the comparison simpler, we grouped the different forest classes in these global data sets into one Forest class. In the Global ecosystems data the grouped classes were Conifer boreal forest, Cool mixed forest, Small leaf mixed woods and Narrow conifers; in the International Geosphere Biosphere Programme data the grouped classes were Evergreen needleleaf forest, Deciduous broadleaf forest and Mixed forest.

Another compared data set is Global Land Cover Data produced by the University of Maryland. It includes 14 classes, and is found at [http://glcf.umiacs.umd.edu/data/]. It is based on supervised classification of the NOAA AVHRR images, the data having a record length of 14 years (1981-1994). Furthermore, this data set included red, infrared, and thermal bands in addition to the NDVI. Their training data consisted of Landsat and LISS images, from which

they selected those cover types about which they were confident (Hansen et al., 2000). In this data set we grouped the classes Evergreen needleleaf forest and Mixed forest into the class Forest.

The last used data set is the GLC2000 (Global Land Cover 2000) classification, which was produced by the Institute of Environment and Sustainability (IES) of the European Commission Joint Research Centre in collaboration with over 30 research teams from around the world. Data is found at [http://www-gvm.jrc.it/glc2000/]. In contrast to the previously described initiatives, the GLC2000 project is a bottom up approach to global mapping. In this project more than 30 research teams have been involved, contributing to 19 regional windows. Each defined region was mapped by local experts, which was aimed to guarantee an accurate classification, based on local knowledge. Each regional partner used the VEGA2000 dataset, providing a daily global image from the Vegetation sensor onboard the SPOT4 satellite. The Northern Eurasian part of this classification is presented in Bartalev et al. (2003). It includes for our study area 27 classes (of which 21 included more than 10 pixels; only these are discussed next). For simplicity, we grouped classes into the following units: Forest (Evergreen Needle-leaf Forest, Deciduous Broadleaf Forest, Needle-leaf/Broadleaf Forest, Mixed Forest, Broadleaf/Needle-leaf Forest, Deciduous Needle-leaf Forest, Fores - Natural Vegetation complexes), Shrublands (Broadleaf deciduous shrubs, Needle-leaf evergreen shrubs), Grasslands (Humid grasslands, Cropland/Grassland complexes), Peat/wetlands (Bogs and marshes, Palsa bogs, Riparian vegetation), Tundra (Prostrate shrub tundra, Sedge tundra, Shrub tundra), Mainly bare (Barren tundra, Bare soil and rock, Urban), and Water bodies (Water bodies).

Results and Discussion

The comparisons between our combined classes and the data sets produced by USGS are presented in Tables 1a and 1b. To conclude shortly, the USGS classifications seem to differ considerably from each other, but none of them seem to have good correspondence with our classification.

Table 1c presents a comparison between our grouped classes and the units of the University of Maryland data. In this classification, the coverage of forested areas was slightly higher than in our classification (35.7% Forests and Woodland vs. 28.1% Forest). The classes Wooded grassland (described as "tree canopy covers 10 – 40 % and trees exceed 5m in height" and so corresponding to forest in our terms) and Closed shrubland are mainly included in our tundra classes. On visual inspection the forest line looks very similar (but only when Wooded grassland is treated as tundra), except in the eastern part of the Usa Basin where an area 20 to 30 km northwards from our forest line was classified as forest. The University of Maryland data is a simplified IGBP classification that does not separate permanent wetlands, in arctic regions mostly different types of peatland. In arctic regions, separation of peatlands is important due to their extensive cover in many areas and their specific hydrological properties.

The GLC2000 classification (Bartalev et al., 2003) was clearly the most accurate in our study region (Table 1d). The areal extent of main vegetation units, e.g. forests, peatlands and tundra was very similar than in our classification. We classified areas where approximately less than half of the ground was non-vegetated to mainly bare class, but in GLC2000 only almost totally non-vegetated areas are in bare area class. There were some differences in exact spatial patterns of the different vegetation units, but at a general level the match is satisfactory.

The regional approach selected in GLC2000 and the use of different season (spring, summer and autumn) SPOT4-VEGETATION images (red, near infra red and short wave infrared channels) are most probably the explanation for the accurate classification product. As this work used the Land Cover Classification System (LCCS) produced by FAO and UNEP their

classes are also relevant for different global change studies. The supervised classification method used by the University of Maryland (with a larger dataset and some additional spectral bands above the NDVI) seems to produce a better match with our data than the data sets of the USGS produced by the unsupervised clustering classification method, but was clearly more problematic than GLC2000 classification. Particularly, the lack of peatlands is noticeable. Hansen & Reed (2000) also compared University of Maryland and USGS datasets, and their conclusion was that core areas were mapped similarly for broad vegetation units, but that the transitional zones between core areas differed significantly. This also seems to be case in our study area, which is located at the taiga-tundra ecotone.

One obvious explanation for the deficiencies of the global data sets in the Usa Basin (especially evident in those that used no regional expertise) is the glaciation history of the lowlands. The upper sediments in the region are thick Quaternary deposits, mostly loamy glacial-marine and lacustrine-alluvial sediments, and no large stones or exposed bedrock are found. Thus, the vegetation cover is more uniform than in most other parts of the Arctic. This evidently leads to exceptionally high NDVI values which, in turn, cause the vegetation in satellite images to appear denser than it is in reality.

To conclude, comparisons with the detailed regional land cover classification for the Usa Basin shows that different global land cover data sets represent such important land cover classes as forest, tundra and peatlands with variable precision. Of the four global data sets used, the GLC2000 product was clearly the most accurate one. Our results are in line with the findings of Achard et al. (2001), who also pointed out the importance of accuracy testing and verification based on field data. A more complete picture will emerge about the precision of different global land cover data sets at high latitudes when comparative analysis are also completed for other subarctic regions.

Acknowledgments

The EC-funded TUNDRA (ENV4-CT97- 0522) and GLIMPSE (EVK2-CT-2002-00164) projects, and the Academy of Finland-funded ARCTICA project (47095) provided financial support for different fieldwork periods and analytical stages of this study.

References

Achard, F., Eva, H. & Mayaux, O. 2001. Tropical forest mapping from coarse spatial resolution satellite data: production and accuracy assessment issues. International Journal of Remote Sensing 22, 2741-2762.

Bartalev, S.A., Belward, A.S., Erchov, D.V. & Isaev, A.S. 2003. A new SPOT4-VEGETATION derived land cover map of Northern Eurasia. International Journal of Remote Sensing 24, 1977-1982.

Hansen, M., DeFries, R., Townshend, J. R. G. and Sohlberg, R. 2000. Global land cover classification at 1km resolution using a decision tree classifier. International Journal of Remote Sensing 21, 1331-1365.

Hansen, M. & Reed, B.C. 2000. A Comparison of the IGBP DISCover and University of Maryland 1 km global land cover products. International Journal of Remote Sensing 21, 1365-1373.

Loveland, T.R., Reed, B.C., Brown, J.F., Ohlen, D.O., Zhu, J, Yang, L. & Merchant, J.W. 2000. Development of a Global Land Cover Characteristics Database and IGBP DISCover from 1-km AVHRR Data. International Journal of Remote Sensing 21, 1303-1330.

Virtanen, T., Mikkola, K. & Nikula, A. 2004. Satellite image based vegetation classification of a large area using limited ground reference data: a case study in the Usa Basin, north-east European Russia. Polar Research 23, 51-66.

Table 1. Comparison of the regional classification to global data sets for the Usa Basin (Northeast European Russia). Values are areal percentages. Forest classes are grouped in the global datasets, grouped classes mentioned in text. a) Global Ecosystems data by USGS, versions 1.2 (left column) and 2.0 (right column). b) International Geosphere Biosphere Programme data by USGS, versions 1.2 (left column) and 2.0 (right column). c) Global Land Cover Data Set produced by the University of Maryland. d) GLC 2000 classification produced by the European Commission's Join Research Centre and the Russian Academy of Science's Centre for Forest Ecology and Productivity.

a)

Our classification: **USGS GE classes:**	**Forests**		**Willow & Meadow**		**Peatland**		**Tundra heaths**		**Mainly bare**		**Water bodies**		**% in USGS GE**	
Forest	8.3	68.5	0.6	31.1	4.2	45.6	0.0	17.0	0.2	3.5	0.5	19.2	3.4	37.1
Wooded tundra	76.1	18.5	90.1	61.3	79.7	40.6	91.2	74.6	19.8	15.9	55.6	41.3	78.2	45.9
Mire	2.9	0.1	1.1	0.2	3.1	0.5	1.5	1.1	0.2	0.2	2.3	0.8	2.1	0.6
Shrub deciduous	11.7	11.8	1.1	1.2	8.5	8.5	0.2	0.2	0.8	0.8	1.4	1.2	5.3	5.3
Cool grassland	0.0	0.0	0.0	0.0	0.3	0.2	0.2	0.3	0.4	0.5	0.9	1.6	0.2	0.2
Upland tundra	0.2	0.3	4.8	4.2	3.4	3.6	6.0	6.0	45.6	45.4	5.3	6.1	6.9	6.9
Barren tundra	0.0	0.0	0.2	0.1	0.0	0.1	0.1	0.1	30.6	30.9	0.1	0.0	2.5	2.5
Polar & alpine desert	0.0	0.0	0.0	0.0	0.0	0.0	0.0	0.0	1.2	0.7	0.0	0.0	0.1	0.1
Urban	0.0	0.0	0.0	0.0	0.0	0.0	0.0	0.0	0.5	0.5	0.0	0.0	0.0	0.0
Inland water	0.6	0.7	2.0	1.9	0.7	0.9	0.7	0.7	0.5	0.4	33.1	29.1	1.4	1.4
% in our classification	28.1		6.0		20.1		35.7		7.9		2.2			

b)

Our classification: **USGS IGBP classes:**	**Forests**		**Willow & meadow**		**Peatland**		**Tundra heaths**		**Mainly bare**		**Water bodies**		**% in IGBP**	
Forest	8.3	68.4	1.0	30.7	4.3	45.6	0.1	16.9	0.4	3.7	1.0	19.5	3.4	36.9
Closed shrublands	11.9	11.9	1.3	1.3	8.5	8.6	0.2	0.2	1.0	1.0	3.0	2.1	5.4	5.3
Open shrublands	75.7	0.3	94.1	4.3	81.8	3.5	97.0	6.0	65.9	45.1	65.6	5.7	84.7	6.9
Woody savannas	0.0	18.5	0.1	61.5	0.0	40.6	0.0	74.9	0.3	16.4	0.2	41.4	0.1	46.0
Grasslands	0.0	0.0	0.0	0.0	0.3	0.3	0.2	0.3	0.4	0.5	1.0	1.2	0.2	0.2
Permanent wetlands	2.9	0.1	1.5	0.1	2.9	0.5	1.5	1.1	0.1	0.1	2.9	0.9	2.1	0.6
Barren or sparse veget.	0.0	0.0	0.1	0.1	0.1	0.1	0.1	1.1	30.9	32.3	0.1	0.1	2.5	2.6
Urban and built-up	0.0	0.0	00	0.0	0.0	0.0	0.0	0.0	0.5	0.6	0.0	0.0	0.1	0.1
Water bodies	1.1	0.7	2.0	2.0	2.0	0.9	0.9	0.6	0.4	0.4	26.1	29.1	1.6	1.4
% in our classification	28.1		6.0		20.1		35.7		7.9		2.2			

c)

Our classification: UM classes:	Forests	Willow meadow	Peat-land	Tundra heaths	Mainly bare	Water bodies	% in UM
Forest	47.4	10.1	7.4	0.5	1.2	5.7	15.8
Woodland	38.4	21.7	24.8	6.2	3.1	16.3	19.9
Wooded grassland	11.1	34.9	42.5	60.6	7.4	27.2	36.6
Closed shrubland	0.4	21.9	18.4	27.8	10.9	28.3	16.5
Open shrubland	0.3	6.5	2.6	2.7	66.9	3.3	7.3
Grassland	1.2	3.5	3.2	1.0	2.4	1.3	1.7
Bare ground	0.0	0.0	0.0	0.0	7.3	0.0	0.6
Urban and built-up	0.0	0.0	0.0	0.0	0.6	0.0	0.1
Water	1.3	1.5	1.2	1.1	0.3	17.9	1.5
% in our classification	28.1	6.0	20.1	35.7	7.9	2.2	

d)

Our classification: IES GLC2000 classes:	Forests	Willow meadow	Peat-land	Tundra heaths	Mainly bare	Water bodies	% in IES GLC2000
Forest	79.9	22.3	32.4	9.2	4.0	15.3	34.21
Shrublands	0.1	3.4	1.0	0.4	0.4	0.3	0.63
Grasslands	0.6	11.1	3.0	1.1	0.3	0.0	1.85
Peat/wetlands	15.7	20.4	27.0	13.9	4.5	36.3	17.18
Tundra	3.3	42.1	36.1	75.2	63.9	25.3	43.20
Mainly bare	0.0	0.2	0.1	0.1	26.0	1.1	2.16
Water	0.4	0.6	0.3	0.1	0.9	21.8	0.78
% in our classification	28.1	6.0	20.1	35.7	7.9	2.2	

Comparison of modelled and observed clouds and radiation in the Arctic

Klaus Wyser, Colin Jones, Ralf Döscher, H. E. Markus Meier

SMHI/Rossby Centre, Norrköping, Sweden

Introduction

The energy budget of the Arctic is largely determined by radiation. However, the processes that govern the absorption and redistribution of radiant energy are still poorly understood, in particular the interaction between clouds and radiation [Randall et al., 1998]. The knowledge about relevant processes needs to be improved, we need to investigate more the seasonal variation of cloud cover, the occurrence of optically thin clouds or diamond dust, the presence of supercooled water in clouds and the size of droplets and ice crystals (effective radius) to name a few of the questions that are not understood..

How well are clouds and radiation represented in climate models? The projects GLIMPSE [Dethloffs et al, 2005] and ARCMIP [Curry and Lynch, 2003] aim at the improvement of parameterizations in regional and global climate models with the Arctic in focus. Here we will look at the skills of several models to reproduce clouds and radiation. We will compare model results against each other, against observations, and against ERA-40 to identify weaknesses in the description of clouds and the implications thereof for the radiation budget.

Experiment setup

Two different experiment setups have been used. The GLIMPSE domain covers the entire Arctic Ocean and part of the surrounding land masses. The same domain is also used for the coupled studies in the GLIMPSE project. In the uncoupled experiment, lateral boundary forcing is from ERA-40 and updated every 6 hours. SST and sea-ice concentrations are also obtained from ERA-40 while temperatures over land are computed within the regional climate models. All models have been integrated for 10 years (1990-99) to provide a reasonable average climate. Three groups have participated in this experiment with their atmosphere-only model: AWI with Hirham [Rinke et al., 2005], met.no with Hirham [Kolzow et al., 2005] and SMHI with RCA [Doescher et al., 2005].

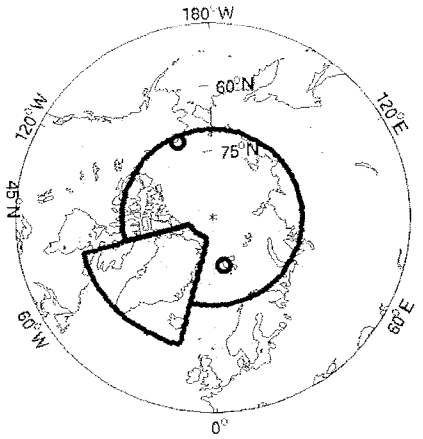

Figure 1: The central Arctic and the Greenland sector that are used for model evaluation. Shown is also the location of the two BSRN station Ny Ålesund (Spitsbergen) and Barrow (Alaska).

The ARCMIP setup covers a small domain over the Beaufort Sea north of Alaska. Lateral boundary forcing is taken from ERA-40 while SST, sea-ice temperature and sea-ice fraction are from the Advanced Polar Pathfinder program. Note that in the ARCMIP setup the sea-ice temperature is prescribed while it is computed by the models in the GLIMPSE setup. The small ARCMIP domain restricts the models to closely follow the synoptic evolution, and the only differences in the results from the different models are due to differences in the model physics. Seven modelling groups have submitted model data for an intercomparison: the same three groups that have participated in the GLIMPSE study, and MISU (with COAMPS), MPI (REMO), CIRES (PMM5 and ArcSYM) and UQAM (CRCM). The ARCMIP experiment is setup to coincide with the SHEBA experiment during which an icebreaker was frozen into the Arctic pack-ice and allowed to drift with the ice for one year [Uttal et al., 2002]. The observations from the SHEBA site are a highly valuable dataset for the validation of the models in the Arctic.

Results

The three regional climate models from the GLIMPSE project have provided fields of monthly averaged radiation and cloud variables. The amount of data is further reduced by looking at timeseries of area averages over the Arctic Sea and in a sector over Greenland (Fig. 1). For the comparison we compute ERA-40 averages for the same timeperiod over the same regions. For comparisons against the BSRN stations Ny Ålesund and Barrow the model output and ERA-40 fields are interpolated to the station location.

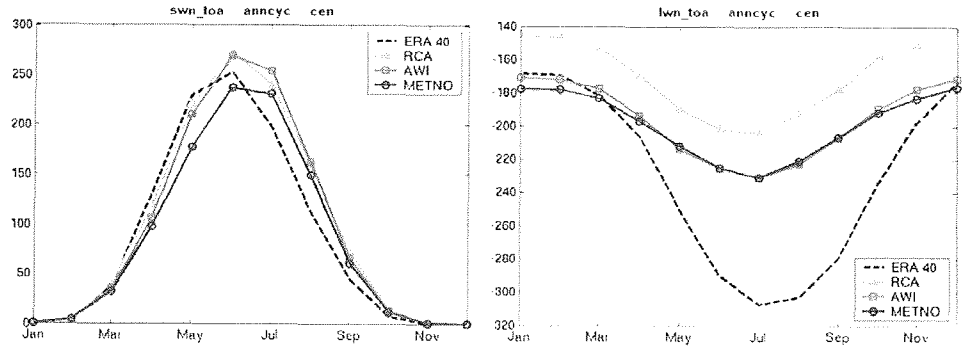

Figure 2: 10-yr averaged annual cycle of SW and LW net radiation at the top of the model, averaged over the central Arctic. Downward radiation is counted positive. Units are W m-2.

Figure 2 shows the annual cycle (averaged over 10 years) of the top of the model net shortwave (SW) and longwave (LW) radiation over the central Arctic. Since the incoming SW radiation is the solar constant and the downwelling LW radiation is negligible the figure can also be interpreted as the difference in the amount of absorbed energy. RCA and AWI are close to each other in the SW, while METNO absorbs less solar radiation. None of the models matches the SW radiation from ERA-40, all models are lower in spring and higher during summer and autumn. The net LW radiation agrees well between AWI and METNO while it is higher (less negative) in RCA with an almost constant bias of 25 W m-2. In winter, AWI and METNO are also close to ERA-40 but during the rest of the year ERA-40 shows much more outgoing LW radiation with the difference exceeding 100 W m-2 in July and August.

When SW and LW radiation are combined we find that all our models absorb more radiation than ERA-40, that is more energy is deposited in the atmosphere-land system (ocean temperature and ice distribution are prescribed). The difference is alarmingly high and need to be investigated in more detail. It is possible that this points to a weakness of the regional climate models in this study, for example the optical properties of clouds in the Arctic.

Another possibility is that ERA-40 may be inappropriate for energy flux and cloud comparisons. Each analysed situation in ERA-40 is a combination of a 6-hr first guess and observations. The 6-hr spin-up of the model is not sufficient to build enough clouds, and the adjustment to the observations destroys the energy balance. Thus, the analysis is not conservative in energy and the cloud field (which is important for the radiative transfer) may be not well adjusted to the synoptic situation. For a more detailed analysis of the result we need to include more observed data, e.g. from satellite programs (APP-x).

The annual cycles of net SW and LW radiation over Greenland show the same qualitative picture as over the central Arctic. The only difference is found in the SW radiation where all models reflect more solar radiation back to space than ERA-40 in summer and autumn, which compensates to some extent the excess downwelling LW. The difference in SW between the central Arctic and Greenland could be a coincidence due to differences in the albedo parameters of ice and snow over sea and land, but it could also be a more fundamental issue. The energy balance over land surface is solved explicitly in the regional climate models, but SST and ice concentration are prescribed over the ocean. Thus, an imbalance in the energy budget over land will feed back to the climate model, but it passes unnoticed over the ocean.

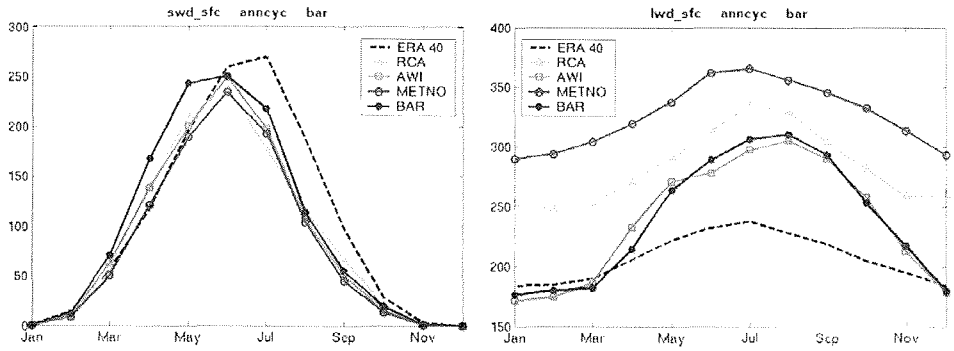

Figure 3: Averaged annual cycle of downwelling radiation (in W m-2) at the surface at Barrow. Model results and ERA-40 data have been interpolated to the location. Observed radiation is shown as BAR.

Figure 3 compares the downwelling radiation at the surface against ERA-40 and observations from Barrow. The SW results from the three models are in fair agreement, but they differ from both observations and ERA-40. However, the overall impression is that ERA-40 deviates more from the observed SW values than our models, especially during summer and fall. In the LW, the three models are distinct with the largest difference in winter and the smallest in summer. AWI follows closely the observations from Barrow while there is more downwelling LW at the surface in the other two models. LW from ERA-40 matches the observations in winter but it is too low during the rest of the year.

ERA-40 agrees poorly with the observed values at Barrow and at Ny Ålesund (not shown). This supports the hypothesis that ERA-40 may not be the best estimate for radiation and therefore not suitable for the validation of radiation of climate models.

For the cloud cover the regional climate models follow closer the annual cycle of ERA-40 than the observations (Fig. 4). The annual cycle of observed cloudiness with a very low minimum cloud cover is fundamentally different from any of the models or ERA-40 where the minimum occurs in spring but is not as deep as in the observations.

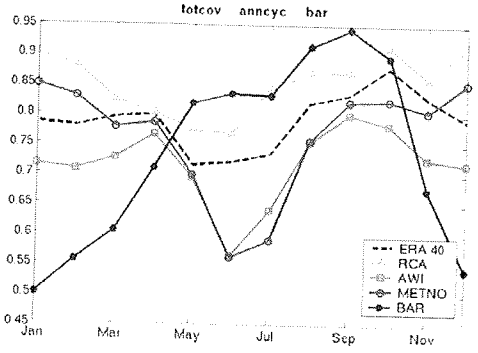

Figure 4: As Fig. 3 but for monthly mean cloud cover.

Cloud cover is an important quantity in climate models, not only for radiation but also for microphysics. It is, however, not straightforward to compare cloud cover from models and observations since the threshold for detecting and counting clouds is different for each instrument [Wyser and Jones, 2005]. Nevertheless, the question arises how models that seem to deviate so much from the observed cloud cover (Fig. 4) are still able to reproduce the radiation at the surface reasonably well (Fig 3). And why do the regional models deviate so much from ERA-40 if the cloud cover is not very different? Are there compensating errors that mitigate the impact from a difference in cloud cover by adjusting the transmissivity or reflectivity of clouds? Further analysis is needed to answer this question.

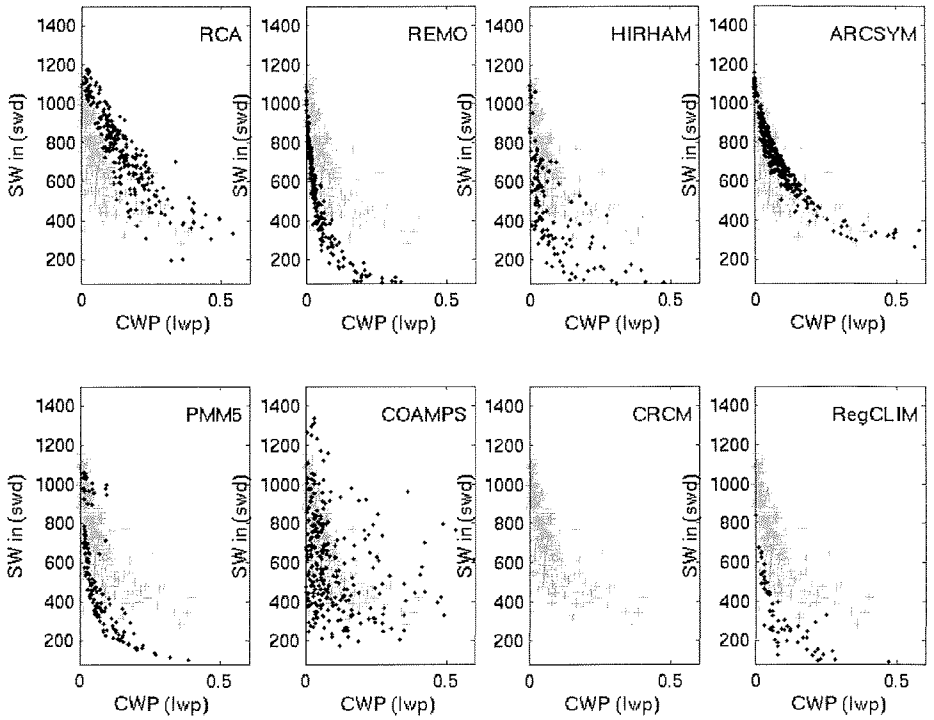

Figure 5: Downwelling SW (in W m-2) at the SHEBA site as a function of the vertically integrated cloud water (liquid plus ice, kg m-2). Results from ARCMIP simulations are shown as black dots, observations are shown as gray crosses. Note that the microwave radiometer detects only liquid water and the observed CWP are likely to be too low. Simulated and observed SW has been normalized by the air mass.

Figure 5 shows an example of how well regional climate models simulate the transmission of solar radiation in clouds. Vertically integrated cloud water (CWP) is plotted on the abscissa and downwelling SW on the ordinate for models and observations. The sum of liquid and ice fraction is plotted for the models, while the microwave radiometer detects only the liquid part and the true CWP is likely to be higher than the values shown. The general trend is well captured by the models, the more cloud water the less radiation to the ground. However, the transmissivity in most models seem to be too low compared to observations. Possibly, the models have been tuned to mid-latitude conditions and fail to reproduce the optical properties of Arctic clouds. ARCSyM which has been developed with the Arctic in mind shows a much better agreement with the observed relationship between cloud water and radiation.

References

Curry J.A. and A.H. Lynch 2002. Comparing Arctic regional climate models. EOS Trans. AGU, 83, 87.

Dethloff, et al., 2005. Overview of GLIMPSE project, in this issue

Doescher R., H.E.M. Meier and K. Wyser 2005. Sensitivities in the Rossby Centre Acrtic models. This issue.

Koltzow et al 2005. Description of RegClim model, in this issue

Randall et al. 1998: Status of and outlook for large-scale modelling of atmosphere-ice-ocean interaction in the Arctic. Bull. Am. Meteorol. Soc., 79, 197-219.

Rinke et al. 2005. in this issue

Uttal T. et al. 2002. Surface heat budget of the Arctic ocean. Bull. Amer. Soc., 82, 255-275.

Wyser K. and C. Jones 2005. Modeled and observed clouds during Surface Heat Budget of the Arctic Ocean (SHEBA). J. Geophys. Res., 110, D09207, doi:10.1029JD004751

4 Appendix

Appendix 1. Work packages of the GLIMPSE project.

- WP1 Intercomparison and Improvements of atmospheric RCMs

will carry out intercomparison of three different Arctic regional atmospheric models on the basis of annual simulations of the SHEBA year October 1997-October 1998. The influence of horizontal resolutions (50 km, 25 km and 10 km), of the domain (whole Arctic Basin and the smaller SHEBA sub-domain), of physical parameterizations (main focus: planetary boundary layer schemes, land-surface models, cloud-radiation and ice-albedo-water vapour feedbacks, uncoupled-coupled models) will be investigated. Improved schemes for the parameterization of land-surface schemes, planetary boundary layer, cloud schemes and permafrost schemes over land points will be implemented. The new schemes will be validated against observational data. Initial and boundary conditions to drive the model simulations are provided as perfect boundary conditions from observations. A serious problem in assessing the performance of simulated regional climate is the availability of good quality high-resolution data for the model validation. Decadal simulations will be carried out to understand natural variability.

- WP2 Intercomparison and Improvements of coupled A-I-O RCMs

will carry out intercomparison of three different coupled regional models of the atmosphere-ocean-ice system. Coupled atmosphere-ice-ocean models will be developed, integrated and validated for the SHEBA year. Series of 10 year integrations with coupled RCM's will be conducted to understand the atmosphere-ice-ocean feedbacks on the variability of the atmospheric circulation. Such a multifaceted approach is necessary to tackle the complex Arctic climate problems.

- WP3 Comparison of Arctic patterns and climate feedbacks in AOGCMs and RCMs

will compare the annual cycle in atmospheric and oceanic key processes and variables with a special focus on the hydrological cycle and water vapour feedbacks. Series of 50 year long simulations of present day climate with two AOGCMs will be used for this intercomparison.

- WP4 Global consequences of improved description of Arctic climate processes and feedbacks in free AOGCM runs

will estimate the implications and global consequences of the improved physical Arctic process parameterizations and feedbacks in two coupled AOGCMs by carrying out 500 year free simulations with constant external forcing parameters. This allows to determine abrupt changes as a result of multiple equilibria in the unforced climate system as e. g. the two states of the thermohaline circulation under the influence of atmospheric and sea-ice feedbacks.

- WP5 Implications of improved Arctic process description on rapid paleoclimatic changes in forced AOGCM runs

will quantify objectively the risk of abrupt changes in the European climate and climate extremes following natural and anthropogenically forced climate changes by carrying out 500 year long simulations with a coupled climate model under the influence of aerosol, solar and carbon dioxide forcing since 1500 BP.

- WP6 Regional assessment of Arctic paleoclimatic and future change

will carry out a dynamical downscaling with regional climate models using the paleoclimatic time slices of the AOGCM simulations carried out in WP5, to assess the potential effect of e.g. a rapid shift similar to the Little Ice Age on the economical and socio systems in Europe and the European Arctic.

Appendix 2. Participants of the workshop.

Surname	First name	e-mail	Organization
Baquero-Bernal	Astrid	baquero@dkrz.de	Meteorological Institute, University Hamburg
Bengtsson	Lennart	bengtsson@dkrz.de	Max Planck Institute of Meteorology Hamburg
Benkel	Andreas	andreas.benkel@gkss.de	GKSS Research Centre, Geesthacht
Brand	Sascha	sbrand@awi-potsdam.de	Alfred Wegener Institute, FS Potsdam
Christensen	Jens Hesselbjerg	jhc@dmi.dk	Danish Meteorological Institute, Copenhagen
Debernard	Jens	jens.debernard@met.no	Norwegian Meteorological Institute, Oslo
Deckelmann	Holger	hdeckelmann@awi-potsdam.de	Alfred Wegener Institute, FS Potsdam
Dethloff	Klaus	dethloff@awi-potsdam.de	Alfred Wegener Institute, FS Potsdam
Dorn	Wolfgang	wdorn@awi-potsdam.de	Alfred Wegener Institute, FS Potsdam
Döscher	Ralf	ralf.doescher@smhi.se	Swedish Meteorological and Hydrological Institute, Norrkoeping
Gerdes	Rüdiger	rgerdes@awi-bremerhaven.de	Alfred Wegener Institute, Bremerhaven
Gluschak	Ksenya	kglushak@awi-potsdam.de	Alfred Wegener Institute, FS Potsdam
Görgen	Klaus	k.goergen@gmx.net	School of Geography and Environmental Science, Melbourne
Handorf	Dörthe	dhandorf@awi-potsdam.de	Alfred Wegener Institute, FS Potsdam
Hebestadt	Ines	hebestad@awi-potsdam.de	Alfred Wegener Institute, FS Potsdam
Holzkämper	Steffen	steffen.holzkaemper@natgeo.su.se	Department of Physical Geography and Quaternary Geology Stockholm University
Jones	Colin	jones@atlas.sca.uqam.ca	Université du Québec à Montréal
Kaleschke	Lars	lkalesch@iup.physik.uni-bremen.de	Institute of Environmental Physics Bremen
Karcher	Michael	mkarcher@awi-bremerhaven.de	Alfred Wegener Institute and O.A.Sys
Kattsov	Vladimir	kattsov@main.mgo.rssi.ru	Voeikov Main Geophysical Observatory, St. Petersburg
Koeberle	Cornelia	ckoeberl@awi-bremerhaven.de	Alfred Wegener Institute, Bremerhaven
Koether	Bernard	bkoether@glaciersociety.org	Glacier Society

Køltzow	Morten	famo@met.no	Norwegian Meteorological Institute, Oslo
Kuhry	Peter	peter.kuhry@natgeo.su.se	Department of Physical Geography and Quaternary Geology Stockholm University
Lange	Manfred	langema@uni-muenster.de	Institute for Geophysics and Centre for Environmental Research
Läuter	Matthias	mlaeuter@awi-potsdam.de	Alfred Wegener Institute, FS Potsdam
Leutert	Beate	bleutert@awi-potsdam.de	Alfred Wegener Institute, FS Potsdam
Martin	Torge	tmartin@awi-bremerhaven.de	Alfred Wegener Institute, Bremerhaven
Maslowski	Wieslaw	maslowsk@nps.edu	Naval Postgraduate School, Monterey
Melsheimer	Christian	melsheimer@uni-bremen.de	Institute of Environmental Physics University of Bremen
Morrison	Hugh	hugh@cloud.colorado.edu	University of Colorado, Boulder
Müller	Gerd	gerd.mueller@dkrz.de	Meteorological Institute of University of Hamburg
Päpke	Jürgen	jpaepke@awi-potsdam.de	Alfred Wegener Institute, FS Potsdam
Ping	Du	ping@obelix.sca.uqam.ca	Université du Québec à Montréal
Reigstad	Marit	maritr@nfh.uit.no	Norwegian College of Fishery Science, University of Tromso
Rinke	Annette	arinke@awi-potsdam.de	Alfred Wegener Institute, FS Potsdam
Rockel	Burkhardt	Burkhardt.Rockel@gkss.de	GKSS Research Centre, Geesthacht
Saha	Subodh Kumar	ssaha@awi-potsdam.de	Alfred Wegener Institute, FS Potsdam
Scherer	Dieter	Dieter.Scherer@TU-Berlin.de	Climatology Section, Institute of Ecology Berlin University of Technology
Schmith	Torben	ts@dmi.dk	Danish Meteorological Institute, Copenhagen
Schröder	David	david.schroeder@dkrz.de	Meteorological Institute, University of Hamburg
Sempf	Mario	msempf@awi-potsdam.de	Alfred Wegener Institute, FS Potsdam
Slagstad	Dag	Dag.Slagstad@sintef.no	Marine Resources Technology SINTEF, Trondheim

Söderberg	Stefan	stefan@misu.su.se	Department of Meteorology Stockholm University
Sokolova	Elena	esokolova@awi-potsdam.de	Alfred Wegener Institute, FS Potsdam
Stenchikov	Georgiy	gera@envsci.rutgers.edu	Department of Environmental Sciences, Rutgers University
Stendel	Martin	mas@dmi.dk	Danish Meteorological Institute, Kopenhagen
Tjernström	Michael	michaelt@misu.su.se	Department of Meteorology Stockholm University
Treffeisen	Renate	rtreff@awi-potsdam.de	Alfred Wegener Institute, FS Potsdam
Wyser	Klaus	Klaus.Wyser@smhi.se	Swedish Meteorological and Hydrological Institute, Norrkoepping

Appendix 3. Author index.

Benkel	9,13,112	Martin	83
Brunner	47	Maslowski	84
Burrows	62	Meier	36,139
Cassano	17,47	Melsheimer	85
Casty	51	Morrison	89
Christensen	51,123	Notholt	62
Debernard	21,26	Reigstad	104
Dethloff	29,41,51,82,94,103,112	Richter	62
Döscher	36,139	Rinke	41,90,94,112
Dorn	41	Rockel	13
Ellingsen	104	Saha	94
Fieg	45	Sander	62
Frickenhaus	41	Schmith	99
Gerdes	41,45,71	Schröder	100
Görgen	47	Sempf	51,103
González-Rouco	13,51	Slagstad	104
Handorf	51,82,103	Söderberg	107,128
Heygster	62,85	Sokolova	112
Hollwedel	62	Stenchikov	116
Holzkämper	58	Stendel	51,99,123
Jacobi	62	Tjernström	107,128
Jones	139	Uotila	17
Kaleschke	62	Virtanen	133
Karcher	41	von Glasow	62
Kattsov	66	Wassmann	104
Kauker	41	Weller	62
Kern	62	Wyser	36,139
Köberle	71	Xie	47
Køltzow	9,73	Žagar	107,128
Kuhry	58,94,133	Zorita	51
Kurgansky	103		
Lange	77		
Läuter	82		
Lestak	47		
Lynch	17,47		